The roles of subtype specific bone marrow stromal cell secretomes

Andrew Philip Stone

PhD

University of York

Biology

February 2021

Abstract

Understanding of bone marrow stromal cell (BMSC) functions is complicated by heterogeneity. Current cell-surface markers are insufficiently selective for functionality, which has profound implications for development of BMSC based therapies. In this thesis I investigated secreted factors of immortalised BMSC clones and their effects on BMSC functions.

I compared the effects of secreted factors from two phenotypically distinct clones on BMSC phenotype. I used Y201, a multipotent and migratory BMSC, and a nullipotent non-migratory clone, Y202. Y201 conditioned media (Y201CM) treatment of Y202 cells resulted in larger colonies in a CFU-F assay. Subsequent tracking of Y202 cells in culture indicated that they migrated further in Y201CM. Increased migration of Y202 cells was driven by heat-labile secreted factors, and was replicated by culturing Y202 on BMSC derived extracellular matrix (ECM). This ECM migration was reduced with a focal adhesion kinase inhibitor.

Proteomics of conditioned media revealed that Y201 secreted proteins significantly enriched for ECM. Periostin and aggrecan were identified as candidate ECM components that could contribute to Y201 phenotype due to high abundance and large fold-changes versus Y202. Extracellular vesicle (EV) protein and miRNAs were also compared between BMSC subtypes, with upregulated Y201 EV proteins enriched for pathways and terms associated with ECM. Nanostring analysis revealed significant upregulation of 10 versus 2 miRNAs in EVs from Y201 and Y202 respectively. Predicted targets of Y201 upregulated miRNAs also indicated ECM involvement.

Immunofluorescence staining of ECM proteins identified by proteomics identified possible BMSC locations in human and murine tissue, with Y201 upregulated ECM components predominantly in endosteal regions. Rare $CD271^{+}$ bone-lining stromal cells were found on top of aggrecan and periostin in trabecular regions of human bone.

I conclude that BMSC subtype heterogeneity is mirrored in secreted factors and that the secretome and ECM components provide important markers of functionality and localization.

Table of Contents

List of Figures

List of Tables

List of accompanying materials

Powerpoint file containing supplementary videos 1, 2, 3 and 4 entitled "Stone_108001093_Supplementary videos"

Acknowledgements

I must begin by thanking my supervisors Paul Genever and Ian Hitchcock who provided me with support and advice throughout this project. I also thank the members of my TAP, Dawn Coverley and Dani Ungar, who regularly saw updates on the work and provided useful guidance and insight.

At York I was lucky to work alongside world experts in the technology facility and thank the imaging and cytometry team with special thanks to Graeme Park and Karen Hogg. I must also thank Meg Stark and Clare Steele-King for guiding me through staining of samples and imaging for electron microscopy. I also want to thank Adam Dowle for his assistance with proteomic work. I also must thank Emma Rand for her help with coding and statistical analyses and her positive attitude and friendship.

I was lucky to work in a fantastic environment and among brilliant colleagues. I am appreciative to all the members of the Genever and Hitchcock labs both past and present for their support. The J0 cell biology labs were also of great help to me.

Importantly I also had a number of friends and colleagues who were particularly involved and I thank them for all they have done to advise and support me, these were Paul Souter, David Kuntin, David Mentlak, Dimi Kioumourtzoglou, Chris MacDonald, Ali Pizzey, Lewis White, Gideon Hughes, Laura Fort, Hannah Spencer, Oliver Herd, Amanda Barnes, Paul Pryor and Alasdair Kay.

I also had some fantastic collaborations and want to thank Rachel Crossland and Xiao-nong Wang from Newcastle for collaborating on EV projects, as well as Tom Dennison at Malvern Panalytical for kindly inviting me to obtain extracellular vesicle size data on their latest equipment.

I have also been lucky to have a family that supported me throughout and I must finally thank my girlfriend Liz, without whom I would not have made it this far.

Declaration

I declare that this thesis is a presentation of original work and I am the sole author. All experiments were performed by the author except; FIB-SEM images were obtained by Jon Barnard from the York Nanocentre, proteomic acquisitions were performed by Adam Dowle from the metabolomics and proteomics lab at York and haematopoietic stem cell survival on extracellular matrices was performed in collaboration with Juan Rubio-Lara. Emma Rand helped with statistical analysis of proteomic data. This work has not previously been presented for an award at this, or any other, University. All sources are acknowledged as References.

Signed 

1 Introduction

1.1 The Bone Marrow Stromal Cell

1.1.1 Bone marrow and the bone marrow stroma

The skeleton is host to a plethora of important cell-types that have fundamental roles in health and disease. Bones provide structural rigidity and support to the human body while also offering physical protection for bone marrow, the highly dynamic organ in which haematopoiesis occurs in healthy adults. The bone marrow is responsible for the production of ~$2.5x10^{11}$ red blood cells in adult humans every day, thus support and regulation of this process is important to maintaining life (Higgins and Mahadevan, 2010). Bone marrow stromal cells (BMSCs) are found in the marrow space of skeletal tissues and are fundamental to the normal development and function of bones and the bone marrow. BMSCs provide structural components of the bone marrow and also contain a pool of stem cells capable of differentiating into bone, fat and cartilage, tissues that are important for the essential functions of the skeleton. BMSCs, specifically osteo-lineage precursors, are present in developing bones before HSCs and are essential for establishing the bone marrow as the haematopoietic organ (Chan et al., 2009; Coşkun et al., 2014). There is significant evidence to indicate that stromal cells are integral for maintenance of healthy haematopoiesis in bone marrow. It is therefore important that we develop our understanding of the various functions of BMSCs in homeostasis so that we are better able to respond to issues related to these cells that might influence disease.

1.1.2 Discovery of bone marrow stromal cells and differentiation competent subpopulations

The discovery of BMSCs that contained stem-cell subpopulations began in the 1960s when Friedenstein and colleagues established evidence for the existence of an osteogenic progenitor in bone marrow through animal transplantation experiments (Friedenstein et al., 1966). Subsequent work demonstrated that colonies, referring to single-cell derived populations, of adherent cells could be isolated from marrow, and it was postulated that these were derived from individual cells. These originator cells were referred to as the colony forming unit fibroblast (CFU-F) (Friedenstein et al., 1970). It was also noted that spontaneous or inducible osteogenic differentiation could occur from cells derived from these CFU-Fs, however, transplant of individual colonies was later shown to demonstrate a more heterogeneous response, with one study demonstrating only 58.8% of CFU-Fs differentiated toward bone *in vivo* (Friedenstein et al., 1970; Kuznetsov et al., 1997).

In the following decades, discoveries revealed that within the CFU-F there was a population of multipotent progenitor cells capable of differentiation towards osteoblasts, adipocytes and chondrocytes, often referred to in the field as tripotent differentiation. This was shown formally by Pittenger et al. (1999) with the isolation and characterisation of the human mesenchymal stem cell (MSC). The term MSC was first coined in 1991, but has produced various controversies over its use and the specificity of the term (Caplan, 1991; Sipp et al., 2018). Reference to these cells as “stem cells” indicated capacity for differentiation towards other lineages. While there was clear evidence for differentiation capacity within cell populations isolated through plastic adherence from bone marrow, there was considerable evidence to highlight the heterogeneity in potency of BMSCs isolated using the same method, with heterogeneity of populations still a problem in research and translation today. Further complication over the definition and nomenclature surrounding the MSC was introduced by discoveries that differentiation competent stromal cells could be isolated from other tissues, with one study highlighting the isolation of MSC-like cells from 10 different post-natal tissues (Meirelles et al., 2006). Subsequently the literature has expanded to include; dental pulp, Wharton’s jelly, adipose tissue, umbilical cord and bone marrow among the most common tissues from which MSCs are derived (Gronthos et al., 2000; Kern et al., 2006; Sarugaser et al., 2005; Wang et al., 2004). This variation in tissue sources for multipotent stromal cells has also led to adoption of common nomenclature to highlight tissue of origin, and with use of the word stromal where stem-characteristics are insufficiently defined (e.g. adipose tissue derived mesenchymal stromal cell/AT-MSC).

The discussion into the terminology used to describe the overall population of differentiation-competent marrow-resident stromal cells is ongoing, but was considered in position statements released in 2005 and 2006 by the International Society for Cell and Gene Therapy (ISCT) (Dominici et al., 2006; Horwitz et al., 2005). In the original statement, the ISCT proposed the term multipotent mesenchymal stromal cell should be applied to fibroblastic, plastic-adherent cells isolated from numerous tissues, and that the term MSC be reserved for cells that had appropriately demonstrated sufficient differentiation capacity. The second position statement, which has superseded its predecessor, expanded upon this and proposed more detailed characterisation criteria to identify cells as multipotent mesenchymal stromal cells. These requirements were:

1) Plastic adherence

2) High expression (≥95%) of CD105 (Endoglin), CD73 (NT5E) and CD90 (Thy-1)

3) Lack, or extremely low expression of (≤2%), haematopoietic lineage markers CD34, CD45, CD14 or CD11b, CD79α or CD19 and Human Leukocyte Antigen-DR isotype

4) Tripotent differentiation capacity towards osteoblasts, adipocytes and chondrocytes *in vitro*

These criteria were established to prevent what was seen as erroneous use of the term 'stem' to describe populations of cells isolated and characterised by plastic adherence, morphology and flow cytometry, but were not always shown to have differentiation potential. The criteria were intended to allow more appropriate comparisons between studies from research groups using different isolation methods and tissue sources, however, these were often interpreted as absolute rules for defining the MSC and have remained controversial and the use of varied terminology to refer to bone marrow derived stromal cells is still common. The use of the ISCT cell-surface marker criteria to categorise cells has been shown to be inclusive of heterogeneous stromal cells from different tissues that vary considerably in their transcriptomes and also in osteogenic differentiation capacity *in vivo* (Reinisch et al., 2015; Sacchetti et al., 2016). In these studies, BMSCs demonstrated a greater *in vivo* osteogenic capacity, with BMSCs exclusively capable of establishing a haematopoietic microenvironment. Another study highlighted how despite several BMSC donors sharing expression of the ISCT markers there was considerable variation in other established markers, secreted factor concentration and ectopic differentiation towards the osteogenic lineage *in vivo* (Samsonraj et al., 2015). The ISCT markers have been shown on multiple occasions to be insufficiently selective for subtypes with multipotent stem cell characteristics. The definitions have also led to treatment of isolated populations that meet the criteria as homogeneous, which disregards the variation in phenotypes within the mixed stromal populations that are isolated. It is likely that numerous BMSC subtypes are isolated by plastic adherence, and that these collectively meet the cell-surface marker criteria with *in vitro* differentiation of these plastic adherent cultures revealing tripotency, however, the relative contribution of individual cells or clones to a positive differentiation assay may be lost. A subset of cells in the plastic adherent culture could differentiate, and possibly even be selected for, when performing *in vitro* experiments, a feature of BMSC population dynamics that was demonstrated using lentiviral fluorescence barcoding and tracing of individual clones (Selich et al., 2016). Thus, cells that do not differentiate (are nullipotent) could remain hidden in the population, and the commonplace treatment of non-clonal BMSC

isolations as homogeneous could help to explain inter- and intra-donor heterogeneity. There have been considerable efforts put towards improving the identification of the multipotent mesenchymal stromal cell populations, particularly from BMSCs, using a variety of alternative cell-surface markers (covered in section 1.3.2), with this work being of particular importance for the development of regenerative cellular therapies through selection of appropriately potent populations.

Throughout this thesis I will predominantly refer to BMSCs, however, I may also refer to studies performed using stromal cells derived from other tissues and will include more characterisation information where the authors explicitly presented it, such as cell surface markers used to classify the population or the tissue of origin.

In addition to the differentiation potential of BMSCs, a number of other important functions have been ascribed to these cells. Through decades of research, the role of BMSCs in communication with immune cells and regulation of immune responses, as well as support of haematopoiesis, have become areas of keen interest, and I will expand on these in the following sections.

1.2 Immunomodulatory potential of MSCs

There have been numerous indications for the use of BMSCs in suppressing inflammation, and some examples of this intriguing functionality are explored here. The immunosuppressive effects of BMSCs on T-cells were first demonstrated using cells isolated from baboons (Bartholomew et al., 2002). The BMSCs were shown *in vitro* to prevent proliferation of lymphocytes in a dose-dependent manner, and prolonged the survival of skin-grafts *in vivo*. A study using human cells released in the same year also demonstrated the suppression of T-lymphocyte proliferation, with a dramatic reduction in proliferative cycles of both $CD4^+$ and $CD8^+$ T-lymphocytes and a positive effect of increasing the ratio of BMSC to T-lymphocyte (Figure 1.1) (Di Nicola et al., 2002). A key observation from this study was that the reduced proliferation was in part driven by paracrine signalling mechanisms, as BMSCs separated by a trans-well were still capable of significantly reducing T-cell proliferation, albeit to a lesser degree. A later comprehensive study using BMSCs in co-culture systems with a variety of different immune cell populations demonstrated a broad capacity to reduce the inflammatory phenotype across various cells (Aggarwal and Pittenger, 2005). In this study, co-cultures with peripheral blood mononuclear cells (PBMCs) resulted in significantly decreased expansion of the PBMCs,

decreased secretion of inflammatory cytokines and an increase by the BMSCs in the expression of the immunomodulatory cytokines interleukin-6 (IL6) and interleukin-8 (IL8), as well as prostaglandin-E2 (PGE2) (Figure 1.1). The study further demonstrated a capacity for BMSCs to modulate expression of cytokines by dendritic cells in response to lipopolysaccharide (LPS), more than halving the expression of inflammatory tumour necrosis factor alpha (TNFα) by monocytic dendritic cells and increasing interleukin-10 (Il-10) expression by plasmacytoid dendritic cells nearly three-fold. The MSCs were also shown to reduce expression of interferon gamma (IFNγ) secretion from IL-2 stimulated natural killer (NK) cells.

Work from the group of Darwin Prockop has comprehensively demonstrated the capacity for BMSCs to suppress inflammation in a variety of mouse models including antigen induced peritonitis, myocardial infarction and damage to the cornea, demonstrating the potent anti-inflammatory capacity of these cells (Choi et al., 2011; Lee et al., 2009; Roddy et al., 2011). These studies collectively argued that secretion of the protein TNFα stimulated gene 6 (TSG-6) by the BMSCs was responsible for the attenuation of inflammation (Figure 1.1). Interestingly, a follow-up study using the corneal inflammation model identified a positive correlation between higher TSG-6 messenger RNA (mRNA) expression levels in BMSCs and efficacy in preventing inflammation (Lee et al., 2014b). The increased efficacy in suppressing inflammation, determined by level of myeloperoxidase as a readout of activated neutrophils, negatively correlated with *in vitro* osteogenic capacity, as determined by an alizarin red staining assay. This was corroborated by overexpression of TSG-6 in a low expressing donor resulting in reduced osteogenic capacity and reduction in myeloperoxidase levels. Osteogenic differentiation in high TSG-6 expressing BMSCs was restored by use of an inhibitor of nuclear factor kappa B (NFκB) which has functions as a transcription factor and is strongly implicated in inflammatory responses. This study also highlighted high donor heterogeneity, and potentially contrasting roles for MSC subtypes or plasticity in MSC function, with possible exclusivism between differentiation and immunosuppression pathways. This consequence of reduced differentiation capacity under inflammatory signalling corroborated a study demonstrating that IFNγ and TNFα produced by T-cells made BMSCs more susceptible to apoptosis and limited their *in vitro* osteogenic differentiation and ability to regenerate bone tissue in calvarial defects (Liu et al., 2011). Murine BMSCs were shown to mediate immunosuppression through a response to IFNγ, confirmed by use of IFNγ-receptor-1 (IFNγR1) knockout mice, demonstrating an inability to suppress immune responses in a GvHD model (Ren et al., 2008).

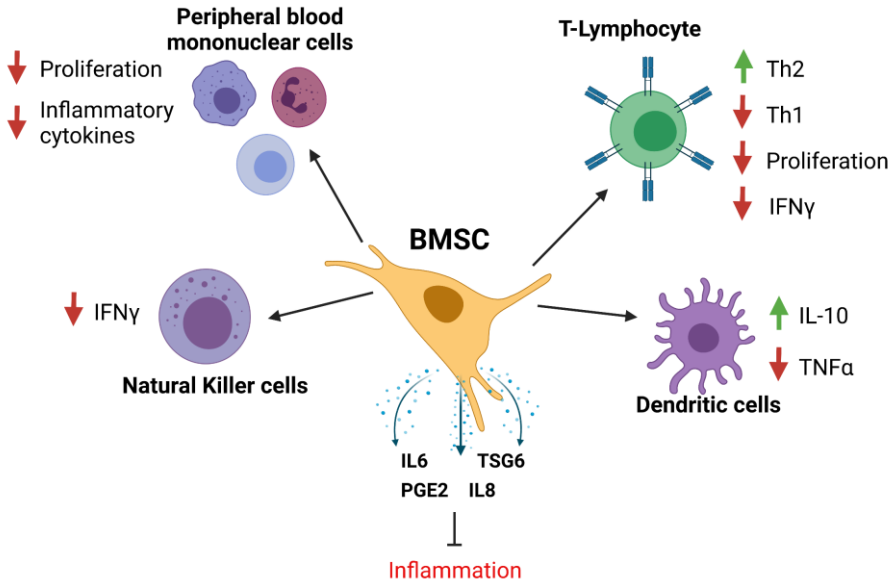

Figure 1.1 BMSCs can modulate immune responses in a variety of cell types

BMSCs have been shown to demonstrate a variety of immunosuppressive effects on both adaptive and innate immune cell types. Shown here are some results of BMSC coculture with a variety of immune cell-types including reduction in proliferation and reduced expression of inflammatory cytokines such as IFNγ and TNFα by immune cells. Such effects were shown to be mediated by paracrine signalling by BMSCs of factors including IL6, IL8, PGE2 and TSG-6.

While the majority of studies have suggested a potential for immunosuppression by BMSCs, there have also been indications that IFNγ and concomitant toll-like-receptor (TLR) activation could result in a pro-inflammatory phenotype (Romieu-Mourez et al., 2009). The authors demonstrated an increase in immune cell infiltration following subcutaneous injection of pre-activated BMSCs with a compounding effect of TLR activation by LPS and IFNγ expression resulting in increased secretion of inflammatory mediators interleukin-12 (IL12) and TNFα. This study also showed an increase in neutrophil chemotaxis towards the BMSCs, indicating a potential role for BMSCs in promoting inflammatory targeting. The pro-inflammatory phenotype could relate to previously established evidence for antigen presentation capacity by BMSCs under low levels of IFNγ stimulation (Chan et al., 2006; Stagg et al., 2006).

Overall, these studies present a complex involvement of BMSCs in the regulation of immune responses and immune cell behaviour which has led to great interest in the development of BMSCs, and of stromal cells isolated from other tissues, in cell-based therapies (covered in 1.6.2).

1.3 BMSCs and the bone marrow/haematopoietic niche

1.3.1 Relationship between the HSC and BMSC

The study of BMSCs and their stem cell subpopulations has often been paralleled by the study of another bone marrow resident stem cell, the HSC. The relationship between these two cell types has been of great interest for understanding haematopoietic development in health and disease, with early studies demonstrating the positive effect of stromal cells in *ex vivo* survival of haematopoietic progenitors (Dexter et al., 1977). Much like the BMSC, the HSC has been repeatedly redefined using more stringent cell-surface markers, allowing a dissection of cellular heterogeneity and identification of more lineage biased/committed progenitors (Kiel et al., 2005; Oguro et al., 2013; Spangrude et al., 1988). That being said, the sorting of HSC subsets capable of reconstituting the entire blood system or specific lineages exemplifies a more comprehensive understanding of the association between cell-surface marker expression and subtype functionality than what is currently known for BMSCs.

Friedenstein's early *in vivo* transplantation experiments of bone marrow and what are now known to be BMSCs, resulted in ectopic bone marrow compartments, acting as an example of the importance of interplay between skeletal progenitors and the haematopoietic system (Friedenstein et al., 1974). More recent studies demonstrating the importance of endochondral ossification and osteogenic precursors in establishing the haematopoietic microenvironment further solidify the link between these cells (Chan et al., 2009; Scotti et al., 2013).

The study of the HSC 'niche', a concept first postulated by Schofield (1978), has been of keen interest, with discussion centring around two key locations in the bone marrow, the endosteal and the perivascular niches (Morrison and Scadden, 2014). A niche refers to the immediate microenvironment in which a cell resides that is capable of facilitating cell functions and maintaining the population *in vivo.* With regards to stem cells this refers to maintenance of the stem cell population and regulation of lineage commitment (Jones and Wagers, 2008). The study of the niche has led to identification of a variety of markers used to distinguish haematopoietic supporting stromal cells, and the specificity and functionality of BMSCs isolated using these markers is explored in the following section.

1.3.2 Candidate markers of bone marrow stromal subpopulations in mice and humans

There has been considerable debate over the localisation of BMSC populations, with intense interest in the identification and refinement of cell-surface markers capable of isolating functionally distinct stromal sub-populations. The improvement and increased accessibility of techniques such as immunolabeling, confocal microscopy, intravital imaging and the development of greater numbers of transgenic reporter mice has resulted in a wave of studies focusing on the localisation of BMSC subsets. The use of markers has also been key for identifying and investigating the location of stem/multipotent subsets that could be classified as MSCs. Identification of discriminating markers has resulted in a considerable number of studies assessing localisation of BMSC populations *in situ*. Studies aiming to define the location of BMSC subtypes have often been done from a haematological perspective, in attempts to understand the role of BMSCs in regulating haematopoiesis and their contribution to the HSC niche. I have summarised a number of proposed markers of BMSC subpopulations, categorised by their cell-surface marker expression in Table 1.1. I expand upon how these populations were defined, their overlapping relations to each other and visualise their localisations in the bone marrow (Figure 1.2). It should be noted that these populations are predominantly defined as a combination of markers after removal or exclusion of haematopoietic and endothelial lineages by use of classical cell-surface markers specific to these lineages.

Low affinity nerve growth factor receptor (LNGFR/CD271) was one of the first markers identified for appropriate selection and enrichment of colony forming human BMSCs that demonstrated tripotent differentiation *in vitro* (Jones et al., 2002; Quirici et al., 2002). It has been consistently observed that CD271 may be a more appropriate *in vivo* marker as its expression is lost rapidly during *in vitro* culture, with one study demonstrating this loss by the second passage (Bakondi et al., 2009). The CFU-F fraction of bone marrow was later demonstrated to be present only in a $CD271^{bright}$ subpopulation of $CD271^{+}$ cells, and that the CFU-F capacity was also enriched in a $CD271^{+}CD56^{+}$ population versus the $CD271^{+}CD56^{-}$ population (Bühring et al., 2007; Venkata Lokesh et al., 2009). The localisation of $CD271^{+}$ BMSCs has also been of interest, with $CD271^{+}CD56^{+}$ cells found exclusively on trabecular bone surfaces, representative of an endosteal BMSC niche (Figure 1.2) (Ilas et al., 2020; Sivasubramaniyan et al., 2018). A study looking to enrich for $CD271^{+}$ BMSCs demonstrated a 65-fold increase in BMSCs isolated from trabeculae versus bone marrow aspirates, again highlighting a more endosteal niche for this population (Jones

et al., 2010). The same pattern of CFU-F capacity and *in situ* localisation is seen when combined with another prospective potency marker, melanoma cell adhesion molecule (MCAM/CD146), as $CD271^{+}CD146^{-/low}$ populations were found as bone lining cells, whereas $CD271^{+}CD146^{+}$ were located perivascularly (Figure 1.2) (Tormin et al., 2011). Single cell sorting and clonal expansion of $CD271^{+}$ BMSCs has also been shown to produce clones with varying potency, with one study demonstrating only 13.3% of clones were tripotent and 13% were nullipotent (Zyrafete et al., 2013). These studies collectively highlight $CD271^{+}$ as a candidate marker of human BMSCs, but also suggests that even within the $CD271^{+}$ population there is considerable heterogeneity, with subpopulations distinguishable by use of additional cell-surface markers or through clonal analyses.

A seminal study by Sacchetti et al. (2007) revealed CD146 to be a marker of a population of tri-potent human BMSCs. CD146 marked a population of perisinusoidal stromal cells in human bone marrow that encapsulated all of the CFU-F capacity of human bone marrow mononuclear cells (Figure 1.2). $CD146^{+}$ BMSCs were capable of establishing ectopic bone and haematopoietic microenvironments *in vivo* through serial transplantation, again highlighting the importance of skeletal progenitors in the haematopoietic niche. The study by Tormin et al. (2011) discussed previously found that $CD271^{+}CD146^{+}$ cells were exclusively located in the perivascular regions of bone marrow using immunofluorescence based approaches. CD146 was further corroborated as a marker of perivascular human stromal cells by Crisan et al. (2008), who demonstrated the $CD146^{+}$ population also expressed neuron-glial antigen 2/chondroitin-sulphate proteoglycan 4 (NG2/CSPG4) and platelet derived growth factor receptor beta (PDGFRβ), although this study did not focus specifically on BMSCs and bone marrow location and presented no evidence of attempts to look at endosteal regions, focusing more on vasculature in various tissues.

Early studies of the HSC niche indicated that HSCs were maintained in endosteal locations, with strong initial suggestions for the involvement of osteoblasts in the early 2000s (Calvi et al., 2003; Zhang et al., 2003). The later identification of HSCs by expression of signalling lymphocyte activation molecule (SLAM) markers revealed some endosteal associated HSCs, but noted a larger percentage of HSCs were found in contact with sinusoidal vasculature (Kiel et al., 2005). Further indication for the perivascular location of the niche was established in a publication demonstrating the importance of C-X-C motif chemokine 12 (CXCL12) by perivascular located BMSCs as a chemoattractive cytokine that maintained the HSC population in bone marrow (Sugiyama et al., 2006). The CXCL12-

abundant-reticular (CAR) cells were found in endosteal or perivascular regions and 94% of phenotypic HSCs identified were found in contact with these cells (Figure 1.2). It was later demonstrated that CAR cells were capable of osteo- and adipogenic differentiation, indicating they represent a multipotent stromal population (Omatsu et al., 2010). Ablation of CXCL12 from perisinusoidal cells by use of leptin receptor (LEPR) or osterix (OSX) or peroxiredoxin (PRX1) CRE mice was later shown to result in a depletion of the HSC pool, highlighting the importance of CXCL12 and the perivascular stromal cells in haematopoietic maintenance (Ding and Morrison, 2013; Greenbaum et al., 2013). It was also established that $CXCL12^+$ expressing populations of perivascular cells nearly completely overlapped with the $LEPR^+$ population (Figure 1.2) (Zhou et al., 2014). CXCL12 expression therefore represents an important feature of haematosupportive BMSCs and is conserved across both mice and humans.

Another combination of markers, platelet derived growth factor receptor alpha (PDGFRα) and stem cell antigen-1 (Sca1), encapsulated the majority of CFU-Fs from the bone marrow of mice after removing haematopoietic lineages (Morikawa et al., 2009). The double positive population was also enriched for cells that demonstrated classical tripotency *in vitro*, although other populations did contain differentiation capacity to varying degrees. Rare $PDGFR\alpha^+Sca1^+$ cells were observed around arterioles in the BM close to cortical bone (Figure 1.2). Use of collagenase resulted in isolation of a greater number of CFU-Fs from bones with an observed increase in $Sca1^+PDGFR\alpha^-$ and $Sca1^+PDGFR\alpha^+$ populations, highlighting a possible greater attachment to the bone surface via collagen adhesions (Houlihan et al., 2012). The PDGFRα single positive cells were shown to express the highest levels of CXCL12, indicating possible overlap with a subpopulation of CAR cells.

The intermediate filament protein nestin has also been identified as a possible marker of HSC supportive multipotent BMSCs, with nestin-green fluorescent $protein^+$ (GFP) BMSCs from transgenic mice shown to localise in close proximity to HSCs and be supportive of maintaining HSCs in the bone marrow niche, with high gene expression of HSC supporting cytokines CXCL12 and stem cell factor (SCF) (Méndez-Ferrer et al., 2010). The nestin-GFP^+ cells demonstrated robust tripotent differentiation *in vitro*. As an intracellular protein nestin-GFP reporters are used to indicate the presence of nestin transcribing cells, however, detection of translated nestin protein was subsequently shown to not correlate with nestin-GFP expression and furthermore the nestin-CreER transgene gave a different pattern of expression to nestin-GFP (Ding et al., 2012). Furthermore it was

argued by Zhou et al. (2014) that perisinusoidal nestin-GFP^{dim} cells were marked by LEPR and that this dim subset of nestin-GFP^{+} cells were the important subset for osteogenic differentiation and haematopoietic support. A rare population of bright nestin-GFP^{+} perivascular cells were later shown to be present in periarteriolar locations whereas dimmer subsets were found perisinusoidally (Figure 1.2) (Kunisaki et al., 2013). Given the role of nestin as an intracellular protein it is unlikely to be a suitable marker for the isolation of stromal subsets, and so further work from the same group highlighted that 60% of nestin-GFP^{+} cells were also double-positive for the cell-surface markers PDGFRα and integrin alpha V (ITGAV/CD51) and these markers were suggested as alternatives to the use of nestin due to significant overlap in cell properties (Pinho et al., 2013). The authors demonstrated that after excluding endothelial and blood lineages that 75% of the PDGFRα^{+}ITGAV^{+} population was nestin-GFP^{+} and that nestin mRNA was enriched in double-positive versus single-positive and double-negative cells. Furthermore, these double-positive cells were capable of the HSC-niche forming activity seen with nestin-GFP^{+} cells. The PDGFRα^{+}ITGAV^{+} population was also identified in human bone marrow, and mirrored the haematosupportive phenotype of the murine counterparts. The human population of double positive cells was notable enriched in foetal bone marrow and represented 16% of the CD146^{+} stromal cell population.

Another key marker of BMSCs that has been established in recent years is LEPR, which was originally shown to mark a collection of perisinusoidal bone marrow stromal cells that expressed high levels of important haematopoietic cytokines SCF and CXCL12 in murine bone marrow (Ding and Morrison, 2013; Ding et al., 2012). This population of perivascular cells was shown to closely overlap (~95%) with populations of perivascular CAR cells that were also a main source of and expressed the stromal marker PDGFRα (Figure 1.2). The LEPR^{+} stromal cells were later shown to differentiate towards bone, fat and cartilage in mouse bone marrow (Zhou et al., 2014). The LEPR^{+} cells were also almost uniformly positive for expression of the stromal markers ITGAV and PDGFRα, again demonstrating consistency in the use of these as confirmatory markers of stromal populations, of note is that ITGAV has also been positively identified in studies of immortalised human BMSCs, highlighting possible conservation across species and candidacy for this as a marker of stromal subsets (Al-Nbaheen et al., 2013; James et al., 2015). Importantly the LEPR^{+} population contained almost all of the CFU-F capacity in the bone marrow, however, LEPR^{+} isolated colonies had varying levels of differentiation capacity. This varied potency highlights that LEPR^{+} did not sufficiently discriminate for an

exclusively stem-cell subpopulation and the heterogeneity within the $LEPR^+$ population has been explored in more recent single cell RNA sequencing (scRNAseq) experiments that further divided the $LEPR^+$ cells into four separate subpopulations (Baryawno et al., 2019; Tikhonova et al., 2019). Despite the ability of LEPR to distinguish stromal cells in murine bone marrow, it has not been readily adopted as a marker of stromal cells in human tissue, although there is evidence to suggest conservation of it as a marker. The functionality of LEPR as a marker in multipotent stromal cells is also appropriate given that its ligand, leptin, has been shown to positively influence differentiation of human BMSCs towards osteoblasts (Thomas et al., 1999).

Within these various studies the evidence for overlap between populations is considerable and as such defining stem cells by their surface marker expression may reach a limit of power beyond which heterogeneous populations can no longer be subdivided by their surface marker expression. The development of scRNAseq approaches, and the more recent development of *in situ* RNAseq, is likely to further improve our understanding of heterogeneous stromal populations and their respective localisations, with the latest studies of stromal heterogeneity explored in section 1.5.3 (Lee et al., 2014a).

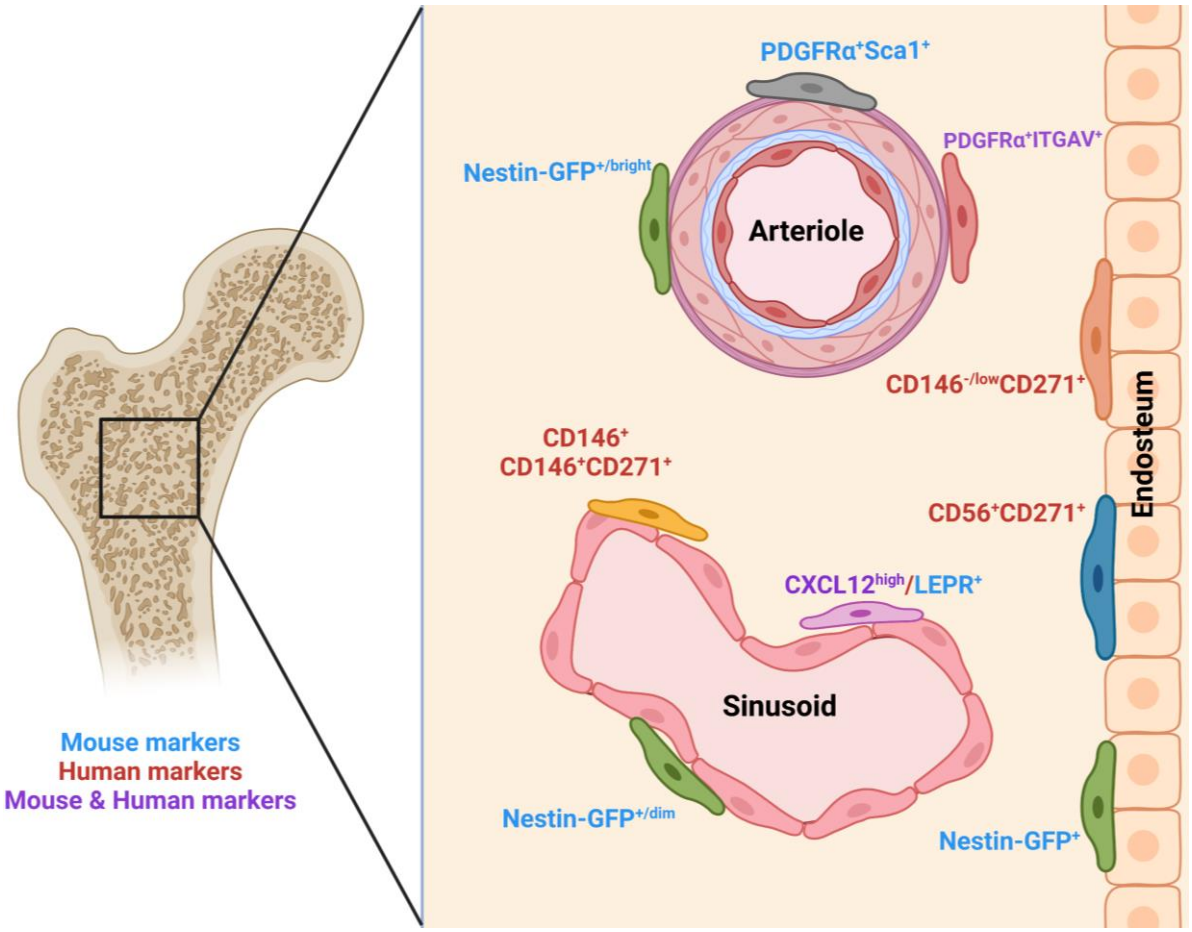

Figure 1.2 The location of various human and murine BMSC in the bone marrow niche
The reported distribution of various BMSC subpopulations in the bone marrow, shown with their identifying markers and their reported locations. Those markers which are associated with murine BMSCs are shown in blue, human markers in red and conserved human and mouse markers are shown in purple. Stromal cell populations are represented by the variously coloured cells. The cell populations are found around vasculature, either periarteriolar or perisinusoidal, and along the endosteum. Nestin-GFP^{+} cells can be subdivided and are found in all locales. The overlapping LEPR^{+} and CXCL12^{+} abundant reticular cells are found perisinusoidally. CD271^{+} cells both endosteal and perisinusoidal and these populations can be distinguished by expression of CD56 and CD146 respectively. PDGFRα is used as a marker of periarteriolar BMSC subpopulations in combination with either Sca1 or ITGAV.

Table 1.1 A table summarising prospective multipotent BMSC markers in mice and humans

Stromal marker(s)	Location	Differentiation capacity	Species	Notes	Refs.
CD146	Perisinusoidal	Bone, fat and cartilage	Human	CD146 expression increases during *in vitro* culture	(Sacchetti et al., 2007; Tormin et al., 2011)
CD271	Perivascular and endosteal	Bone, fat and cartilage	Human	$CD146^{+}CD271^{+}$ were perisinusoidal. $CD146^{low/-}$ $CD271^{+}$ are endosteal. CD271+/CD56+ cells trabecular surfaces.	(Jones et al., 2002; Quirici et al., 2002; Tormin et al., 2011)
CXCL12	Perisinusoidal and endosteal	Bone and fat	Mouse and Human	Rarer expression of cxcl12-gfp in endosteal cells, large overlap with $LEPR^{+}$ BMSCs	(Omatsu et al., 2010; Sugiyama et al., 2006
LEPR	Mostly perisinusoidal	Bone, fat and cartilage	Mouse	Overlaps almost completely with other marker populations including CXCL12 and PDGFRα	(Ding and Morrison, 2013; Ding et al., 2012; Zhou et al., 2014)
Nestin	Endosteal and perivascular	Bone, fat and cartilage *in vitro*, bone and cartilage *in vivo*	Mouse	Intracellular protein – not suitable for antibody sorting. Protein seems not expressed by nestin-GFP^{+} cells and different expression pattern with Nes-CreER. Heterogeneous Nes-GFP^{bright} and Nes-GFP^{dim} populations that are arteriolar and sinusoidal respectively	(Kunisaki et al., 2013; Méndez-Ferrer et al., 2010)
$PDGFR\alpha^{+}ITGAV^{+}$	Perivascular close to bone in human foetal bone	Bone, fat and cartilage	Mouse and human foetal bone	Large overlap with nestin-GFP cells, potential alternative cell-surface markers to identify this population	(Pinho et al., 2013)
$PDGFR\alpha^{+}Sca\text{-}1^{+}$	Periarteriolar near endosteum	Bone, fat and cartilage	Mouse	PDGFRα single positive high CXCL12 expression. From crushed bones rather than marrow	(Morikawa et al., 2009)

1.4 The BMSC secretome

1.4.1 BMSC secreted factors

BMSCs are known to co-ordinate the development of bone and bone marrow through differentiation towards skeletal lineages as well as participating in regulation and support of other cell-types such as HSCs. Collectively all secreted factors can be included within the umbrella term of the “secretome”. Understanding the secretome of cells is important for discerning possible autocrine and paracrine signalling functions, which in turn may aid identification of functionally distinct subtypes. Paracrine signalling has been shown in bone marrow dendritic cells to exert fine control over cellular heterogeneity at a single cell level, and in macrophages heterogenenous secretion profiles of individual cells influenced overall population secretion responses following stimulation with LPS (Shalek et al., 2014; Xue et al., 2015). The signalling of BMSC populations to each other may similarly regulate overall population function. A considerable amount of work on the secreted factors of BMSCs *in vitro* has been undertaken to understand the effects that these cells may have when applied in therapeutic settings. Native *in vivo* functionality is inherently more difficult to study, however, the use of stromal lineage restricted knockout mice has in recent years highlighted the importance for secreted CXCL12 and SCF from BMSCs for maintenance of HSCs in the bone marrow microenvironment (Ding and Morrison, 2013; Ding et al., 2012; Greenbaum et al., 2013).

The role of secreted factors from BMSCs is not limited to soluble cytokines, with ever increasing interest in other secreted molecules such as extracellular vesicles (EVs) and the role of the extracellular matrix (ECM) being studied as important functional compartments of the secretome.

1.4.2 Extracellular Vesicles

EVs are small, bi-lipid membrane vesicles that are secreted by cells and can be further categorised based upon their path of biogenesis (Raposo and Stoorvogel, 2013). Apoptotic bodies are released from apoptosing cells and tend to be the largest EVs, roughly ranging from 1000nm to 5000nm. Microvesicles range in size from 80-500nm and are released directly from the plasma membrane. Finally, exosomes are formed when a multivesicular body formed intracellularly fuses with the plasma membrane, releasing vesicles of roughly 40-200nm in size. There has been considerable interest in the signalling

potential of vesicles as they are known to carry various proteins and nucleic acids (mRNA, DNA, miRNA and lncRNA) which can drive signalling responses in the recipient.

EVs have become of increasing interest, particularly with regards to translation of these potent signalling molecules for therapeutic purposes, as well as their roles in homeostasis and disease. There are numerous ongoing efforts to translate these paracrine factors into effective therapies, although the understanding of their native functionality in the bone marrow is currently limited.There is evidence that EVs may be capable of recapitulating or signalling to drive known aspects of BMSC phenotype, including osteogenic differentiation (Qin et al., 2016).

1.4.3 Extracellular Matrix and BMSC functions

The ECM is the proteinaceous scaffolding which is secreted by cells in their local microenvironment and comprises a subcompartment of the secretome. The ECM is made up of a large number of proteins and proteoglycans and is important for providing structural support, sites for cellular adhesion and acting as a source of biochemical signalling (Frantz et al., 2010). The local microenvironment is important for facilitating the function of all cell types and its role in the regulation and support of stem cells is of particular interest for fundamental understanding of stem cell functionality and maintenance, as well as for the design of regenerative therapies (Donnelly et al., 2018; Gattazzo et al., 2014; Watt and Huck, 2013). There are a considerable number of proteins that play roles within or interact with the ECM and the interest in this field with regards to the ECM in health and disease has led to the development of a curated database of proteins known to contribute to the ECM, with this collection referred to as the matrisome (Hynes and Naba, 2012; Naba et al., 2012).

Cells secrete ECM comprised of proteins and proteoglycans into their environment, subsequently patterning their niche for specific functions, however, deposition of ECM into the local microenvironment also leaves these molecules accessible to other cell types for signalling and adherence (Frantz et al., 2010). During development there are various niches for the maintenance of the HSC pool and HSCs migrate from foetal liver to colonise bones and produce a bone marrow haematopoietic niche from which adult haematopoiesis is driven. It has been shown that physical cues, as well as the highly characterised cytokine signalling, are capable of mediating changes in HSC differentiation, adhesion and migration (Choi and Harley, 2017; Lee-Thedieck et al., 2012).

The structural role of ECM in bone and bone marrow is particularly well documented as during development a collagenous matrix is steadily mineralised through calcium phosphate deposition during the process of ossification (Mackie et al., 2008). This ossification provides the extreme stiffness necessary for the skeleton to support the body, with the stiffness of bone measured in gigapascals while other human tissues barely reach beyond the 100 kilopascal range (Buxboim et al., 2010; Zysset et al., 1999). It is noted that even within the bone marrow microenvironment there is an extreme contrast in mechanics, with stiffness measurements varying by orders of magnitude between cortical bone, trabecular bone, marrow regions and the growth plate with a recent study highlighting heterogeneity of elasticity even within these regions (Chen et al., 2020). The stiffness of ECM has been shown to be a key regulator of cell fate decisions. In a seminal study by Engler et al. (2006) BMSCs with adherence to soft matrices upregulated expression of neurogenic transcription factors while stiff matrices promoted osteoblast specific transcription factor production *in vitro*. This effect of matrix stiffness driving BMSC differentiation was inhibited through blocking the action of non-muscle myosins with blebbistatin, highlighting the important role of these proteins in co-ordination of cellular morphology and migration. The elasticity of a hydrogel matrix was also recently used to demonstrate a significant increase in clustering of tumour necrosis factor receptors (TNFRs) on MSCs cultured on soft ECMs that is more indicative of the environment at the endothelial niche (Wong et al., 2020). Interestingly, even softer gels than those used in the aforementioned inflammation study were shown to induce quiescence in BMSCs (Klein et al., 2009; Winer et al., 2008). These studies show the integral role of the mechanics of matrix in both regulating differentiation and inflammatory responses, key aspects of the BMSC phenotype. Scientific understanding of the role the ECM plays in multicellular organisms has developed beyond simply providing architectural support to tissues to a level where the role of ECM in cellular function and in driving cell-signalling is much more appreciated.

The ECM not only provides mechanical input but, by providing sites for adhesion, can exhibit control over cell morphology. The organisation of cellular geometry has been identified as a regulator of key processes such as apoptosis and differentiation. Studies on adherence of endothelial cells to ECM coated substrates patterned in different shapes and sizes demonstrated the requirement for sufficient adherence to allow growth and avoid apoptosis (Chen et al., 1997). Further work on cellular geometry using BMSCs revealed that artificial induction of square and circular cell shapes resulted in osteogenic and

adipogenic differentiation respectively (McBeath et al., 2004). The use of other shapes has further shown the influence of geometric co-ordination of cell shape through adherence to patterned ECMs on differentiation (Kilian et al., 2010; von Erlach et al., 2018). The effect of changes in mechanical environment can be studied through the use of cell-culture compatible materials and gels, however, these systems tend to isolate how the mechanical inputs of the matrix alter cell behaviour and do not consider the important function of the ECM in biochemical signalling. The ECM can also act as a repository for signalling molecules, with matrix glycoproteins known for facilitating the presentation of proteins to cells and also to act in protecting them from cleavage and degradation. Key examples of this powerful interaction of growth factors and ECM were demonstrated by the protective role of endothelial cell ECM, in particular the role of heparan sulphate, in binding fibroblast growth factor (bFGF) (Saksela et al., 1988; Vlodavsky et al., 1987). It has also been demonstrated that in knockouts of the ECM proteins biglycan and decorin that BMSC numbers are reduced and that the sequestration of Transforming growth factor beta 1 (TGFβ1) is impaired, with the study concluding that the increased availability of the TGFβ1 led to increased apoptosis of BMSCs (Bi et al., 2005). TGFβ1 is a cytokine with a highly studied association with ECM. TGFβ1 is sequestered in the ECM in an inactive form attached to one of four latent transforming growth factor β proteins (LTBP) which facilitate the binding and interaction of the cytokine with a variety of proteins (Hinz, 2015; Todorovic and Rifkin, 2012). TGFβ has further been implicated in control of various BMSC functions and in regulation of functions of the haematopoietic niche, including regulation of HSC proliferation and quiescence, therefore the ECM plays and important role in the bone marrow microenvironment (Zhao et al., 2014).

Hyaluronic acid (HA), a glycosaminoglycan (GAG), contributes to the molecular patterning of the ECM and in the cell microenvironment was demonstrated to facilitate BMSC migration through the HA-receptor CD44 (Zhu et al., 2006). HA has also been implicated with enhancement of CXCL12 mediated migration of HSCs by HA with decreased HSC numbers in bone marrow of mice with triple knockdown of the hyaluronic acid synthase enzymes (Goncharova et al., 2012). Additionally, HA can be bound by a variety of proteins, including the key anti-inflammatory TSG-6 and the proteoglycan aggrecan, perhaps suggesting a role for HA in co-ordination of BMSC signals and the niche. Other glycan molecules known to bind ECM, namely heparan sulphate, have also been implicated in the presentation and binding of cytokines, including CXCL12, which is important for retention of HSCs (Murphy et al., 2007).

BMSC derived ECM is likely integral for various stromal and stem cell functions. Fibronectin has previously been shown to be important for BMSC migration ECM derived from BMSCs was shown to enhance the colony-forming capacity and better preserved differentiation capacity of primary BMSCs during culture (Lai et al., 2010b; Rakian et al., 2015). This indicated the positive effect of culture conditions more representative of the *in vivo* niche provided by the presence of ECM. This ECM niche can also be disrupted during diseases such as primary myelofibrosis, where an accumulation of ECM components results in a fibrotic marrow environment and bone marrow failure, with BMSCs implicated as major sources of the fibrosis (Decker et al., 2017; Leimkühler et al., 2020).

Overall the involvement of the ECM in the bone marrow microenvironment is a key area of research with a need to better define the acellular components of specific niches and how they impact the maintenance of cell phenotypes *in vivo.*

1.5 BMSC heterogeneity

1.5.1 Evidence for functionally heterogeneous BMSCs

Since the early studies on BMSCs there have been observations of heterogeneity, with clear differences in CFU-F capacity seen even during Friedenstein's early clonogenic assays. Heterogeneity exists in many forms, and in referring to MSCs this can also include tissue sources (Wilson et al., 2019a). In this thesis I have focused on BMSCs and so in limiting the study to a single tissue source reducing the heterogeneity. Inter-donor heterogeneity has revealed variable potencies in osteogenic differentiation capacities and growth kinetics, originally demonstrated by Phinney et al. (1999). The study of 17 healthy donors revealed no significant correlation between BMSC osteogenic response or growth rate and donor age or sex. This corroborated previous assessments that single BMSC CFU-Fs transplanted *in vivo* resulted in variable osteogenic capacity (Kuznetsov et al., 1997). Intra-donor heterogeneity refers more to differences in specific subpopulations of BMSCs that occurs at a cellular level. A study of 185 individual clones of BMSCs, isolated from various donors between 5 months and 30 years of age, indicated a hierarchical level of differentiation capacity, with various tri-, bi- and uni-potent colonies (Muraglia et al., 2000). This study also highlighted the potential for paracrine signalling from FGF-2 to improve the maintenance of multipotent characteristics in isolation of BMSCs. Further studies have corroborated the heterogeneity seen between donors, with several indicating that the age of donors didn't reliably predict differentiation phenotype (Andrzejewska et al., 2019; Herrmann et al., 2019). Another large-scale study of *in vitro* heterogeneity within BMSCs

indicated that only half of all CFU-Fs from bone marrow preparations were capable of tri-potent differentiation across two donors, with varied numbers of bi-, uni- and nullipotent cells making up the rest (Russell et al., 2010). Collectively these studies highlight a high level of heterogeneity in BMSC functions and phenotypes of isolated cells both intra- and inter-donor.

Heterogeneity in morphology was noticed early in studies by Mets and Verdonk who categorise BMSC cultures with distinct large, flat cells and more spindle shaped cells (Mets and Verdonk, 1981a, b). Morphological heterogeneity was shown to increase during *in vitro* culture along with replication times and cell shape changes through repeated imaging in studies by Whitfield et al. (2013) and Rennerfeldt et al. (2019). These studies potentially associatie this heterogeneity with cell cycle stage and lineage commitment with some variation arising even in single cell derived colonies. Interestingly a clonal expansion experiment using umbilical cord derived stromal cells indicated a strong impact of clonal competition, highlighting that *in vitro* heterogeneity may be reduced over time (Selich et al., 2016).

Variation in other functionalities has also been seen, with a study of five murine BMSC clones indicating differential capacity to reduce T-cell proliferation, however, pre-treatment of clones with TNFα and IFNγ resulted in equal inhibition of T-cell proliferation (Szabó et al., 2015). This study highlighted inherent heterogeneity between BMSC subtypes, but also plasticity, with heterogeneous cell-types capable of responding collectively given an appropriately strong stimulus. Isolation of variably potent clones and subsequent determination of differences in their inflammatory signalling has also been shown in immortalised clones and is covered in section 1.5.2

1.5.2 hTERT immortalised BMSCs as a model of cellular heterogeneity

The need to distinguish between heterogeneous BMSCs is not only important for basic understanding of the role of these cells in normal biology, but also for their translation to cell and cell-based therapies. Our ability to study BMSCs *in vitro,* however*,* is limited due to cellular senescence induced by the shortening of telomeres over multiple rounds of replication (Baxter et al., 2004). In order to circumvent senescence, transduction with a lentivirus to induce expression of human telomerase reverse transcriptase (hTERT) has previously been shown to prevent cellular senescence and to maintain osteogenic potential in BMSCs (Shi et al., 2002; Simonsen et al., 2002). A study release the same year utilised

clonal isolation of hTERT immortalised stromal cells to demonstrate that hTERT immortalised MSCs resulted in isolation of subpopulations of varying differentiation capacity, with the majority of clones incapable of *in vitro* differentiation (Okamoto et al., 2002).

Our group has previously used viral transduction of cells from a single donor, and subsequent clonal isolation, to identify functionally distinct clones that presented with varying immunomodulatory phenotypes and differentiation characteristics (James et al., 2015). Of key interest in this work was the identification of the Y201 clone, which displayed "classical" multipotent BMSC characteristics. The Y201 had an elongated morphology and was highly migratory in culture. This line was equally capable of differentiation towards the osteo-, adipo- and chondrogenic lineages.

The study also identified a more committed BMSC progenitor cell, the Y101, that had a similar fibroblastic morphology and migratory phenotype to Y201, and was potently osteogenic. The Y101 was also capable of differentiation towards the chondrogenic lineage, however, its adipogenic differentiation was poor.

In contrast to the Y201 and Y101, the Y202 line had a significantly larger cell surface area and was flatter and less migratory, tending to form densely packed colonies. Through *in vitro* differentiation assays the Y202 line appeared nullipotent, unable to differentiate towards the three classical lineages. Gene expression profiling of the Y202 cells also revealed an expression signature that contrasted to the Y201 and Y101 lines, with upregulation of pathways related to immune and inflammatory pathways. The line was also distinguishable from Y101 and Y201 by surface expression of the marker CD317 (Bone marrow stromal antigen 2, BST2) which has a known role in tethering virions such as human immunodeficiency virus-1 (HIV-1) to the plasma membrane (Neil et al., 2008). There has not yet been marker identified that was capable of distinguishing between Y201 and Y101 subtypes, demonstrating a limit of power for cell-surface markers in discerning between variably potent subpopulations.

These clonal lines all met the criteria established by the ISCT for cell-surface marker expression and plastic adherence, indicating that they were all mesenchymal stromal cells, but with some lacking the relevant potency requirement. Gene expression data generated through a microarray from these cell lines has subsequently assessed using a classification model generated from datasets of known mesenchymal stromal cell cultures (Rohart et al.,

2016). Despite the clear behavioural differences between these cells this model independently classified all three stromal lines as mesenchymal stromal cells (unpublished data). A summary of their characteristics is available in Table 1.2.

These clonal lines provide a snapshot of distinct BMSC subtypes, removing the issues commonly associated with mixed populations and inter- and intra-donor heterogeneity, providing a highly reproducible model through which to study essential BMSC biology *in vitro*.

Table 1.2 Summary of characteristics associated with three hTERT Immortalised BMSC clones produced by the Genever lab

	Y201	Y101	Y202
Osteogenic	+	++	-
Chondrogenic	+	+	-
Adipogenic	+	-	-
Migratory	+	+	-
Morphology	Fibroblastic	Fibroblastic	Flat
ISCT Cell Surface Markers	Yes	Yes	Yes
Basal inflammatory gene expression	Low	Low	High

1.5.3 The future of studies into BMSC heterogeneity

Investigations into heterogeneity have increased in power and depth following the development of scRNAseq methods in 2009 (Tang et al., 2009a). This technique has resulted in a number of publications revealing considerable heterogeneity in stromal populations in mice and humans at a single-cell level, revealing heterogeneity in populations previously treated as more homogeneous. A comprehensive single-cell study by Baryawno et al. (2019) proposed the identification of 17 different stromal subpopulations in mice and suggested different differentiation competencies and hierarchies for these subtypes. They subdivided the LEPR positive population of stromal cells into four populations, a finding that was also corroborated by Tikhonova et al. (2019) in a separate scRNAseq study of non-haematopoietic cells in bone marrow. This second study used cell-surface markers to

identify and separate osteoblasts, endothelial cells and stromal cells, using LEPR as the marker of stroma. Another scRNAseq study focusing on BMSCs identified 7 subsets, with categorisation of one multipotent BMSC at the top of a hierarchy and 6 subpopulations of more committed progenitors (Wolock et al., 2019). Interestingly this study indicated a diverse expression of LEPR across 4 of the subsets, again corroborating a potential identification of distinct subsets in the heterogeneous $LEPR^{+}$ population of murine BMSCs. The ability to study single cells allows a more powerful dissection of cellular heterogeneity and could lead to the identification of more surface-markers or alternative methods of determining sufficiently potent BMSCs.

1.6 The use of BMSCs in therapies

The study of BMSCs and their potential in therapy can roughly be divided into two groups based upon the therapeutic end goal. The development of research into stem cells and their ability to differentiate and produce functional tissue resulted in the birth of the field of regenerative medicine. During the study of BMSCs it has also been noted that they are capable of imparting immunomodulatory and immunosuppressive effects, which are also of high interest in the treatment of various diseases. Overall this lead to the development of therapeutic potential for MSCs in both regenerative and immunomodulatory therapies.

1.6.1 Regenerative BMSC therapies

The replicative power of stem cells and their capacity to differentiate to produce functional tissues has been an attractive prospect for the field of medicine for decades. HSCs in bone marrow transplants were first performed in the 1950s and have been used to treat a plethora of haematological disorders (Hatzimichael and Tuthill, 2010). In the 14 years since the first reports of identification of induced pluripotent stem cells (iPSCs) in human cells the field of regenerative medicine has continued to look forward to the development of effective therapies to treat diseases through appropriate regeneration of damaged or diseased tissue by stem cells (Takahashi et al., 2007).

BMSCs, and more specifically their multipotent subsets, have long been heralded for their potential in regenerative therapies, with particular attention to their role in alleviating musculoskeletal disorders such as osteoarthritis (OA) due to their osteogenic and chondrogenic differentiation capacity. OA is categorised as a degeneration of the cartilage in the joint space resulting in loss of mobility, pain and swelling. The current gold standards for the treatment of hip and knee OA is surgical intervention by whole hip and knee

replacement, which are highly involved, especially considering the age-associated prevalence of OA. A recent study in the UK indicated that over a third of men and nearly half of all women over the age of 75 in the UK have diagnosed OA (Swain et al., 2020). While hip and knee replacements are effective, there is a clear need for alternatives given theaging populationis likely leading to increased prevalence of OA and prolonged life with OA. The requirement for highly invasive surgery leads to the potential of infection and presents a greater risk in the elderly and as such preventative or curative treatments using cell therapies could present a significant improvement. Autologous transplantation of chondrocytes was the first use of cells shown to successfully repair damaged cartilage, providing a promising insight into cellular therapy for OA (Brittberg et al., 1994). MSCs were assumed to present a possible source of regenerative chondrogenic cells capable of repairing the joint through differentiation after application, although this proved to produce tissues inconsistent with functional meniscus in a rabbit model of OA using BMSCs transplanted into the damaged tissue in a collagen scaffold (Walsh et al., 1999). The potential for BMSCs to prevent damage to cartilage was demonstrated in a goat model of OA which saw promising improvement of damaged meniscus using GFP transduced BMSCs versus vehicle treated controls, although relative engraftment of the cells was low (Murphy et al., 2003). Potential for cell therapies in humans have resulted in a number of clinical trials taking place for the application of BMSCs to treat OA in humans. Another trial comparing autologous BMSC with autologous chondrocyte transplantation in the knee indicated the potential benefit of this as an effective alternative to chondrocytes (Nejadnik et al., 2010). Equally, in a clinical trial looking at cartilage defects in patients that utilised intra-articular injection there was a significant improvement in knee quality scoring at two years post injection (Wong et al., 2013).

Evidence for further regenerative medicine applications of multipotent bone marrow progenitors can be found in their osteogenic potential. A 1998 study using a canine BMSCs loaded into an implant drastically improved healing of a non-union fracture (Bruder et al., 1998). In a small cohort of human patients, concentrated autologous bone marrow aspirates were used to heal non-union fractures with a correlation between fracture healing and the number of CFU-Fs derived from the same donor aspirate (Hernigou et al., 2005). This presents a non-selective but effective approach to cell therapy utilising an inherently recognised osteogenic potency within the BMSC population.

1.6.2 Immunomodulatory BMSC therapies

The capacity for BMSCs to modulate immune responses has resulted in strong interest in the use of these cells for the treatment of inflammatory disorders. One disease with proven efficacy of BMSC therapy is graft versus host disease (GvHD), which can prove highly destructive to organs following allogeneic HSC transplants. An initial case study in one patient was highly successful in the treatment of GvHD, which was expanded into phase I & II clinical trials showing positive responses to BMSC treatment and increased survival at one and two year follow-up (Le Blanc et al., 2008; Le Blanc et al., 2004; Ringdén et al., 2006). Interestingly, in the phase II trial, the detail of criteria used to select MSCs was that of a spindle shaped morphology, adherence to ISCT cell-surface marker criteria and high (>95%) cell viability but there was no mention of proof of tripotent differentiation capacity. A BMSC therapy (Prochymal) was approved for use in acute GvHD in 2012 in Canada after proving suitable efficacy and safety (Kurtzberg et al., 2014; Prasad et al., 2011). In another use of BMSCs for the treatment of inflammation there have been positive outcomes in clinical trials for safety and efficacy in assessing the capacity for BMSCs to be used in the treatment of acute respiratory distress syndrome, systemic lupus erythematosus (Wilson et al., 2015a; Zheng et al., 2014; Zhou et al., 2020).

1.6.3 BMSC secreted factors could be used for cellular therapies

The potential for BMSCs in cellular therapies is enticing, however, issues associated with the use of cells in therapy persist and provide significant roadblocks to their development. These include potential for rejection of a cell therapy. The function and therapeutic potential of MSCs has often been ascribed as a result of paracrine signalling and so interest is developing into the use of secreted factors from BMSCs as alternatives to cell-therapies. It was shown by Kinnaird et al. (2004) that murine BMSCs were capable of improving recovery from hind-limb ischaemia after application from a proximal site in the muscle through paracrine action as suggested by increased pro-angiogenic cytokines such as vascular endothelial growth factor (VEGF). These cell-free indications provide significant advantages due to lack of cellular material capable of inducing immune response and the potential to produce a more assayable, standardised and reproducible therapeutic product.

BMSC secrete various factors, and uses for these factors are being identified, including with a view to therapeutic development. BMSCs had previously shown promise in the treatment of myocardial infarction, and BMSC conditioned medium (BMSC-CM) was assayed for its potential to replicate this benefit in a cell-free manner in pigs (Strauer et al., 2002; Timmers et al., 2008). In a comparison between adipose tissue derived stromal cells

and BMSC, conditioned media from the latter demonstrated greater efficacy in reducing damage by LPS induced inflammation to various organs, particularly in the lungs (Elman et al., 2014). In an antigen-induced-arthritis model in mouse the use of BMSC-CM was capable of reducing joint swelling and cartilage degradation (Kay et al., 2017). Although the specific factor that ameliorated damage was not identified, it suggests potential in the development of BMSC secreted factors in developing therapies.

There is promising indication for the potential of BMSC EVs in the treatment of bone disorders and fractures upregulated osteogenic differentiation of BMSCs *in vitro* and promoted regeneration of calcified bone in a calvarial defect model (Qin et al., 2016). BMSC EVs have also shown further showed promise in the treatment of myocardial diseases, in this case injury caused by ischemia, with the application of BMSC EVs (Arslan et al., 2013). This study utilised EVs isolated from a human embryonic stem cell derived MSC line to significantly improve myocardial infarct size and reduce neutrophil influx. Of importance for the development of EV therapies will be the improved understanding of heterogeneity of the EV source to inform and produce consistent product

1.6.4 The problem of MSC heterogeneity in cellular therapies and the need for better definitions

Multipotent MSCs are strong candidates for use in regenerative therapies. In order to use cells as a therapeutic agent there needs to be consistency in output and this has resulted in most cell therapy populations being defined by a strategy of selecting the therapeutic population by cell-surface markers (Figure 1.3). The importance of high levels of characterisation and reproducibility of small molecular therapeutics and biologics is imperative during standard drug development pipelines and It is to be expected that the use of cells in therapy are subject to similar scrutiny (Wilson et al., 2019b). With regard to the direction of therapies for highly intricate processes such as tissue regeneration, as has long been the case with BMSCs, the importance of appropriately applying sufficiently potent subsets is clear. The therapeutic application of a population that lacks differentiation capacity, or worse, one that may exacerbate a condition, presents a key problem for the development of cell therapies.

While there are a number of cell-surface markers currently used to define the multipotent populations of BMSCs these are still insufficiently selective and other methods for the defining of appropriate populations may be required should surface markers become limited in power. The use of TSG-6 mRNA expression (detailed in section 1.2 paragraph 2)

by Lee et al. (2014b) highlights a mechanism by which cellular heterogeneity may be appropriately navigated for the identification and isolation of cell populations that offer appropriate efficacy for applications whereby the anti-inflammatory properties of BMSCs are desired for therapeutic effect.

There is already evidence that single-cell derived colonies perform better in regenerative therapies of myocardial infarction when meeting previously determined selection criteria (Zhang et al., 2006). This adds emphasis to the idea of potential hazards and risks of a lack of therapeutic response when using insufficiently defined or non-clonal population of BMSCs in therapy. The prevalence of heterogeneous differentiation and the potential differences in immune responses make clear the necessity to better define stromal cell subpopulations. Current definitions for the isolation of multipotent BMSC populations still result in isolation of heterogeneous populations which may negatively affect development of cell-based therapies if they are insufficiently reproducible, effective and potent.

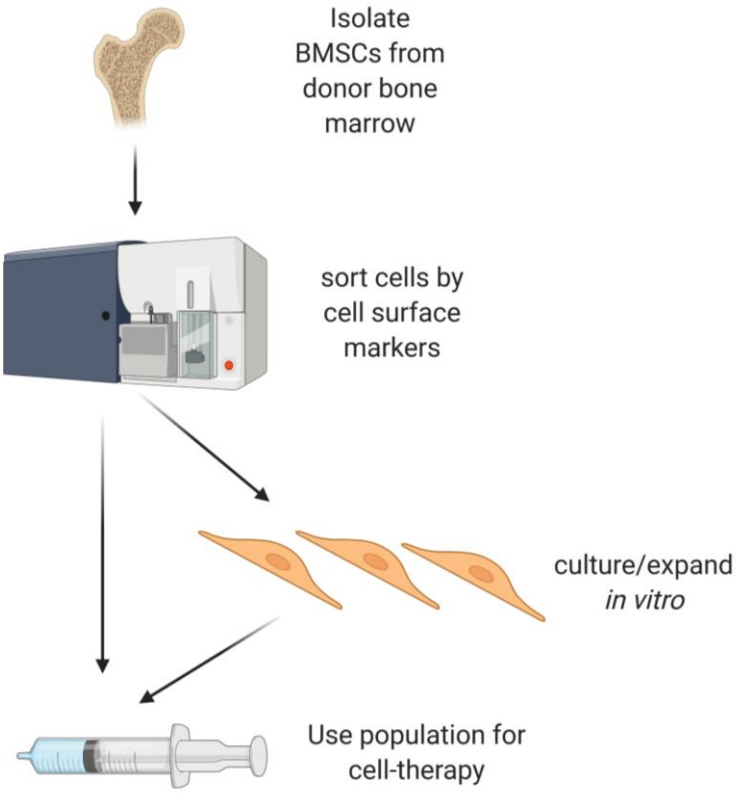

Figure 1.3 Isolation of cells for use in therapy

A simplified interpretation of the commonly accepted pipeline for isolation of refined populations of BMSCs for cellular therapy by use of antibodies and sorting based upon expression of cell-surface markers followed by direct application of cells or subsequent *in vitro* expansion.

1.7 Aims of this thesis

Investigations into the functions of BMSCs have often been established with heterogeneous populations of isolated stromal cells, with conclusions drawn as if they were homogeneous, however, there is clear evidence for heterogeneity with the isolation of functionally distinct subtypes. There have been considerable efforts in recent years to better identify BMSC populations using cell-surface markers, however there is still evidence for overlap in these populations. The function of MSCs has often been ascribed as a result of paracrine signalling, and so in this thesis I aim to investigate the secreted factors produced by BMSC subtypes in order to identify possible differences in the secretomes of functionally diverse subpopulations and whether this may correlate with differences in subpopulation functions. The heterogeneity of BMSCs has also been considered with regards to their effects on other cell-types, however, the effects they have on each other in culture has been explored far less. I therefore also aim to determine if there is potential for signalling from some BMSC subsets to co-ordinate the functions of heterogeneous populations.

1.7.1 Summary of aims

- Use different immortalised BMSC clones to identify differences in cellular secretomes from stromal subsets
- Determine the effect of stromal secretomes on subtype-specific functions and identify if there is plasticity in phenotype controlled by secreted factors
- Identify possible niche locations for subpopulations of BMSCs that correspond with secreted factors
- Use understanding of the differences in BMSC secretomes between subsets to inform potential choices of BMSC subsets for cellular therapies

2 **Methods**

2.1.1 Standard *in vitro* culture of hTERT BMSCs

The hTERT immortalised BMSC clonal lines were cultured in Dulbecco's Modified Eagle Medium (DMEM) containing 10% foetal bovine serum (FBS), 100units/mL penicillin and 100µg/mL streptomycin and incubated at 37ºC in a 95% air/5% CO_2 humidified atmosphere. Cells were passaged using trypsin-EDTA upon reaching 70-80% confluency.

2.1.2 Isolation and concentration of conditioned medium

For functional assays cells were grown to ~80% confluency in T175 flasks before washing 2x with PBS and adding 17ml of serum-free DMEM + 100units/mL penicillin and 100µg/mL streptomycin to each flask and incubated as normal for 24h. Media was collected and then centrifuged at 300g to remove any large cell debris. Cells from the flasks used to generate the conditioned media (CM) were trypsinised and counted using a countess haemocytometer (Thermofisher). The collected medium was diluted with serum-free DMEM + 100units/mL penicillin and 100µg/mL streptomycin to achieve a concentration of 80,000 cells/mL of media. Diluted media was then stored at -70ºC until required. Where indicated, heat inactivation of CM was performed by incubating CM in a water bath to 80ºC for 15 minutes before cooling to 37ºC prior to application to cells.

For proteomic analyses CM was collected from 2x T175 flasks of each hTERT immortalised line (Y101, Y201 and Y202). Cells were grown to ~80% confluency under their standard conditions before washing 2x with PBS. Cells were then incubated as normal for 24 hours in 17mL of serum-free DMEM without phenol-red (Thermofisher) supplemented with 4mM L-glutamine (Thermofisher) and 1mM sodium pyruvate so as to match the standard cell culture formulation. Medium was collected and centrifuged at 300xg to remove any large cell debris. Medium was stored at -80ºC until required. For proteomic analyses, the medium was concentrated in Vivaspin 3kD molecular weight cut-off tubes (GE Healthcare) at 4500xg until concentrated to ~1mL in volume. The protein concentration of conditioned media was calculated using a Quick-start Bradford protein assay (Bio-Rad) and compared against a bovine serum albumin (BSA) protein standard curve made by diluting the 2mg/mL BSA standard (Thermofisher) in the phenol-red free DMEM formulation used above according to manufacturer recommended dilutions.

2.1.3 Colony forming unit fibroblast assays

For CFU-F assays, cells were seeded at 10 cells/cm^2 in 6-well plates using DMEM supplemented with 20% Hyclone FBS, 100units/mL penicillin and 100µg/mL streptomycin. CM (from section 2.1.2) was defrosted overnight at 4^{o}C then collected and centrifuged at 300g to remove cell debris, and the number of cells was counted. The CM was then diluted with additional serum-free DMEM to give 12ml CM/million cells. This medium was then supplemented with a final concentration of 20% Hyclone FBS for use in CFU-F assays. For CFU-F assays, primary cells and cell lines were seeded in unconditioned Hyclone medium and media changes were performed every 4 days post-seeding. Cells were fixed and stained at day 10 for cell lines and day 14 for primary cells due to quicker growth of cell lines. At assay endpoint, plates were stained by aspirating media and covering the well surface with 0.05% crystal violet + 1% formaldehyde + 1% methanol in PBS at room temperature for 20 minutes. Crystal violet was aspirated before, plates washed with tap water and left to air dry before imaging (See section 2.1.4) Alternatively for gene expression analyses lysates were collected (see section 2.1.9).

In experiments using the focal adhesion kinase inhibitor (FAKi) PF-573,228 (Generon) medium was aspirated from wells 2 hours after seeding and replaced with either fresh medium containing FAKi or dimethyl sulfoxide (DMSO) vehicle control. PF-572,228 was made at a stock concentration of 10mM using DMSO.

2.1.4 CFU-F image analysis pipeline for crystal violet stained colonies

Crystal violet stained plates scanned on an Epson Perfection 4990 photo scanner at 1200dpi. The image analysis programme CellProfiler was used to produce a custom analysis pipeline to accurately detect and measure colonies in a more automated fashion (Lamprecht et al., 2007). The scanned image was loaded into CellProfiler and converted to a greyscale image using the ColorToGrey module, splitting the image into red, green and blue channels. The blue channel was then thresholded to 0.99 to include all features identified as completely black. Well edges were then identified as primary objects of size 1000-2000 pixel units in diameter and with a manual threshold of 0.99 to include all features, this reproducibly identified the well edges as primary objects. In order to fit this as a complete circle a grid was defined using DefineGrid and then true circles were placed using the IdentifyObjectsinGrid module. The circle was shrunk by 10 pixels in diameter to prevent running over the edge of the well. The UnmixColors module was used to create an image without any blue absorbance (red and green absorbance of 1, blue absorbance of 0) which

was effective in detecting objects stained with crystal violet. The area of this image outside of the wells was cropped using the 10 pixel shrunken circles. Illumination correction was then calculated (block size 20, median filter and object size filter with median object size of 80 pixels), and applied by subtraction method to remove lighting inconsistencies. The edges of features were enhanced using the Sobel method in the EnhanceEdges module which identified cells that had dispersed away from a tight colony. Cells were then included into nearby colonies through a Closing module using a diamond shape with a reach of 10 pixels. Colonies were subsequently detected by an IdentifyPrimaryObjects module with typical diameter between 60-800 pixels and using the RobustBackground with a Mode averaging method. Manual correction of colony detection could then be applied in CellProfiler. The colonies were measured for size and shape characteristics and used as a mask to analyse other features of the colonies such as intensity. Other available colony analysis tools were unsuitable for this due to the dispersion of many BMSC colonies. A visual summary of this pipeline can be seen in Figure 2.1.

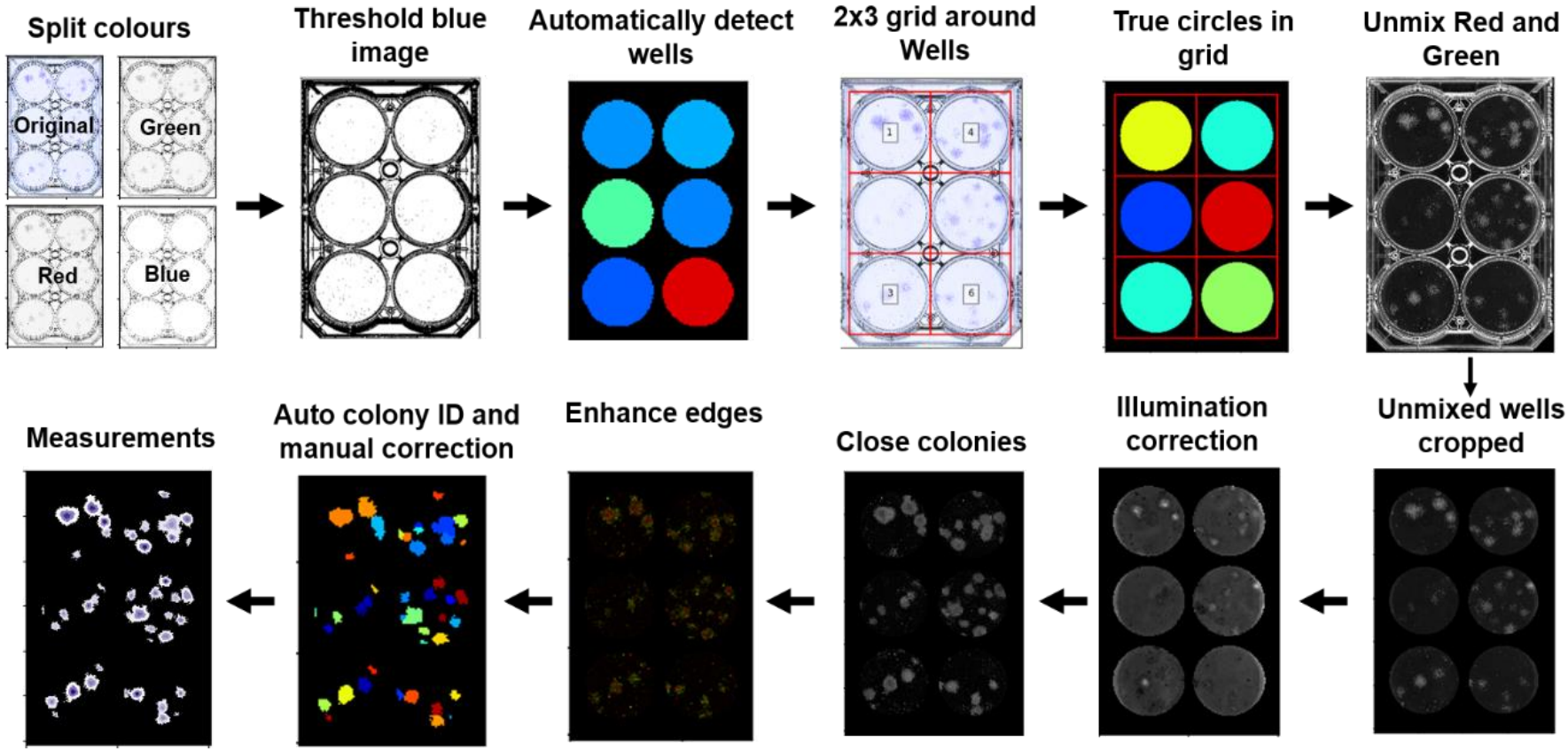

Figure 2.1 CellProfiler CFU-F image analysis pipeline summary

Outline of the processing steps used in the CellProfiler colony analysis pipeline after input of a 1200dpi scanned TIF of a CFU-F assay in a 6 well plate. The images shown represent the outputs of the image processing modules and their titles.

2.1.5 Isolation and *in vitro* aging of primary BMSCs from femoral heads and tibial plateaus

Primary BMSCs were isolated from tibial plateaus received from Clifton Park Hospital, York, under informed consent following routine knee replacements. Cells were isolated by explant culture onto plastic petri dishes and plastic adherence of stromal cells. Donor HS739 was purchased from Lonza. All work involving human samples was approved by the University of York Department of Biology Ethics committee. Primary cells were cultured in DMEM containing 15% batch-tested FBS, 100units/mL penicillin and 100µg/mL streptomycin in a 95%air/5% CO_2 humidified atmosphere. Cells were routinely passaged with a one-in-five split upon reaching approximately 80% confluency in T75 flasks. Primary cells were cultured to beyond passage 10 for use in *in vitro* aging experiments, with a noted increase in time between passages.

2.1.6 Ptychography, cell tracking and image analysis

For cell migration and morphology analysis cells were seeded as 6-well CFU-F assays (as in section 2.1.3) and imaging performed using a VL21 Livecyte (PhaseFocus) imaging platform for live cell tracking. The LiveCyte allowed imaging in a 37^{o}C humidified chamber with 5% CO_2. This system has advantages in allowing high-contrast imaging of cells in culture over time without the need for perturbation of the cells with chemical labelling (Marrison et al., 2013). For CM experiments the media was changed immediately prior to imaging and images were taken continuously at 20-26-minute intervals (dependent on fields of view and distances between colonies being imaged) for 96 hours at 4 days post-seeding. For experiments using ECM, colonies were tracked at 3-hours post-seeding. Images were processed and analysed using the PhaseFocus Analyse software using a custom analysis pipeline which is summarised with example images in Figure 2.2. Images were first processed with a rolling ball algorithm to remove background features before smoothing was applied to remove low frequency noise. Points of maximal brightness, indicating areas of high phase-contrast corresponding to cell nuclei, were identified in the smoothed image and were used as seeding points for the identification of individual cells. Seed points were consolidated where points that did not change in pixel intensity within a threshold were removed, this enabled removal of multiple seed points in a single cell. Thresholding and segmentation levels were then set to define the area which was part of a cell against the background. This processing pipeline was applied to all images in an experiment. The output images then allowed tracking of cells and using a spatial and temporal dot plot, along

with quantification of various morphological metrics such as dry-mass, area, width and length. Small debris was removed by an exclusion gate removing objects that were less than 250pg in dry mass and less than 1000µm^2. Large doublets and debris were excluded if having an area over 25,000µm^2. Manual removal of debris was also performed by visual assessment. To be included in analyses, cells had to be tracked for a minimum of 20-frames. For cell tracking, n=3-6 colonies were imaged as technical replicates per condition at each time point and the data from these colonies were then averaged to represent one biological replicate. Metrics from individually tracked cells were exported and statistical tests comparing mean results performed in GraphPad Prism.

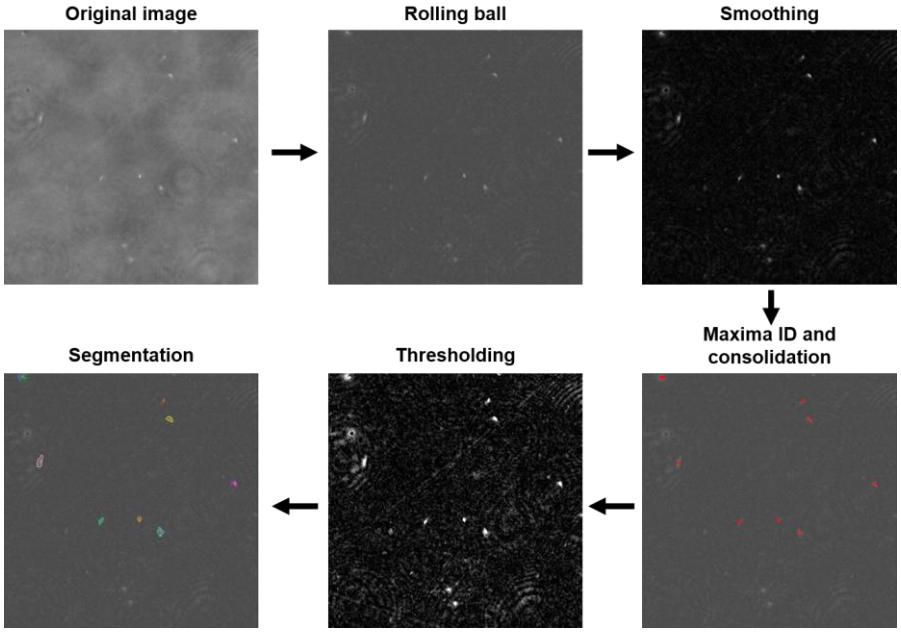

Figure 2.2 PhaseFocus image processing pipeline overview
Outline of the output of respective image processing steps using prior to the tracking of cells in the PhaseFocus Analyse software package. Images shown are representative of outputs of a single frame.

2.1.7 Preparation of MSC-derived Extracellular Matrix

ECM was prepared from *in vitro* cell cultures using a protocol adapted from Ng et al. (2014). Y201 and Y202 cells were seeded at 1000 cells/cm^2 for 6 well plates or 13mm coverslips in 24 well plates and allowed to grow for 14 days. For 96 well plates this was adapted to 500 cells/well (equivalent to 1562cells/cm^2) due to the tendency of cells to settle in the centre of the wells and not fully expand towards the edges. Between days 1-7 of culture, cells were grown in standard culture medium before supplementing this medium at days 8-14 with 50µM L-Ascorbic acid to enhance matrix deposition. Medium changes were performed every 3 days. At day 14, medium was aspirated and cells were washed 1x with

phosphate buffered saline (PBS). A cell clearing solution of 20mM Ammonium Hydroxide (Sigma) with 0.5% Triton X-100 (Sigma) in PBS was used to remove cells and retain deposited ECM. Cells were incubated in the clearing solution for 5 minutes at room temperature with occasional shaking to ensure full coverage of the growth surface. After clearing, plates were washed once with PBS before three washes with sterile distilled water (dH_2O). Plates were left to dry in a sterile laminar flow cabinet before covering and wrapping in parafilm. Plates were wrapped in parafilm and stored at 4^{o}C and were used within 1-month of cell-clearing.

2.1.8 Focal adhesion imaging and assessments

Y201 and Y202 cells were seeded onto sterile 13mm glass coverslips in 24-well plates in standard culture medium at low density and left to adhere. At 24 hours after seeding, medium was isolated and cells were fixed by a 5 minute incubation in 4% (w/v) methanol-free paraformaldehyde (PFA) in PBS (Thermofisher) before washing 3x with PBS. Cells were permeabilised in 0.1% Triton X-100 (Sigma) in PBS for 30 minutes and washed 3x with PBS. Samples were blocked for 30 minutes with 10% goat serum in PBS at room temperature. Samples were incubated with mouse-anti-vinculin antibody (Sigma, V9131) in 1% BSA at 1 in 400 dilution overnight at 4^{o}C. After primary antibody staining, cells were washed gently 3x with PBS before incubation of secondary antibodies and phalloidin for 1 hour at room temperature in the dark. Cruzfluor594 (CF594) conjugated phalloidin (Santa Cruz, sc-363795) was reconstituted by addition of 30µl of DMSO and aliquoted before storing at -20^{o}C. Alexafluor488 conjugated goat-anti-mouse secondary antibody (Thermofisher, A11001) was diluted 1 in 300 while phalloidin was diluted 1 in 1000. Coverslips were washed 3x with PBS and nuclei counterstained with 0.2µg/mL 4′,6-diamidino-2-phenylindole (DAPI) in PBS for 10 minutes before rinsing in dH_2O and gently dabbing off excess moisture onto clean tissue. Coverslips were mounted onto a microscope slide with 10µl of Prolong gold antifade hard setting mounting medium (ThermoFisher) and left to cure overnight. Images were captured using a Zeiss LSM880 or LSM710 confocal microscope. Focal adhesion sizes were subsequently determined using the ImageJ software package for individual cells by a thresholding setting followed by the analyse particles module. Data was exported as a CSV before statistical tests performed in GraphPad Prism.

2.1.9 qRT-PCR for inflammatory gene expression

Y201 cells and Y202 cells were cultured as CFU-F assays with either Y201 conditioned media (Y201CM), Y202 conditioned media (Y202CM) or UCM. At assay endpoint cells were lysed with 350µL RA1 lysis buffer (Machery Nagel) + 3.5µL β-mercaptoethanol per condition before purification of RNA with the NucleoSpin RNA kit (Machery-Nagel). The manufacturer's protocol was followed except for a modification to the final elution, whereby samples were eluted twice using the same 40µL of RNAse-free water to improve yield and concentration. RNA concentration was estimated using a Nanodrop2000 (Thermofisher). Resultant RNA was reverse transcribed to cDNA using Superscript IV (SSIV) reverse transcriptase (Thermofisher) with volumes used to match the lowest concentration sample collected. All reactions were performed in a DNA Engine thermocycler (MJ research). Primer annealing was performed using 1µL of 10mM dNTP mix + 1µL of 50uM Oligo $d(T)_{20}$ primer + template RNA up to 11µL and made up to 13µL with nuclease-free water. The solutions were mixed in an RNAse-free tube and flicked to mix before centrifuging briefly. The mix was heated to 65^{o}C for 5 minutes then incubated on ice. A reverse transcriptase master-mix was made using 4µL SSIV reaction buffer + 1µL 100mM DTT + 1µL RNAseOUT + 1µL SSIV per reaction. 7µL of mastermix was added to each reaction, mixed and centrifuged. The reactions were incubated at 55^{o}C for 10 minutes before inactivating at 80^{o}C for 10 minutes. cDNA was diluted with 80µL of RNAse-free water before storing at -20^{o}C. Changes in gene expression of 8 interferon upregulated genes (LY6E, HERC5, IFI44L, ISG15, MX1, MX2, EPSTI1 and RSAD2) were assessed by quantitative real time PCR, performed using a 2x SyGreen Blue mastermix (PCRBiosystems) on a QuantStudio3 system (Thermofisher) with a 20µL final reaction volume. These genes were previously used to produce an interferon signature (Raterman et al., 2012). Fold changes were calculated using ΔΔCT relative to the expression of the house-keeping gene RPS27a. Data were normalised against expression of these genes in Y201 cells grown in unconditioned medium (UCM). Primer sequences used in qPCR are found in Table 2.1.

Table 2.1 Primer sequences for genes used in qPCR assessment of inflammatory gene expression in Y201 versus Y202 BMSCs

Target	Forward primer sequence	Reverse primer sequence
EPSTI1	TGC ATA CAC CTT GAT AGC ACC AA	TCC TGC TCC GCA ATT CTT TG
HERC5	GAG CTA AGA CCC TGT TTG G	CCA CCT TCC ACA TGC TAT C
IFI44L	TGC TCC TTC TGC CCC ATC TA	TGC TCC TTC TGC CCC ATC TA
ISG15	ATG TCG GTG TCA GAG CTG AAG	GTT ATT CCT CAC CAG GAT GCT C
LY6E	CCT GGA GTC TTA CGG TCC AA	GTA CAC AGC CAG GCA CAC AT
MX1	TTC AGC ACC TGA TGG CCT ATC	GTA CGT CTG GAG CAT GAA GAA CTG
MX2	CAG AGG CAG CGG AAT CGT AA	TGA AGC TCT AGC TCG GTG TTC
RSAD2	GTG GTT CCA GAA TTA TGG TGA GTA TTT	CCA CGG CCA ATA AGG ACA TT
RPS27a	TGG ATG AGA ATG GCA AAA TTA GTC	CAC CCC AGC ACC ACA TTC A

2.1.10 Scanning Electron Microscopy (SEM)

Imaging of the topographical surface of ECM samples was performed by SEM. ECMs cultured onto glass coverslips were fixed after removal of cells for 30 minutes in a mix of 4% PFA + 2.5% glutaraldehyde in 100mM phosphate buffer (pH 7.0) at room temperature. Samples were washed twice for 10 minutes each with phosphate buffer before secondary fixation with 1% Osmium tetroxide for 30 minutes at room temperature. Samples were washed 2 more times with phosphate buffer for 10 minutes, then dehydrated in an ethanol series of 25%, 50%, 70%, 90% and 3 X 100% at 15min each stage. Samples were covered with hexamethyldisilazane for 15 minutes before aspirating and allowing to air dry. Samples were imaged with a JEOL 7800F Prime.

2.1.11 Focused Ion Beam Scanning Electron Microscopy (FIBSEM)

FIBSEM was performed to examine the organisation of ECM in a cross-sectional manner and to expand upon topographical information derived from SEM and observe interaction between cells and ECM. Samples were prepared by fixing in 2.5% glutaraldehyde in 100mM phosphate buffer for 1h before 3x 15 minute washes with phosphate buffer. A secondary fixation with 1% OsO_4 in 100mM phosphate buffer was performed for 1h before 3x 5min washes with ddH_2O. Samples were then blocked in 1% Uranyl Acetate in ddH_2O for 1h. Samples underwent dehydration in an ethanol series with 15 minutes in 30%, 50%, 70%, 90% and 2x15 minutes in absolute ethanol. The samples were then washed 2x 5minutes in epoxy propane before infiltrating with Epon-araldite resin (Epon 812, Araldite CY212) overnight. Excess resin was removed by centrifugation of coverslips held upright in a 15ml falcon tube at 1000g for 1 minute before the resin was

polymerised at 60°C for 48h. Prior to FIBSEM, a carbon coating was sprayed onto the matrix surface to provide a conductive sheath. The sample was protected from the ion beam by deposition of a 2 to 3 µm layer of nanocrystalline platinum (Pt) and amorphous carbon.

An FEI NOVA 200 FIBSEM was used for ion beam milling and imaging. A triangular trench was initially milled into the sample using a 7nA ion probe. Cleaning scans were then performed with smaller ion probe currents of 1 nA, 300 pA, 50 pA, all at 30 keV. Finally the sample could be tilted to ensure that optics were as close to the milled surface as possible for imaging. Tiled scans of the sample surface were stitched together by hand or using a plugin in ImageJ (Preibisch et al., 2009).

2.1.12 Osteogenic Differentiation *in vitro* and Alizarin Red staining for calcium deposition

For osteogenic differentiation, cells were seeded at 1000 cells/cm^2 in 24-well plates using DMEM + 10% FBS + 100units/mL penicillin, 100µg/mL streptomycin to allow expansion of cells and spreading over the ECM layer. Cells were left to grow until reaching confluency before supplementing medium with 50µg/mL L-ascorbic acid-2-phosphate, 5mM β-glycerophosphate and 10nM Dexamethasone to produce osteogenic media. Fresh osteogenic media changes were performed every 3 to 4 days. Time-points were collected at days 0, 7, 14, and 21. At each timepoint, medium was aspirated and the cells washed once with PBS. Cells were subsequently fixed with 4% PFA in PBS for 5 minutes at room temperature. Cells were then washed 3x with PBS before covering in PBS and storing at 4°C until staining. At assay endpoint all fixed plates were washed once with PBS before addition of 40mM Alizarin Red S in distilled water adjusted to pH4.2 with hydrochloric acid for 20 minutes at room temperature. After staining, cells were washed 3x with PBS and subsequently with gently running tap water to remove non-specific staining. Plates were left to air-dry before scanning on an Epson Perfection 4990 Photo scanner at 1200dpi.

2.1.13 EV Isolation

Y201 and Y202 MSC lines were cultured as described above, but using FBS that had been depleted of EVs by an 18-hour centrifugation at 100,000g to pellet and discard serum-derived EVs; the supernatant was retained and filtered through a 0.2µm filter before adding to media. Cells were grown to ~80% confluency in T175 flasks before washing with PBS and adding 17ml of EV-depleted medium. Cells were incubated as described above for 48h before conditioned medium was collected and stored at -70°C. Media was thawed overnight at 4°C before isolating EVs using a differential ultracentrifugation protocol adapted

from Théry et al. (2006). All centrifugation steps were carried out at 4°C and samples were kept on ice. Media was centrifuged at 300g for 5 minutes before transferring media to new tubes and spinning again at 2000g. Supernatants were carefully decanted into 70ml Polycarbonate tubes (Beckman Coulter) for centrifugation at 10,000g for 45 minutes using a Type 45 Ti rotor (Beckman Coulter). Supernatants were transferred to fresh Polycarbonate tubes and centrifuged for 90 minutes at 100,000g. Supernatants were then discarded and pellets resuspended in a total of 1ml Dulbecco's PBS (Gibco). Resuspended pellets were transferred to 1.5ml polypropylene tubes (Beckman Coulter) and centrifuged at 100,000g in a TLA100.3 rotor fitted with delrin adapters (Beckman Coulter) for 90 minutes. Supernatants were carefully discarded before resuspending the EV pellet in 100µL of DPBS. EV's were then stored at -70°C until required.

2.1.14 Transmission electron microscopy

BMSC-derived EVs were imaged by transmission electron microscopy (TEM). For this, 6µL of resuspended EVs (from 2.1.13) was pipetted onto a formvar/carbon support filmed copper grid and left for 5 minutes at room temperature. The grid was washed briefly with distilled water and negatively stained with 1% uranyl acetate. Samples were imaged using a Tecnai 12 BioTWIN working at 120kV.

2.1.15 Proteomic analysis of MSC secretomes

For proteomic analysis, 50µg of concentrated conditioned-media samples (from section 2.1.2) or EVs isolated from 8xT175 of cells (as described in 2.1.13) were added to 8M urea with 20mM HEPES and a phosphatase inhibitor cocktail comprising 1mM sodium orthovanadate, 1mM β-glycerophosphate and 2.5mM sodium pyrophosphate. Protein was in-solution reduced and alkylated before digestion with a combination of Lys-C and trypsin proteases. Resulting peptides were analysed over 1-hour LC-MS acquisitions using an Orbitrap Fusion (Thermofisher). Peptides were eluted into the mass spectrometer from a 50cm C18 EN PepMap column. Three biological replicates for each cell line were run. Tandem mass spectra were searched against the human subset of the UniProt database using Mascot and peptide identifications were filtered through the Percolator algorithm to achieve a global 1% false discovery rate (FDR). Identifications were imported back into Progenesis QI and mapped onto MS1 peak areas. Peak areas were normalized to total ion intensity for all identified peptides. Relative protein quantification was performed using relative peak areas of non-conflicting peptides. Proteins were accepted for analysis provided they were detected with ≥2 peptides and ≥1 unique-peptide in at least one sample. Relative fold differences and associated p-values for differential abundance between

pairwise comparisons of cell lines was calculated in Progenesis QI by ANOVA. A heatmap of protein expression for the 201 proteins identified with significant differences in expression was produced using the http://www.heatmapper.ca./ online tool, with clustering performed by a complete-cluster algorithm (Babicki et al., 2016).

2.1.16 Nanoparticle tracking analysis

Nanoparticle tracking analysis (NTA) was used to quantify and determine size distribution of EVs isolated from BMSC clones. EV samples were diluted in PBS before running under flow conditions on an NS300 with a 405nm laser (Malvern-Panalytical). Scattered light from particles was tracked and the Brownian motion of particles used to calculate their hydrodynamic radius. EV sizes are binned by one nanometre increments beginning at 0.5nm, and so size distributions are represented by percentage contribution of each bin to the overall population.

2.1.17 Analysis of EV microRNAs

EVs from BMSC clones were thawed and allowed to reach room temperature. RNA was extracted using the Total Exosome RNA and Protein Isolation kit (Invitrogen). Samples were thawed and diluted with 1x PBS to 200µL total volume in an RNAse-free tube. 200µL of pre-warmed denaturing solution was then added and mixed before incubating samples on ice for 5 minutes. 400µL of Acid-Phenol:Chloroform was then added to each sample and they were vortexed for 60 seconds before centrifuging at 13,000g for 5 minutes at room temperature. The aqueous (upper) phase was then transferred to a fresh RNAse-free tube and the volume recovered was recorded and then used in purification. The elution solution was pre-heated to 95^{o}C and 100% ethanol left at room temperature. The aqueous phase was diluted with 1.25x volumes of 100% ethanol and mixed. The aqueous-phase/ethanol mix was loaded onto a filter cartridge in a fresh tube and centrifuged at 10,000g for 15 seconds. The flow through was discarded and the cartridge was then washed by centrifuging with 700µL of miRNA wash solution 1 at 10,000g for 15 seconds. Flow through was discarded and then 2x washes with 500µL of miRNA wash solution 2/3 were performed at the same settings. The cartridge dried with a spin of 10,000g for 1 minute. The cartridge was then removed and placed into a fresh collection tube and the RNA was eluted using 50µL of pre-heated elution solution and centrifuging at 10,000g for 30 seconds. The eluate was then passed through the cartridge a second time to improve yield. After RNA purification the sample were concentrated using Amicon Ultra 0.5ml centrifugal filters (Sigma-Aldrich) by first topping up to 400uL with RNAse-free water. Samples were

centrifuged at 14,000g for 88 minutes before inverting and collecting RNA in a fresh tube at 8000g for 2 minutes. Total RNA was then quantified on a Bioanalyzer 2100 (Applied biosystems) using a Pico chip.

Between 3 and 5µL of RNA was used in the NanoString miRNA ligation reaction, dependent on concentration. NanoString was performed following manufacturer's miRNA sample preparation protocol using the nCounter Human v3 miRNA expression assay codeset (NanoString). MiRNA counts were normalized using spike-ins from the NanoString procedure before miRNAs with >20 counts in ≥1 sample were filtered for analysis. Comparisons of EV miRNAs was performed in the R programming language. All relevant code used to produce figures can be found in Appendix 7.1.

The TargetScan database was used to identify predicted targets of miRNAs. Targets were included in analyses if satisfying a threshold cut-off of a context score <-0.6 (the more negative a score the more evidence that the gene is a true target of the miRNA).

2.1.18 Gene Ontology term enrichment and clustering

Gene Ontology (GO) enrichment was performed using the ClueGO plugin for the Cytoscape software package (Bindea et al., 2009; Shannon et al., 2003). Gene lists were assessed for enrichment against the Biological Process and Molecular function GO-genesets with Benjamini-Hochberg False Discovery Rate (FDR) corrected p-values. Redundancy of GO terms was reduced by using the GO-fusion setting in ClueGO before automated clustering of significant GO terms (FDR-corrected $p<0.05$). Cluster diagrams were generated from ClueGO results using the AutoAnnotate plugin to facilitate organisation and labelling of like-terms and to generate titles for clusters based upon common words (Kucera et al., 2016). Clusters were moved to aid visualisation.

2.1.19 KEGG Pathway enrichment

Lists of significantly more abundant genes and proteins were analysed for pathway enrichment against the curated Kyoto Encyclopedia of Genes and Genomes (KEGG) database using the Molecular Signatures Database website on version 7.2 (Kanehisa and Goto, 2000; Liberzon et al., 2011; Subramanian et al., 2005). Enrichment was performed for significantly different protein lists and results filtered to exclude terms with FDR corrected p-values (q) of >0.05. To minimise the effect of confounding and relatively uninformative terms, a filter excluded gene-sets containing more than 500 genes. Where p-values for

enriched pathways were the same, samples were ordered by the MSigDB k/K ratio where k = the number of proteins identified in the geneset and K = the total number of proteins in that set. Enrichments were presented in bar-charts generated in Graphpad Prism.

2.1.20 FunRich Venn diagrams

Lists of proteins were imported into the FunRich (version 3.1.3) programme and were used to generate Venn diagrams (Pathan et al., 2015). Lists of proteins identified in other experiments were downloaded from the Vesiclepedia database through FunRich for comparisons with my datasets (Pathan et al., 2018).

2.1.21 Matrisome annotations

Proteins were annotated for involvement in the Matrisome using the MatrisomeDB database at www.http://matrisomeproject.mit.edu/ (Shao et al., 2019). Chi-squared tests were performed in Graphpad Prism.

2.1.22 Statistical analyses

Unless otherwise stated, statistical comparisons were performed in GraphPad prism version 8. Data were assessed for normal distributions by Shapiro-Wilk normality tests. Normally distributed data were analysed using appropriate parametric tests while data that was not normally distributed was analysed with an equivalent non-parametric test.

2.1.23 Processing and embedding of mouse femurs

Femurs were dissected from C57Bl/6 mice at ages 8-12 weeks immediately after sacrificing. Collagen type VI knockout femurs were kindly supplied by Paolo Bonaldo and Francesco da Ros (University of Padua, Italy). These femurs were taken from 6-month-old mice and fixed and processed using the same steps, as described below. All work was carried out under ethical approval from the University of York Department of Biology Ethics Committee.

Muscle tissue was removed and femurs were fixed in 3mL of 4% PFA in a 12-well plate, one femur per well, for 24hours at 4^{o}C. After fixing, the PFA was aspirated and femurs washed once with PBS. Bones were then decalcified using 10% ethylenediaminetetraacetic acid (EDTA) in PBS weight to volume (w/v) at pH 7.5 for 24 hours at 4^{o}C. After decalcification, femurs were cryoprotected by submerging in 30% sucrose in PBS (w/v) for 24 hours at 4^{o}C. Before embedding, femurs were dabbed dry on paper towels and aligned

in vinyl cryomolds. Bones were then covered with Optimal Cutting Temperature (OCT) compound and left for 5 minutes. A slurry comprising dry-ice pellets and 100% ethanol was made to supercool the ethanol for rapid cooling of the OCT. Cryomolds were floated at the surface of the slurry. After OCT became opaque and solidified, samples were transferred onto dry-ice and excess ethanol removed with a tissue. Samples were stored long-term at -70^{o}C.

2.1.24 Processing and embedding of human bone pieces

Human femoral heads from routine hip and knee replacements were donated following informed consent from Clifton Park hospital under ethical approval from the local NHS Research Ethics committee and the Department of Biology Ethics Committee. A CleanCut bone saw (deSoutter medical) was used to cut chunks from femoral heads which were then dissected into roughly 1cm^3 pieces using a fresh scalpel. Processing steps were carried out at 4^{o}C. Bone pieces were fixed in 4% PFA for 24 hours. After fixation, bone pieces were washed once with PBS before decalcifying for 48hours in 10% EDTA in PBS at pH 7.5. Bone pieces were then cryoprotected by submerging in 30% sucrose in PBS for 24 hours. Bone pieces were cut again using a scalpel into smaller pieces before embedding in OCT on a dry ice ethanol slurry as in section 2.1.24.

2.1.25 Cryosectioning

Prior to sectioning, embedded samples were placed in an OTF5000 cryostat (Bright) for one hour to equilibrate to the temperature of the chamber. Samples were attached to brass chucks with OCT and mounted into the microtome. The OCT block-face was trimmed until bone and marrow appeared. Sections were cut at 8-10µm using a tungsten-carbide tipped blade, with a sample temperature of -19^{o}C and a chamber temperature of -21^{o}C. Sections were collected onto SuperFrost plus microscope slides (Thermofisher) and left to adhere at room temperature for several hours before subsequently storing upright at -70^{o}C in slide boxes.

2.1.26 Immunofluorescent staining of bone tissues

Slides were removed from -70^{o}C storage and allowed to reach room temperature for at least 1 hour. Sections were blocked for 45 minutes in 10% goat serum (Sigma) + 0.1% Tween-20 in PBS or 10% donkey serum (Sigma) + 0.1% Tween-20 in PBS if a goat primary antibody was used. Blocking solution was removed by tilting and leftover moisture was gently dabbed dry with a tissue, avoiding contact with the section. A hydrophobic pen was

used to separate sections on the same slide. Primary antibodies were diluted in 1% IgG free Bovine Serum Albumin (Sigma) + 0.05% Tween-20 (Sigma) at the concentrations shown in Table 2.2. Primary antibodies were incubated in the dark at 4°C overnight in a humidified chamber. After primary antibody staining the sections were washed 3 times for five minutes with PBS. All secondary antibodies were then added at 1:300 dilution in PBS for 1 hour at room temperature in the dark. Details of antibodies used are provided in Table 2.2. Three five-minute washes were performed before staining for 10 minutes with 0.2µg/mL 4′,6-diamidino-2-phenylindole (DAPI) in PBS. Slides were left in the dark to dry slightly before mounting a #1.5 thickness glass coverslip (Scientific Laboratory Supplies) using hard setting Prolong Gold antifade mounting medium (Invitrogen). Slides were left to cure at room temperature in the dark for 24 hours before imaging.

2.1.27 Confocal Imaging and slidescanner

High power images of bone tissues were captured on LSM880 or LSM780 (Zeiss) confocal microscopes. The same laser wavelengths were used for excitation of fluorophores on both LSM780 and LSM880 microscopes, these were 405nm, 488nm, 561nm and 633nm. Whole bone images of collagen VI stained femurs were captured using a Zeiss AxioScan slidescanner. Slides were stored at 4°C in the dark.

For optimal viewing of all immunofluorescent images it is recommended to use a digital copy of this thesis rather than printed reproductions.

2.1.28 Haematopoietic stem cell survival and proliferation assay

HSCs from C57Bl/6 mice were isolated collectively from femurs, tibias, pelvic bones and spines of mice. Bone marrow was flushed and bones crushed in 10ml of PBS + 2% FBS + EDTA (PBSFE). Cells were collected into 50ml tubes through a cell strainer and pelleted for 7 minutes @ 300g before red cell lysis by adding 3mL PBSFE and 5mL NH_4Cl and incubating on ice for 10 minutes with a vortex at 5 minutes. Tubes were topped up to 20ml with PBSFE before cells pelleted at 300g. Supernatant was discarded and cells resuspended with 500µL/mouse of PBSFE, taking into account the volume of the pellet. The cells were depleted of lineage marked populations by use of an EasySep™ mouse hematopoietic progenitor cell isolation kit (Stemcell Technologies) sorted as single cells using a MoFlo (Beckman coulter) using an ESLAM Sca-1^{high} strategy as performed by Wilson et al. (2015b) into individual wells of a 96 well plate coated with the ECM derived from Y201 cells, Y202 cells or plastic. Sorted HSCs were cultured for 10 days in serum-free

StemSpan media (Stemcell Technologies) supplemented with 20ng/mL Interleukin-11 (R&D), 300ng/mL stem Cell Factor (R&D), L-glutamine, 100units/mL penicillin and 100µg/mL (Sigma), 2mM L-glut (Sigma) and 0.2% β-mercaptoethanol. At day 10 the number of wells that had formed colonies was manually counted.

Table 2.2 Table of all immunolabelling reagents used

Immunolabelling reagents used for immunofluorescence imaging and flow cytometry. Shown are targets, catalogue or antibody specific clone numbers and the dilution at which the antibody was used in experiments. All experiments where targets were identified in both mouse and human tissue were performed using the same antibody due to reported cross-reactivity by the manufacturer.

Primary/Secondary/Isotype	Target	Clone/Cat. No	Manufacturer	Species and isc	Conjugate	Dilution
Primary	Aggrecan	13880-1-AP	Proteintech	Rabbit	-	1 in 50
Primary	Biglycan	16409-1-AP	Proteintech	Rabbit	-	1 in 200
Primary	CEMIP/KIIAA1199	21129-1-AP	Proteintech	Rabbit	-	1 in 100
Primary	Leptin receptor	BAF497	R&D biosystems	Goat	Biotin	1 in 100
Primary	Type VI collagen	AB6588	Abcam	Rabbit	-	1 in 200
Primary	Periostin	AB14041	Abcam	Rabbit	-	1 in 100
Primary	ITGAV	SC-9969	Santa Cruz	Mouse IgG1, κ	-	1 in 100
Primary	Lumican	EPR8898(2)	Abcam	Rabbit	-	1 in 400
Primary	CD31 (PECAM)	MEC13.3	BD Biosciences	Rat IgG_{2a}, κ	-	1 in 200
Primary	CD317/BST-2	NBP2-27154	Novus Biologicals	Rabbit	-	1 in 50
Primary	CD271	ME20.4	BioLegend	Mouse IgG_1, κ	-	1 in 100
Primary	mouse CD45	30-F11	BioLegend	Rat IgG_{2b}, κ	BV421	1.5µL in 100µL staining buffer per whole mouse bone marrow
Primary	mouse CD117	2B8	BioLegend	Rat IgG_{2b}, κ	APC/Cy7	1µL in 100µL staining buffer per whole mouse bone marrow
Primary	mouse/human CD11b	M1/70	BioLegend	Rat IgG_{2b}, κ	APC	1µL in 100µL staining buffer per whole mouse bone marrow
Primary	mouse Ly-6G/Ly-6C	RB6-8C5	BioLegend	Rat IgG_{2b}, κ	PE/Cy7	1µ in 100µL staining bufferl per whole mouse bone marrow
Primary	mouse CD3	17A2	BioLegend	Rat IgG_{2b}, κ	PE	1µl in 100µL staining buffer per whole mouse bone marrow
Primary	Sca-1	D7	BioLegend	Rat IgG_{2a}, κ	BV605	0.5µl in 100µL staining buffer per whole mouse bone marrow
Primary	mouse EPCR	RMEPCR1560	Stem Cell Technologies	Rat IgG_{2b}, κ	PE	
Secondary	Rat IgG	A11077	ThermoFisher	Goat	AlexaFluor 568	1 in 300
Secondary	Rabbit IgG	A21244	ThermoFisher	Goat	AlexaFluor 647	1 in 300
Secondary	Goat IgG	A21447	ThermoFisher	Donkey	AlexaFluor 647	1 in 300
Secondary	Rabbit IgG	A11011	ThermoFisher	Goat	AlexaFluor 568	1 in 300
Secondary	Mouse IgG	A11001	ThermoFisher	Goat	AlexaFluor 488	1 in 300
Streptavidin Secondary	Biotin	S32354	ThermoFisher	-	AlexaFluor 488	1 in 300
Isotype control	-	Poly29108	BioLegend	Rabbit	-	Matched to 1°
Isotype control	-	BAF108	Novus Biologicals	Goat	Biotin	Matched to 1°
Isotype control	-	eBR2a	eBioscience	Rat IgG_{2a}, κ		Matched to 1°
Isotype control	-	MPC-11	Biolegend	Mouse IgG1, κ		Matched to 1°

3 Functional effects of BMSC secretomes

3.1 Introduction

3.1.1 BMSC heterogeneity and control of population phenotype

BMSCs can regulate the function of other cell types through paracrine signalling. Given that heterogeneous BMSC subtypes can be isolated by clonal expansion of single cells from a population (as evidenced through our immortalised stromal lines) I investigated how secreted factors from different subsets of BMSCs influence the behaviour of other subsets. I previously highlighted the problem of heterogeneity within BMSC isolations due to the use of unsuitably discriminatory cell-surface markers in chapters 1.1 and 1.5. Understanding how BMSC subpopulations may influence each other's behaviour is an important but often underappreciated area of investigation. The majority of studies focus on the role BMSCs play in driving phenotypic changes in other cell types, with little regard for the way heterogeneous subpopulations may influence each other. The interactions between cells in a mixed population could give us a better understanding of how BMSC subtypes may be specialised for specific functions and may play different roles in health and disease. For the purposes of this work I used two of our highly characterised, hTERT immortalised BMSC subtypes with contrasting phenotypes introduced in section 1.5.2, Y201 and Y202 (James et al., 2015). We aimed to demonstrate subtype specific functions using these cell lines.

3.1.2 Functionality of BMSC subtype secretomes

The role of BMSCs both *in vivo* and in therapeutic settings has often been attributed to paracrine signalling, such as BMSC secreted chemokine CXCL12 permitting HSC maintenance, or the paracrine effect of TSG-6 in regulating inflammatory signalling during peritonitis (Choi et al., 2011; Greenbaum et al., 2013; Sugiyama et al., 2006). The ability of BMSCs to alter inflammatory responses has led to investigations into the use of BMSCs to treat diseases such as rheumatoid arthritis and graft versus host disease (Augello et al., 2007; Le Blanc et al., 2004). The application of cells to treat such diseases poses problems commonly associated with the translation of cellular therapies, notably, the risk of cellular rejection and providing appropriate quantities of cells with sufficient therapeutic potency. The use of cells in a therapy adds a level of complexity that can potentially be avoided by the use of cell-free products. The functional effects of BMSCs in treating various diseases has often been attributed to a paracrine action imparted by a secreted factor(s) from an BMSC. Recent interest has ventured towards using the secretome of BMSCs for cell-free

therapies (Vizoso et al., 2017). However, the variability in secretome between heterogeneous BMSCs is understudied and may still prevent a roadblock to clinical development. More research is needed to identify cell populations which produce consistent secreted factors with therapeutic benefit. Our human telomerase reverse transcriptase (hTERT) immortalised cell lines provide an excellent resource for the study of BMSC secreted factors from specific subtypes through expansion of clones to develop mono-cultures. The cell lines also provide a model to better inform BMSC selection criteria from primary donors for cellular therapies. I therefore aimed to understand the potential functionality of secreted factors produced by our BMSCs.

3.1.3 Extracellular matrix as a driver of cellular phenotype

The production of ECM by cells has clear function in maintenance of niche architecture and chemical signalling but can also have profound effects on cellular phenotype, including alteration of stem cell fate (Guilak et al., 2009). BMSCs *in vivo* are likely to produce matrix that may act as a substrate for the adherence and growth of other cells, as well as a mechanical and/or biochemical signalling to alter cell behaviour. Heterogeneous BMSCs may reside in distinct niches *in vivo,* although current understanding of heterogeneity makes identifying these populations difficult. The current practices of culturing heterogeneous populations of cells *in vitro* may lead to a homogenisation of cell phenotype over time, as cells adapt to the collective microenvironment that they produce in 2D culture and/or cellular competition dictates that some less resilient BMSC subsets are lost. Studies of BMSC matrices *in vitro* may reveal important information about their function and identifying enriched or unique secreted extracellular matrix proteins by distinct stromal subpopulations these proteins could also be used for potential niche localisation *in vivo*.

3.1.4 Aims

In this chapter I aimed to expand upon previous work investigating BMSCs to determine if secreted factors from clonally derived heterogeneous BMSC subsets were capable of altering various aspects of BMSC phenotype. Understanding heterogeneity of BMSCs and developing understanding of how subpopulations are capable of influencing behaviour of the overall population may prove useful for future investigations to identify heterogeneity. Key aims of this work were to:

- Develop an understanding of how secreted factors from heterogeneous BMSC subtypes are capable of driving aspects of the cellular phenotype, including migration, morphology, inflammatory gene expression and differentiation

- Identify signalling pathways through which secreted factors influence changes in cellular phenotype

- Identify if Y201 and Y202 produce structurally distinct ECMs

3.2 Results

3.2.1 Effects of BMSC subtype conditioned media on colony size and morphology

To determine if secreted factors produced by heterogeneous BMSC subtypes were capable of inducing changes in colony formation, Y201 and Y202 BMSCs were cultured in Y201CM, Y202CM or UCM in a CFU-F assay alongside respective heat-inactivated CM controls. Colonies were fixed and stained with crystal violet at day 10 and assessed for changes in colony size and morphology. I noted an increase in colony size in both Y201 and Y202 cells treated with Y201CM, with this effect nullified by heat inactivation of the CM (Figure 3.1). Subsequent quantification of colony size revealed that Y202 cells cultured in Y201CM presented significantly increased mean colony size versus Y202CM ($p=0.0157$) or UCM ($p=0.0018$) (Figure 3.2).

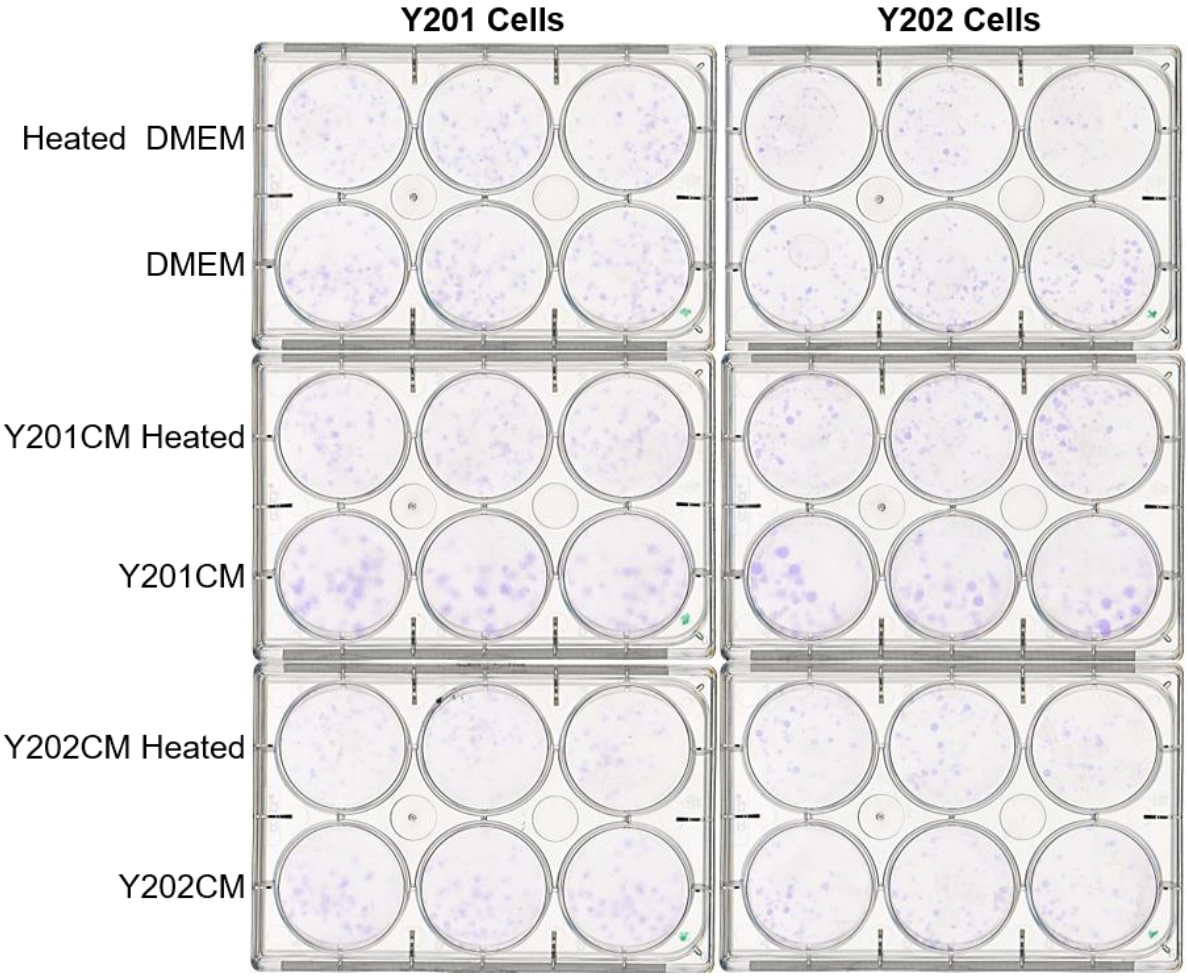

Figure 3.1 CFU-F assays of Y201 and Y202 with Y201CM or Y202CM and heat inactivated controls

Representative crystal violet stained colonies of Y201 and Y202 cells from CFU-F assays after 10 days of culture in either UCM, Y201CM, Y202CM or respective heat inactivated controls of each treatment.

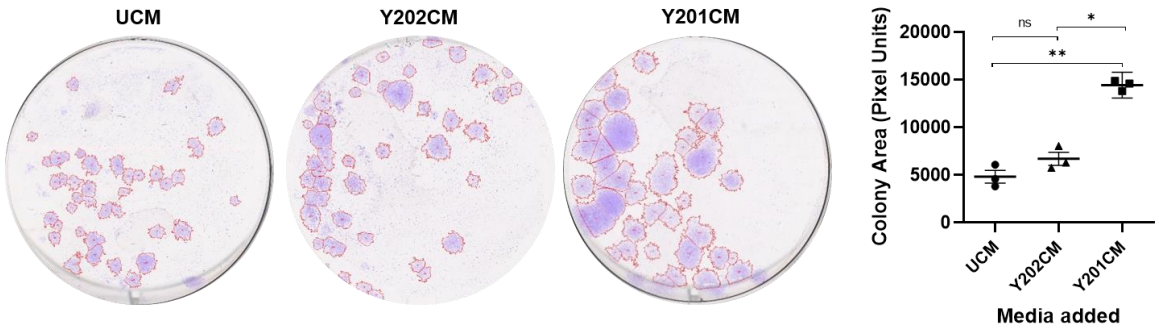

Figure 3.2 Colony area metric of CFU-Fs of Y202 treated with UCM, Y202CM or Y201CM

Representative crystal violet stained colonies of Y202 cells at day 10 of a CFU-F assay with individual colonies marked by a red outline generated by the CellProfiler colony detection pipeline. Mean colony area (graph, far right) shows quantification of mean colony areas per experiment after culture in UCM, Y202CM or Y201CM. Mean ± SE, n=3, (ANOVA: F (1.130, 2.260) = 60.05; *p*=0.0113).

Observation of these colonies at higher magnification with a light microscope indicated cellular and colony morphology was also changing, possibly as a result of increased cellular dispersion by migration of cells within a colony (not shown). Y202 colonies were subsequently imaged using a ptychographic imaging method at regular intervals for 96h. Proprietary software was used to track the movement of cells in colonies in response to treatment with Y201CM or Y202CM and the change of colony morphology can be seen with an increase in dispersion of cells visible in Y201CM treated cells at 96h (Figure 3.3, bottom). Tracking of individual cells Y202 within each colony revealed that Y201CM changed morphology of Y202 cells, resulting in a significantly increased mean length:width ratio (p=0.0293) while also increasing overall cell migration speed (p=0.0141) and an increased displacement of each cell from its point of origin (p=0.0012) (Figure 3.4). This increase in migration and dispersal of Y202 cells is evident when comparing videos of cells after addition of Y202CM or Y201CM (Supplementary videos 1 & 2).

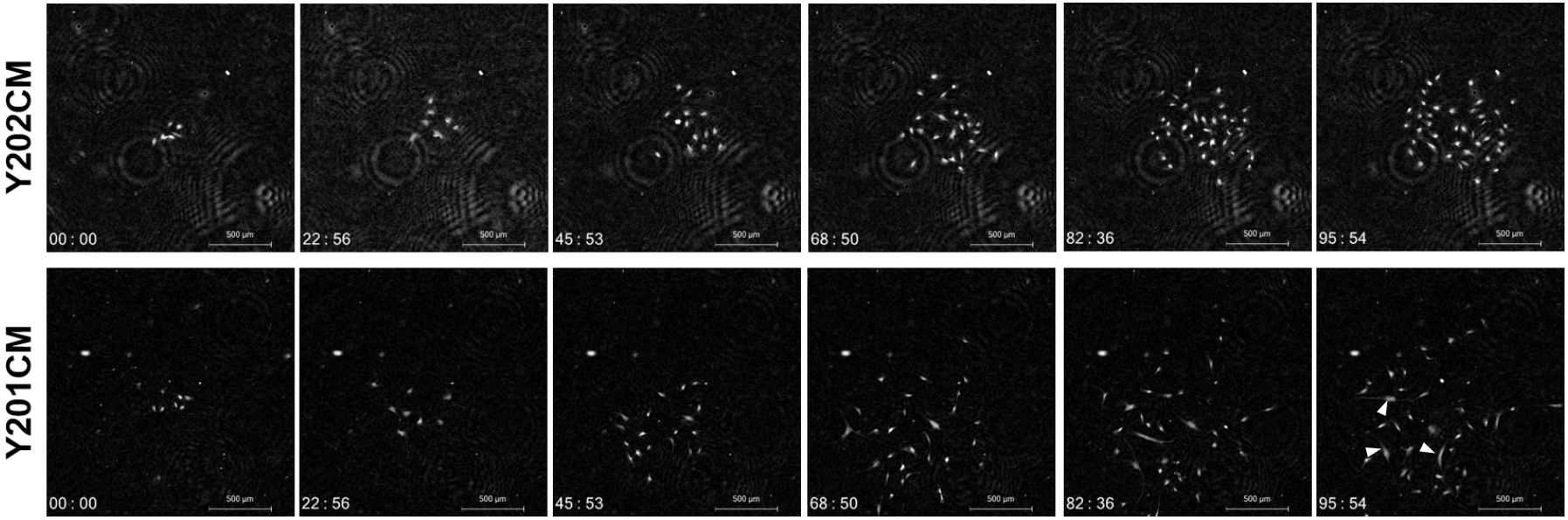

Figure 3.3 PhaseFocus tracking of Y202 colonies exposed to Y202CM or Y201CM

Individual frames of phase-contrast images after image processing from PhaseFocus ptychographic tracking of a representative single colony of Y202 BMSCs in a CFU-F assay treated with either Y202CM (top) or Y201CM (bottom) for a 96 hour period. Elongated cells are marked by white arrows in the final frame of Y201CM treated samples.

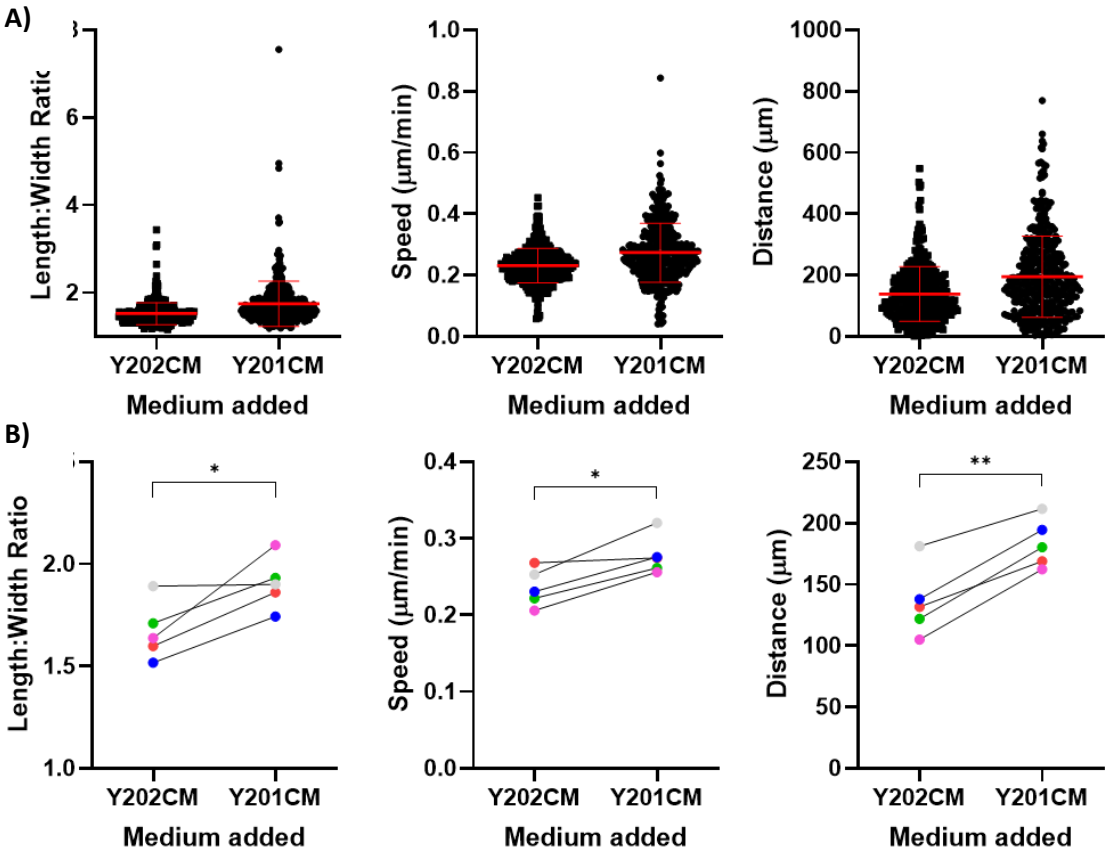

Figure 3.4 Morphometrics and migration of Y202 cells cultured in Y202CM vs Y201CM

A) Representative graphs for migration and morphological metrics calculated from tracking of Y202 cells in colonies cultured in either Y201CM or Y202CM for 96h. Mean cell length:width ratio, mean cell speed and mean displacement. Error bars are means ± SE B) Mean metrics as calculated from individual experiments (n=5) for length:width ratio, cell speed and displacement. Lines between points indicate experiments performed at the same time with cells seeded from the same flask. Significance determined by paired t-test. *p<0.05, **p<0.01.

The effect of Y201CM was also compared against UCM in a CFU-F performed on Y202 cells. This revealed an increase in cell length:width ratio and migration distance but a variable change in cell speed (Figure 3.5).

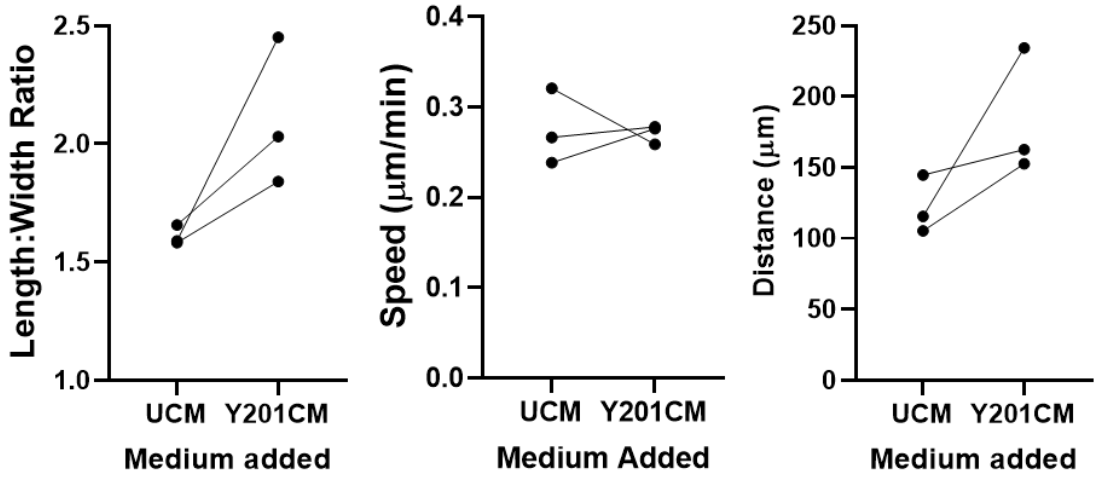

Figure 3.5 Morphometrics and migration of Y202 cells cultured in Y201CM vs UCM
Metrics calculated from individual experiments comparing the effect of UCM vs Y201CM on Y202 cell migratory and morphological characteristics when cultured in a CFU-F (n=3). Shown left to right are the mean length:width ratio, mean cell speed and mean displacement of Y202 cells over 96-hours of tracking during culture in UCM or Y201CM.

3.2.2 Conditioned media from hTERT BMSCs alters colony survival and size of *in vitro* aged primary BMSCs

Considering the striking effect of Y201CM on cell morphology and migration I tested the effect of the potent signalling on five primary cultures of BMSCs that had been *in vitro* aged through serial passaging, to determine if secreted factors from the Y201 or Y202 promoted an increase in CFU-F capacity or colony size. Colonies were cultured from 5 primary donors in a CFU-F assay with either UCM, Y201CM or Y202CM. At day 14 resultant colonies were stained with crystal violet and imaged (Figure 3.6). Quantification of colony characteristics using a CellProfiler pipeline revealed no statistically significant increase in colony number upon treatment with Y202CM ($p=0.3183$) or Y201CM ($p=0.0547$). However, there was a significant increase in mean colony area for primary cells cultured in Y201CM ($p=0.0004$) and Y202CM ($p=0.0122$), with one donor (K136) demonstrating a complete recovery of colony forming capacity when cultured with CM versus UCM (Figure 3.7).

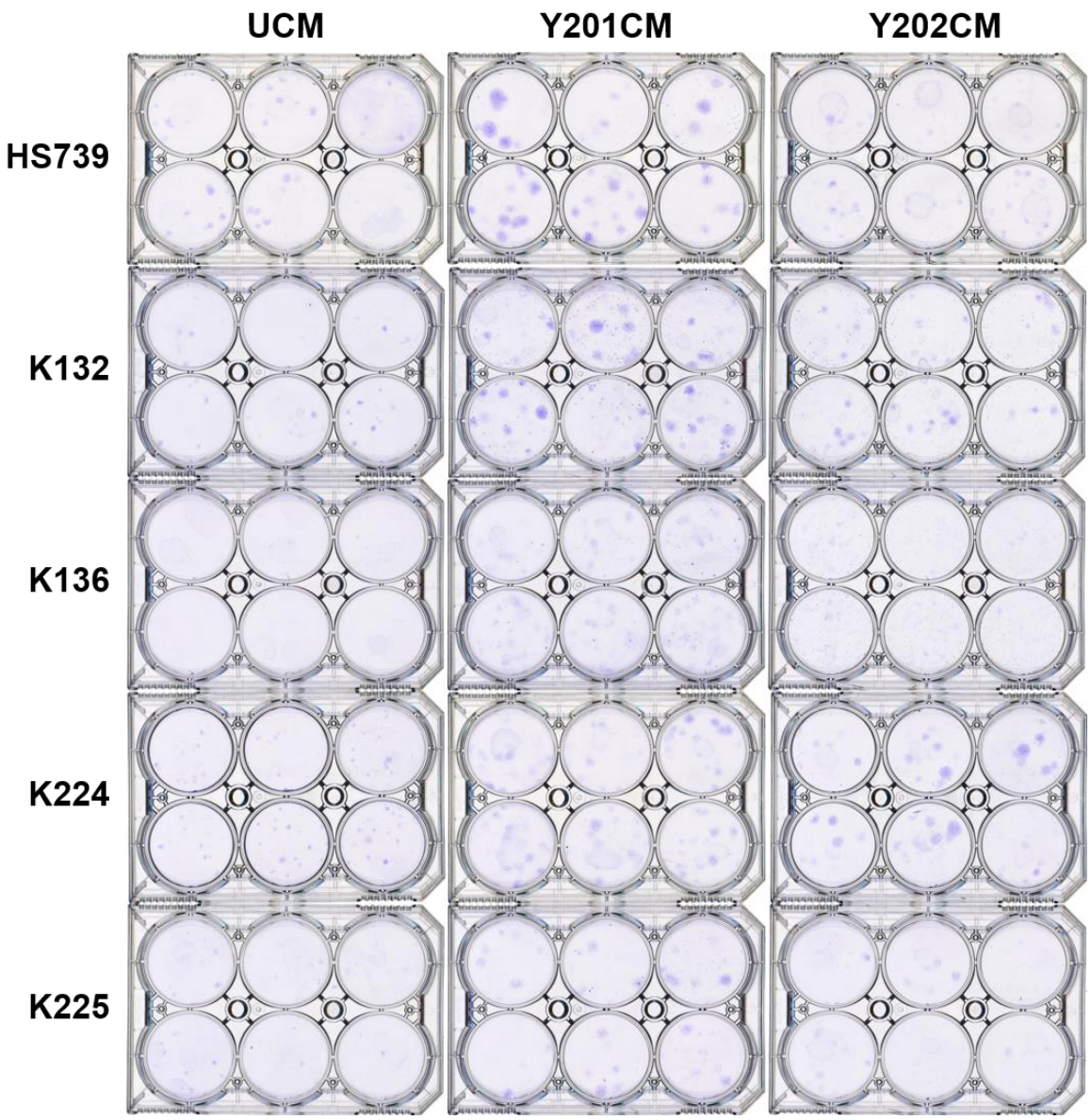

Figure 3.6 CFU-F assays of *in vitro* aged primary BMSCs with Y201CM or Y202CM

Scans of crystal violet stained CFU-F assays fixed at day 14 from 5 primary donors that were *in vitro* aged beyond passage 10. Primary cells were cultured in either UCM, Y201CM or Y202CM. 6 wells were captured per condition.

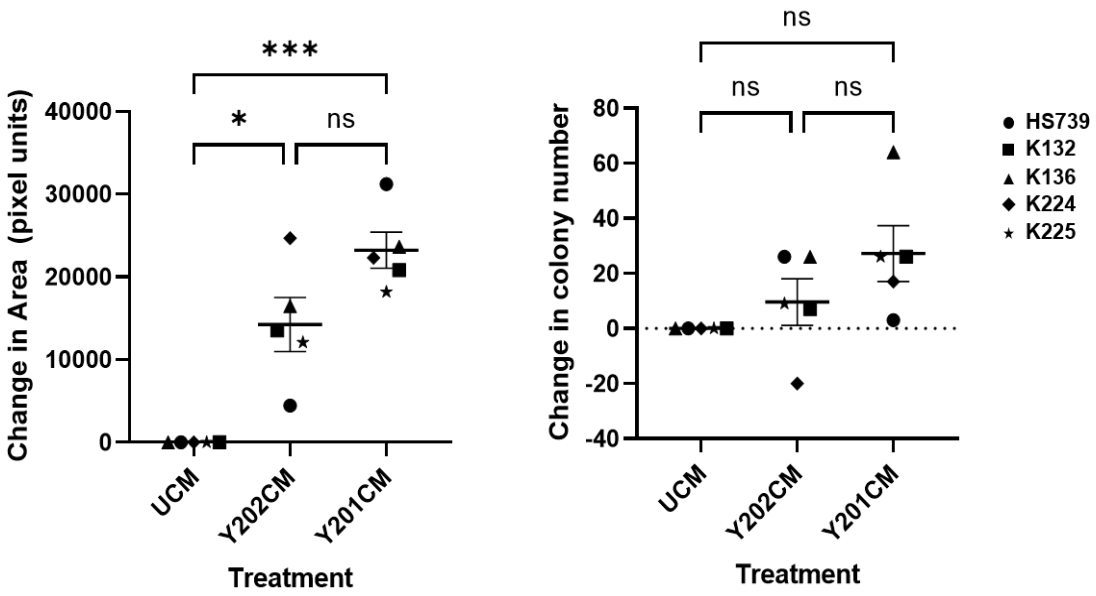

Figure 3.7 Metrics of *in vitro* aged primary BMSC CFU-Fs grown in Y201CM or Y202CM

Change in mean colony area (left) and mean colony number (right) of *in vitro*-aged primary BMSCs cultured in Y201CM or Y202CM versus UCM. Pairwise comparisons were performed by one-way ANOVA. Mean ± SE. Sample IDs are shown to demonstrate changes in individual donors due to treatments.

3.2.3 The effect of Y201CM on Y202 morphology and focal adhesion morphology

Changes in cell morphology and migratory characteristics may be driven by alterations in focal adhesions and the organisation of the actin cytoskeleton. To assess any changes in focal adhesions and actin cytoskeleton during CM treatment I used immunofluorescence staining to image the actin cytoskeleton and focal adhesions of Y201 and Y202 cells seeded onto glass. Actin cytoskeleton was revealed by phalloidin and focal adhesions using an anti-vinculin antibody. I identified distinct differences in cellular morphology, highlighted by differences in the actin cytoskeleton where Y202 cells presented with more obvious stress fibres that ran perpendicular to each other while Y201 samples appeared to have more diffuse, thinner filaments (Figure 3.8i&ii). These images also clearly demonstrate the differences in cellular morphology between the clonal lines, with a more fibroblastic shape in Y201, as well as a more peripheral localisation of actin. Y202 cells also presented with a significantly increased number of focal adhesions per cell that were also found to cover significantly larger areas and were longer than in Y201 cells ($p<0.0001$) (Figure 3.8iii-v).

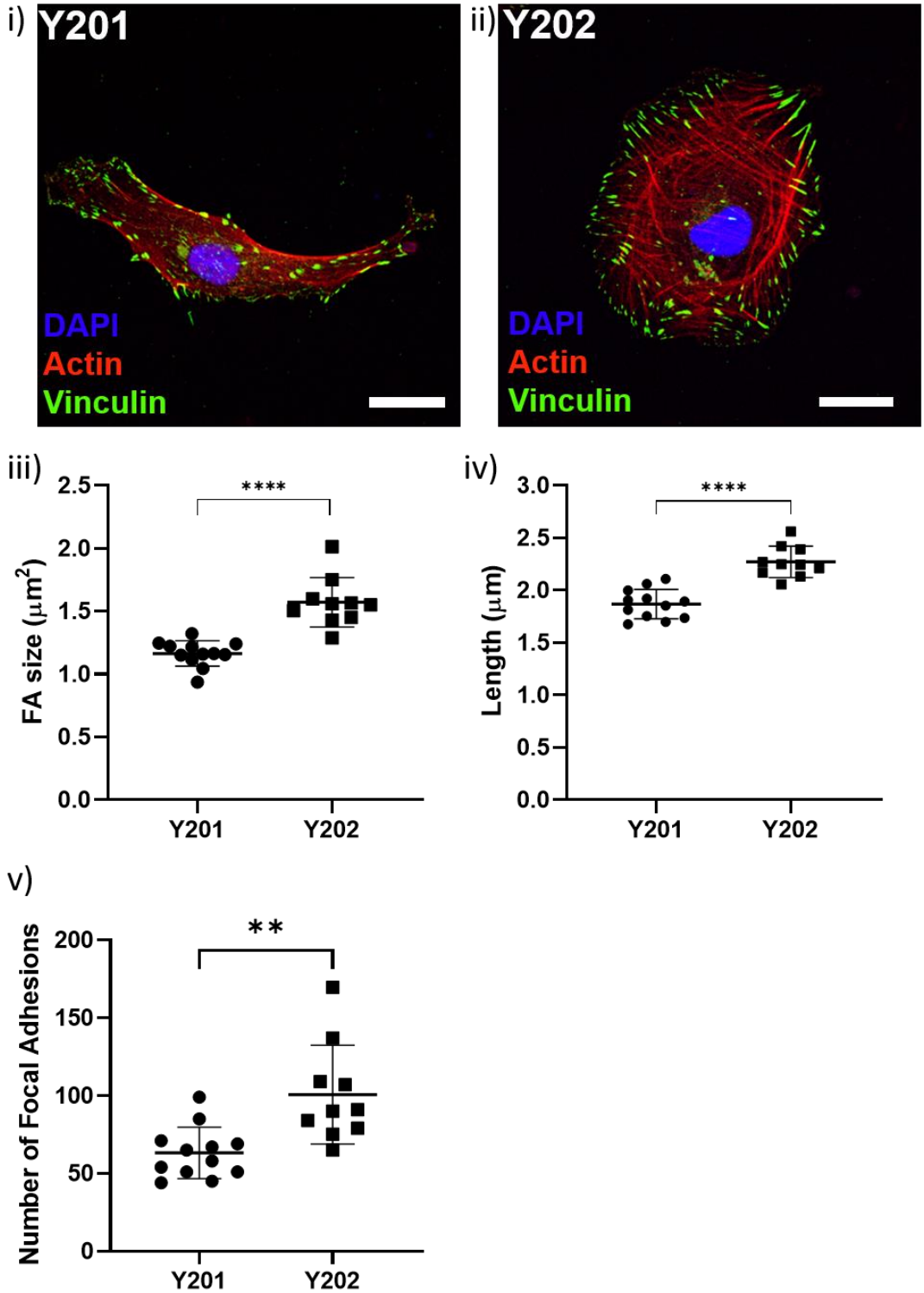

Figure 3.8 Images and analysis of Y201 and Y202 focal adhesions and actin cytoskeleton

Representative images of a i) Y201 cell) and ii) Y202 cell with phalloidin stained actin cytoskeleton (red, CF594), focal adhesions marked by mouse anti-vinculin antibody (AF488, green) and DAPI stained nuclei (blue) on glass coverslips. Focal adhesion iii) area, iv) length and v) number (n=10-12). Scale bar 20μm. Statistical significance determined by *t*-test. **p<0.01 ****p<0.0001

Y202 cells increased migration upon exposure to Y201CM and to assess whether this correlated with a change in focal adhesion size and shape upon exposure to CM I measured the size of focal adhesions of Y202 cells after 24 hours of culture in Y201 or Y202 CM. Y201CM proved highly effective in altering the morphology of Y202 cells to become more similar to that of Y201, despite obvious changes in cellular morphology of Y202 cells to a morphology more similar to Y201 (Figure 3.9). There was no statistically significant change in mean focal adhesion area or length between Y201CM and Y202CM treatments ($p=0.459$ and 0.695 respectively) however, the number of focal adhesions per cell was significantly lower with Y201CM vs Y202CM ($p=0.0445$). Despite no difference in focal adhesion size and length in Y202 cells treated with Y201CM and Y202CM it was noted that adhesion size in both Y201CM and Y202CM treated Y202 cells was smaller than that identified of 202 cells cultured in normal media. The organisation of actin cytoskeleton seemed to differ in between CM treated and untreated Y202 cells, with actin in Y202 cells appearing more aligned versus the untreated counterparts.

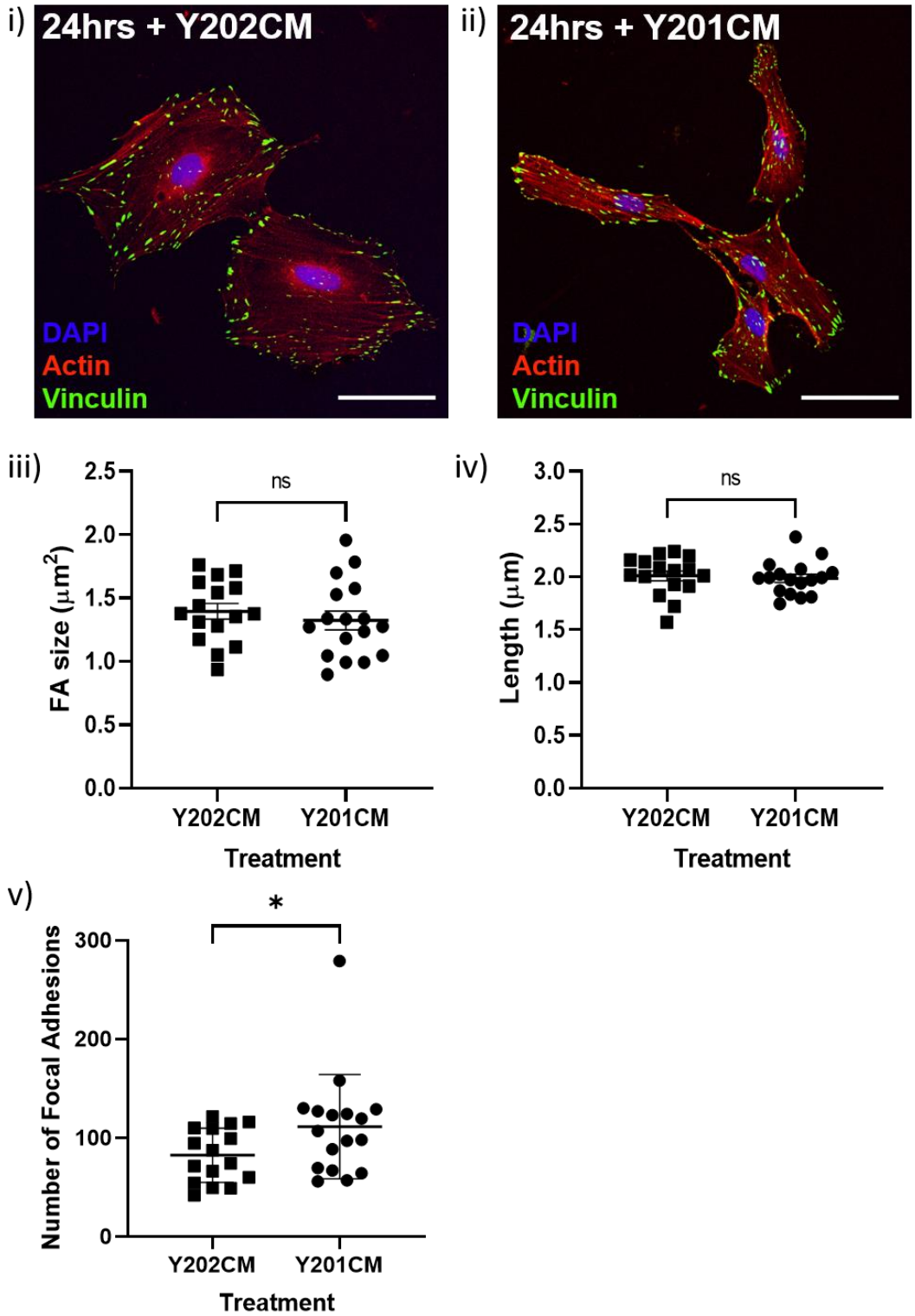

Figure 3.9 Images and analysis of focal adhesions and actin cytoskeleton of Y202 cells treated with Y201CM or Y202CM

Phalloidin stained actin cytoskeleton (red, CF594), focal adhesions marked by mouse anti-vinculin antibody (AF488, green) and DAPI stained nuclei (blue) of Y202 cells cultured for 24hours in i) Y201CM or ii) Y202CM. Quantification is shown in the graphs for focal adhesion iii) area iv) length and iv count). N=16-17. Scale bar 20um. Statistical significance determined by *t*-test. *p<0.05 ns = not significant.

3.2.4 Effect of BMSC conditioned media on inflammatory gene signature

Unpublished data from our lab has revealed that Y202 cells express a high basal level of 8 inflammatory genes when compared to Y201 cells. I cultured Y202 and Y201 cells in a CFU-F with UCM, Y201CM or Y202CM to determine if secreted factors were capable of altering inflammatory gene expression. At assay endpoint, cells were lysed and the expression level of the 8 classical inflammation related genes was determined by RT-qPCR (Figure 3.10). In Y202 cells there were significant increases in expression for MX2, EPSTI1, RSAD2, HERC5, IFI44L and MX1 when cultured in Y202CM versus UCM. The increase in expression for Y202CM treated cells was also significant against Y201CM treatment for MX2, EPSTI1, HERC5, IFI44L and ISG15. Significant changes in expression in Y201 cells was observed only for IFI44L and LY6E, with the increase being significantly higher in Y202CM treated versus UCM treated cells for both genes. The highest mean level of expression for all genes was consistently seen in the Y202CM treated Y202 cells.

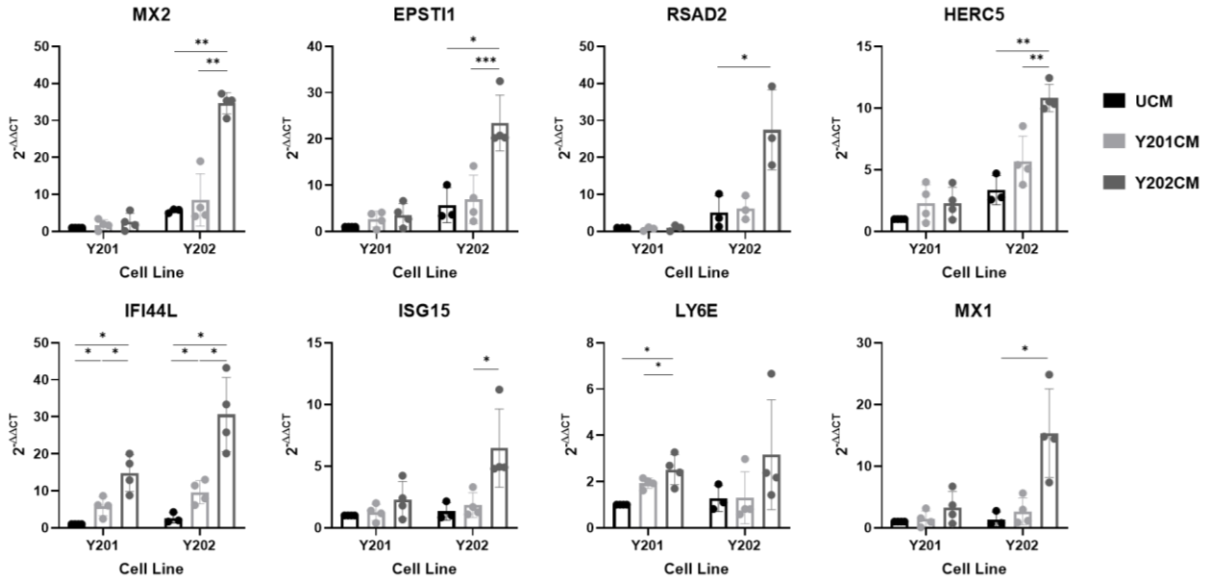

Figure 3.10 Gene expression of 8 inflammatory genes in Y201 and Y202 cells treated with UCM, Y201CM or Y202CM

Relative gene expression levels of 8 classical inflammatory genes from Y201 and Y202 cells cultured in CFU-Fs with either UCM (black), Y201CM (light grey) or Y202CM (dark grey). All values are normalised around the Y201 untreated control. *N = 3-4.* Statistical significance was determined by Mixed effects analysis with a Fisher's LSD post-hoc test by comparing changes in gene expression between treatments within each cell line. *p<0.05, **p<0.01, ***p<0.001

3.2.5 MSC subtypes produce structurally varied extracellular matrices

ECM proteins are a substantial contributor to the total cell secretome, providing a suitable environment for cell attachment and growth. Y201 and Y202 were cultured for 2 weeks to allow deposition of a layer of ECM onto the cell culture surface. After removal of the cell layer there was a clear distinction between the structure of the ECMs produced by these BMSC subtypes between when visualised by light microscopy (not shown). I used SEM to observe the topographical surface of the matrix at high magnification and to interrogate its structure (Figure 3.11). The matrix made by Y201 appeared to be more compacted and with larger and potentially deeper pits or holes. In contrast the matrix produced by Y202 cells appeared more fibrous, with distinct fibres visible at both high and low magnifications.

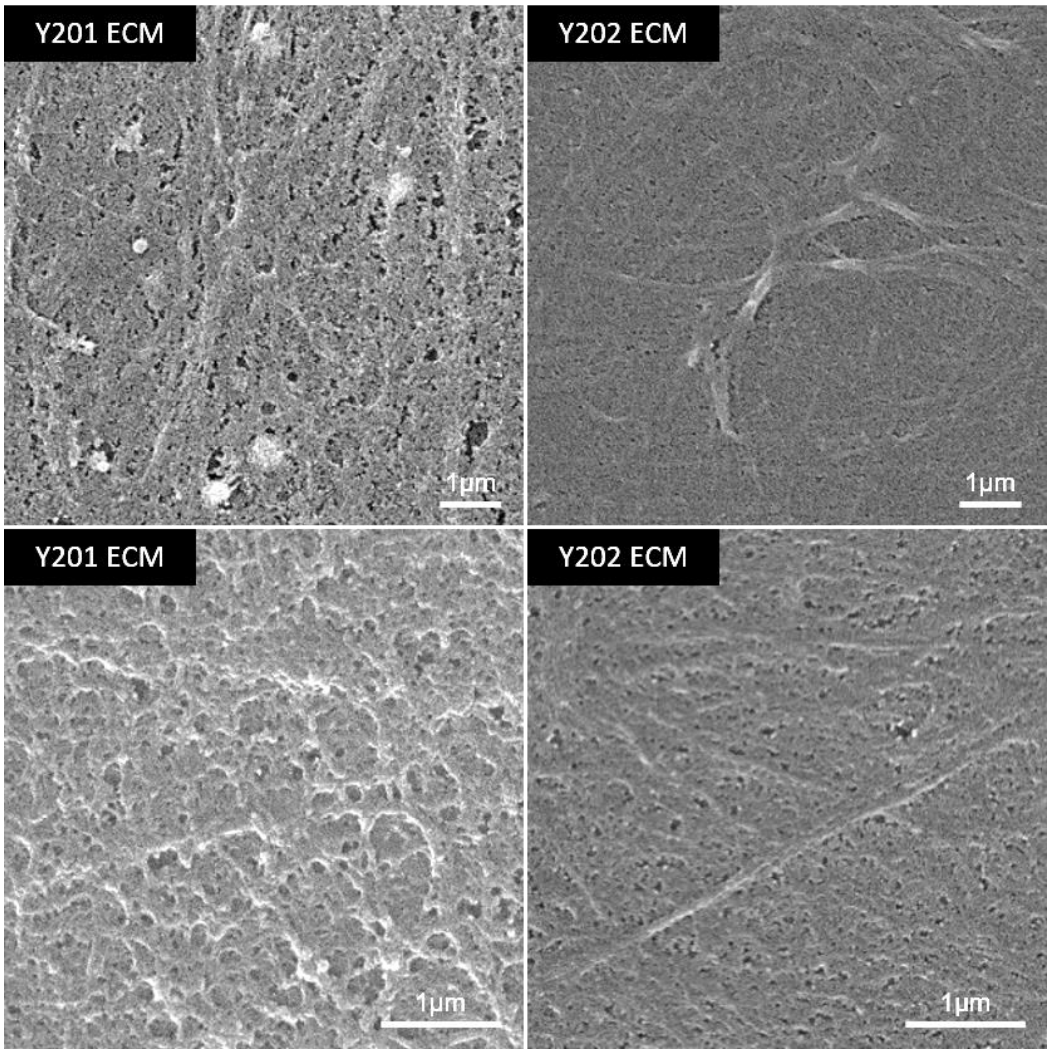

Figure 3.11 Scanning electron microscopy of Y201 and Y202 ECMs

Scanning electron micrographs of ECM deposited by Y201 and Y202 BMSCs on glass coverslips at two different magnifications reveals topographical differences between the matrix deposited between two subtypes.

This difference in topography of the matrix was further evident when performing Focused Ion Beam SEM (FIB-SEM) of the same samples. The overall architecture of the ECM was apparent when observed at low magnification prior to initial FIB-SEM experiments. Y201 matrix appeared as a consistent mat of dense fibres whereas Y202 ECM presented as a more disperse meshwork with irregular patches of more fibrous matrix (Figure 3.12, Top). FIB-SEM was utilised to section through the ECM and image, revealing that ECM produced by Y201 cells was notably thicker than that produced by Y202 cells (Figure 3.12, Bottom). The FIB-SEM was repeated using samples embedded in resin to better preserve the architecture of material from damage by the ion beam. Cells were not cleared from the matrix in these samples in order to observe interaction between the ECM and the cells. The images captured corroborated the finding that Y201 cells deposited a thicker ECM as can be seen in Figure 3.13.

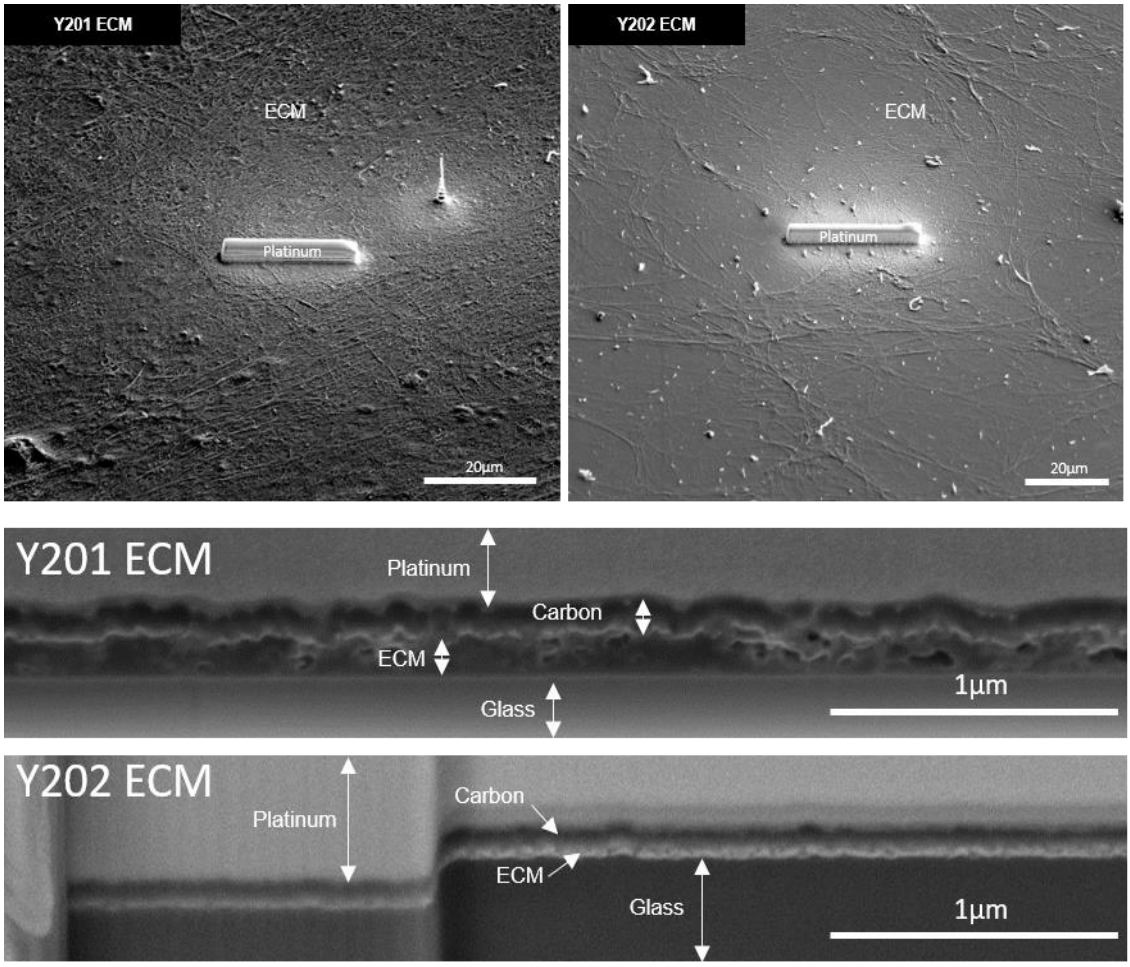

Figure 3.12 Focused-ion beam SEM of Y201 and Y202 extracellular matrices without cells

Scanning electron micrographs of the ECMs produced by Y201 and Y202 cells after carbon coating and the addition of the protective layer of platinum (TOP). FIB-SEM images showing cross sectional view of matrices after ion beam milling are shown in the long panels (BOTTOM).

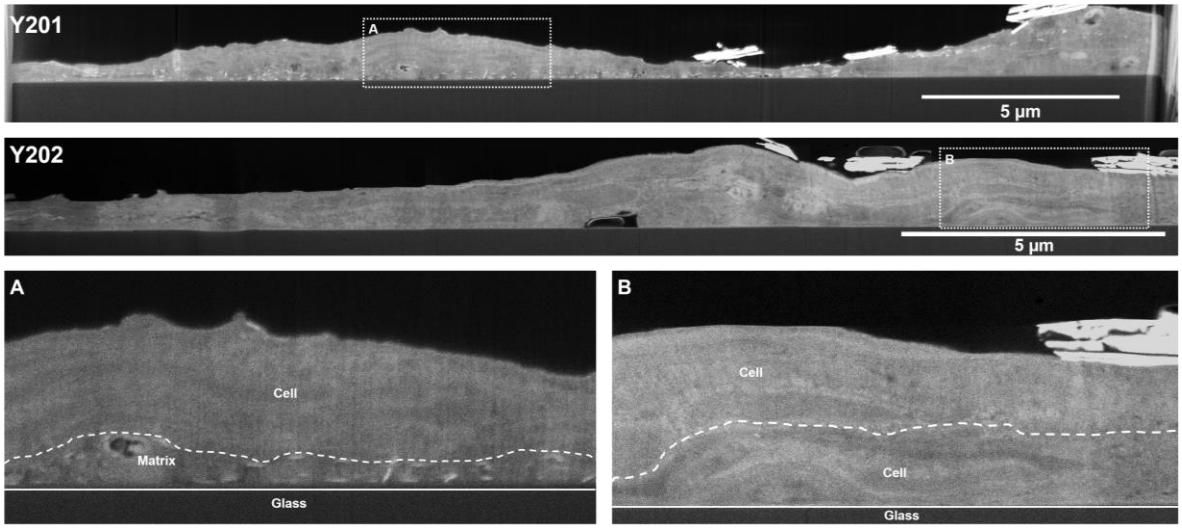

Figure 3.13 Focused-ion beam SEM of Y201 and Y202 extracellular matrices with cells

Scanning electron micrographs of the focused ion beam milled extracellular matrix with cells still attached. The small white flecks visible in the Y201 (Top) are indicative of regions of deposited ECM. Enlarged views of regions marked by dashed boxes are shown in the bottom panels for Y201 (A) and Y202 (B).

3.2.6 Effect of ECM on osteogenic differentiation versus tissue culture plastic

I investigated the potential for ECMs from BMSC subtypes to alter osteogenic differentiation through a 21 day osteogenic assay. Representative alizarin red staining for calcium deposition demonstrating osteogenic differentiation is shown in Figure 3.14. Alizarin Red staining of plastic cultured controls confirmed osteogenic differentiation of Y201 cells and limited differentiation of Y202 by day 21 in the presence osteogenic supplements. The end wells contained no cells so as to demonstrate the absence of calcium deposition or acellular calcium binding capacity of Y201 ECM or Y202 ECM. There was a slight increase in staining of Y201 cells cultured on either Y201 ECM or Y202 ECM versus plastic by day 14 with notably darker staining at the centre of wells by day 21. Furthermore, there was an increase in alizarin staining of Y202 cells grown on Y201 ECM or Y202 ECM versus plastic by day 21.

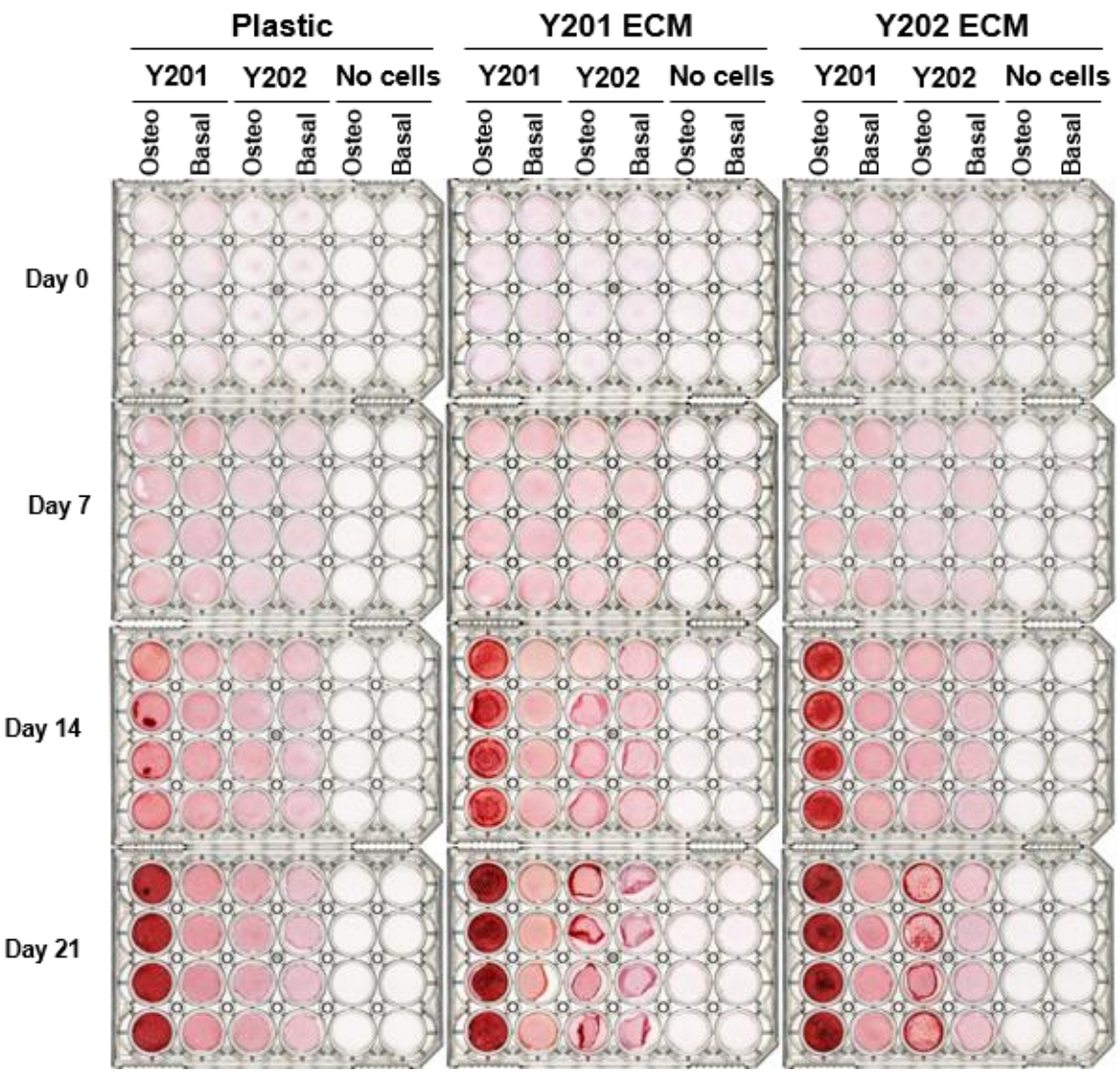

Figure 3.14 Osteogenic differentiation of Y201 and Y202 cells cultured on Y201 or Y202ECM

Alizarin red staining for calcium deposition of osteogenic differentiation assays at day 0, 7, 14 and 21 for Y201 and Y202 cells cultured on plastic (left), Y201 ECM (middle) or Y202 ECM (right). Cells were treated with either osteogenic differentiation supplements (Osteo) or standard culture medium (Basal). Staining is representative of n=3 experiments.

3.2.7 MSC derived extracellular matrices improve migration of Y202 BMSCs

ECM deposited by BMSC subtypes appeared structurally distinct and so I hypothesised that this may result in an altered capacity to facilitate migration of BMSCs. I showed using non-destructive imaging of Y202 cells seeded onto ECM over time resulted in an increase in migration of cells compared to those that were cultured on plastic. Y202 cells seeded onto plastic displayed typically flattened and spread morphologies that persisted during colony formation (Figure 3.15 top row and supplementary video 3). In contrast, those cells cultured on ECMs appeared more fibroblastic and were considerably more motile (Figure 3.15 middle and bottom row and supplementary video 4).

Assessment of cell motility characteristics through tracking analysis software revealed that Y202 cells cultured on either Y201ECM or Y202ECM significantly altered their morphology to become elongated as shown by the increased length:width ratio (Figure 3.16A). Y202 cells cultured on ECMs also migrated further from their point of origin and at an increased speed versus Y202 cells grown on plastic (Figure 3.16B&C). I also identified that Y202 cells cultured on either ECM altered their morphology dramatically, with cells often becoming more elongated with a higher length:width ratio and with occasional exceptionally elongated cells.

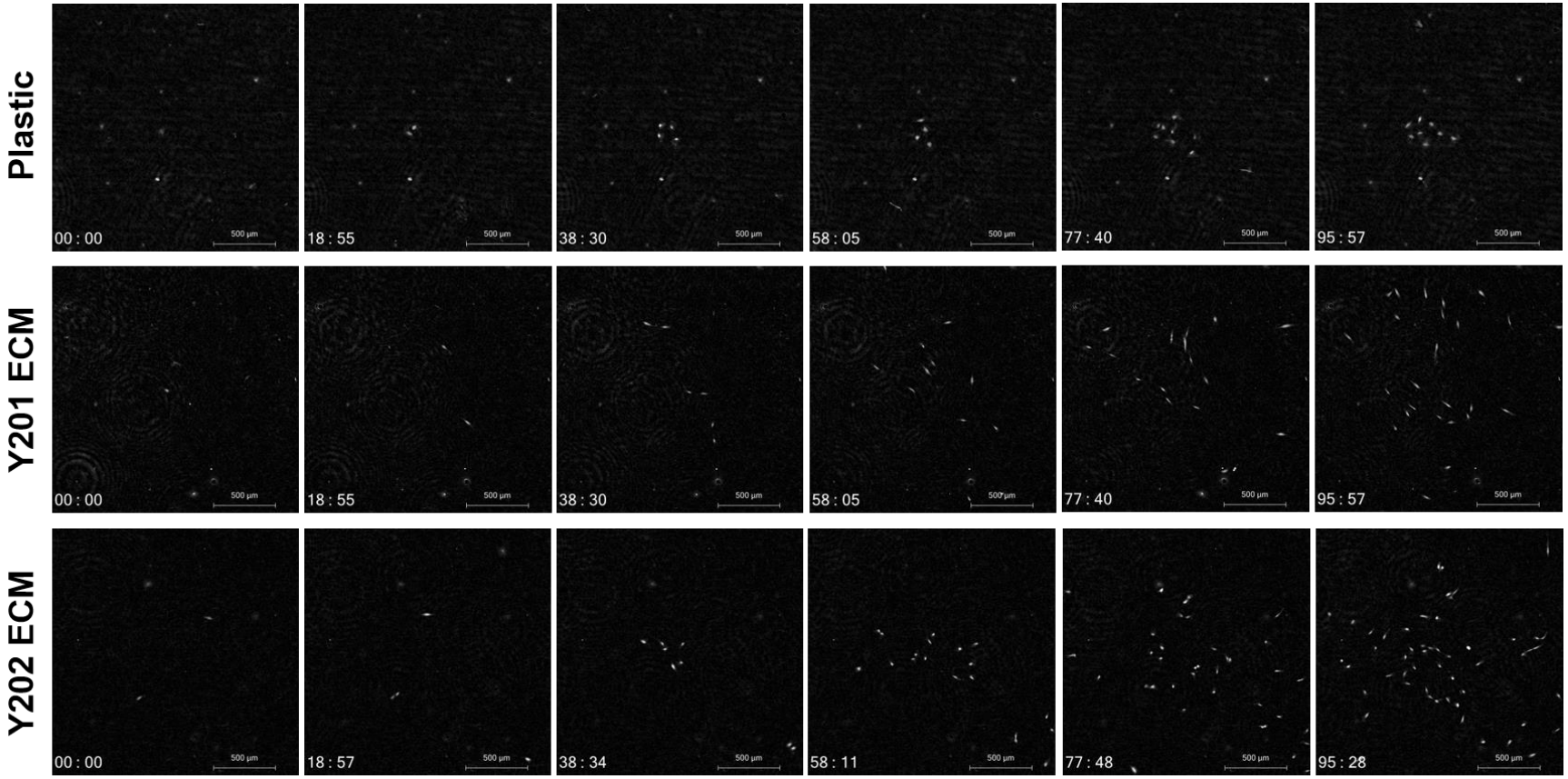

Figure 3.15 PhaseFocus tracking of Y202 colonies cultured on plastic, Y201ECM or Y202ECM

Individual frames from PhaseFocus ptychographic imaging of Y202 BMSCs in CFU-F assays cultured on plastic, Y201 ECM or Y202 ECM. Images were captured at regular intervals for 96 hours. Time of capture for frames is shown in the bottom left of each panel.

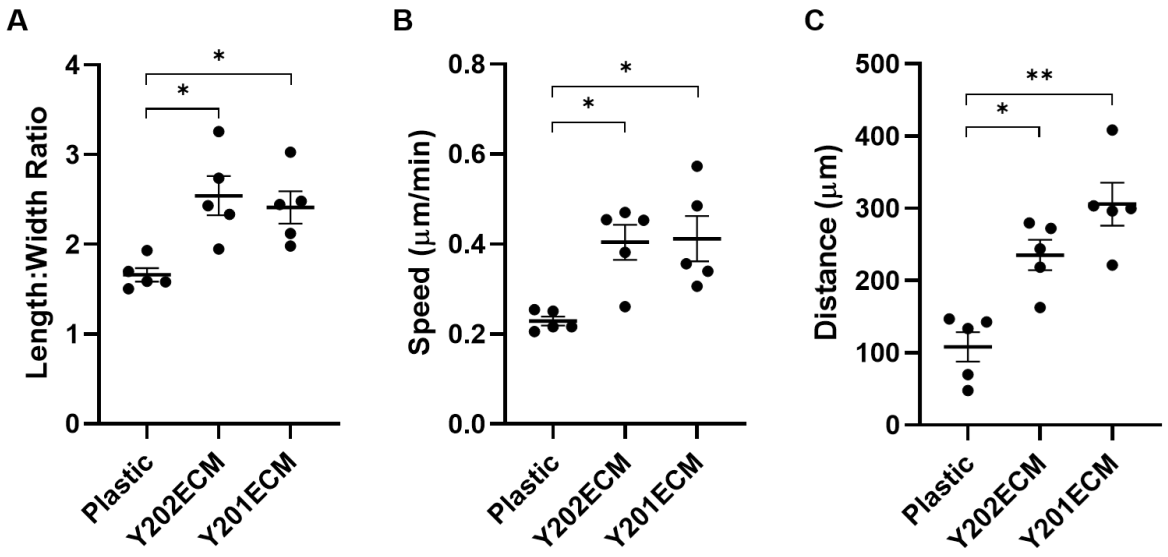

Figure 3.16 Morphometrics and migration of Y202 cells cultured on plastic, Y202ECM or Y201ECM

Cell metrics calculated from Y202 cells cultured on different surfaces and tracked over 96h using a PhaseFocus ptychographic imaging platform. The A) length:width ratio, B) Speed and C) Displacement from point of origin are shown as mean ± SE. Significance determined by one-way ANOVA with Tukey's multiple comparisons test. *p<0.05. **p<0.01. N = 5.

3.2.8 Inhibition of Focal Adhesion Kinase inhibits migration on BMSC ECMs

I demonstrated that the Y201 ECM drove significant increase in migration of Y202 cells and that this increase in migration was occurring through a focal adhesion kinase (FAK) dependent mechanism through use of a small molecular inhibitor. The FAK inhibitor (FAKi) (PF573228) did not significantly alter the length:width ratio of Y202 cells on ECM at any of concentrations. I observed no increase in cell-death in response to inhibitor, however, proliferation appeared to be reduced (data not shown). At 10μM the FAKi significantly inhibited the mean speed at which cells migrated and the displacement of individual cells from their starting point was significantly lower for Y202 cells treated with 3 and 10μM of inhibitor (Figure 3.17). Overall there appeared to be a dose-dependent effect of FAK inhibition on the migration of Y202 cells on ECM.

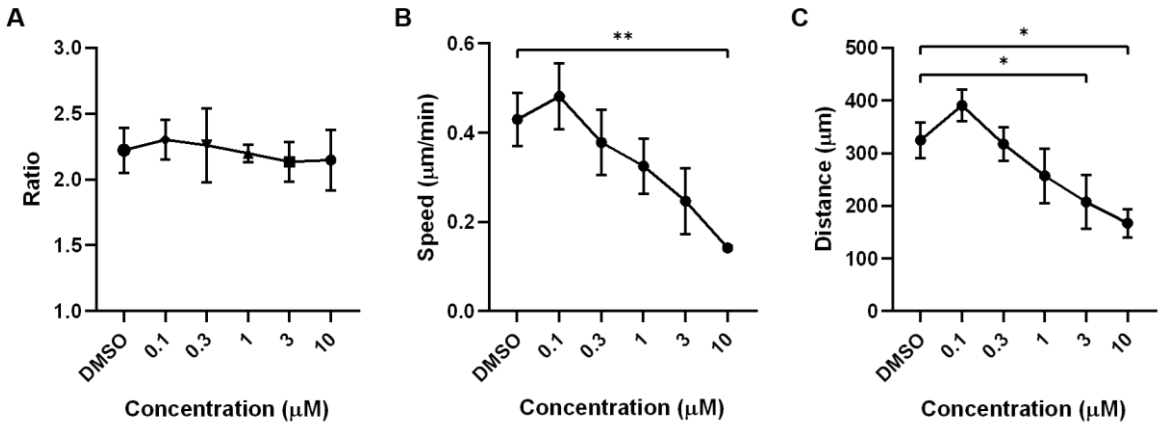

Figure 3.17 Morphometrics and migration of Y202 cells cultured on Y201ECM with a FAK inhibitor

The mean A) length:width ratio, B) speed and C) displacement of Y202 cells seeded onto Y201 ECM and tracked for 96 hours in the presence of varying concentrations of FAK inhibitor (PF573228) or DMSO vehicle control equivalent to the top concentration of inhibitor used. Mean ± SE. ANOVA of comparisons against DMSO control. *p<0.05, *p<0.01. N=4.

3.3 Discussion

It is understood that within the heterogeneous population of bone marrow stromal cells there are phenotypically distinct subsets, and it is reasonable to assume that the secreted factors of these subtypes are also likely to differ in accordance with other aspects of cell phenotype such as potency and migratory capacity. I presented in this chapter evidence for differential effects of secreted factors from two distinct BMSCs, and that the phenotype of a non-migratory, pro-inflammatory Y202 subtype can be altered by the secreted products of another more classical multipotent MSC subtype.

The significant increase in Y202 colony size upon exposure to Y201CM indicated the presence of trophic factors secreted by Y201 cells that drive proliferation of cells from a single cell, a feature of BMSC secretomes that has been reviewed extensively in the context of their effects on other cell types (Caplan and Dennis, 2006). Inactivation of this function by heat treatment suggested this effect was likely imparted through secreted proteins that lost their function by denaturing under heating. Further interrogation of these colonies revealed an altered colony and cellular morphology suggesting an increased migration of cells, which I confirmed by experiments using non-destructive label-free ptychographic imaging. The Y202 cells adapted to a more classical ‘stromal’ morphology more similar to Y201, and became more migratory, in response to Y201CM. This suggests that Y201 migration seen in normal culture may be driven by continual secretion of migration inducing factors. Cell biophysical properties including cell shape have previously been demonstrated to have some use in predicting the capacity for a BMSC to both differentiate and provide immunosuppressive capacity (Klinker et al., 2017; Lee et al., 2014c; Poon et al., 2015). The non-migratory Y202 significantly increased displacement, the distance travelled from point of origin, upon exposure to Y201CM, indicating an increased presence of a chemotactic or migration inducing factor(s) in the Y201CM. This factor may have been responsible for altering other aspects of cellular phenotype, including the observed elongation in cell shape which is of key interest given that the shape and biophysical properties of BMSCs *in vitro* previously have been used as a predictor of functionality. A recent study even highlighted high migratory capacity as a feature of BMSC phenotype that correlated with improved therapeutic benefit in the treatment of degeneration of the nervous system in mice (Danielyan et al., 2020). The observed change in morphology indicated that plasticity in cell shape may be reflective of subsequent plasticity in cell function. Equally, the morphology change could mask true cell functionality by induction of morphological change by secreted

factors from migratory BMSCs without a subsequent change in other properties such as differentiation potential. Overall the increased migration of Y202 cells in response to Y201CM highlights a potential for phenotypic plasticity, and that aspects of the Y202 phenotype from primary cells akin to Y202 may not be maintained when cultured as part of a heterogeneous BMSC mix. Though these cells are defined as BMSCs by their cell surface marker expression, there is little understanding of where these BMSC subtypes may reside *in vivo.* As such, the change in cellular phenotype is likely to occur as a result of removal of these cells from a phenotype-maintaining niche into a 2-dimensional plastic culture system where they are perhaps more readily exposed to secreted factors from other BMSC-like cells that reside in a different niche. Our Y202 lines may preserve their phenotype due to being cultured as a mono-culture, a phenomenon that is seen in other studies that use cells cultured from single cells (Russell et al., 2010). Y202-like cells represent a small proportion of BMSCs and as such exposing them to conditioned media from Y201 cells may represent a model of the dynamics of how Y202-like primary cells undergo changes in *ex-vivo* cultures with other BMSCs.

The increased proliferation of *in vitro*-aged primary cells cultured in Y201CM gives further evidence for the trophic capacity of secreted factors from Y201 cells, with the complete rescue of colony forming capacity in one donor (K136) evidence for a potential use of such secreted factors in the *ex vivo* treatment of both allogeneic or autologous donor cells. It would be of interest to extend studies with primary BMSCs, and specifically clonally isolated primaries, to determine if other aspects of their phenotype including migration, cell morphology and differentiation potential are changed in a similar way or are maintained with BMSC secreted factors. Such studies could begin to reveal if there are dominant clones within the BMSC population that are capable of driving positive selection or altering phenotypes of a plastic population. The effect of Y201CM may be consistent with preventing senescence of primary cells, identifying a niche function of Y201 cells.

The lack of difference in focal adhesion size between Y202CM and Y201CM exposed Y202 cells was unexpected given the significant increase in cell motility that was observed with Y201CM versus Y202CM. It was noted, however, that the mean focal adhesion size decreased versus untreated Y202 cells for both CM treatments (1.572µm in Y202 cells versus 1.395µm and 1.323µm in Y201CM and Y202CM respectively). This might suggest that a decrease in focal adhesion size is related with increased motility. Other work in mouse embryonic fibroblasts demonstrated a biphasic relationship of adhesion size with

cell speed, highlighting how both smaller and larger average focal adhesions could positively correlate with increased migration (Kim and Wirtz, 2013). This study used a normalised, rather than absolute, measure of focal adhesion size and so the adhesion size at which maximal cell speed is reached may peak at a different absolute adhesion size in BMSCs. This decrease in focal adhesion size could correlate with a response to a factor that induces increased migration. Focal adhesion size and distribution offer informative metrics although it would be of interest to determine the rate at which the focal adhesions turnover in cells exposed to conditioned media, as this might indicate more effectively the functional impact of cell speed with different treatment.

As well as morphological changes in hTERT BMSCs cultured in the presence of CM we also identified changes in gene expression of Y201 or Y202 cells upon exposure to Y201CM or Y202CM. Y202 cells exposed to Y202CM consistently presented with the highest expression level of 8 classical inflammatory genes, with significant fold changes over cells cultured without conditioned media. A comparatively slight, but significant, increase in expression for IFI44L and LY6E in Y201 cells exposed to Y202CMsuggests that a factor was present in the media that could drive inflammatory gene expression but that the cells differ in their capacity to respond to this factor, with Y202 more likely to upregulate inflammatory genes upon exposure. This might suggest a role for Y202 cells in driving inflammatory responses through signalling in the bone marrow microenvironment, although this may further present a model of how Y202-like BMSCs may be harmful in a therapeutic or regenerative setting were they to perpetuate inflammatory signalling in other cell-types through paracrine signalling. A microarray looking at global gene expression in Y202 had previously revealed increased expression of a number of immune-pathway related genes. Follow up revealed high basal expression for the 8 genes which suggests further that when cultured as a mono-culture that a factor expressed by the Y202 may facilitate the perpetuation of high basal expression. The implications of this in a disease setting could be that inflammatory gene expression is modulated by maintenance of the pro-inflammatory Y202 population numbers, a disproportionate expansion of such “inflammatory” BMSCs may result in an autocrine feedback loop of secreted factors perpetuating the increase in gene expression. This further has important implications for regenerative therapies as it was previously demonstrated inflammatory signalling can prevent differentiation of BMSCs toward bone (Lacey et al., 2009). This autocrine loop could explain the increased expression of some genes in response to Y201CM may be explained by the previously noted trophic capacity of Y201 CM in colony forming assays. Increased numbers of Y202

cells may have resulted in proliferation of Y202 cells and a subsequent feedback of Y202 secreted signals onto these cells driving increased inflammatory gene expression. This experimental system also only observed the effect of secreted signals on gene expression in other BMSCs, however, *in vivo* BMSCs are exposed to a plethora of cell types including immune populations and the effect of secreted factors on these cells could further indicate differences in functionality.

Extracellular matrices produced by Y201 and Y202 subtypes were structurally different and this offers a potential mechanism through which BMSCs may dictate the behaviour of cells in their local environment. There was minor improvement in osteogenic efficiency when culturing BMSCs on either matrix, however, subtle indication of increased calcium deposition in the Y202 clone (which ordinarily do not differentiate) suggests a potential to drive differentiation when cultured on a proteinaceous matrix, although differences between matrices were indiscernible. Previous work demonstrated how primary adherent-marrow-cell ECM was capable of maintaining *in vivo* potency of primary BMSCs cultured *in vitro* and that BMSC derived matrix performed similarly under serum-free conditions. In support of this work and in relation to the previous indication that Y202 cells have increased inflammatory signalling it was shown by Waterman et al. (2010) that a more pro-inflammatory subset of BMSCs produced less fibronectin matrix. This work presents a refinement of these studies, with matrices derived from homogeneous cell populations. By elucidating how the matrices of different cell-types may impart these beneficial expansion and stem-maintenance functions we may be able to develop reproducible materials for treatment of cells prior to therapy. Experimental evidence indicates plasticity in cell behaviour can be driven through biophysical properties such as surface elasticity, with cells cultured on soft gels more capable of responding to inflammatory stimuli, and so our evidence that there are inherent differences in the matrix production of BMSC subtypes indicates that this may also occur naturally through a co-ordinated of biological signalling via ECM biophysical properties to regulate cell and population phenotype (Wong et al., 2020). A study by Gomariz et al. (2018) demonstrated a strict adherence of CAR cells to ECM proteins collagen IV, laminin and perlecan that were also notably thicker in peri-sinusoidal regions and thicker still in peri-arteriolar areas, although the selection of ECM proteins immunostained for was limited. Of note was the observation that osteogenic differentiation of Y201 cells was accelerated on ECMs regardless of the BMSC that produced them which correlates with previous work with heterogeneous BMSC mixes demonstrating improved preservation of potency as well as potentiation of differentiation by

BMSC derived ECM (Chen et al., 2007; Novoseletskaya et al., 2020; Rakian et al., 2015). There was a slight increase in calcium deposition by Y202 cells cultured on matrices. Previous work has highlighted that 'young' BMSC matrices may rescue replication and osteogenesis in aged BMSCs, and thus our matrices may rescue such capacity in Y202 via a similar method (Sun et al., 2011).

Y202 cells cultured on ECMs from either Y202 or Y201 became more fibroblastic in shape and migrated further on average than cells cultured on tissue culture plastic, recapitulating some of the increased migration seen with Y201CM treatment. Previously soluble ECM components, specifically tropoelastin, have been shown to increase MSC migration and so soluble ECM components could be responsible for the increased migration (Yeo and Weiss, 2019). The change in cell migration in response to both matrices suggests that it may be simply the decreased deposition of Y202 matrix, demonstrated by SEM and FIB-SEM that preserves the overall cellular phenotype. Threshold levels of matrix components required to drive morphological change and increased migration are likely surpassed considerably when a layer of established matrix is provided. I showed that the increased migration of Y202 cells on Y201ECM was FAK dependent, highlighting a role for this important intracellular signalling protein in co-ordination of BMSC migration, although more experiments to identify the membrane bound ECM binding proteins signalling through FAK are required to determine the mechanism behind BMSC migratory plasticity. ECM is known to drive migration of BMSCs via integrin and CD44 signalling and so attempts to target these bindings proteins may be necessary (Veevers-Lowe et al., 2011; Zhu et al., 2006).

3.4 Conclusions

Y201CM is capable of inducing a change to a more migratory and fibroblastic phenotype in Y202 cells, and does so more effectively than Y202CM. Y201 cells produce a thicker ECM than Y202, however, both ECMs appear to improve cell migration versus plastic and this process appears to be FAK dependent on Y201 ECM. The ECM did not appear to induce differentiation capacity in nullipotent Y202 cells, however, ECM did appear to accelerate osteogenesis *in vitro* of Y201. Y202CM also increased expression of 8 classical interferon upregulated genes in Y202 cells, potentially highlighting a positive feedback of inflammation by these cells. Y201CM therefore contains trophic and pro-migratory factors, likely released at higher concentrations per cell than in Y202, while the Y202 secretome may perpetuate inflammatory signalling. This highlights a stark contrast in

secretomes which has implications for how culturing of mixed populations of BMSCs may lead to phenotypic drift through paracrine signals. This also highlights how selection of refined populations for MSC secretome based factors is necessary given the variation in function between subpopulation secretomes.

4 Characterisation of Secreted Factors from Heterogeneous BMSCs

4.1 Introduction

4.1.1 The BMSC secretome and heterogeneity in secreted factors

The factors that are collectively secreted into the extracellular milieu may be referred to as the secretome. The secretome is of great interest for identification of biomarkers and for establishing functions of cells through their paracrine signalling actions (Stastna and Van Eyk, 2012). The role that BMSCs have in modifying immune responses, as well as their support of the haematopoietic niche, have been related in part to their paracrine signalling capacity. BMSCs are known to secrete important cytokines and chemokines such as CXCL12 for maintaining HSCs in the bone marrow (Greenbaum et al., 2013). BMSCs, however, are highly heterogeneous, and I have demonstrated in chapter 3.2 that CM isolated from two phenotypically contrasting clonal lines can have vastly different impacts on cell migration, morphology and inflammatory gene expression. These functions were shown to be driven by heat-labile secreted factors, and thus I aimed to identify the differences in these factors between BMSC clones that were likely responsible for this variation in function.

There have been numerous studies that have investigated and compared the total secretomes and subcompartments such as extracellular vesicles produced by BMSCs, and even comparisons between stromal populations isolated from different tissues, undergoing differentiation or exposed to inflammatory cytokines (Anderson et al., 2016; Baberg et al., 2019; Kim et al., 2012; Lai et al., 2016; Maffioli et al., 2017; Mizukami et al., 2019). Collectively these studies and others have highlighted considerable heterogeneity in secretomes in different conditions, however, the interrogation of heterogeneity in secreted factors between BMSC subpopulations has been largely ignored. Considering the stark differences in potency between subsets it is possible that heterogeneity is reflected in their paracrine signalling. This work represents a novel approach to assess heterogeneity of BMSC subtype secreted factors by omics approaches using clonally derived BMSC lines. I compare expression of secreted proteins in BMSC CM between clones by a liquid chromatography tandem mass spectrometry (LC-MS/MS) approach. In comparisons I will refer to interrogation of the CM as total secretome, given that it will contain all secreted factors. I further investigate the contribution to the cell secretome that may be played by EVs. In addition to the use of the tripotent clone Y201, and the nullipotent clone Y202, I also

investigated the secreted factors in CM from Y101, an osteochondral restricted clone (James et al., 2015). This clone represents a more committed progenitor than Y201, capable of only bipotent differentiation capacity. Y101 sits between the other two clones in terms of potency, providing a useful comparison for identifying differences between potent and nullipotent subsets, as well as being able to compare differences between cells at different levels of the differentiation hierarchy.

4.1.2 Extracellular Vesicles

The term EV is used to refer to a number of bilipid-membrane encapsulated vesicles that bud from the surface of a cell and are released into the extracellular environment (Raposo and Stoorvogel, 2013). These vesicles are biologically distinguished through the pathways by which they are generated and are predominantly classed into 3 main groups (Raposo and Stoorvogel, 2013). EVs can vary in size, with apoptotic bodies generally the largest EVs (between 500-5000nm in diameter) that bud from the plasma membrane during cell-death. Microvesicles can be considerably smaller (100-1000nm) and are produced through budding directly from the plasma membrane. The final class of vesicle is the exosome (30-150nm), these form intracellularly in a multivesicular body (MVB), the MVB then fuses with the plasma membrane and releases the exosomes. There are various methods for isolation of extracellular vesicles with currently no single 'gold-standard' method, given the various benefits and trade-offs in accessibility, cost, ease of use and purity of isolation between methods such as ultracentrifugation, precipitation, size exclusion chromatography and sucrose density gradient centrifugation (Sidhom et al., 2020). The terms exosome and microvesicle are sometimes used in studies where vesicles are categorised purely by size, however, there is considerable overlap in possible sizes leading to inclusion of multiple EV types in preparations. There are currently no absolute markers of distinct EVs that suitably segregate different subtypes. In a position paper presented by the International Society for Extracellular Vesicles (ISEV) in 2018 it was recommended that the term EV be used where there lacked definitive proof of biogenesis pathway (Théry et al., 2018).

EVs are capable of transporting proteins, lipids and nucleic acids between cells, thus delivering powerful signalling cocktails, and the roles that EVs have in regulating functions in homeostasis and in disease is rapidly expanding. I therefore used an analogous LC-MS/MS approach to the total secretome interrogation to examine protein content in EVs of heterogeneous BMSC subtypes isolated by differential ultracentrifugation. As well as

functionality of EVs driven by protein content there has also been considerable interest in the role of miRNAs in driving BMSC EV functionality is of particular interest and so I used NanoString technology that uses fluorescence barcoded tags to directly quantify over 800 miRNAs without the need for amplification (Geiss et al., 2008). Both miRNA and EV protein interrogation revealed considerable differences in vesicle content, again highlighting how cellular heterogeneity is reflected in secreted factors that may impart varied functions.

4.1.3 The MSC secretome and MSC EVs as an avenue for cell-free therapy

Beneficial effects of MSCs are often ascribed to potent paracrine signalling mechanisms and considerable emphasis has now been placed on the development of these paracrine signals into cell-free therapeutics for a variety of diseases through the modulation of immune responses and regenerative medicine applications (Ranganath et al., 2012; Vizoso et al., 2017). There are numerous studies demonstrating the positive effects of the MSC secretome, and more recently, the effects of EVs. The use of vesicles for cell-free therapies is of increasing interest, with the native contents of vesicles shown to directly impart therapeutic benefits in models of disease and injury (Gnecchi et al., 2005; Kilpinen et al., 2013; Lai et al., 2010a; Lee et al., 2012; Qin et al., 2016; Zhang et al., 2019). Secreted factors and EVs provide an interesting avenue for MSC based therapy as they avoid many of the complications of rejection that can arise with cell-based therapies. Despite considerable interest in such treatments, the development of biologic therapies is complicated by variability in secreted cell products introduced by inter-donor and intra-donor variation. Here I present data from well characterized, clonal MSC lines with high level of reproducibility in their secreted products and phenotypes (James et al., 2015).

4.1.4 Aims

The role of BMSC secreted factors in driving functionality is well understood, however, the heterogeneity of BMSCs means that understanding of subpopulation secretomes is limited, and therefore understanding of subpopulation functions is equally limited. In this chapter I aimed to identify whether there were significant differences in the content of heterogeneous BMSC secretomes and whether any differences might reflect subtype functionality. Specific aims of this chapter were to

- Use LC-MS/MS approach to interrogate total secretome and EVs from heterogeneous BMSC subtypes and determine if there are differences in secreted proteins

- Use Nanostring analysis to identify differences in heterogeneous BMSC EV miRNA content
- Use bioinformatic approaches to infer functionality from any differences in secretomes

4.2 Results

4.2.1 Comparison of secretomes from three functionally distinct clonal lines

Using an LC-MS/MS approach I identified significantly different abundance of 201 proteins in pairwise comparisons of CM isolated from Y101, Y201 and Y202 clones (ANOVA, $p<0.05$) (Figure 4.1). Biological repeats from each clonal line clustered together in a heatmap of expression of these 201 proteins, with Y201 and Y202 segregated as the most divergent samples. The clustering of the Y101 clone indicated a greater level of similarity to Y201, however, the expression pattern of proteins in Y101 seemed to overlap with both Y201 and Y202. This was further made evident when comparing proteins that were significantly more highly abundant in one clone than the other two. Y201 and Y202 expressed 14 and 17 proteins at significantly higher levels than the other two clones respectively, while Y101 did not express any protein more significantly than *both* Y201 and Y202 (Table 4.1).

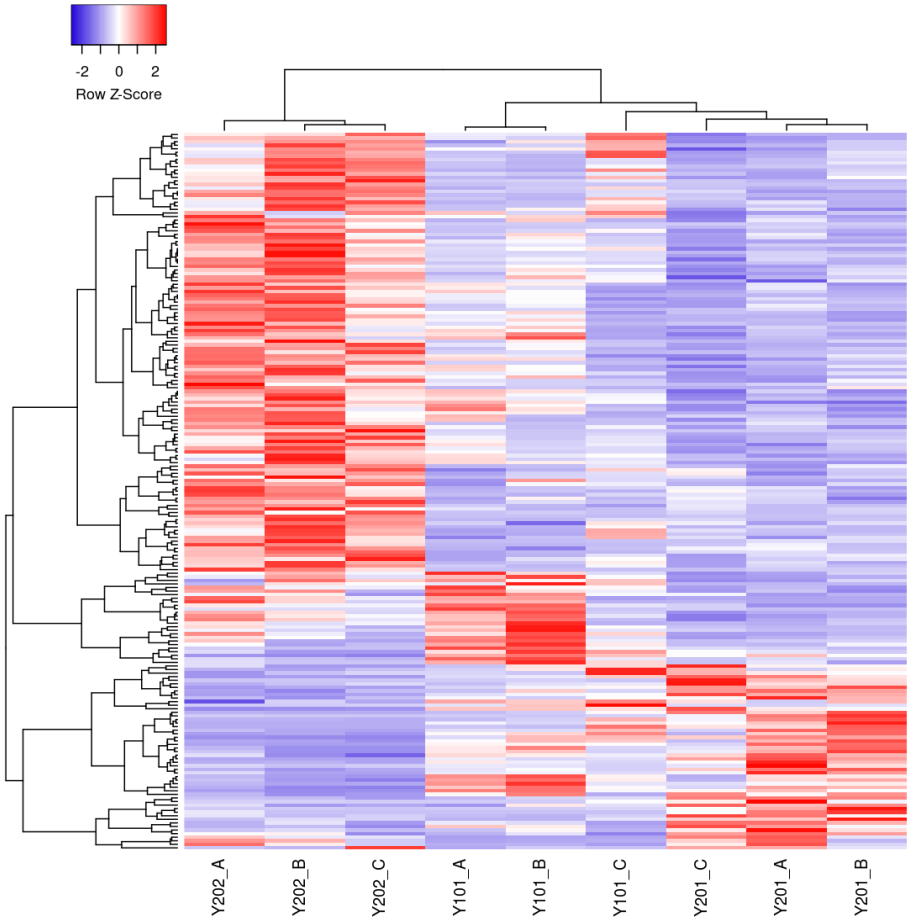

Figure 4.1 Heatmap of significant differences in protein expression between three clonal BMSC lines
Clustered heatmap of 201 proteins that were identified to have significant differences in expression between Y101, Y201 and Y202 from ANOVA tests in Progenesis QI ($p<0.05$). Colours are scaled according to Z-score from low abundance (blue) to high abundance (red). N=3 per clone.

Table 4.1 Table of proteins that were identified as significantly more highly expressed in one hTERT immortalised BMSC clone than the other two

Comparison of protein abundance	Proteins
Y201 > Y101 and Y202	ACAN, POSTN, C2, SERPINB2, TNFRSF11B, ADAMTS1, THBS2, ENPP2, MYLK, CYTL1, JAG1, BGN, THBS1, NOTCH2
Y202 > Y101 and Y201	QPCT, OLFML1, MATN2, NPR3, PDLIM1, EMILIN2, LUM, COL12A1, DKK3, ULBP2, AXL, COL5A2, CFH, HYOU1, FHL1, SCRN1, XPNPEP1
Y101 > Y201 and Y202	-

4.2.2 Comparisons of Y201 vs Y202 total secretome protein content

Given the stark polarisation between the Y201 and Y202 I further interrogated the proteins identified by LC-MS/MS from CM of these clones, identifying a total of 861 proteins across both lines. Of these proteins, 44 were significantly more abundant in Y201CM compared to 129 proteins upregulated in Y202CM (ANOVA, $p<0.05$). The log2 fold changes in expression of all proteins can be seen in the volcano plot in Figure 4.2 and fold-changes for significantly different proteins are available in Supplementary Table 1 and Supplementary Table 2. It was clear from this that aggrecan and periostin were highly enriched in Y201 versus Y202 secretome, and that this increase had a high level of statistical significance.

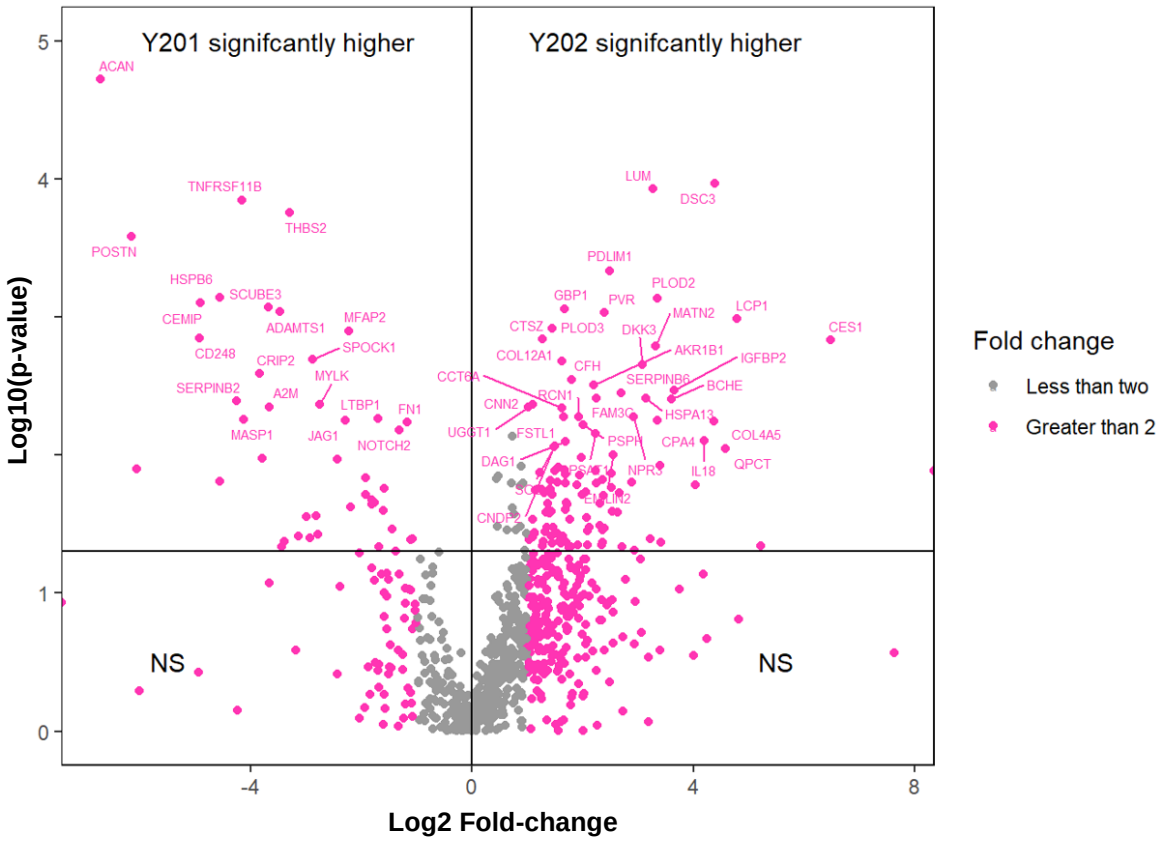

Figure 4.2 Volcano plot of proteins identified in conditioned media from Y201 and Y202 clonal lines

861 proteins were identified by LC-MS/MS in conditioned media from Y201 and Y202 clones. Shown are the log2 fold-changes of these proteins versus the p-value of their difference in expression. Proteins with a fold change >2 between cell lines are shown in pink with fold changes <2 are in grey. The two upper quadrants contain proteins that were determined as significantly different between Y201 and Y202 by ANOVA ($p<0.05$). This figure was made by Emma Rand.

The Y201 and Y202 cell lines were previously characterised by a microarray experiment comparing their gene expression to the parental primary donor population from which they were isolated, femoral head 181 (FH181) (James et al., 2015). Using this dataset I compared the expression level of the differently expressed proteins identified in Y201 and Y202 CM at the mRNA level (Figure 4.3). The heatmaps indicated a similar pattern of increased gene expression for the majority of significantly differently expressed proteins, corroborating the findings of the proteomics. Periostin and aggrecan were two of the most highly abundant proteins in Y201 with large fold-changes in expression, which is corroborated by the mRNA expression data indicating higher mRNA levels in Y201 clones. The cytokine interleukin-18 (IL18) was present at low level in CM in both clones, but with a

large fold-increase in abundance versus Y201 which is in agreement with the mRNA expression data.

The 44 proteins that were more highly expressed in the secretome of Y201 versus Y202 are presented in order of normalised abundance in Figure 4.4 to provide context of protein abundance to the fold-change data shown previously. The two most abundant of the 44 upregulated proteins in Y201 secretome, fibronectin and collagen type VI alpha chain 1 (col6a1), are structural components of the ECM. I also determined that periostin (POSTN) and aggrecan (ACAN) were the third and fourth most highly abundant proteins identified (Figure 4.4A) from the significantly upregulated proteins in Y201 vs Y202 secretome and presented with the largest log2 fold changes of 6.16 and 6.71 versus Y202 respectively (Supplementary Table 1). Alpha-2-macroglobulin (A2M), latent TGFβ binding protein 1 (LTBP1) and osteoprotogerin (OPG, also known as tumour necrosis factor 11B) were the highest expressed non-ECM structural proteins identified in Y201CM. Latent TGFβ binding protein 2 (LTBP2), a member of the same family as LTBP1 was also upregulated in Y201 secretome, albeit at around 13-fold lower abundance than LTBP1. The key haematopoietic chemokine CXCL12, a feature of a subset of BMSCs called CAR cells, was also identified in the secretome of Y201 at higher abundance than in Y202, with a log2 fold increase of 2.99, although there was no statistical significant difference between Y201 and Y101 in CXCL12 expression.

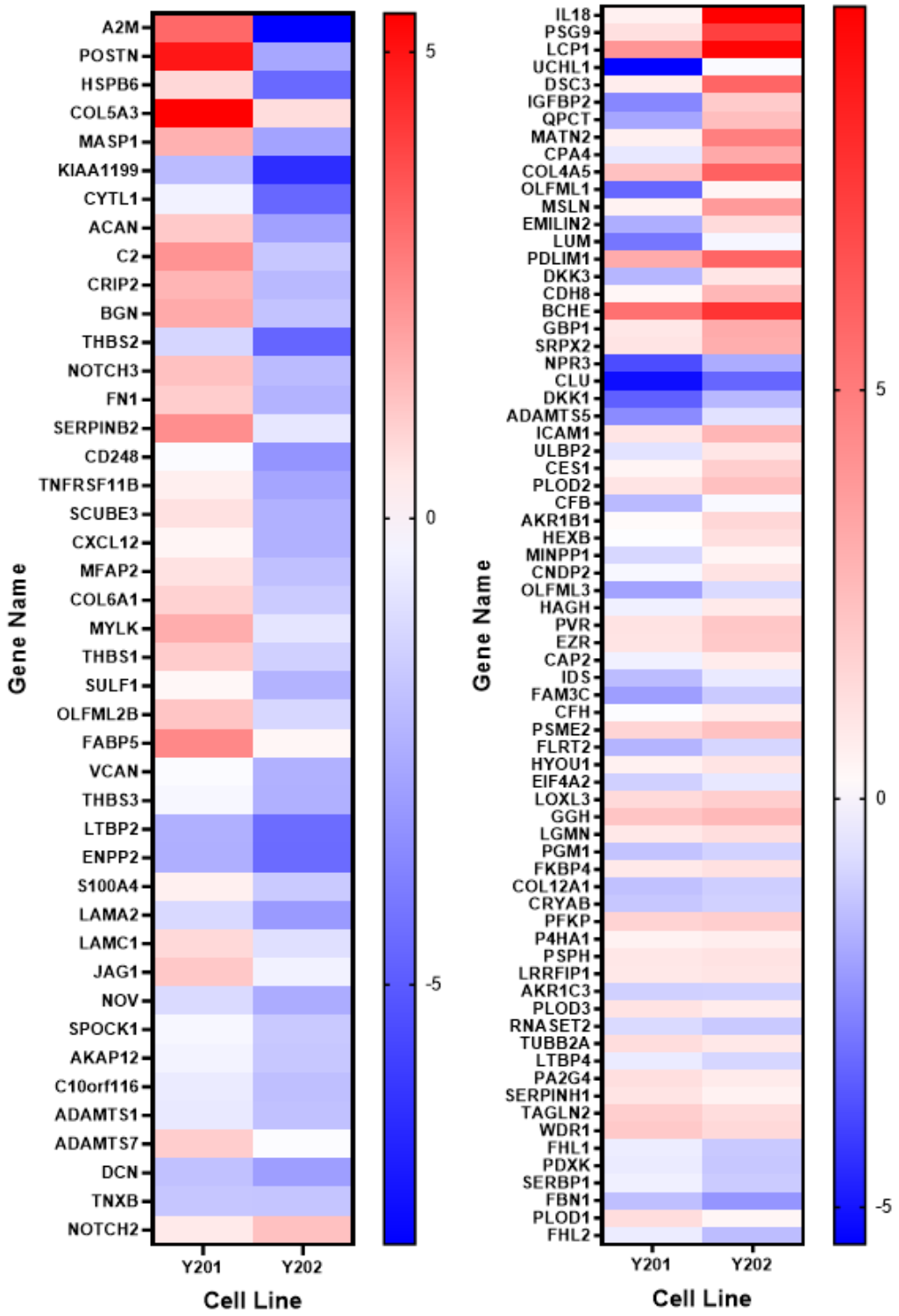

Figure 4.3 Heatmap of mRNA level expression for proteins significantly different at the protein level between Y201 and Y202

Heatmaps of gene expression data previously generated from a microarray comparing Y201 and Y202 mRNA. Gene expression is calculated as a Log2 fold-change against the parental primary cells (Femoral head sample 181). The gene expression data, where available, is shown for the proteins significantly more highly expressed in Y201 (left heatmap) and Y202 (right heatmap). Gene expression data was available for 43/44 proteins upregulated in Y201 secretome and 71/129 proteins upregulated in Y202 secretome.

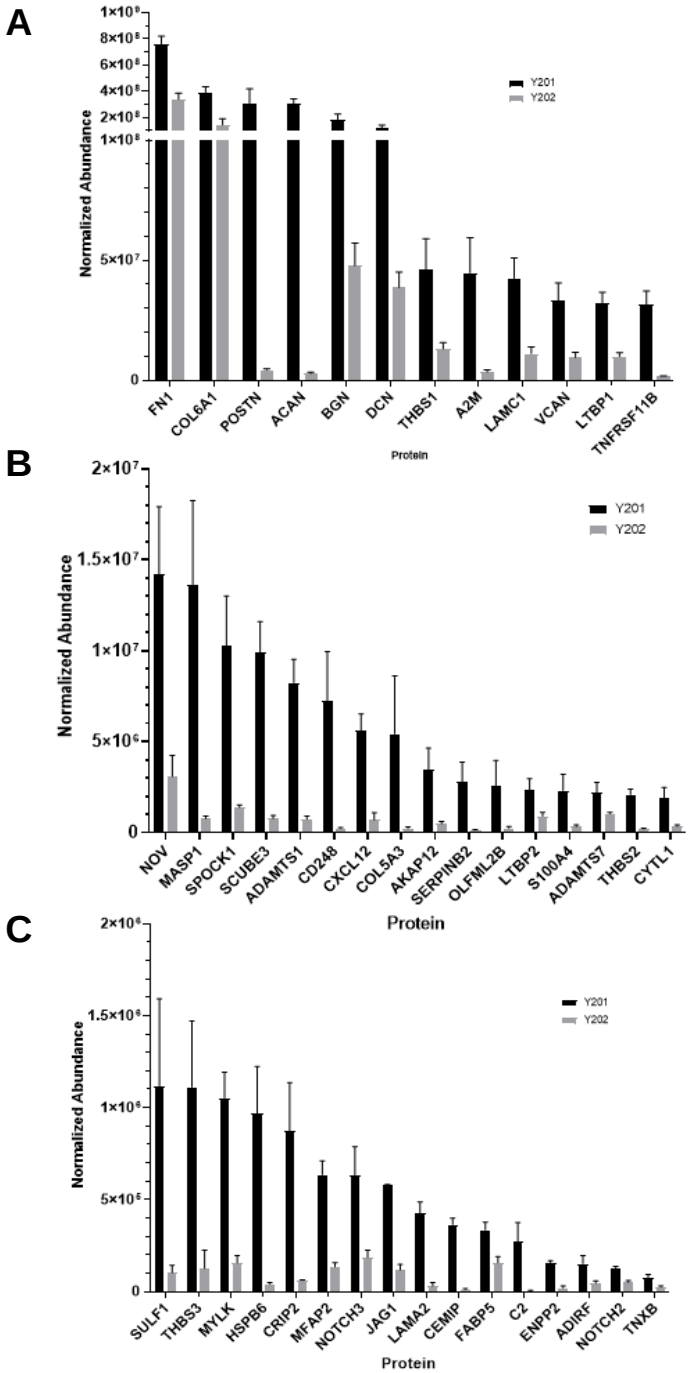

Figure 4.4 Normalized abundance of significantly differently expressed proteins from Y201 versus Y202 secretome

Mean normalized abundance of 44 proteins significantly more highly abundant (ANOVA, $p<0.05$) in Y201 secretome (black) compared to Y202 secretome (grey). Linear scale used across 3 axes to improve visualisation of differences and with proteins ordered by mean normalized abundance from highest to lowest. Axes are split by arbitrarily High (A), Medium (B) and Low (C) expression. N=3, error bars ± SE.

The 129 proteins significantly upregulated in the Y202 secretome are organised by mean normalized abundance in Figure 4.5. Like with Y201, the Y202 secretome also significantly enriched for some structural components of the ECM versus Y201. I detected a high abundance of fibrillin-1 (FBN1), although the log2 fold-increase was only 1.09, and lumican (LUM), another structural ECM protein, was the third most highly abundant of the 129 different proteins in Y202 secretome, with a significant log2 fold increase of 3.28 over Y201 (Figure 4.5A). Interestingly, the least abundant significantly upregulated protein in Y202 was dikkopf related protein 1 (DKK1) and this was identified with an infinite fold change, with no ions representative of DKK1 peptides identified from any Y201 sample during LC-MS/MS. Another of the DKK family, dikkopf related protein 3 (DKK3) was significantly upregulated in Y202 and was more highly abundant than DKK1. The other proteins in the latent TGFβ binding family, 3 and 4 (LTBP3 and LTBP4), were found at higher levels in Y202 secretome, in contrast to the high LTBP1 and LTBP2 in Y201 secretome, although only LTBP4 was significantly enriched (Figure 4.5C). Even though it was expressed at a low level, the IL18 was significantly upregulated in Y202 with a log2 fold change of 4.2. Overall the analysis of Y202 secretome indicated a greater number different proteins enriched, however, a large proportion of these proteins were found at a low total abundance (Figure 4.5B&C).

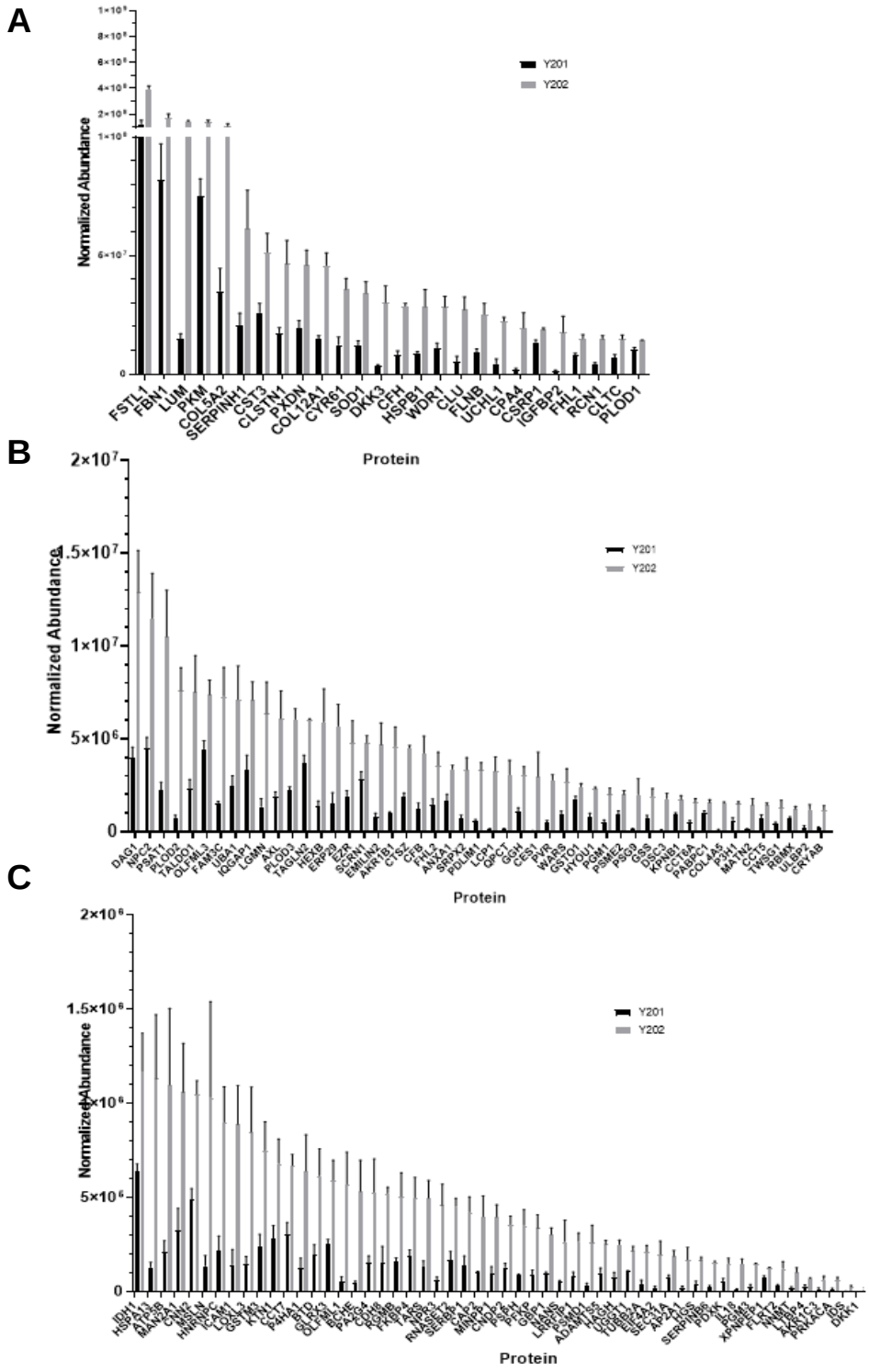

Figure 4.5 Normalized abundance of significantly differently expressed proteins from Y202 versus Y201 secretome

Mean normalized abundance of 129 proteins significantly more highly abundant (ANOVA, $p<0.05$) in Y202 secretome (grey) than Y201 secretome (black). Linear scale used with separation to improve visualisation of differences across the range and with proteins ordered by mean normalized abundance from highest (top) to lowest (bottom). N=3, error bars ± SE.

4.2.3 GO term and KEGG pathway enrichment for differently secreted proteins

GO term enrichment and clustering was performed using the ClueGo plugin in Cytoscape for the 44 and 129 proteins that were significantly more highly expressed in Y201 and Y202 secretomes respectively. Clustering of significantly enriched terms from the "Biological Process" and "Molecular Function" ontologies revealed that the most significantly enriched terms for the more abundant Y201 secreted proteins related to involvement in the ECM (Figure 4.6A). The "proteoglycan metabolic process" and "glycosaminoglycan heparin binding" clusters are indicative of ECM functions. The specific node corresponding to the GO term "extracellular matrix organisation" was also identified in the network of GO terms enriched for by the 129 more abundant Y202 secreted proteins, although with a smaller number of contributing proteins, shown by the smaller node-size, and an overlap with basement membrane organisation (Figure 4.6B). The "ascorbic acid amino modification cluster" indicates a potential difference in extracellular protein modification capacity. It was also noted that GO terms related to immune-cell-related pathways were clustered within the cell-lipoprotein particle cluster and that the "interleukin-12 mediated signalling pathway" was un-clustered but with a high degree of significance ($p<0.0005$).

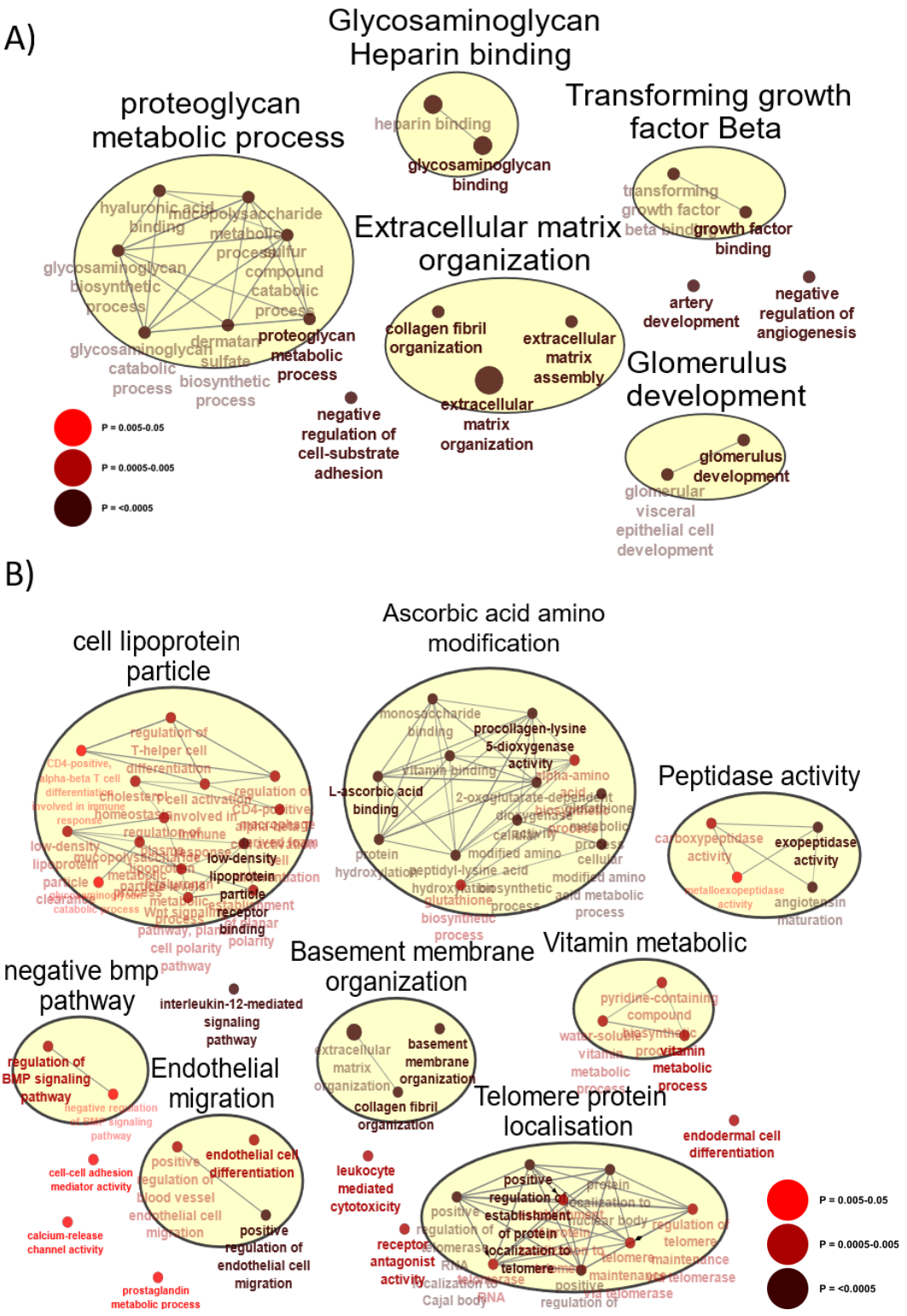

Figure 4.6 GO-term enrichment of differentially upregulated proteins in Y201 and Y202 secretome

A network view of the Gene Ontology Biological Process and Molecular Function terms (red nodes) that were significantly enriched (FDR corrected p<0.05) for the 44 proteins significantly more abundant in the secretomes of Y201 (A) and the 129 proteins significantly more abundant in Y202 (B). Size of the red circular nodes is relative to the number of proteins identified. Yellow circles with black headers indicate clusters of similar GO terms. Size of individual nodes increases relative to the number of proteins from that overlapped in the respective GO term. Darker nodes indicate a smaller p-value. Links between terms in the GO-term hierarchy are shown by grey lines.

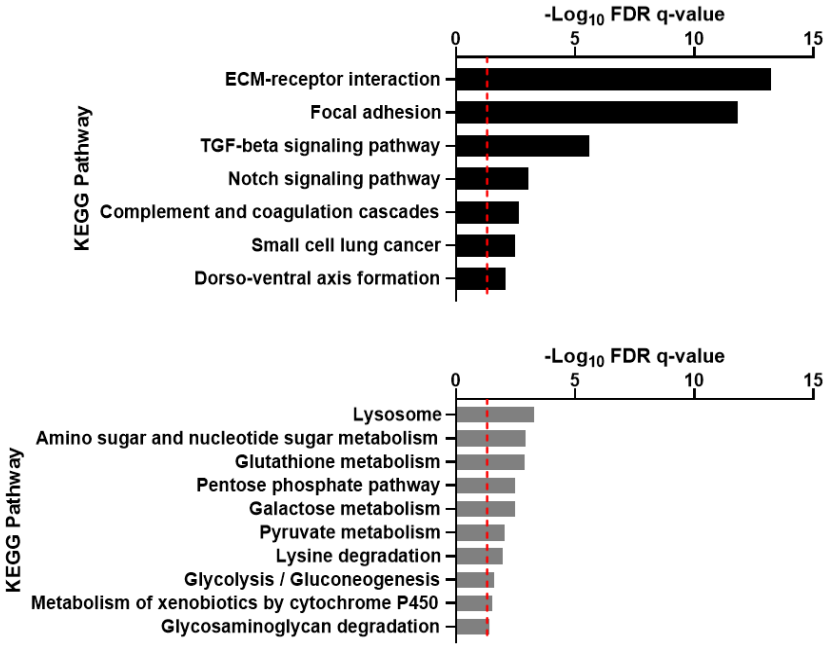

Figure 4.7 KEGG pathway enrichment for proteins significantly more abundant in Y201 versus Y202 secretome

The 44 significantly more abundant Y201 and the 129 proteins significantly more abundant in Y202 secretome proteins were analysed for their enrichment in the KEGG biological pathway database to determine potential functionality. Seven pathways were enriched in Y201 (black) and ten in Y202 (grey) . Enrichment was performed using the molecular signatures database server and ordered by False Discovery Rate corrected p-value (q). Red line indicates where q=0.05.

Potential functionality of the differently secreted proteins was interrogated further using KEGG Pathway enrichment for the 44 and 129 differently abundant Y201 and Y202 proteins respectively (Figure 4.7). The more abundant Y201 secreted proteins revealed a high level of enrichment for the cell matrix and adhesion related pathways “ECM-receptor interaction” and “Focal adhesion” ($p=6.24x10^{-14}$ and $1.45x10^{-12}$ respectively). KEGG enrichment also highlighted the “TGF-beta signalling” and “Notch signalling” pathways. The more abundant proteins in Y202 secretome enriched for various KEGG metabolic pathways and with the lysosome pathway, all at a low significance.

4.2.4 Matrisome enrichment of Y201 and Y202 conditioned media proteins

The recurring references to ECM in GO-term and KEGG pathway enrichment was investigated further by comparing all proteins identified in LC-MS/MS of Y201 and Y202 secretome against the matrisome database (Naba et al., 2012). This is a curated database of human proteins known to contribute to or associate with ECM through either structure, interaction or regulation. From 861 identified proteins in soluble secretome, 175 (20.3%) were annotated in the matrisome, with 85 labelled as “core matrisome” and 90 “matrisome associated**” (**Figure 4.8**).** Assuming that all proteins were equally likely to be upregulated in Y201 or Y202 I would expect 8.9 matrisome associated proteins to be enriched in the 44 significantly upregulated Y201 secreted proteins and 26.2 from the 129 upregulated Y202 proteins. Chi-squared tests revealed a significant enrichment for observed matrisome annotated proteins in Y201 (28/44) significantly upregulated proteins (χ^2 = 50.97, d.f.= 1, p<0.0001) whereas Y202 significantly upregulated proteins (25/129) did not differ from expected amounts (χ^2 = 0.1576, d.f. = 1, p = 0.69). Of the 175 matrisome proteins in total secretome 122 proteins did not differ significantly between Y201 and Y202, and the relative abundances and log2 fold changes in these proteins is shown in Supplementary Table 5.

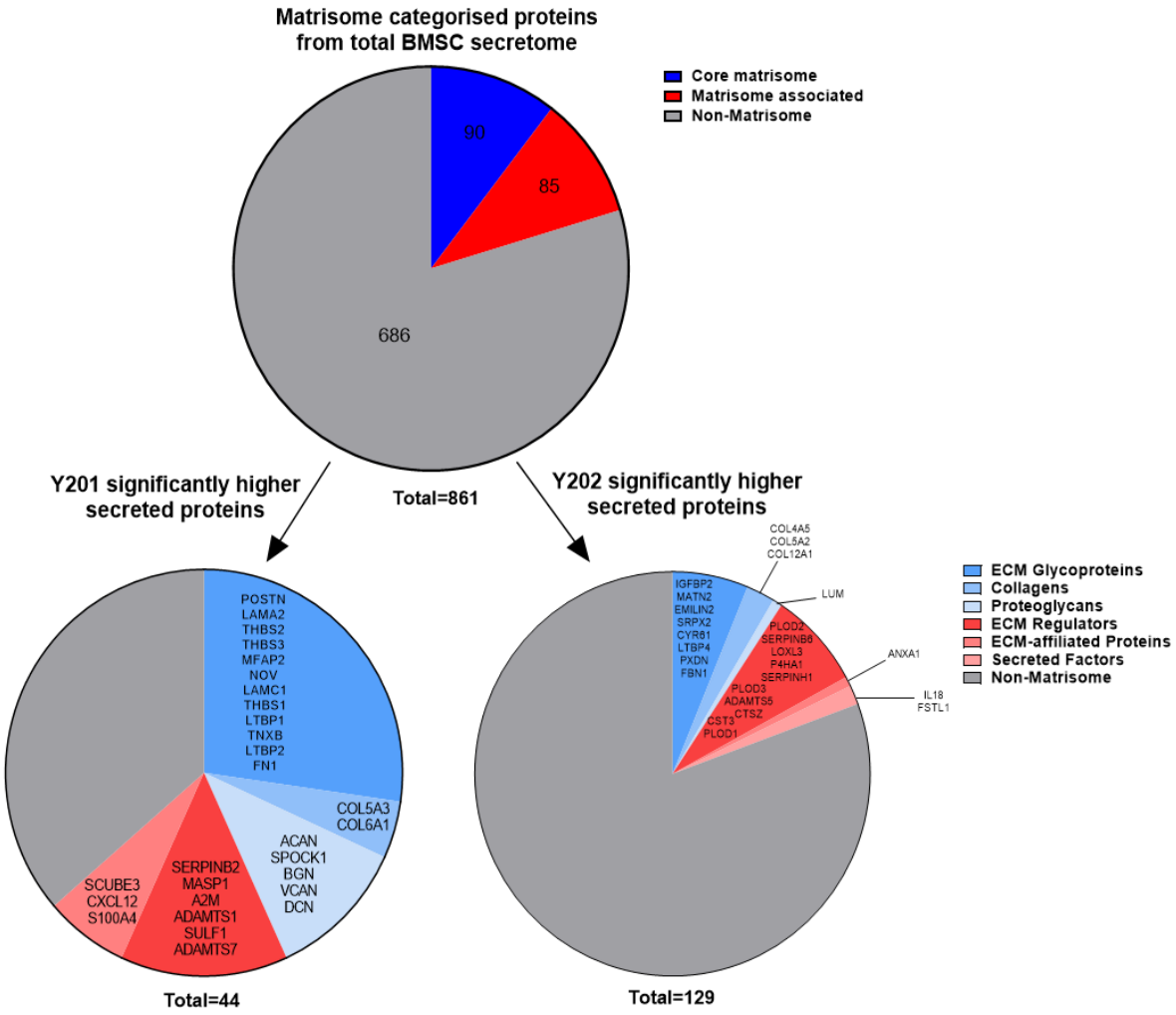

Figure 4.8 Relative contribution of matrisome proteins in total secretome of Y201 and Y202

Proportional contribution of proteins annotated in the matrisome database and shown by the categories “Core matrisome” (blue), “Matrisome associated” (red) and “Non-Matrisome” (grey) among all proteins identified in proteomic analysis of BMSC secreted protein (TOP). Annotation of proteins by matrisome categories in the significantly more abundant proteins found in the secretome of Y201 (bottom left) and Y202 (bottom right) secretome. The categories of core matrisome proteins (light blues) and matrisome associated proteins (light reds) are broken down into subgroups in the bottom pie charts. Proteins contributing to each subgroup are shown on charts.

4.2.5 Characterisation of EVs from Y201 and Y202 BMSC clones

Total secretome proteomics demonstrated stark differences in protein content between Y201 and Y202, however, the contribution of EVs to the secretome may be underappreciated in these data and I therefore isolated EVs by differential ultracentrifugation to identify differences in EVs between Y201 and Y202. The presence of EVs secreted by Y201 and Y202 cells was confirmed by TEM after EV isolations. These images revealed presence of cup shaped vesicles from both cell lines that were between 80 and 150nm in size (Figure 4.9).

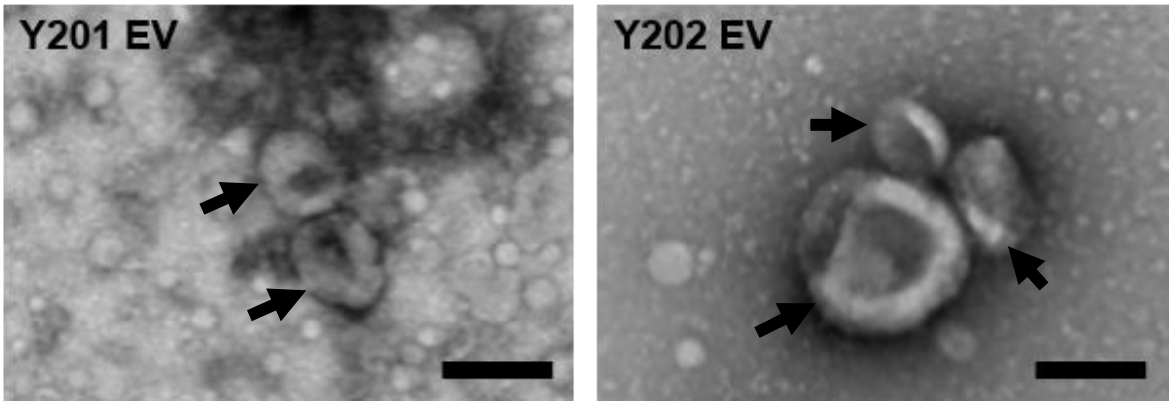

Figure 4.9 TEM of EVs isolated from Y201 and Y202
Transmission electron micrographs of EVs (arrows) isolated by ultracentrifugation of conditioned media from Y201 (left), Y202 (right). Scale bars = 100nm.

Size distribution of EVs was determined by NTA and revealed a modal peak at 84.5nm in Y201 EVs (Figure 4.10). In contrast, Y202 EVs presented a multimodal distribution with two prominent peaks at 74.5nm and 98.5nm. Both Y201 and Y202 EVs presented a prominent shoulder at around 140nm in size, with overall size distribution of samples appearing similar with the majority of EVs being detected at less than 250nm in size for both clones.

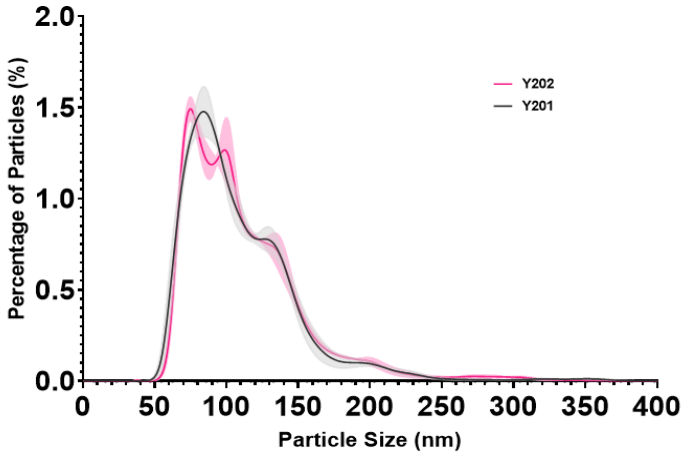

Figure 4.10 Nanoparticle tracking analysis of EVs from Y201 and Y202
Size distribution of EVs calculated by Nanoparticle Tracking Analysis normalized by percentage of total particles Y201 (Black) and Y202 (Pink). Vesicle sizes were binned in 1nm size increments beginning at 0.5nm. N=3, shaded area is ± SE.

The proteins identified in our total secretome using LC-MS/MS were likely to contain EV associated proteins and equally the isolations of EVs were likely to pull-down associated secreted proteins that may bind to the surface or be encapsulated within EVs. To provide a general indication of overlap between the total secretome and the EV protein contents I used the FunRich tool to compare the lists of proteins identified in the EV and total secretome experiments. This revealed that 326 proteins were identified in both EV and total secretome, whereas there were 333 and 535 proteins uniquely identified in EV and total secretome respectively (Figure 4.11A). I compared the proteins identified by our LC-MS/MS experiment against lists available in the FunRich analysis programme imported from the VesiclePedia database. I compared datasets that were derived from experiments using cells registered under the term “bone marrow mesenchymal stem/stromal cells” or “mesenchymal stem cells”, revealing that 325/659 of all proteins had been previously identified in other proteomic experiments investigating similar cell types (Figure 4.11B).

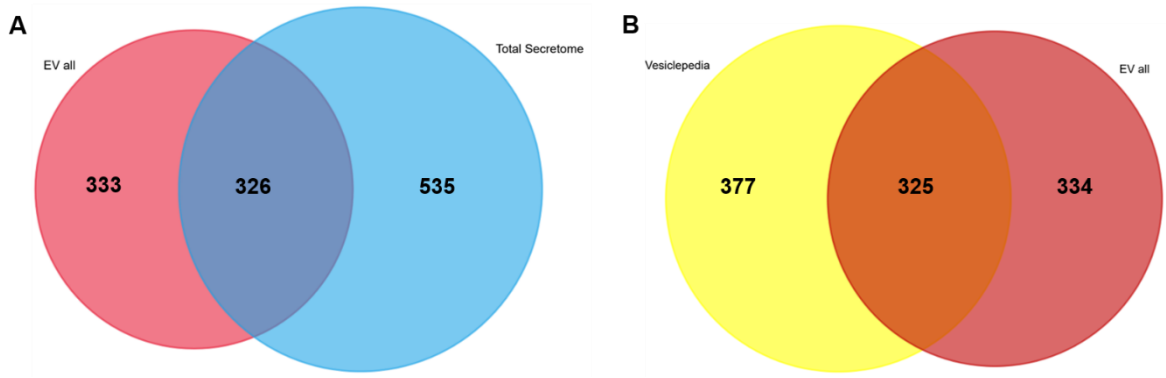

Figure 4.11 Comparisons of proteins in EV isolations versus total secretome and curated EV proteomic databases

Venn Diagrams demonstrating overlap between A) all proteins identified from total secretome (blue) and EV isolations from the hTERT immortalised BMSC lines (red) and B) proteins from public datasets identified in previously performed proteomic experiments investigating mesenchymal stromal/stem cell EVs listed in the Vesiclepedia database (yellow) and the proteins identified in our EV proteomics (red).

4.2.6 EV proteomics from Y201 and Y202

EVs isolated from Y201 and Y202 cells were analysed by LC-MS/MS to determine protein content. A total of 663 proteins were identified across all samples with a significant increased abundance of 162 proteins in Y201 EVs versus 14 proteins upregulated in Y202 EVs (ANOVA, $p<0.05$) (Figure 4.12). Relative log2 fold changes for the significantly different proteins are available in Supplementary Table 3 and Supplementary Table 4.

In the EV fraction there was evidence for a large number of membrane bound proteins, including the identification of integrins alpha-1, -3, -4, -5, -6, -7, -8, -v, and beta-1, -3 and -5 between all samples. Of these integrins only itgα11, itgα4 and itgα7 were significantly differently expressed between samples (all higher in Y201, $p<0.05$). It was also noted that the cytokine transforming growth factor beta 1 (TGFβ1) was detected with a significantly higher abundance in Y201 EVs, with a log2 fold-increase of 2.47. The ECM protein matrillin-2 (MATN2), which was observed to be increased in total secretome of Y202, was also significantly more abundant Y202 EVs, with a log2 fold-increase of 4.08 in EVs and 3.31 in total secretome.

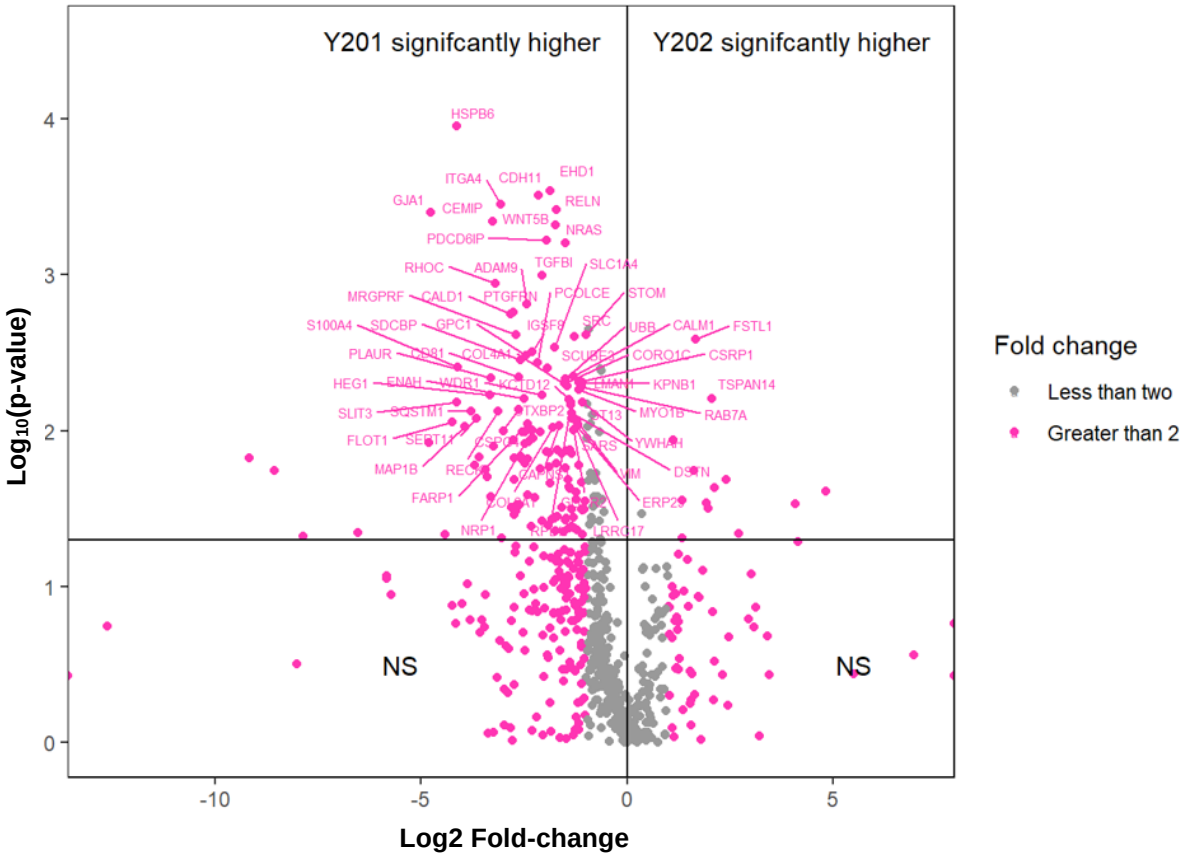

Figure 4.12 Volcano plot of proteins identified in EV isolations from Y201 and Y202 clonal lines

Volcano plot of fold change for the 663 proteins identified from LC-MS/MS analysis of extracellular vesicles isolated from Y201 and Y202. Proteins with a fold change >2 between cell lines are shown in pink with fold changes <2 in grey. The two upper quadrants contain proteins that were significantly different between Y201 and Y202 as determined by ANOVA ($p<0.05$). This figure was produced by Emma Rand.

4.2.7 Gene Ontology and KEGG pathway enrichment for Y201 upregulated EV proteins

GO term enrichment using the 162 proteins significantly more abundant in Y201 EVs versus Y202 EVs revealed significant enrichment for 307 GO terms (FDR-corrected $p<0.05$). Complexity of this network was reduced by clustering of terms based upon similarity (Figure 4.13). This revealed a number of small clusters of terms with highly significant FDR corrected p-values ($p<0.0005$) associated with “Extracellular matrix organisation”. Around this cluster were other significantly enriched terms associated with the ECM including “collagen fibril organisation”, “extracellular matrix disassembly” and “proteoglycan glycosaminoglycan process”. The “adhesion cell substrate” cluster contained the largest number of significantly enriched GO terms with 23. There were also strongly significant clusters associated with “myeloid immune leukocyte” and “axon morphogenesis”. Subsequent KEGG pathway enrichment corroborated findings from GO-term clustering by highlighting the “Focal adhesion” and “ECM-receptor interaction” pathways as the most significantly enriched terms of the 50 that were identified (Figure 4.14). The 14 proteins more abundant in Y202 EVs did not enrich for any GO terms or KEGG pathways ($p>0.05$). Other cell-substrate and cell-cell binding pathways were also enriched including “Adherens junction”, “tight junction” and “gap junction”.

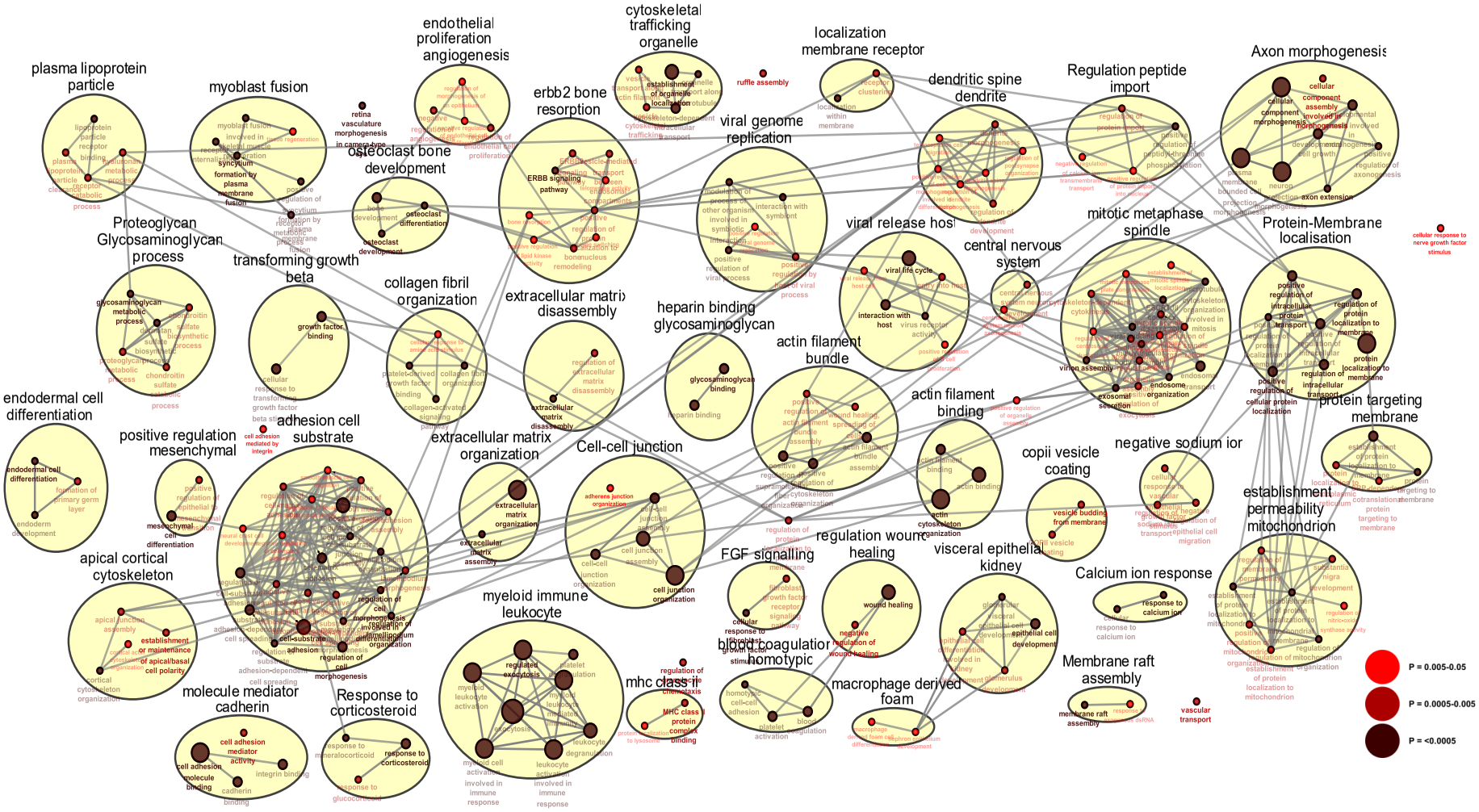

Figure 4.13 GO term enrichment and clustering for proteins significantly enriched in Y201 EVs
Clustered network of significantly enriched (FDR corrected p<0.05) Biological process and Molecular function GO terms (Red nodes) for the 162 proteins that were significantly more abundant in Y201 EVs. Relationships between GO terms are demonstrated by adjoining grey lines. Yellow circles with black headers encapsulate GO terms clustered by similarity in ClueGO. The size of a node is relative to the number of proteins from the 162 that overlap with the pathway. Significance of enrichment is shown by colour of the node with darker red from more significant terms.

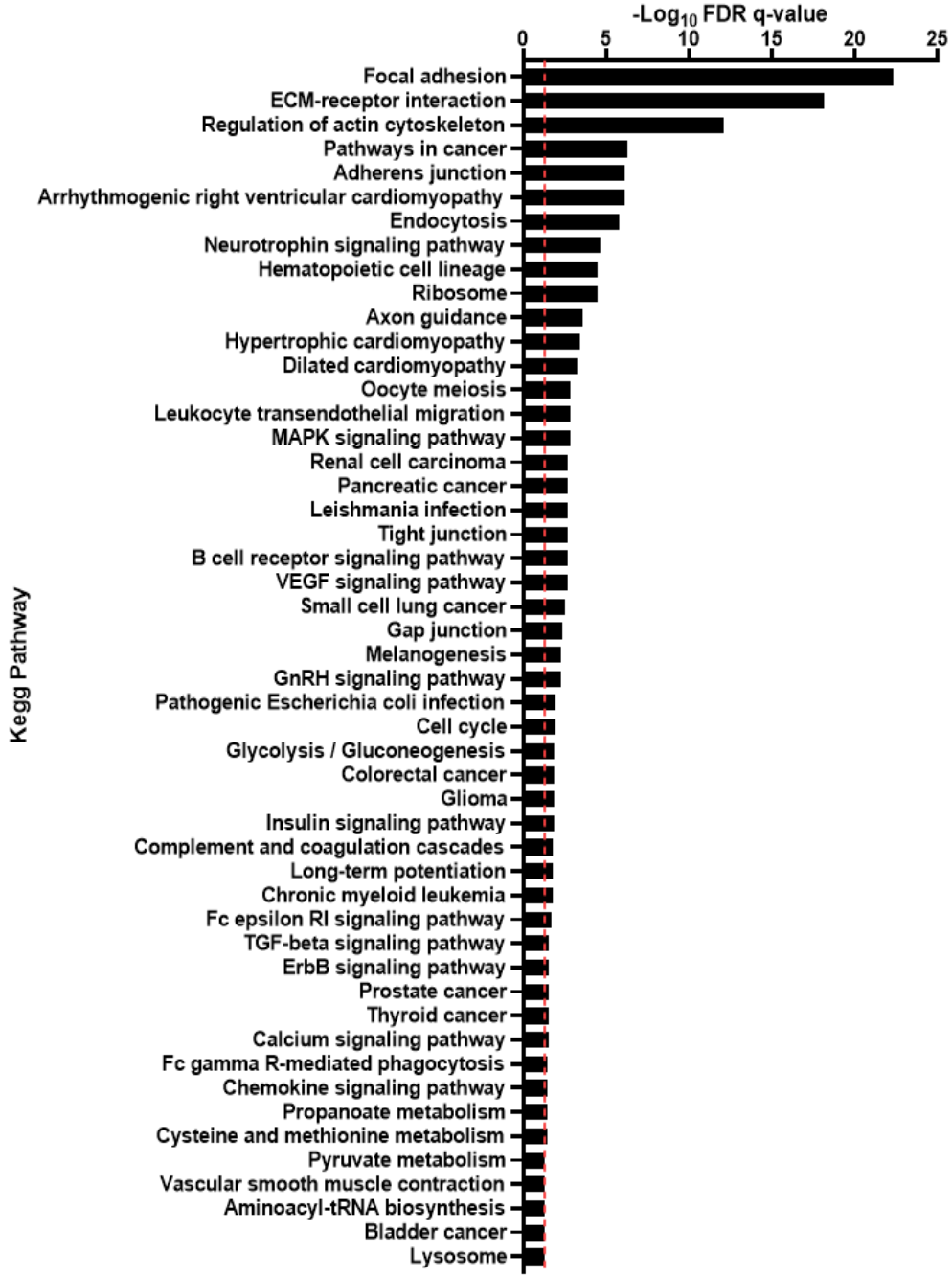

Figure 4.14 KEGG pathway enrichment for proteins significantly more abundant in Y201 versus Y202 EVs

50 significantly enriched KEGG pathways (FDR corrected p-value <0.05) from the 162 proteins identified as significantly more abundant in Y201 EVs. Red line indicates where $-Log_{10}(0.05)$.

4.2.8 Comparison of miRNA quantification from Y201 and Y202 EVs

I investigated the miRNA content of EVs from Y201 and Y202 using Nanostring technology that utilises fluorescence barcoding and absolute counts of detected miRNAs without amplification. Counts of 828 different miRNAs compared between Y201 and Y202 EVs revealed significant upregulated expression for 10 different miRNAs from Y201 EVs versus 2 from Y202 EVs ($p<0.05$) (Figure 4.15). The relative fold changes between EVs are shown in Table 4.2 along with their mean counts. The largest fold change in Y201 EVs was found in miR-100-5p while miR-6721-5p presented the largest fold increase in Y202 EVs respectively. Two of the three miRNAs comprising the highly conserved miR-29 family (miR-29a-3p and miR-29b-3p) were upregulated in Y201 EVs. Of the miRNAs upregulated in Y201, miR-125b-5p presented with the highest mean miRNA count, however, it had a low relative fold-change compared to other miRNAs, only 3.31-fold higher than Y202.

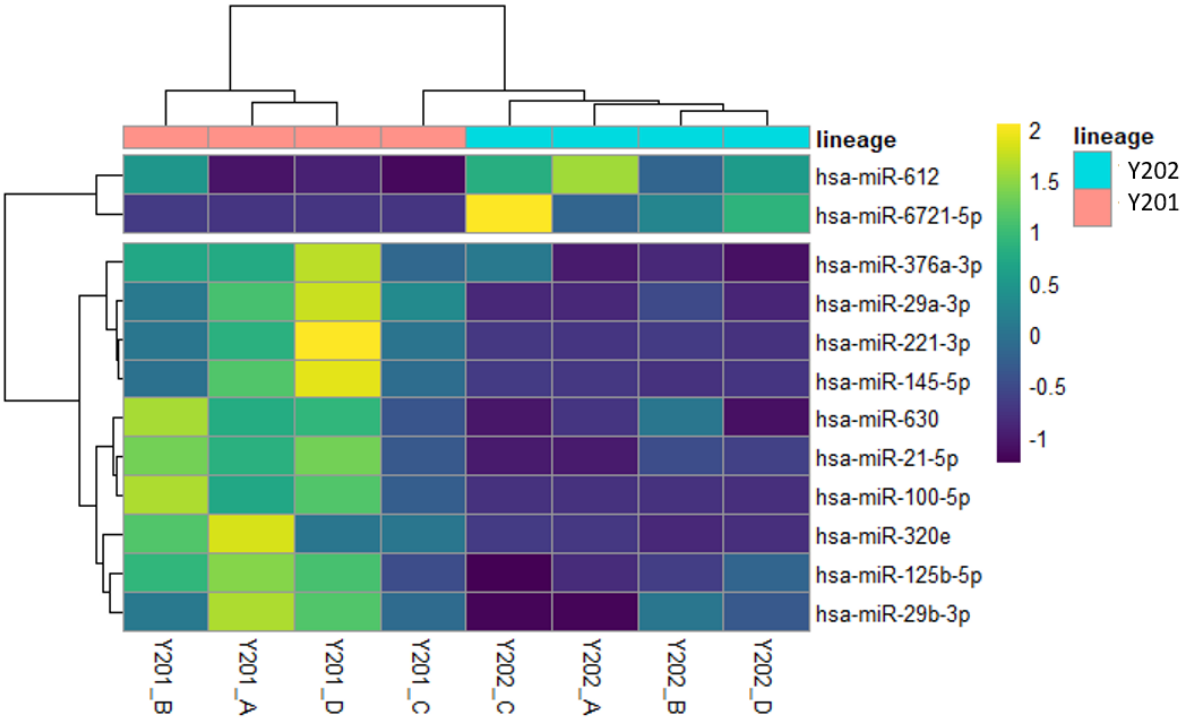

Figure 4.15 Heatmap of differently expressed miRNAs from Y201 and Y202 EVs
Clustered heatmap of 12 significantly differently expressed miRNAs identified in EVs after Nanostring miRNA quantification between Y201 (pink cluster) and Y202 (blue cluster) cells. 10 miRNAs were upregulated in Y201 EVs versus 2 in Y202 EVs. N=4, ANOVA, $p<0.05$. Colour scale is representative of z-score.

Table 4.2 Relative fold changes for miRNAs identified as significantly different between Y201 and Y202 EVs.

miRNA	Mean count Y201 (±SEM)	Mean count Y202 (±SEM)	Fold change Y201 vs Y202
hsa-miR-376a-3p	33.07 ± 6.23	8.49 ± 4.5	3.90
hsa-miR-29a-3p	91.92 ± 19.98	8.39 ± 4.82	10.96
hsa-miR-221-3p	65.9 ± 19.89	4.49 ± 1.04	14.68
hsa-miR-145-5p	56.1 ± 17.39	3 ± 0.8	18.70
hsa-miR-630	85.3 ± 18.84	19.7 ± 11.95	4.33
hsa-miR-21-5p	138.21 ± 29.8	22.01 ± 10.38	6.28
hsa-miR-100-5p	90.94 ± 21.93	3.89 ± 0.6	23.38
hsa-miR-320e	30.11 ± 7.73	3 ± 0.8	10.04
hsa-miR-125b-5p	481.61 ± 94.95	145.49 ± 50.14	3.31
hsa-miR-29b-3p	67.84 ± 14.2	22.08 ± 10.63	3.07
hsa-miR-612	27.29 ± 11.89	68.7 ± 11.1	0.40
hsa-miR-6721-5p	1.33 ± 0.28	24.47 ± 7.54	0.05

4.2.9 Bioinformatic analysis of Y201 and Y202 EV miRNA targets

I used the TargetScan miRNA target prediction algorithm to identify possible targets for the collectively upregulated miRNAs from both Y201 and Y202 EVs. The 10 miRNAs upregulated in Y201 produced 378 predicted targets while the 2 Y202 miRNAs targeted a possible 743 mRNAs (total-context++ -<0.6). The list of potential targets for each miRNA was collectively assessed for GO term enrichment. The most significantly enriched GO terms ($p<0.0005$) with the largest number of overlapping genes were “extracellular matrix organisation” and “vasculature development” indicating a downregulation of these pathways if truly targeted by the miRNAs (Figure 4.16). Clustering of like terms indicated that control of extracellular matrix was a strongly overlapping target with the cluster “Extracellular matrix PDGF” containing highly enriched terms. The same identified targets were also used to test for enrichment in the KEGG pathway databases. I found further enrichment for the “Focal adhesion” and “ECM-receptor interaction” pathways (Figure 4.17). Despite having a greater number of predicted targets the Y202 EV miRNA targets did not collectively enrich for any GO terms, however, when compared against KEGG pathways, six pathways were enriched at low significance, with the “Cell adhesion molecules” pathway most significant.

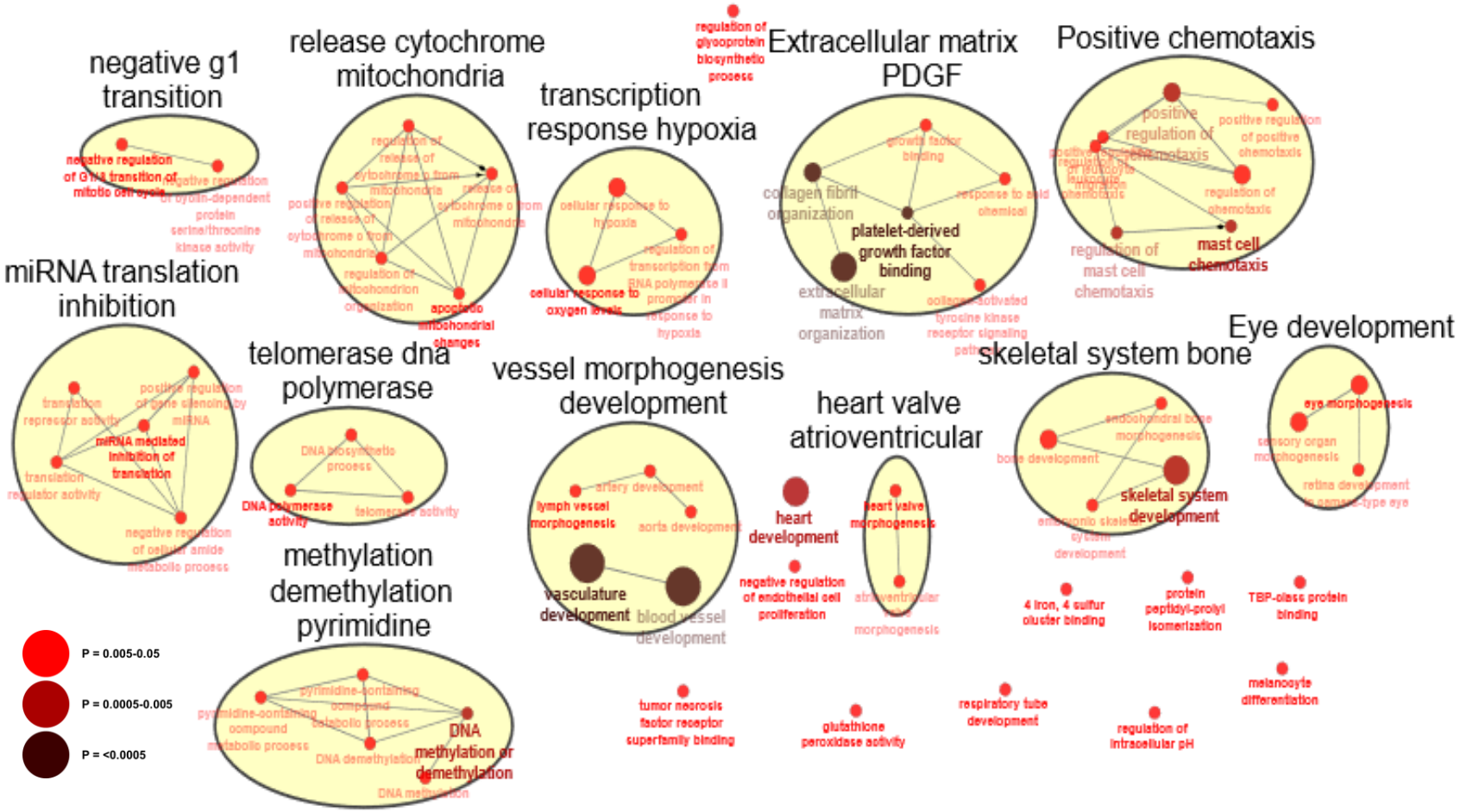

Figure 4.16 GO term enrichment and clustering for predicted targets of miRNAs significantly enriched in Y201 EVs

Clustered network of significantly enriched (FDR corrected p<0.05) Biological process and Molecular function GO terms for the 377 targets of the 10 miRNAs that were significantly more abundant in Y201 EVs. Yellow circles with black headers indicate terms collated by similarity. The size of each node is relative to the absolute number of proteins from the 378 miRNA targets that overlap with that pathway. Relative significance of enrichment is shown by colour of the node with an increasingly darker reds indicating a smaller p-value.

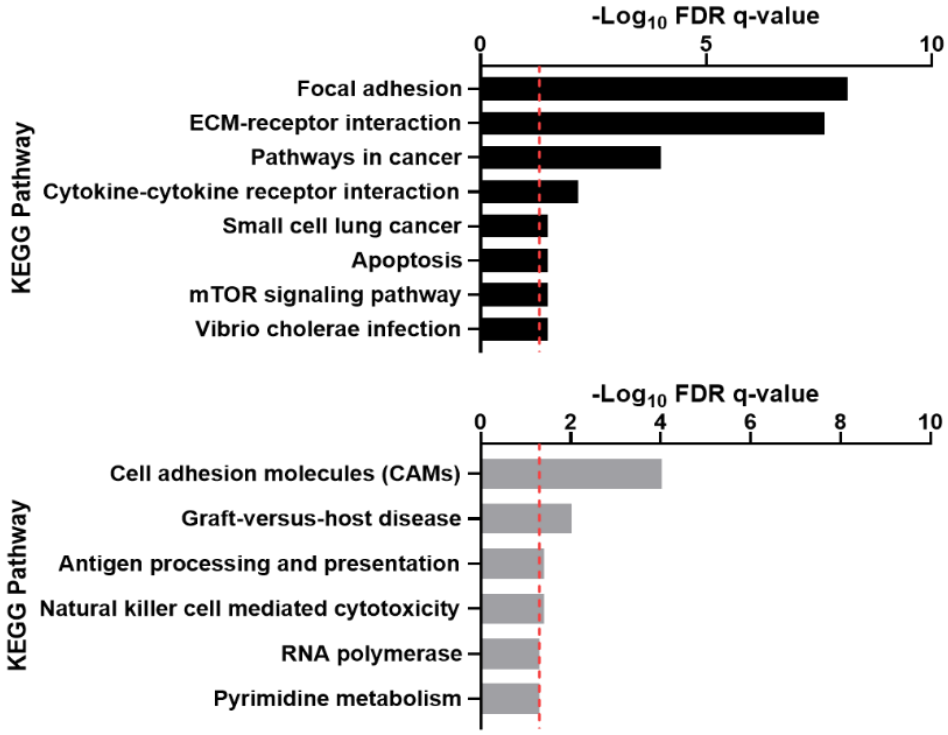

Figure 4.17 KEGG pathway enrichment for predicted targets of miRNAs that were more abundant in Y201 vs Y202 EVs

Significantly enriched KEGG pathways (FDR corrected q-value < 0.05) for genes that were predicted targets of the 10 miRNAs that were more abundant in Y201 EVs (Top, Black) and Y202 EVs (Bottom, grey) as determined by Nanostring. Red line marks q < 0.05. q = FDR corrected p-value.

EVs secreted into the local microenvironment during *in vitro* culture may be taken up by cells and therefore deliver miRNAs in an autocrine fashion. I hypothesised that predicted targets identified from Y201 EV miRNAs would show reduced expression at the protein level in Y201 cells versus Y202 cells due to autocrine action of miRNAs. Of the 378 predicted targets of miRNAs upregulated in Y201 EVs, 26 were also detected by LC-MS/MS in the CM of Y201 and Y202 (section 4.2.2). Of these 26 proteins, 14 were included in the KEGG pathway "ECM-receptor interaction". I assessed whether these 14 proteins were significantly decreased in expression as hypothesised and demonstrated that col4a5, fam3c, col3a1, fbn1 and col5a3 were significantly different in abundance at the protein level between Y201 and Y202 ($p<0.05$) (Table 4.3). Col5a3, despite being a target of miRNAs secreted by Y201, was upregulated in Y201 (23.59-fold increase vs Y202), however, fbn1, col3a1 and fam3c were all significantly more abundant in Y202.

Table 4.3 Comparisons of miRNA predicted targets versus their fold-change in expression in MSC secretome

A comparison between 26 TargetScan predicted miRNA targets and their Total context++ scores identified from miRNAs that were significantly more abundant in Y201 EVs and the fold-change in abundance for those proteins that were also identified by LC-MS/MS in the total secretome of Y201 versus Y202 cells.

Protein	Targeting miRNA	Total context++ score	Proteomic Fold Change	Sig. diff Proteomics
COL4A5	miR-29-3p	-0.72	0.05	Yes
PSMA1	miR-630	-0.83	0.05	
FAM3C	miR-29-3p	-0.71	0.21	Yes
ATP6V1G1	miR-376-3p	-0.53	0.31	
COL5A2	miR-29-3p	-0.94	0.32	Yes
COL3A1	miR-29-3p	-1.71	0.39	
GMFB	miR-145-5p	-0.82	0.40	
TPM3	miR-145-5p	-0.74	0.40	
TPT1	miR-145-5p	-0.73	0.45	
FBN1	miR-29-3p	-0.61	0.47	Yes
CCT4	miR-221-3p	-0.6	0.49	
FSCN1	miR-145-5p	-1.05	0.52	
VPS29	miR-376-3p	-0.75	0.54	
COL5A1	miR-29-3p	-0.87	0.78	
PDIA6	miR-376-3p	-0.55	0.91	
COL1A1	miR-29-3p	-2.76	0.96	
IFI30	miR-29-3p	-0.82	0.98	
COL4A1	miR-29-3p	-0.7	1.01	
HNRNPA0	miR-376-3p	-0.76	1.01	
SPARC	miR-29-3p	-0.75	1.02	
FKBP3	miR-145-5p	-0.6	1.06	
LOX	miR-29-3p	-0.8	1.17	
COL1A2	miR-29-3p	-1.1	1.19	
COL11A1	miR-29-3p	-0.8	1.57	
ADAMTS2	miR-29-3p	-0.77	1.94	
COL5A3	miR-29-3p	-0.73	23.59	Yes

4.3 Discussion

The data I have presented here gives strong evidence for the importance of understanding BMSC heterogeneity, given the considerable variation in cell secreted factors between phenotypically distinct subtypes. There have been a number of studies that investigated by proteomic analysis the secretome and EVs of BMSCs and other stromal subtypes under native conditions and following inflammatory cytokine exposure (Anderson et al., 2016; Baberg et al., 2019; Kim et al., 2012; Kshitiz et al., 2019; Lai et al., 2016; Maffioli et al., 2017). Here I have presented an alternative approach through the use of clonal BMSCs to demonstrate how the heterogeneity of primary/donor populations should be considered during studies of BMSC secretomes. This data indicates how better definition of subtypes is needed, particularly for use in deriving cell-free therapies from secreted products, and may help in the explanation of variation seen in experimental data by suggesting highly variable secretomes.

The Y201 and Y202 clonal lines are examples of highly contrasting BMSCs and this is clearly shown in the variation in secreted proteins produced by these lines. Interestingly, the Y101 line, which also demonstrates potency, also had a differing secretome to the Y201 and Y202, although was more similar to Y201 overall. This status as an overlapping and possibly transitional secretome between Y202 and Y201 suggests a change in secretory phenotype according to the level of potency beyond simply differentiation competent vs incompetent, and the use of proteins that differ between potent and nullipotent subsets may be useful for identification of potency markers.

Collectively the proteomic comparison of Y201 and Y202 cell secretomes across the total secretome and the EVs revealed a common theme of differences in ECM associated proteins. Of interest was the relative enrichment for different ECM proteins detected in the total secretome from the 2 lines, with Y201 upregulated proteins containing significantly more matrisome annotated proteins than would be expected. The ECM enrichment was also highlighted through GO and KEGG pathway enrichment. The striking upregulation of numerous ECM components in Y201 suggests that this cell subset may function as a matrix synthesising BMSC, capable of patterning the marrow through production of ECM proteins to create a supportive niche for BMSCs. The potential for Y201 ECM functions are of particular interest given its tripotent differentiation potential. It was also noted that not all ECM proteins differed significantly between stromal subsets, which could also be indicative of a “core” versus “functional” matrisome, with the proteins that

differ between subsets from these core proteins capable of driving aspects of cell phenotype.

Some Y201 upregulated ECM proteins were higher in expression than both Y101 and Y202, indicating that some ECM proteins may specifically play essential roles in the support of the tripotent MSC phenotype, such as aggrecan and periostin which were considerably more highly expressed in Y201 than the other clones. This also reveals the potential for ECM to be used as a biomarker to segregate BMSCs of varying differentiation competency. Equally, matrillin-2 and lumican were both expressed at higher levels in Y202 than Y201 and Y101, highlighting these as potential markers of nullipotent or inflammation responsive BMSCs. The differences in ECM protein abundance likely resulted in the differences in ECM structure and organisation seen by SEM in Figure 3.11 and could explain how conditioned media was capable of inducing migration in non-migratory BMSCs through differential abundance of migration promoting ECM components in the Y201CM.

Within the secreted protein data, significant fold-increases and high overall abundance were noted for ECM components periostin and aggrecan in the Y201 secretome. Periostin has a well-documented role in co-ordination of the ECM structure and the expression of it is known to be upregulated in response to TGFβ1 (Horiuchi et al., 1999; Norris et al., 2007). Among phenotypic differences in Y201 and Y202 the contrast in differentiation capacity is perhaps most striking, and the secretion of periostin may function in Y201 to facilitate osteogenic differentiation, having previously been linked to osteogenic potential of MSCs *in vitro* and to the control of osteogenic potential by periosteal stem cells *in vivo* (Coutu et al., 2008; Duchamp de Lageneste et al., 2018). Periostin has also been shown to be important for imparting tensile strength in tissues through regulating collagen fibrillogenesis, which could possibly explain why Y201 cells that secreted considerably more periostin produced a thicker and more complex ECM (see Figure 3.12), although experimental interrogation of these matrices would be required to demonstrate different biophysical characteristics (Norris et al., 2007). In a study of epithelial cell-derived periostin, collagen matrices produced through stimulation of the TGFβ signalling pathway by periostin resulted in stiffer matrices, and so this increased stiffness could be expected for Y201 ECM vs Y202ECM (Sidhu et al., 2010). Other proteins significantly upregulated in Y201 secretome have been associated with positive (CEMIP, BGN, THBS2, JAG1) and negative (THBS1) regulation of osteogenic differentiation (Bailey Dubose et al., 2012; Chen et al., 2019). This highlights the possible priming of an extracellular environment for differentiation

by potent MSC subsets, but with suppression of lineage commitment in the absence of appropriate stimuli. There appeared to be other proteins differentially expressed between the clones that also have associated roles with the TGFβ signalling pathways, such as LTBP 1, 2, 3 and 4, which could indicate a differential mechanism of TGFβ signalling between clones. Previously high TGFβ expression/overexpression has been associated with inhibition of differentiation towards osteogenic and adipogenic and induction towards chondrogenic lineages (Denker et al., 1995; Fierro et al., 2011). The presentation and binding of TGFβ is likely different between clones due to differential expression of LTBPs and the TGFβ activating ECM component THBS1 (Schultz-Cherry et al., 1994). The potential for autocrine signalling to control TGFβ signalling and cell functionality may also be present via miRNA regulation of gene expression, as miR-21, which was significantly more highly expressed in Y201 EVs, downregulates TGFβ receptor 2 (TGFβR2) and TGFβ1 and with mir-21 knockout murine BMSCs demonstrating reduced anti-inflammatory signalling and mir-21 shown to regulate differentiation of BMSCs (Wu et al., 2015). Follow up studies will be important to assess the role secreted TGFβ may play in co-ordination of heterogeneous phenotypes.

Presence of increased aggrecan was also interesting as it is an important ECM component and a key proteoglycan required for cartilage formation, and was previously shown to be constitutively expressed by BMSCs (Mwale et al., 2006). Secretion of this protein at high levels could correlate or be predictive of chondrogenic differentiation capacity. Binding of various ECM components in conditioned media to integrins may drive the migratory phenotype and the inherently high enrichment for matrix production in Y201 cells could explain their migratory profile. It would be of interest to develop investigations into biophysical properties of these matrices as they may reflect functionality *in vivo* as MSCs are likely to reside within specific niches. In Figure 3.3 and Figure 3.4 I demonstrated how secreted factors from Y201 were more potent in inducing migration in non-migratory Y202 cells compared to Y202 signals, also resulting in a change in overall cell morphology. ECM proteins such as fibronectin have previously been shown to facilitate migration of BMSCs, mediated through integrin binding (Veevers-Lowe et al., 2011). Fibronectin was found at high levels in both Y202 and Y201, albeit significantly higher in Y201 secretome.

The increased expression of CXCL12 in Y201 was also noted. High expression of this cytokine is associated with chemotactic responses for HSCs, and could represent possible differential *in vivo* functionality for Y201-like BMSCs (Sugiyama et al., 2006). There

was no significant difference in CXCL12 expression between Y201 and Y101 however, indicating that expression of this cytokine may also correlate with stem-functions, and highlighting how there may be heterogeneity within CXCL12 abundant BMSC populations. Interestingly murine CAR cells overlap highly with the LepR population of murine BMSCs and this population has been shown to be heterogeneous by scRNA-seq and so Y201 and Y101 may be representative of analogous heterogeneity in humans (Tikhonova et al., 2019; Zhou et al., 2014)

The most highly abundant differentially expressed proteins in Y202 secretomes included Follistatin-like-1, Fibrillin-1 and Lumican. Follistatin-like-1 has been implicated as an inflammatory signalling molecule which may contribute to the pathogenesis of arthritis and could be a candidate for explaining upregulated inflammatory gene expression of Y202 when exposed to Y202 secreted factors (Chaly et al., 2012; Miyamae et al., 2006). Fibrillin-1 has shown to regulate the availability of TGF-β, a signalling protein with key roles in regulating ECM production (Chaudhry et al., 2007; Massagué, 2012). The increased expression of Lumican in Y202 secretome could also further explain the decreased migratory capacity and high basal inflammatory signalling of Y202 cells as Lumican has been shown to impede migration of MSCs and has also been implicated in inflammatory cell chemotaxis in corneal and was recently shown to play a role in inflammation induced in osteoarthritis by facilitating activation of inflammatory signalling by Toll like receptors (Barreto et al., 2020; Carlson et al., 2007; Malinowski et al., 2012).

Collectively these differences in secreted ECM protein expression between these lines may help to explain the functional differences and could be used to direct functionality and behaviour of MSC subtypes.

To develop a greater appreciation for differences in secreted signalling capacity between our lines I also investigated the content of EVs. I demonstrated here that there was a shift in significantly different proteins with Y201 derived EVs enriched for a greater number of different proteins, suggesting a more diverse or concentrated packaging of EVs with protein cargo, given that isolations were performed from roughly the same number of cells. The presence of various membrane bound ECM binding proteins in the EVs, such as integrins, gave confidence that the proteomics was identifying EV associated protein, and this was corroborated with TEM and NTA supporting the presence of EVs. Equally, it was noted that only 50% of proteins identified in EV isolation were also found in total secretome, highlighting this as a distinct sub-compartment of the secretome. I showed that both Y201

and Y202 produced EVs with similar size distributions determined by NTA and demonstrated presence of classical cup-shaped EVs by TEM, although this shape is associated with collapse during TEM preparation (Raposo and Stoorvogel, 2013).

While Y201 and Y202 appear to produce physically similar EVs, the protein content of vesicles varied dramatically, implying a differential capacity to signal via EVs. The presence and specific enrichment of particular matrix binding proteins within Y201 EVs also seems to correlate with the idea of patterning the immediate niche with EVs. The cells may produce a matrix layer and subsequently secrete vesicles capable of binding the matrix, these vesicles could then act as signalling packages to other cells that migrate over the matrix, an important function reviewed by Rilla et al. (2019) and Rackov et al. (2018). I noted increased presence of all 3 type VI collagen chains necessary to form a functional collagen type VI helix in Y201 EVs, which were also upregulated in Y201 secretome (albeit only col6a1 was upregulated significantly) compared to Y202. Interestingly the relative abundance was reversed between the total secretome and the EV compartments with col6a1 most abundant in secretome and col6a3 most abundant in EVs, suggesting that col6a3, which is the largest of the three chains, may be enriched during the EV isolation process. This enrichment could be coincidental due to size or could indicate that col6a3 may be bound preferentially by EV associated molecules preferential binding substrate for EVs.

Only 10 miRNAs presented significantly higher expression in Y201 versus Y202 and analysis of the predicted targets of these again highlights a potential targeting cell function towards control of the ECM. Combining this with the previous proteomic analyses provides a consistent interpretation that Y201 cells are contributing largely to the ECM that is laid down and signalling to control the organisation and constituents laid down by other cells via paracrine interference through miRNAs.

In addition to the protein level comparisons, the increased abundance of miR-29a-3p and miR-29b-3p in EVs from Y201 provided further evidence of a concerted effort by Y201 to alter the expression of various ECM proteins in their microenvironment as the conserved miR-29 family has well documented roles in regulation of ECM proteins (Roderburg et al., 2011). There is a further indication that miR-29 could have roles in regulating osteogenesis as previously it was shown to also target DKK1, a negative regulator of osteogenesis that was exclusively detected in the secretome of non-potent Y202 cells. A recent study also demonstrated that mi-29a was capable of improving

osteogenesis and angiogenesis (Lu et al., 2020). This finding again highlights a possible role in co-ordination of the local environment by secreted factors, given the important roles of vascularising and mineralising tissue. It should be noted that the Nanostring analysis performed is limited by quantifying a filtered set of miRNAs and that use of a sequencing approach may result in greater differences between BMSC subtype EV miRNAs being detected.

4.4 Conclusions

Collectively these findings show the considerable emphasis of a tri-potent BMSC subset in producing a suitable extracellular environment and could highlight how BMSC phenotypes are maintained through the production of appropriate ECMs in *in vitro* culture. The data also makes clear the large variation in secreted factors between BMSC subpopulations which will need to be strongly considered when selecting populations for development of cell-free BMSC therapies, as well as indicating potential origins of BMSC secreted factors in a mixed population. It also highlights another method through which we can distinguish heterogeneity, in a potentially non-destructive manner, through the use of secreted factors.

5 Immunolocalisation of MSC subtypes and ECM components

5.1 Introduction

5.1.1 Localisation of MSC subtypes

Localisation studies using cell-surface markers, fluorescent reporter mice and lineage tracing experiments have identified BMSCs expressing LEPR, CD146, CD271, Nestin and other cell surface markers at perivascular and endosteal locations (Jones et al., 2002; Méndez-Ferrer et al., 2010; Sacchetti et al., 2007; Zhou et al., 2014). The Y202 clone has previously been shown to express the cell surface marker CD317 and primary human MSCs sorted for CD317 expression recapitulate the proinflammatory expression profile of these cells (unpublished data and James et al. (2015)). Recently, comparative gene expression analysis revealed correlation between murine peri-sinusoidal stromal cells and $CD317^+$ BMSCs (Balzano et al., 2019). $LEPR^+$ has been shown to mark perisinusoidal stromal cells *in vivo* and so I therefore aimed to show evidence for $CD317^+LEPR^+$ stromal cells in mouse bone marrow to mark an equivalent subpopulation of these cells.

The heterogeneity of stromal populations has gained increasing interest with the advent of scRNAseq approaches revealing heterogeneity within populations of BMSCs defined by the same cell-surface markers (Baccin et al., 2020; Baryawno et al., 2019; Tikhonova et al., 2019; Wolock et al., 2019). Dissection of heterogeneity and determination of cell functionality by cell surface markers may be limited in capacity, as was shown by subdivision of the $LEPR^+$ population in the aforementioned studies into 4 distinct subgroups. Subpopulations may have overlapping cell surface markers and the functionality of subtypes will likely be defined more by their gene expression profiles and paracrine signalling functions. This further complicates the isolation of functionally distinct stromal populations if the differential expression does not reveal sufficiently discriminatory surface markers. For *in vivo* localisation it may help to understand whether subpopulations isolated by the same surface-marker expression have differences in their secretomes. The presence of subtype enriched or specific factors in the local environment of a cell may help to better identify subtypes by non-destructive assessment of secreted factors, as well as providing markers to identify specific locations *in vivo*. Localisation and composition of the niches of functionally distinct BMSCs is particularly important for fundamental understanding of how BMSCs function under homeostasis and in response to diseases and injury. In the previous chapter I have revealed differences in secreted products of clonally derived stromal subpopulations *in vitro*. I postulated that, akin to the use of cell-surface markers, secreted

factors may also be useful for defining the location and identity of stromal cell subtypes. Soluble factors may have potent local functions; however, they may be capable of diffusion or transport away from the immediate microenvironment (as has been suggested with CXCL12, an important stromal derived niche factor). I utilised my observations of differentially expressed ECM proteins by three contrasting stromal cell subtypes *in vitro* to inform selection of six candidate niche-marking ECM components that may discriminate between nullipotent (Y202), bipotent (Y101) and tripotent (Y201) BMSCs. The ECM protein lumican was more highly expressed in Y202 than both Y101 and Y201; CEMIP and collagen VI were more highly expressed in both Y101 and Y201 than Y202; aggrecan, periostin and biglycan were upregulated in Y201 versus Y101 and Y202 (Table 4.1). I used immunofluorescence labelling of sections of mouse and human bone marrow to identify location of these ECM proteins *in vivo*. I used the commonly accepted stromal marker LEPR for murine BMSCs and selected the marker CD271 in human tissue, which has been shown to contain the CFU-F stromal fraction of human marrow (Jones et al., 2002; Quirici et al., 2002; Zhou et al., 2014). I also hypothesised that BMSCs that produce periostin may utilise this protein for adherence and migration and so also looked for expression of the known periostin binding integrin ITGAV which has further been implicated as a possible marker of BMSCs (Pinho et al., 2013).

5.1.2 ECM proteins in the BMSC niche

Investigations into the bone marrow niche predominantly focus on the haematopoietic and stromal compartments, with emphasis on the cellular constituents. Beyond the cellular makeup of the niche, we must also strive to define the soluble factors and matrix components. Self-renewal and differentiation capacity are key features of stem cells, and these features of BMSC behaviour that are known to be facilitated through ECM adherence *in vitro* (Chen et al., 2007). Investigation into the matrix may therefore give key insight into functionality of distinct stromal niches *in vivo.* There have been various studies to identify ECM proteins within bone marrow, including collagens-IV and VI, tenascin-C, fibronectin, laminin and periostin, although most of these have not focused on finding the exact localisation of specific ECM components with respect to BMSCs, but have focused more on overall distribution of protein within the bone marrow (Coutu et al., 2017; Klein et al., 1995; Nakamura-Ishizu et al., 2012; Nilsson et al., 1998).

ECM proteins are of high importance in the cellular niche, both for structural support and also for the co-ordination of biochemical signals and their availability to cells (Gattazzo

et al., 2014). Biomechanical forces experienced by a cell such as stiffness are likely linked to the microenvironment and the niche ECM composition will influence this, which can have dramatic implications for stem cell fate and even immune responses (Engler et al., 2006; Wong et al., 2020). Developing a more complete understanding of the composition of the immediate microenvironment and niche of BMSC subtypes could lead to more appropriate *in vitro* recapitulation of the niche to expand and maintain important multipotent subtypes *ex vivo* which could in turn facilitate the development of regenerative therapies using multipotent BMSCs. Equally, it could help to understand how the niche can alter during disease or act aberrantly to support disease progression which is a key area of interest in haematology (Duarte et al., 2018; Medyouf et al., 2014).

The localisation of the niche within the complex bone marrow microenvironment is also likely to be important for the understanding of the native functions of BMSC subpopulations. The architecture of bone marrow varies considerably between endosteal regions and diaphysis and between cortical and trabecular bone, which may have consequences for locations of specific subtypes, as has been suggested by a group highlighting varied potency in BMSCs isolated from different bone regions (Herrmann et al., 2019). As mentioned previously a large amount of this work has been done with respect to the HSC supportive populations of BMSCs, with evidence for a predominantly perivascular localisation. The localisation of potent stromal subsets outside of their roles in the heamatopoietic niche has been limited, although recent studies have emphasised the importance of growth plate regions for identification of osteo-chondral and stromal committed progenitors (Chan et al., 2018; Chan et al., 2015). By developing an understanding of the distribution of BMSC subpopulations, we may not only be better capable of isolating specific subtypes but we may learn more about the specific niches and how these are capable of maintaining phenotypes.

5.1.3 Haematopoietic stem cells and ECM components

In this chapter I performed immunofluorescence studies in mouse and human bone marrow to localise proteins that were identified as significantly differentially expressed between the Y201 and Y202 BMSC subtypes. I hypothesised that these matrix proteins may be important for the maintenance of Y201 stem-cell functions and may therefore mark stem-cell matrix and subsequently stem-cell localisations *in vivo*. I demonstrate that the Y201 upregulated matrix proteins have diverse distributions but are only all found in the endosteal regions of femurs. Furthermore, I show how these proteins can be found in the

immediate microenvironment of a subset of $CD271^+$ bone lining stromal cells in human tissue, a known population of multipotent stromal cells (Jones et al., 2002; Quirici et al., 2002).

5.2 Results

5.2.1 Survival of HSCs on BMSC derived ECM

The relationship between BMSC and HSC has been long documented with suggestions of BMSC support of HSC survival. I aimed to determine if the ECM produced by different BMSC subsets were capable of facilitating survival of HSCs *ex vivo*. Single HSCs were seeded onto Y201 ECM, Y202 ECM or tissue culture plastic in 96 well plates and cultured for 10 days under serum-free conditions. At assay endpoint, survival of individual HSCs was calculated by visual identification of colonies by light microscopy. Counts of colonies per plate revealed a significant increase in survival of HSCs when cultured on Y201 ECM (p=0.0008) or Y202 ECM (p=0.0106) versus tissue culture plastic (Figure 5.1). Observations of the colonies indicated that colony sizes of HSCs cultured on ECM tended to be smaller than those that survived on plastic (data not shown).

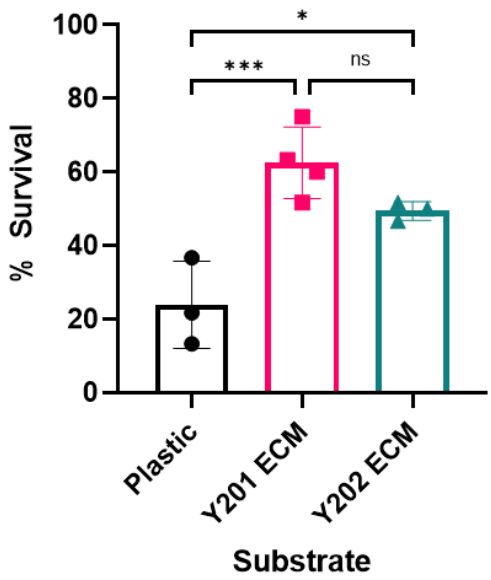

Figure 5.1 Analysis of the effects of Y201 and Y202 derived ECM on HSC survival ex vivo

Survival of single mouse HSCs at day 10 post seeding into individual wells of a 96 well plate (60 per plate). HSCs were isolated by FACS onto plastic or layers of ECM deposited onto plastic by Y201 (pink) or Y202 (green) cells. HSC survival was determined by manual counting of colony formation in vitro at day 10. N=3-4. Kruskal-Wallis, *p<0.05 ***p<0.001 ns = not significant. This work was performed in collaboration with Juan Rubio-Lara.

5.2.2 Localisation of CD317^{+} MSC subtype in murine bone marrow

The cell-surface marker CD317 was previously shown to be selective for Y202-like cells from BMSC populations and we have shown that primary human BMSC cultures sorted using this marker recapitulate their phenotype (James et al., 2015). I looked for colocalisation of CD317 and LEPR^{+} stromal cells and found at low frequency some CD31^{-} LEPR^{+}CD317^{+} cells in perisinusoidal locations (Figure 5.2). CD317 expression was detected in other regions of the marrow but only colocalized with LEPR staining in the perisinusoidal locations. Clear positive staining for these markers is shown versus the isotype control (Figure 5.3)

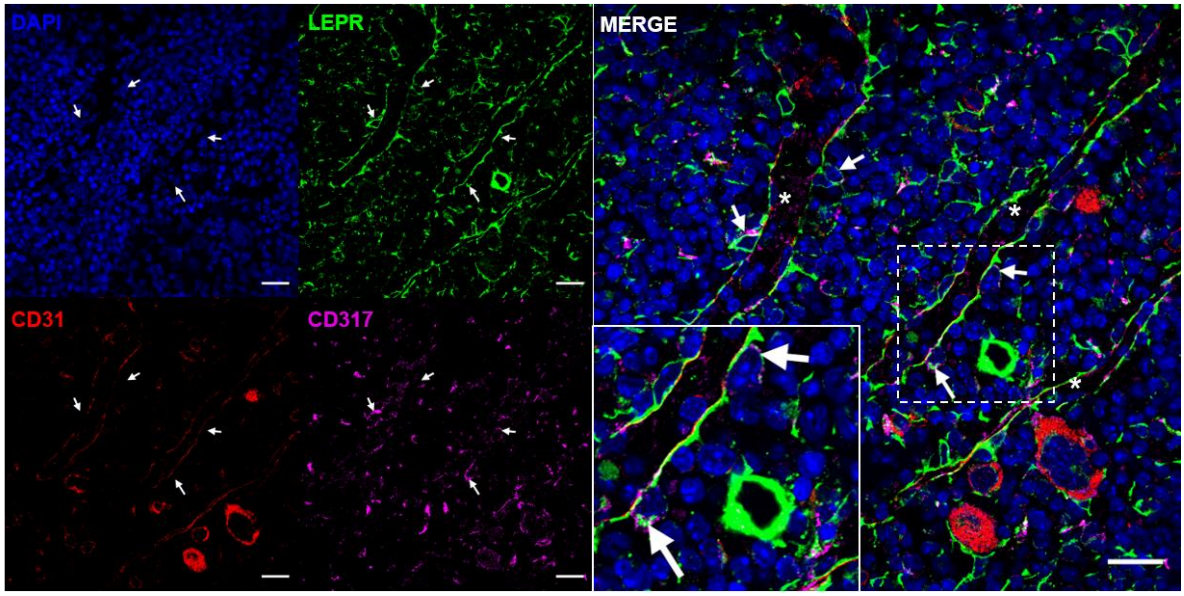

Figure 5.2 Immunofluorescence images of CD317⁺ stromal cells in mouse bone marrow

Immunofluorescence detection of the Y202 stromal cell marker CD317 (violet, AF647) with the stromal cell marker LEPR (green, AF488) in mouse bone marrow, arrows. CD31 was used as an endothelial and megakaryocyte marker (red, AF568) and nuclei are shown (blue, DAPI). * = sinusoid. Inset is an enlarged view of the dashed box. Scale bar = 50μm.

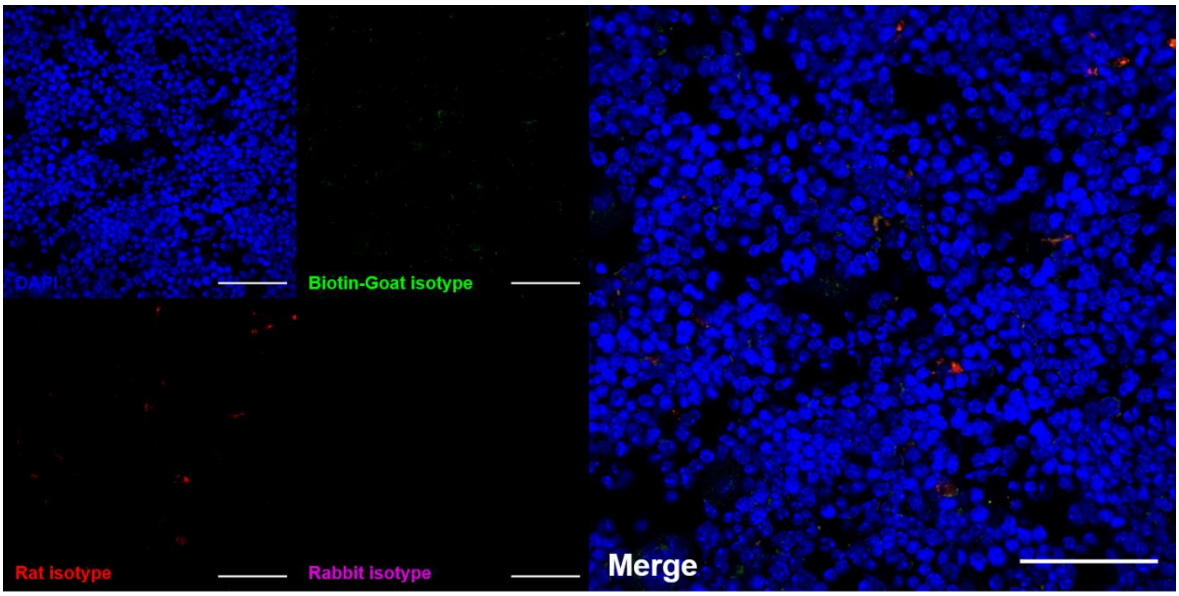

Figure 5.3 Isotype control immunostaining for LEPR, CD31 and CD317 in mouse bone marrow

Immunofluorescent imaging of appropriate isotype control stained mouse femurs secondaries added for detection. There was minimal fluorescence activity, likely as a result of autofluorescence in the bone marrow. Biotin conjugated goat-anti-mouse isotype (green, AF488), Rat-anti-mouse isotype (red, AF568) and Rabbit anti-mouse isotype (purple, AF647) and nuclei stained (blue, DAPI).

5.2.3 Differentially expressed Y201 and Y202 ECM proteins in murine bone marrow

Using immunofluorescence labelling and confocal imaging of mouse femurs, I detected presence of six ECM proteins (collagen VI, biglycan, aggrecan, periostin, CEMIP and lumican) identified from the proteomic interrogation of BMSC secretomes in chapter 5 (Figure 5.4). Aggrecan and periostin were highly upregulated by Y201 cells *in vitro* and presented possible stem-cell specific or enriched ECM proteins, therefore the *in vivo* location of these ECM proteins in the bones was evaluated. Aggrecan and periostin were detected around chondrocytes and in periosteum respectively, which are known sites of expression, but were also detected at low frequency in close proximity to, or lining, the endosteal surface in both epiphyseal and diaphyseal regions (Figure 5.4C,D,I&J). Expression of aggrecan and periostin appeared more prevalent in the trabecular regions of the epiphyses, as is shown in the expanded views in Figure 5.5. The morphology of aggrecan and periostin expressing cells in the epiphyses did not appear to resemble the typical cuboid shape associated with osteoblasts. Biglycan was detected at high abundance along the majority of the endosteum and along trabecular bone in the epiphyses as well as in cartilage (Figure 5.4B&H). There was also less frequent expression of biglycan in some possible perivascular areas, and high expression around megakaryocytes. Collagen VI was found endostealy as well as in a fine meshwork in the marrow and this distribution is further covered in section 5.2.4. CEMIP also presented expression predominantly in the endosteal region of bone marrow (Figure 5.4E&K). Lumican, which was significantly more highly expressed in Y202 secretome, was revealed to have a broad distribution pattern, prevalent along the endosteum and throughout the marrow as well as in the pericellular matrix of chondrocytes (Figure 5.4F&L). The endosteal/trabecular surface was the only area where all proteins could be found.

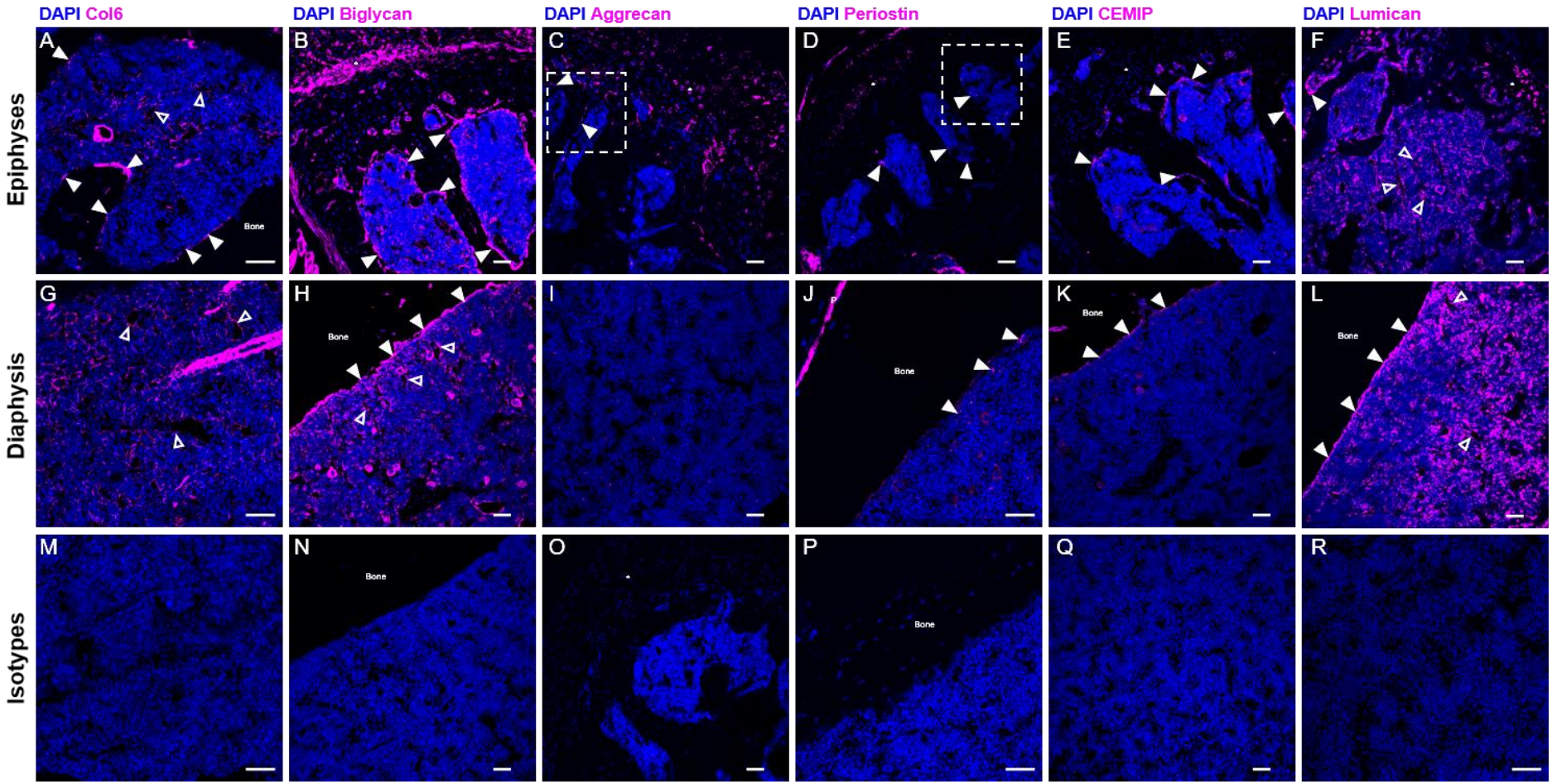

Figure 5.4 Immunofluorescence images of ECM proteins in mouse bone marrow

Immunofluorescence microscopy of various ECM proteins (violet) in mouse bone marrow with DAPI (blue) nuclear stain. Top row shows imaging of epiphyses regions of mouse femur. Middle row shows regions from the diaphysis of the femur. The bottom row shows isotype controls for respective stains. Confocal images of mouse bones in the femoral epiphyses showing antibody staining for collagen VI (A,G&M), biglycan (B,H&N), aggrecan (C,I&O), periostin (D,J&P), CEMIP (E,K&Q) and lumican (F,L&R). Expression along the endosteal surface is marked by solid arrows. Expression of protein around possible endothelial vessels is marked by open arrows. * = cartilage and hypertrophic chondrocytes. P = Periosteum. White boxes indicate regions expanded in Figure 5.5. Scale bars = 50μM

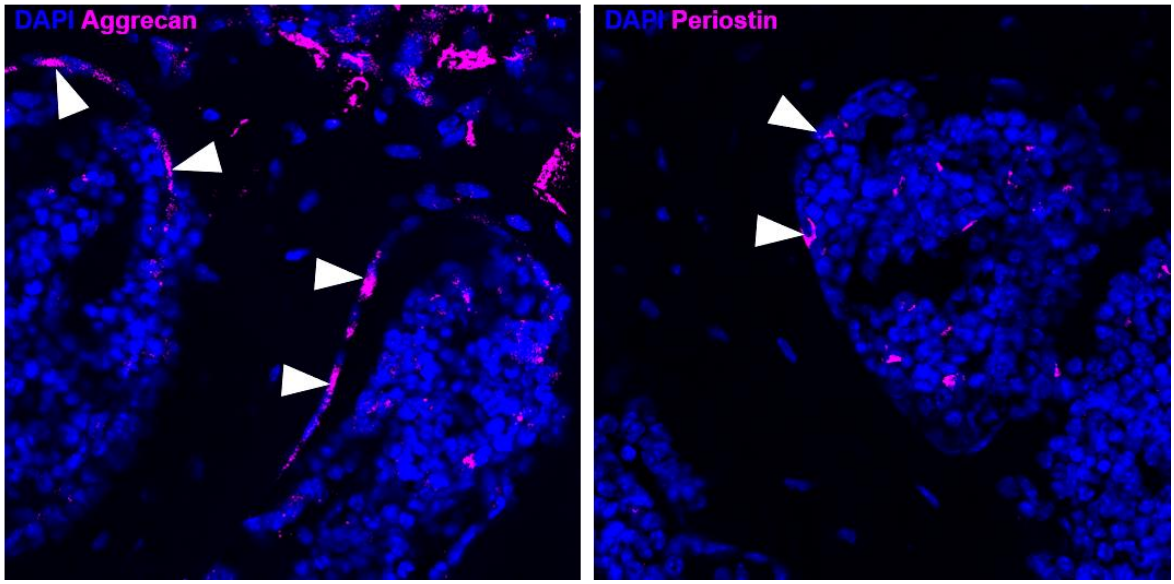

Figure 5.5 Enlarged views of immunofluorescence labelling of aggrecan and periostin in trabecular regions of mouse bone marrow

Enlarged frames corresponding with white boxes from Figure 5.4C (left) and D (right). These panels highlight the primarily endosteal localisation of aggrecan (left) and periostin (right) in bone marrow. Arrows point to cells in direct contact with the endosteum.

Collagen VI has a polarised distribution in mouse femurs

I used immunolabelling of collagen VI to determine its distribution in mouse femoral bone marrow (Figure 5.6). In Y201 secretome Col6a1 was detected at significantly higher levels, and the other collagen chains (Col6a2 and Col6a3) were increased, albeit not statistically significantly. Collagen type VI has been implicated with a role in promoting haematopoietic cell adhesion and but its function in the bone marrow has yet to be fully determined (Klein et al., 1995). In the EV proteomic experiments, all three chains were significantly more highly expressed in Y201 EVs. By immunofluorescence I observed a widespread distribution of collagen VI in adult mouse femurs, with strong staining in articular cartilage, skeletal muscle and in smooth muscle cells surrounding bone marrow arteries and arterioles (Figure 5.6). Increased exposure revealed more subtle expression of collagen VI in the marrow space. As shown in Figure 5.4A and Figure 5.6 expression was high in endosteal regions, particularly along trabeculae in the epiphyses. When imaging the entire bone the meshwork pattern of collagen VI was notably enriched towards the epiphyses, and was particularly striking in the distal diaphysis and in both epiphysis (Figure 5.6A,D&E). In the diaphysis the distribution appeared to be most prevalent at the endosteal edge and in the medial diaphysis with a decrease in expression between these regions (Figure 5.6D). The targeting of the type VI collagen antibody was confirmed with a Col6a1 knockout mouse that is known to result in total absence of whole collagen VI and an isotype control is shown for the whole mouse femur staining (Figure 5.7and Figure 5.8).

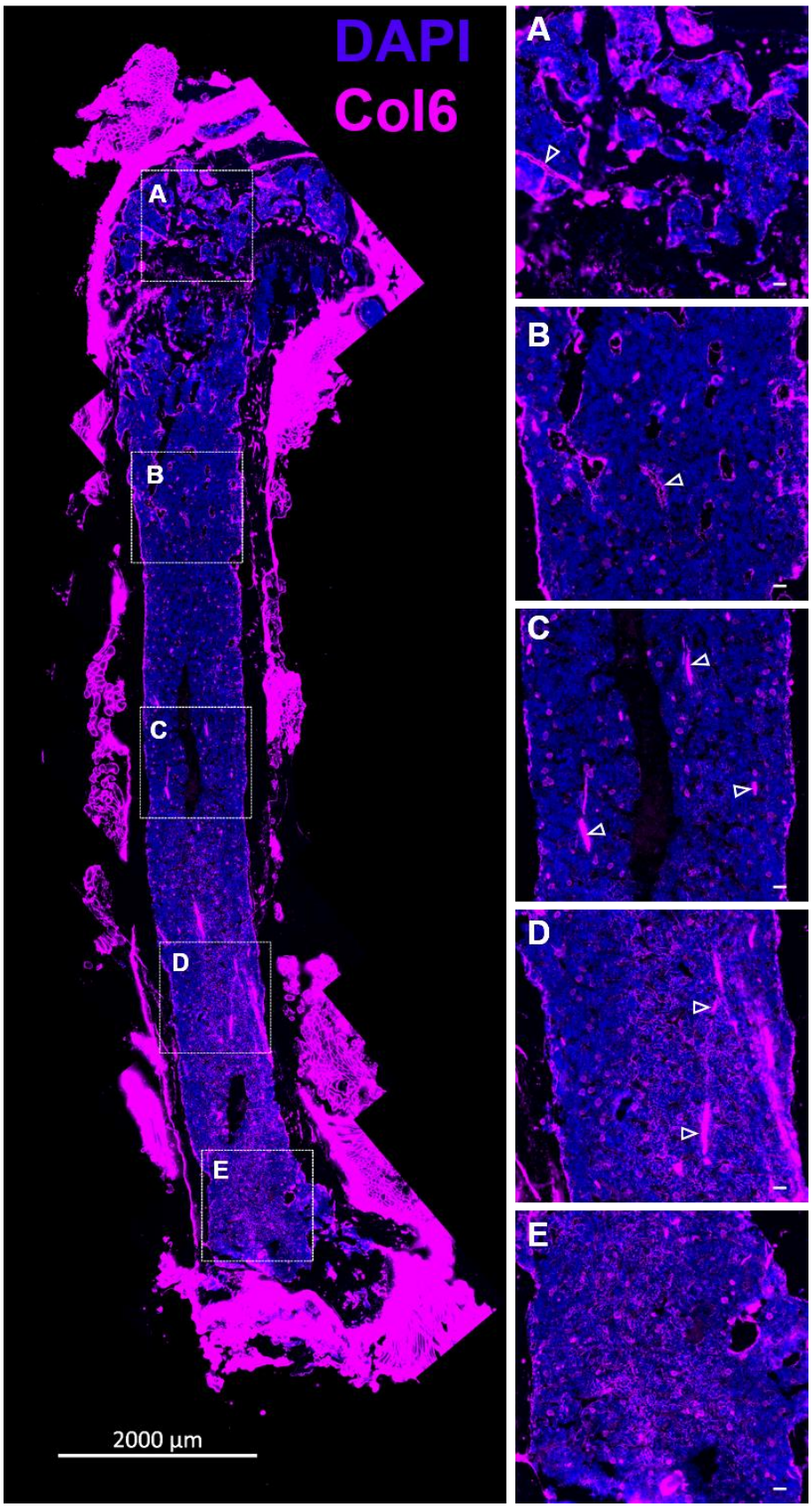

Figure 5.6 Immunofluorescence images of collagen VI distribution in mouse femur

Representative immunofluorescence of a mouse femur for nuclei (blue, DAPI) and collagen VI (violet, AF647) with higher magnification images taken from A) Proximal epiphysis B) Proximal diaphysis C) Mid diaphysis D) Distal diaphysis E) Distal epiphysis. Arrows point to smooth muscle labelled arteries and arterioles. Scale bars in insets are 50µm.

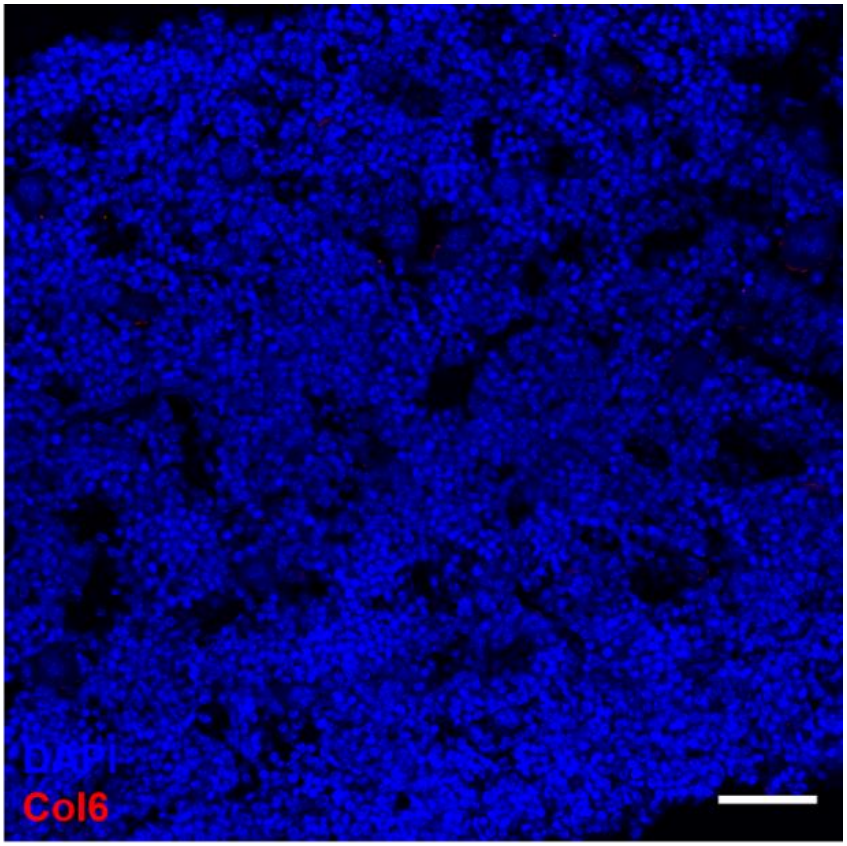

Figure 5.7 Col6 antibody targeting confirmed in a col6a1 knockout mouse femur
Immunofluorescence imaging demonstrating highly specific targeting of rabbit-anti-col6 antibody in bone marrow demonstrated by complete absence of fluorescence signal in the bone marrow of a col6a1 knockout mouse. Demonstrated appropriate targeting of the antibody used in Figure 5.6. Scale bar = 50μm

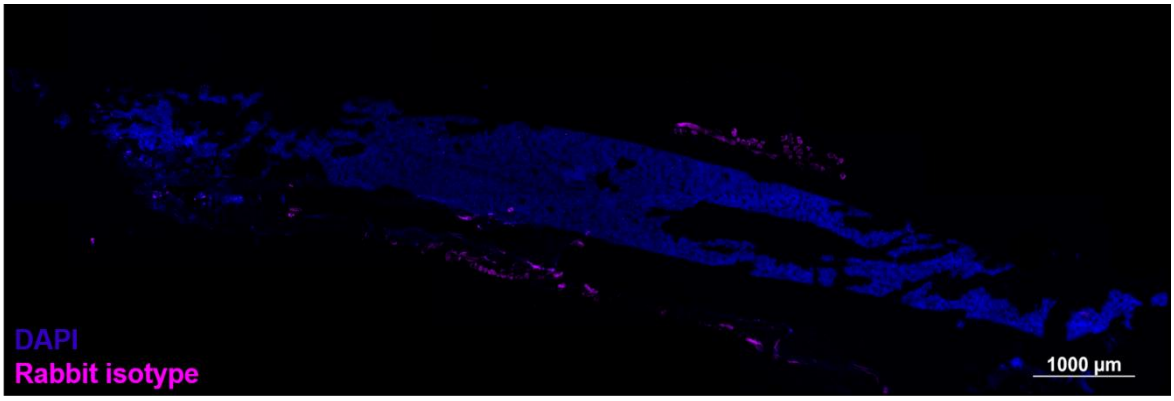

Figure 5.8 Isotype control for collagen VI staining in whole mouse femurs

Immunofluorescence detection of signal from rabbit-anti-mouse isotype stained femur showing a lack of staining in response to goat-anti-rabbit 647 conjugated secondary antibody. There is evidence of some autofluorescence in skeletal muscle tissue but absence in bone and bone marrow regions incidcating appropriate targeting of the anti-col6 antibody in Figure 5.6.

5.2.4 Stromal subtype ECM proteins are identifiable in human bone

Using immunofluorescence labelling I identified expression of five ECM proteins differentially upregulated by Y201 BMSCs (collagen VI, biglycan, aggrecan and periostin) or Y202 BMSCs (lumican) in sections taken from human femoral heads (Figure 5.9). Given the diversity of human bone marrow structure I attempted to look for expression of these proteins against trabecular bone and in haematopoietic cell rich marrow regions (Figure 5.9). I demonstrated a broad expression pattern of collagen VI and lumican in both endosteal bone lining regions and in marrow rich regions (Figure 5.9A,E,F&J). In contrast, biglycan was highly abundant in bone lining regions but with no detectable expression in marrow (Figure 5.9B&G). Periostin was found associated with bone lining cells, as well as at low levels throughout the marrow and with particularly strong expression by some round cells found in close proximity to trabecular bone (Figure 5.9D&I). Aggrecan was observed primarily in contact with trabecular bone (Figure 5.9C&H). Overall the only site where expression of all these proteins was identified was trabecular bone lining regions. ECM components were not always found in the direct presence of a cell, suggesting deposition and migration away by cells.

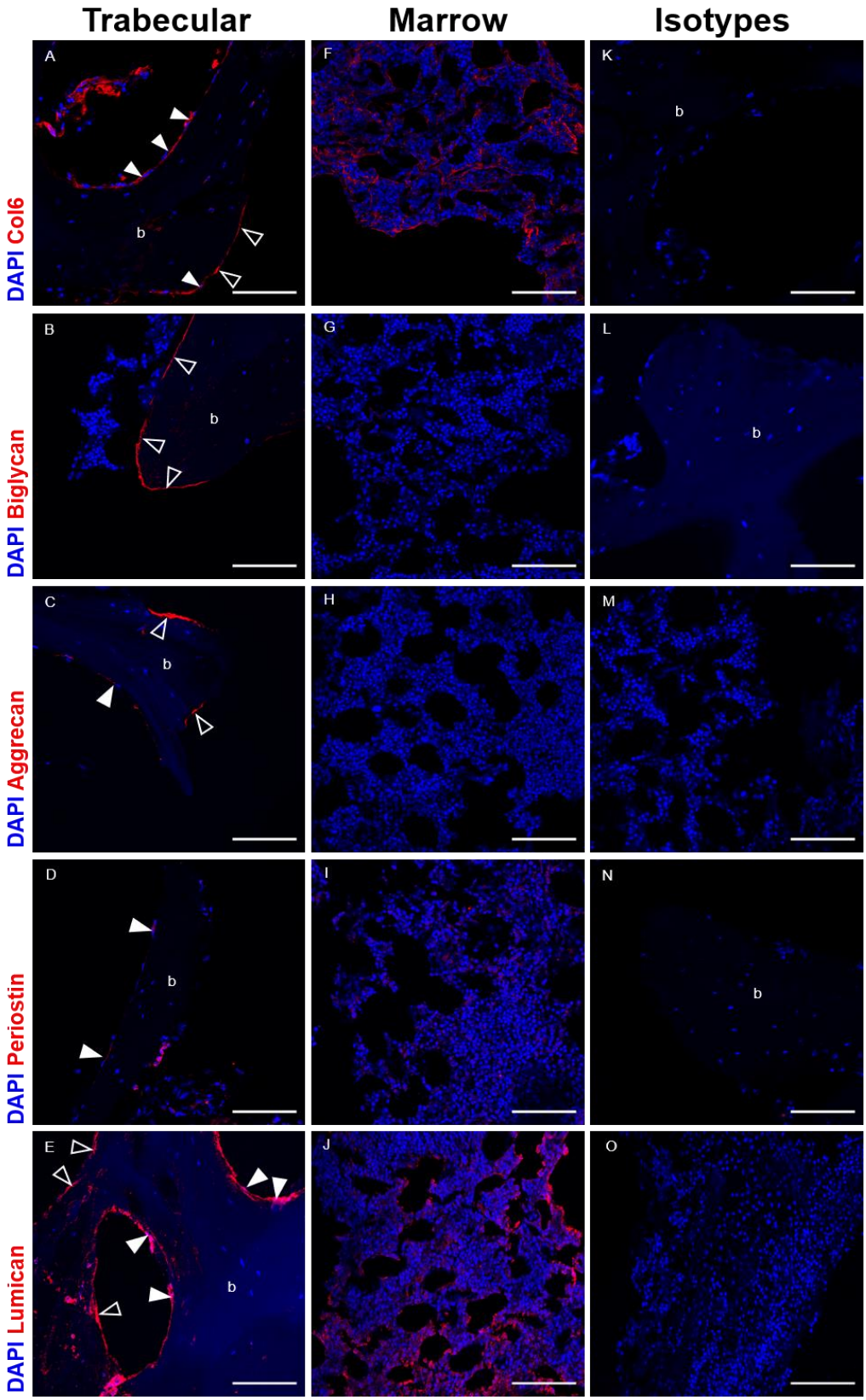

Figure 5.9 Immunofluorescence detection of ECM proteins in human bone sections
Immunofluorescence detection of various ECM proteins (red) in cryosections of bone from human femoral heads. Shown are areas with trabecular bone pieces (left column), marrow regions (middle column) and the respective isotype controls used to set detection limits (right column). Nuclei were stained with DAPI (Blue). Open arrows indicate where ECM protein is found in a bone lining region but not with an associated nucleus, closed arrows show areas where a nucleus and the ECM protein are both present. b = Bone. Scale bars = 100µm.

5.2.5 Colocalisation of periostin and aggrecan with CD271$^+$ stroma

Proximity of CD271$^+$ stromal cells to aggrecan and periostin was assessed due to being the two most highly different ECM proteins in Y201 secretome (Figure 4.4). Periostin and aggrecan are ECM proteins more commonly associated with periosteal and cartilage distributions and their significant abundance in tripotent undifferentiated BMSCs was unusual, I therefore utilised these as candidate markers of a possible Y201-like BMSC population *in vivo*. Using CD271 as a marker of human BMSCs with high potency I demonstrated co-localisation of CD271$^+$ bone lining stromal cells with periostin and aggrecan in sections of human femoral heads (Figure 5.10 and Figure 5.11). Some CD271$^+$ cells were found colocalised with periostin coated regions of trabecular bone (Figure 5.10). There were also regions of positive endosteal CD271$^+$ that did not colocalise with any periostin (Figure 5.10, arrows). Aggrecan was also identified in regions where elongated CD271$^+$ cells were in contact with trabecular bone. It was noted that not all CD271$^+$ cells lining trabecular bone were found on top of or in proximity to periostin or aggrecan but those that did appeared bright. Another key observation was that CD271$^+$ cells found in marrow regions were devoid of significant aggrecan or periostin expression (Figure 5.12). The positive expression of these proteins was set against isotype controls that showed limited fluorescence (Figure 5.15).

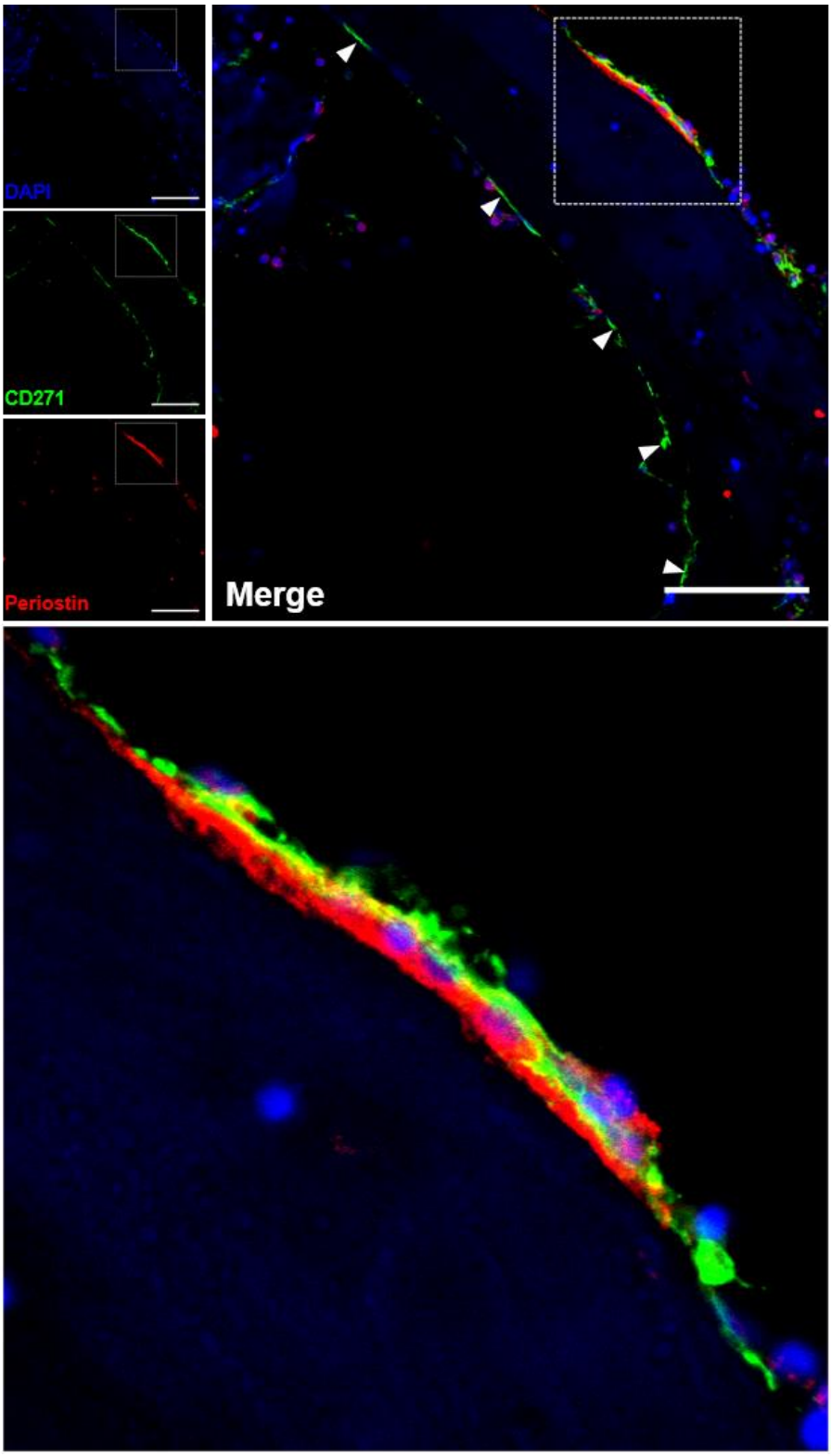

Figure 5.10 Immunofluorescence images of CD271^{+} bone lining cells and periostin in human bone

Immunofluorescence detection of a group of prospective bone lining stromal cells, expressing CD271 (green, AF488) and over the top of a periostin ECM (red, AF568) with nuclei (blue, DAPI). White box area is expanded in the bottom panel. White arrows show positive CD271^{+} staining with no evidence for underlying periostin. Scale bar = 50µm.

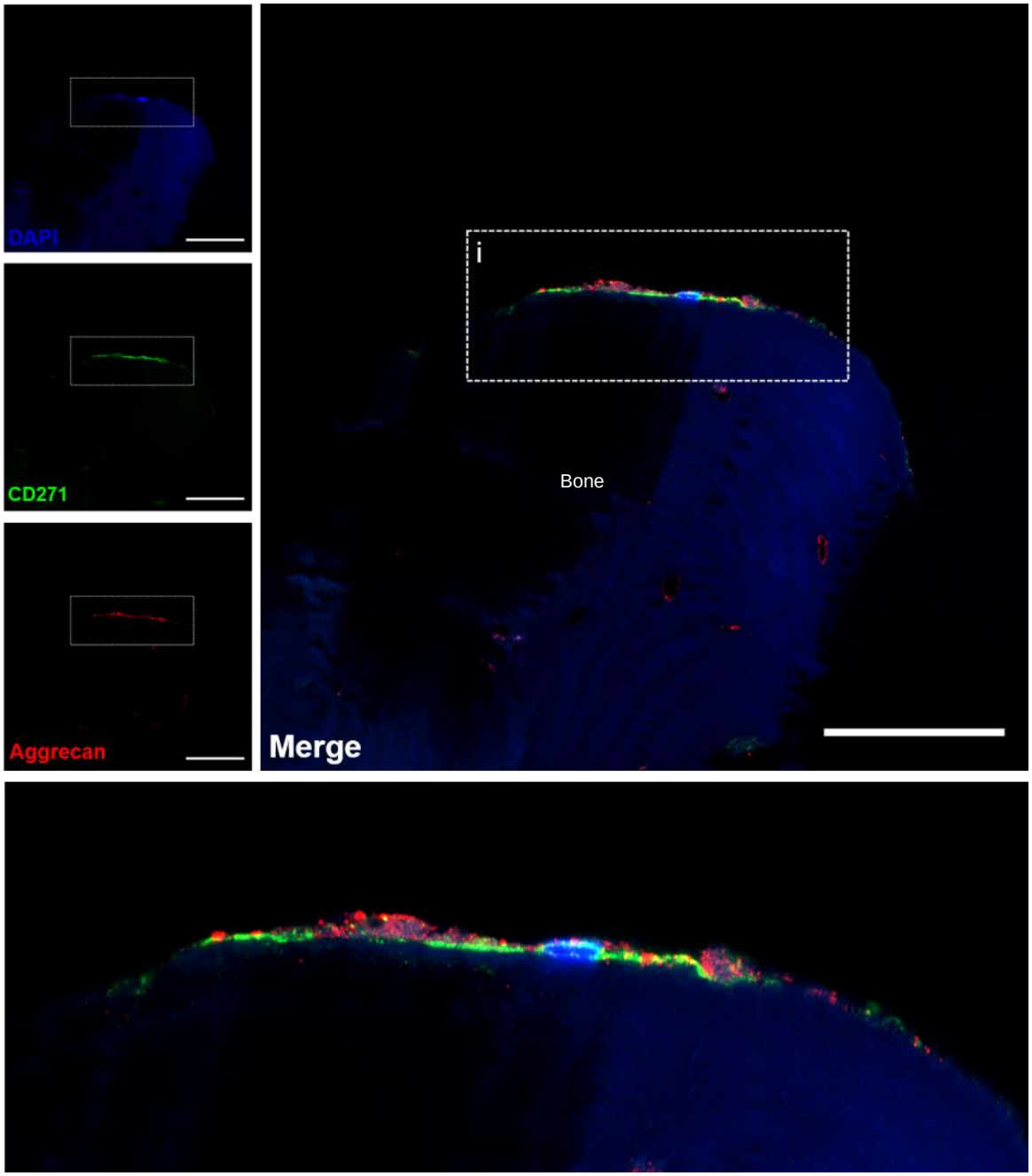

Figure 5.11 Immunofluorescence images of CD271^{+} bone lining cells and aggrecan in human bone

Immunofluorescence detection in human bone tissue of a prospective bone lining stromal cell marked by CD271 expression (green, AF488) found localised on top of aggrecan on ECM (red, AF568) and nucleus (blue, DAPI). White box area (i) is enlarged in the bottom panel. Scale bar = 50μM.

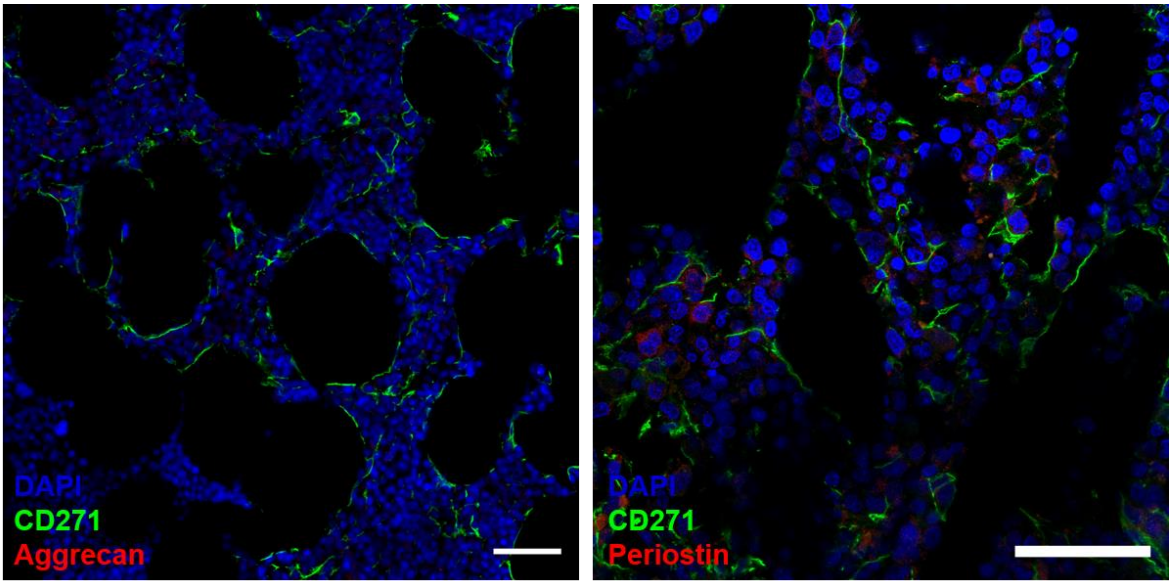

Figure 5.12 Immunofluorescence labelling of periostin and aggrecan with CD271 in marrow rich regions of human bone

Immunofluorescence detection of CD271^{+} reticular cells (green, AF488) in human bone marrow regions with absence of detection of aggrecan (left) or periostin (right) (both red, AF568). Scale bar = 50μm.

5.2.6 ECM markers of a stromal niche and ITGAV

Given the role of the ECM in driving BMSC migration, as identified previously in section 3.2.7, I hypothesised that endosteal lining BMSCs may use specific integrins to bind and drive migration *in vivo*. Integrin-alpha-V (ITGAV/CD51) is known to form integrin alpha-beta dimers that can bind periostin and has been shown to be expressed by MSCs and is expressed by Y201 and Y202 cells (unpublished data, (Li et al., 2010)). I used an anti-ITGAV antibody to detect colocalisation of ITGAV expressing cells and periostin on the surfaces of trabecular bone (Figure 5.13). Given the similar distribution patterns observed for aggrecan and periostin, I also determined the localisation of ITGAV and aggrecan, identifying colocalisation in the trabecular bone region of elongated ITGAV^{+} cells identified against trabeculae in contact with aggrecan (Figure 5.14).

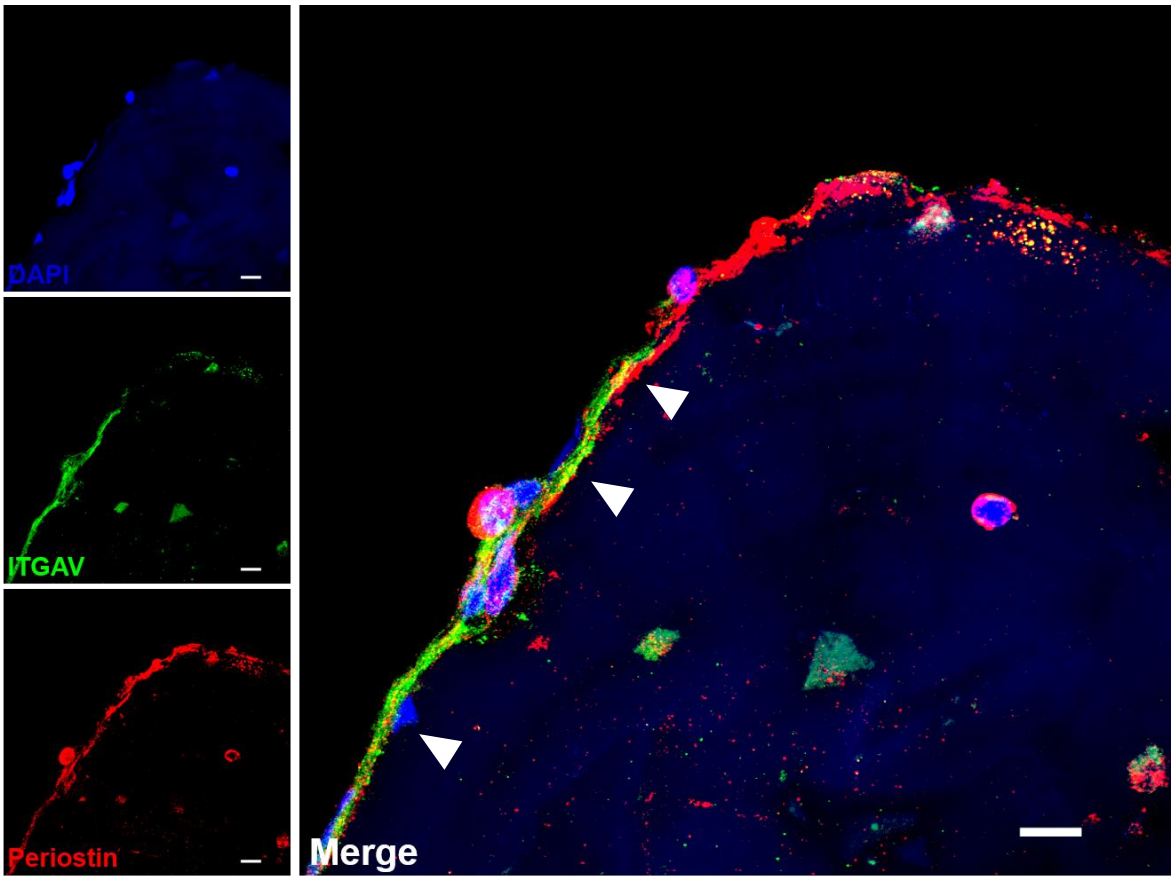

Figure 5.13 Immunofluorescence detection of ITGAV and periostin in human bone

Maximum intensity projection immunofluorescence image of a section of human bone. Nuclei (blue, DAPI), ITGAV (green, AF488) and periostin (Red, AF568) are shown. White arrows indicate where ITGAV expressing cells may crossover with extracellular matrix containing Aggrecan. Scale bar = 10µm.

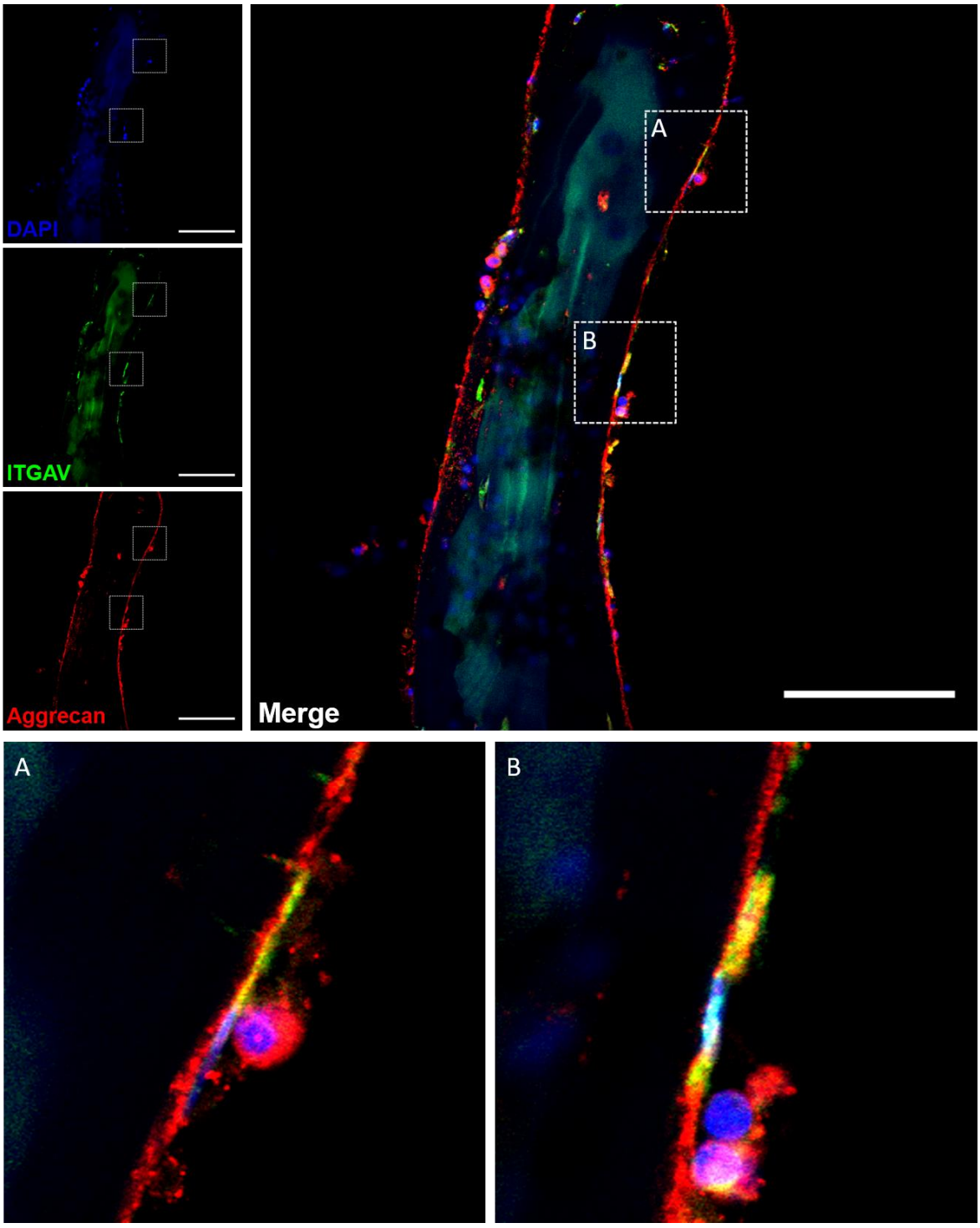

Figure 5.14 Immunofluorescence detection of ITGAV and aggrecan in human bone lining cells

Immunofluorescence of human bone tissue with nuclei (blue, DAPI), ITGAV (green, AF488) and aggrecan (Red, AF568). Zoomed views of two ITGAV^{+} cells surrounded by aggrecan are shown in A and B. Scale bar = 50µm.

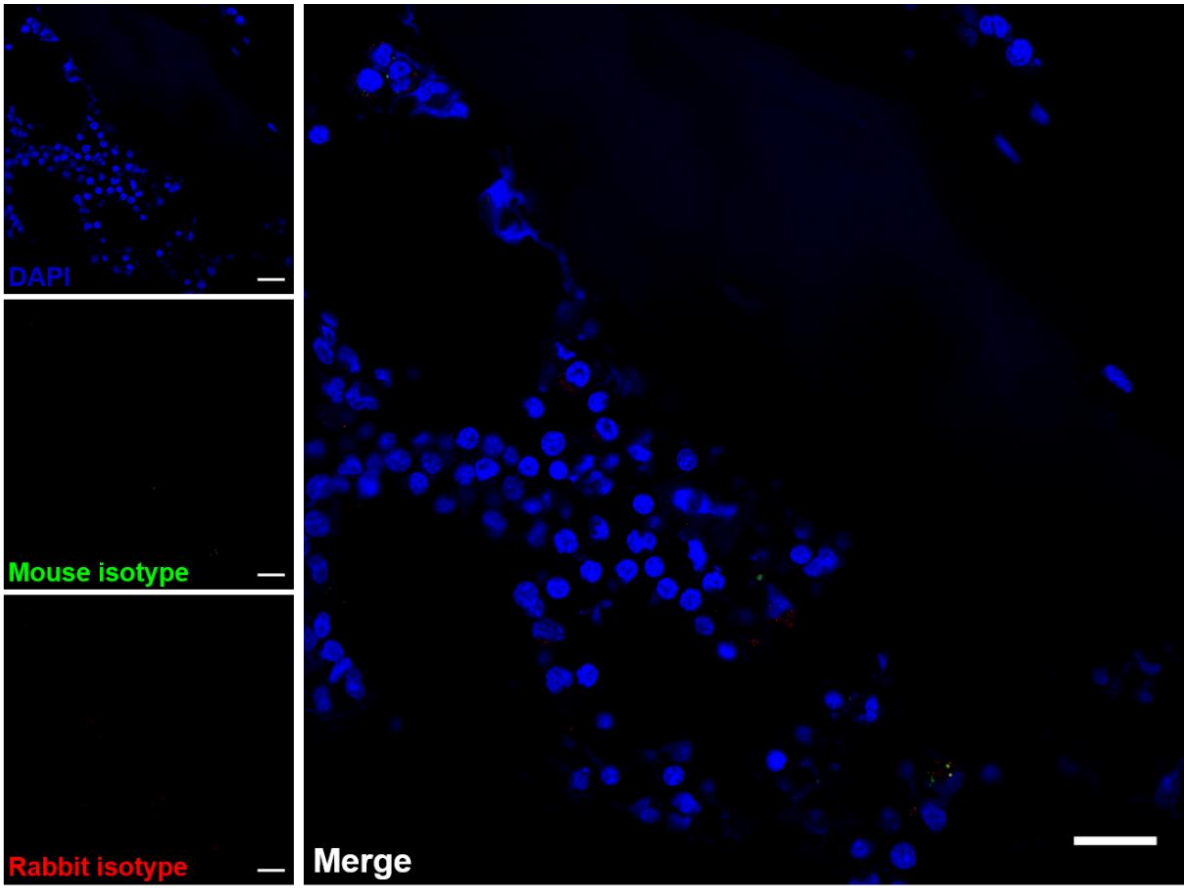

Figure 5.15 Isotype control for periostin and aggrecan co-staining with ITGAV and CD271 in human bone

Immunofluorescence image of human bone stained with isotype control antibodies for periostin/aggrecan (rabbit, red) and ITGAV/CD271 (mouse, green) captured using the same settings used in Figure 5.13 and Figure 5.14. There is clear absence of significant detectable green and red fluorescence in the control stained sample. Scale bar = 50μm.

5.3 Discussion

In this chapter I attempted to identify the localisation of a CD317$^+$ stromal subset in murine tissue and determine if secreted ECMs from different stromal subsets were capable of improving survival of HSCs. I also aimed to demonstrate whether the secreted ECM components of heterogeneous BMSCs determined from proteomic analysis of secretome could be used as markers of the *in vivo* localisation of phenotypically distinct subtypes *in vivo*.

The relationship between MSCs and HSCs has been extensively described and developmentally MSCs are resident in the niche before HSCs arrive and may play a role in patterning the microenvironment to suit the HSC, with chemoattractive CXCL12 expression helping to maintain the cells in the niche (Ding and Morrison, 2013; Greenbaum et al., 2013). We demonstrated a significant improvement in *ex vivo* survival of murine HSCs on our hTERT derived ECM, with the Y201 matrix increasing survival more than 2-fold on average, although we did not observe increased expansion as has been suggested in previous experiments using BMSC derived ECM (Kräter et al., 2017). The matrix likely provides pro-survival signals through a combination of mechanical or biochemical signals and indicates further how MSCs may act to support haematopoiesis *in vivo* through the development of appropriate niches. The *in vitro* MSC matrix produced by Y201 and Y202 cells may present an environment akin to the *in vivo* haematopoietic niche, hence the improved survival.

The identification of CD317$^+$ stromal cells *in vivo* in perisinusoidal locations potentially highlights a population of stromal cells in mouse that is orthologous to our Y202 human stromal subset. It should be understood that CD317 is upregulated in response to interferon alpha and at age 8-12 weeks a naïve laboratory mouse is unlikely to have been exposed to significant immunological insult as to cause a spike in interferon (Kawai et al., 2008). Expression of CD317 in BMSCs may therefore be lower than in human BMSC donors who will have likely been exposed to infections and inflammatory stimuli. It would be of interest to see if CD317 expression in murine stromal cells spikes with inflammatory responses. This could also help to explain the considerable variation seen in CD317$^+$ stromal population percentage seen in adult femoral head donors, if this population increases or CD317 expression increases under inflammatory conditions. The perisinusoidal location of this population may also correlate with the distribution of lumican in mouse and human tissue. This ECM protein was enriched in Y202 secretome and was more abundant in perivascular/central marrow locations than ECM proteins expressed more

abundantly by Y201 cells, corroborating a possible niche location for Y202-like stromal cells in perivascular locales. The potential contribution of lumican to a perivascular niche may further correlate with the pro-inflammatory phenotype of Y202/CD317^{+} BMSCs, as lumican has been implicated in promoting inflammatory responses in colitis and was recently shown to exacerbate inflammation of chondrocytes during osteoarthritis (Barreto et al., 2020; Wu et al., 2007). A 2019 study using microarray data showed a correlation between the gene expression profiles of Y202 cells and those of perisinusoidal stromal cells in murine bone marrow, indicating further the concept of unique niches and appropriate localisation of this subset (Balzano et al., 2019).

Collagen VI has been predominantly investigated for its role in skeletal muscle, however, there have been indications for an important role of this collagen in bone architecture and bone marrow function (Bonaldo et al., 1998). This functionality may be conserved between species given that the meshwork expression seen in mouse bones was also observed in sections of human femoral head. The interesting distribution of collagen VI potentially reveals a functional compartmentalisation of marrow. Collagen VI has been shown to act as a cytoadhesive for haematopoietic lineages which correlates with a function of stroma in haematopoietic support (Klein et al., 1995). The col6a1 knockout mouse, which results in complete loss of total collagen VI, was shown to have decreased trabecular bone formation, also highlighting the potential importance of this collagen to appropriate development of bones from skeletal stem cells as trabecular regions in mouse bone are found towards the epiphyses (Alexopoulos et al., 2009; Christensen et al., 2012). NG2, a prospective stromal cell marker, has a binding site for collagen VI, and could therefore indicate a function for collagen VI in stromal cell migration (Tillet et al., 2002). Despite collagen VI being statistically significantly upregulated in Y201 secretome versus Y202 it was still relatively highly abundant in the Y202 cells, indicating that this may be an important ECM protein for a variety of stromal subtypes. This could help to explain the extensive expression of this ECM protein in bone marrow.

I showed previously that the Y201 multipotent stromal subset had a highly contrasting secretome to that of the Y202 nullipotent stromal cell. The major differences in secreted protein were largely enriched for ECM components (Figure 4.8). Here I have revealed the localisation of these ECM proteins in bone marrow in both mouse and human tissue suggesting some conservation of function in the role of these ECM proteins. The use of cell surface markers to identify stromal cell subtypes has long been key for identification

and sorting for specific cell function and potency, however, I demonstrate that secreted outputs may allow further discrimination of subtypes and may also sufficiently identify their *in vivo* location if sufficiently discriminatory ECM proteins are selected.

Truly multipotent progenitors of skeletal lineages are likely to be rare in adult tissue, and the composition of their niche may be specialised to promote their maintenance. The deposition of varied ECM proteins could be important for maintenance of cell-function *in vivo* and *in vitro* and offers a potential secreted marker of cell functionality. Collectively the localisation data highlight that the primary location where all Y201 upregulated proteins were identified was along the endosteal or trabecular region of bones, although expression of proteins such as collagen VI, biglycan and CEMIP were fairly ubiquitous and may not powerfully discriminate a distinct niche. CEMIP expression in mouse bone corroborated previous in-situ-hybridization work in human bone indicating expression in endosteal locations (Chen et al., 2019). Aggrecan and periostin demonstrate high fold-increase in the secretome of Y201 versus Y202 and in human tissue were found underlying and colocalised with some, but not all, $CD271^{+}$ bone lining cells. These proteins could help demarcate presence of a unique stem cell niche in bone marrow along the endosteal region of bone trabeculae, where previously multipotent progenitors, including $CD271^{+}$ cells have been shown to preside (Jones et al., 2010; Nuttall et al., 1998). I hypothesise that these ECM components are important for the generation of a specific niche to complement their appropriate maintenance *in vivo* and that assaying for matrix composition of extracted cells *in vitro* may help to identify appropriately potent populations. Together, the multipotent characteristics, high CFU-F capacity and the *in vivo* colocalisation of CD271 and ECM components highlights how ECM could be used to identify stem cell niche *in vivo*. It would be of interest to expand the immunofluorescence work to look for dual-labelled $periostin^{+}aggrecan^{+}$ niches along with more markers of known stem cell populations such as CD146, CD56 and CD164 (Chan et al., 2018; Sacchetti et al., 2007). To determine the importance of periostin and aggrecan to the stromal niche it would also be of interest to sort primary human stem cells with known criteria into plastic culture and assess their matrix production. Functional assessment of periostin and aggrecan containing matrices on stem cell characteristics such as differentiation and self-renewal would also be of interest.

Periostin has previously been linked with controlling the regenerative potential of periosteal skeletal stem cells, as well as supporting HSCs in the foetal liver niche and regulating their quiescence (Biswas et al., 2020; Duchamp de Lageneste et al., 2018). The

observation of low abundance periostin by immunofluorescence in mouse bone marrow was extremely rare and was not reported in larger assessments of protein distribution across whole long-bones, although BMSC-derived periostin has also been shown in mouse to have functional effects in leukaemia, suggesting it is present in marrow (Coutu et al., 2017; Duchamp de Lageneste et al., 2018; Ma et al., 2019). Aggrecan has a well characterised role in cartilage development, however its role in trabecular bone and stem cell niches is understudied. Aggrecan in cartilage facilitates compression resistance but this key proteoglycan has also been shown to act as a binding partner for hyaluronan (HA), which is capable of maintaining MSC quiescence, and may therefore indicate a potential functional role for aggrecan in the MSC matrix (Watanabe et al., 1997; Wong et al., 2017). An elegant lineage tracing study using an aggrecan-Cre mouse revealed expression of aggrecan by mesenchymal progenitors in epiphyseal marrow during development which could correlate with the expression of aggrecan seen in trabecular lining stromal cells (Ono et al., 2014).

Co-expression of ITGAV with the ECM proteins further indicates a potential mechanism for integrin binding to matrix, and could highlight the mechanisms by which these cells interact with their local microenvironment and actively migrate across the trabecular surface. ITGAV has also previously been shown to identify quiescent bone lining cells that are capable of contributing to the osteogenic lineage, this population also had some overlap with MSCs by surface marker expression and could correlate with a similar population of cells (Matic et al., 2016).

Overall, I have identified proteins that could be important for functionality of prospective multipotent BMSC niche that correlates with $CD271^{+}$ BMSC localisation *in vivo*. This work reveals the potential candidacy for use of markers of the niche, in addition to cell-surface markers, to identify stromal subpopulations.

6 General Discussion

6.1 The aims

The aims of this PhD were to utilise a panel of heterogeneous BMSC clones to identify variation in paracrine signalling between subpopulations and establish if secreted factors were capable of altering the phenotype of other BMSC subtypes. -Omics approaches were employed to screen for differences in the secretomes before using differentially expressed secreted proteins to identify the localisation of distinct subsets *in vivo*.

6.2 Summary of key findings

CM from migratory Y201 cells was capable of increasing migration on non-migratory Y202 cells. This was accompanied by a change in cellular morphology resulting in Y202 cells appearing more fibroblastic. I subsequently demonstrated that this increase in migration could be recapitulated by culturing Y202 on ECM derived from either cell line, and I showed that this migratory capacity was FAK-dependent. These findings demonstrating induction of a migratory phenotype by soluble factors led me to interrogate the secreted factors of these cell types using omics approaches. I performed LC-MS/MS and NanoString analyses to identify differences in secreted proteins, extracellular vesicle proteins and miRNAs. I observed that the secretome of the tri-potent Y201 clone was highly enriched for ECM products when compared to Y202. Subsequent investigation of the ECM produced by Y201 and Y202 cells revealed considerable structural differences which were apparent by SEM and FIBSEM.

I concluded from these *in vitro* studies of BMSC clones that the secretome of subtypes was important for maintaining cellular phenotype, and I used information from our proteomic approach to select candidate markers of a multipotent stromal cell ECM *in vivo*. I identified the expression of 6 ECM proteins (5 upregulated in Y201 and 1 upregulated in Y202) in mouse bone marrow, with these proteins found primarily in the endosteal regions. I subsequently identified the expression of periostin, aggrecan, biglycan, collagen VI and lumican in human bone marrow sections. Periostin and aggrecan were the two most highly differently expressed proteins in Y201 secretome versus Y202 secretome. I identified rare expression of periostin and aggrecan, predominantly lining trabecular regions in human bone. I then used CD271 and ITGAV, well characterised markers of BMSCs, to demonstrate colocalisation with periostin and aggrecan, exclusively in the trabecular regions, although

not all CD271$^+$ or ITGAV$^+$ cells were positive for periostin or aggrecan, highlighting the potential of these proteins to mark a subtype of BMSC.

Overall I highlighted how secreted factors from stromal subtypes are capable of influencing BMSC behaviour, particularly migration. These data also re-iterate that more stringent classifications are required to identify functionally distinct stromal cell populations and that assessment of cell-secreted factors may provide an assayable approach to identify subtypes.

6.3 Secreted factors and their potential in understanding heterogeneity and relation to cell phenotype

There have been various studies analysing the secretome of BMSCs by proteomic approaches, including in comparisons with MSCs isolated from alternative tissue sources. This thesis represents a novel approach to investigate the secretome of distinct BMSC subpopulations through comprehensive analysis of two compartments of the secretome, investigating the soluble proteins and EV encapsulated proteins and miRNAs. The use of the secretome to predict cell functionality is not a new concept for BMSCs, and has been utilised in combination with transcriptomics to predict responses to possible inflammatory situations *in vivo* (Chinnadurai et al., 2018). This approach, however, did not use clonal populations and looked more generally at overall population responses, which are likely heterogeneous.

I identified functional differences in secretomes between heterogeneous BMSCs and subsequently identified varied abundance of secreted factors that mirrored this heterogeneity. The ECM was consistently identified as a major difference in the secretomes of phenotypically distinct BMSCs subtypes.

6.3.1 ECM as a regulator of BMSC function

Observations of differential ECM expression show promise as a candidate approach for the localisation of potent subsets, but could also help in identifying the functionality of distinct subpopulations. Given the upregulation of aggrecan and periostin in a multipotent progenitor there is potential that these proteins may act to facilitate the maintenance of the stem cell phenotype and be important in other aspects of the stem cell niche. Considering the maintenance of the immortalised BMSC phenotypes *in vitro*, secreted ECM potentially indicates a mechanism through which phenotype is maintained by the production of a “niche” environment by deposition of ECM.

The importance of periostin in stem cell niches was established in knockout mice presenting with malformation of long-bone trabecular regions, potentially indicative of an exhaustion of stem cell progenitors, and they also have a reduced capacity for repair from periosteal skeletal stem cells in a model of fracture healing (Duchamp de Lageneste et al., 2018; Rios et al., 2005). Furthermore, in HSCs, a link between ITGAV and periostin has been established in regulation of stemness with increased proliferation and faster loss of primitive progenitor cells in periostin knockout mice (Khurana et al., 2016). This finding of periostin and the regulation of HSCs could possibly correlate with the functionality I identified of improved HSC survival on the Y201 ECM *ex vivo*, although evidence for incorporation of the periostin in the ECM would be needed. It may also highlight a mechanism through which BMSC subtypes are able to support haematopoiesis *in vivo* through interaction between BMSC ECM and HSCs.

In contrast to periostin there is little known about aggrecan in the role of stem cell maintenance, perhaps due to its prevalence as a marker of cartilage and chondrogenic differentiation, although expression of aggrecan has been seen in other studies of BMSCs (Mwale et al., 2006). Despite the lack of information regarding aggrecan and its role in stem cell maintenance, there is characterisation of its role in the binding of hyaluronic acid (HA) which is a key glycosaminoglycan of ECM (Kiani et al., 2002). HA has important roles in cell migration and has been implicated in maintenance of stem characteristics in embryonic stem cells when cultured in a 3D hydrogel environment but not in a 2D culture (Gerecht et al., 2007). Presentation of HA may therefore be important for function and could explain functionality of Y201 ECM. The protein CEMIP, a hyaluronan binding protein, was also present at higher levels in the Y201 matrix, further implicating a possible role of HA in modifying the ECM.

The structure of the ECM produced by Y201 was visibly different to that of Y202 and there is considerable evidence to suggest that the mechanics of growth surfaces are capable of influencing differentiation and other cellular phenotypes such as inflammatory signalling. The influence of surface topography and structure has been demonstrated to be of fundamental importance for maintenance of stemness through manipulation of the surface experienced by BMSCs, indicating that a native matrix may produce a topography with similar characteristics (McMurray et al., 2011). It would be interesting to determine if the mechanics of Y201 and Y202 matrices altered inflammatory signalling differently, given the inherently high basal expression of inflammatory genes in Y202. This could correlate

with recent work performed using hydrogels of varying stiffnesses that demonstrated BMSC inflammatory signalling could be enhanced by a softer matrix (Wong et al., 2020). The Y202 may naturally produce a matrix that perpetuates a high basal inflammatory gene expression. The presence of soluble matrix components in CM may also help to explain the dramatic increase in expression of the 8 inflammatory genes in Figure 4.10 if binding to these components is sufficient to trigger increase gene expression. This soluble expression of ECM components from Y201 could also link to the increase in cell migration seen with Y201CM on Y202 and how this was recapitulated using decellularized ECM.

Interestingly, TGFβ1 was identified at higher levels in the EV fraction of Y201 samples and the binding partners of TGFβ1, LTBP1 and LTBP2 were identified at significantly higher levels in secretome. LTBP1 has been shown to bind TGFβ1 and facilitate its attachment to ECM (Taipale et al., 1994). TGFβ1 also has a role in chemotactic migration of BMSCs as well as acting to negatively regulate osteogenic differentiation, potentially highlighting a role in maintenance of stem-cell functionality (Maeda et al., 2004; Tang et al., 2009b). This interplay between the ECM and the role of TGFβ1 could help to explain the regulation of the stem cell phenotype and the considerable effort that is exerted by the Y201 tripotent BMSC clone into producing and patterning its ECM. There is also a potential coinciding role of the stromal marker ITGAV in the activation of TGFβ1 with various integrin heterodimers contained ITGAV demonstrated to facilitate release of latent bound TGFβ1 or bind it in its latent form (Annes et al., 2004; Asano et al., 2005; Mu et al., 2002; Munger et al., 1998). Overall the findings indicate a strong influence of ECM on driving heterogeneous cell functions with potential regulation by both mechanics and presentation of cytokines.

Clear distinctions between functionally heterogeneous BMSC populations can be drawn from their secretory phenotype. The use of ECM in particular provides an attractive prospect for the development of studies into subtype localisation and phenotype as I have demonstrated clear differences in the ECM produced by heterogeneous stromal cell types, and now efforts to understand the function of these ECMs and how they control BMSC phenotype may help us to understand essential biology with regards to functions such as migration, inflammatory response and stemness.

6.3.2 ECM as markers of *in vivo* BMSC subtype localization

Periostin and aggrecan subsequently proved to colocalize with CD271$^+$ and ITGAV$^+$ bone lining cells *in vivo*. CD271$^+$ BMSCs have previously been shown to occur in endosteal regions, so the colocalisation in this region indicates an appropriate localisation (Ilas et al.,

2020; Tormin et al., 2011). Given the tripotent phenotype of Y201 it could be that the expression of these matrix proteins is capable of marking tripotent subpopulation locations *in vivo* (Figure 6.1). Follow up work to isolate CD271$^+$ aggrecan and periostin expressing primary cell subsets is necessary to determine if these possible biomarkers of potency are consistent and selective. This use of ECM components presents a novel approach to aid localisation of specific BMSC subtypes, and expands upon the work that has previously been undertaken to identify the localisation of BMSCs *in vivo*. The majority of previous studies demonstrated localisation and potency but without complete characterisation of heterogeneity within populations collectively expressing the same surface markers.

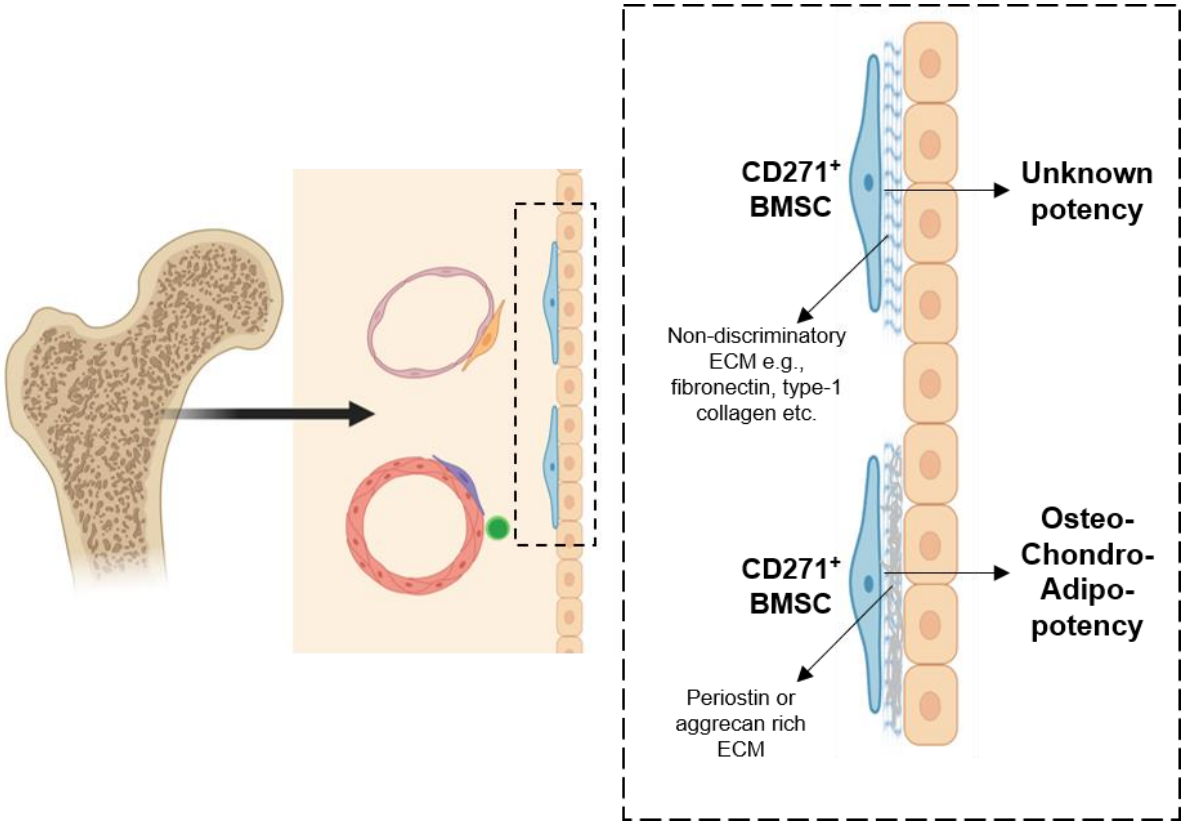

Figure 6.1 The ECM may mark functionally distinct population locations *in* vivo

A schematic of the putative bone marrow niche of endosteal/trabecular located CD271$^+$ cells (blue) demonstrating how the ECM components periostin and aggrecan could potentially highlight the location of tripotent clones in vivo. CD271$^+$ BMSCs are shown lining the endosteal region.

6.4 Heterogeneity in the context of modern single-cell approaches

BMSCs have often been studied as if they were homogeneous populations, despite considerable evidence for heterogeneity in their morphology, behaviour, potency and gene expression. Heterogeneity exists both intra- and inter- donor and advances in identifying subtypes by surface markers has proven useful at dissecting this heterogeneity to a degree (Table 1.1). However, it is evident from the latest scRNAseq studies that provide comprehensive profiling of heterogeneity at the transcriptomic level, that better markers, or alternative ways of classifying cells, are required to unravel functionally distinct subtypes and their locations (Baryawno et al., 2019; Tikhonova et al., 2019; Wolock et al., 2019). These studies investigated non-haematopoietic, skeletal lineages and BMSCs through varied isolation and separation strategies, however they all independently clustered murine $LepR^{+}$ BMSCs into 4 subgroups, confirming a level of heterogeneity within the population. Despite this, looking at expression within these groups in the study by Baryawno et al. (2019), which offered a larger number of clusters with which to define stroma and progenitors, there still appears to be variation within these subgroups and considerable overlap, even in expression of markers commonly used to help define subgroups such as LepR and CXCL12.

It is difficult to categorically state where the immortalized clones used in this study fit in the cell-type clusters as defined in these studies, both because they are performed in mouse rather than human cells and equally that they are categorized by relative expression across a large number of cell subpopulations, which makes determining high and low expression by relative comparisons tricky. For instance, CXCL12 is more highly expressed by Y201 versus Y202 yet there could feasibly be other stromal cells that express considerably higher CXCL12 than even Y201. However, when looking at the publicly available datasets from Baryawno et al. (2019) and Tikhonova et al. (2019) for aggrecan and periostin, both indicated an upregulation of the respective genes for these ECM proteins within primitive osteolineage precursors or LepR MSCs, suggesting a potential for these to mark potent populations, although neither study confirmed potency of cells in their relative subcompartments, as lineage was inferred from gene expression analyses. These studies at the single cell level undoubtedly provide considerable power for compartmentalizing, however, the observed level of variation and stochasticity seen in transcriptomes and the attempts to compartmentalize these may be artefacts of an absolute approach to cell identity, when in actuality the plasticity and variation seen in BMSCs may mean that the

overlap in phenotypes results in no true cell subgroups, but rather indicates a more plastic and dynamic mix of phenotypes. The fluctuation in phenotypes means other methods of distinguishing cells that overlap more closely are needed, particularly for the selection of appropriate populations for therapies. Interestingly a study of dendritic cells by Shalek et al. (2014) that utilized an elegant microfluidic mechanism for blocking paracrine signalling between cells highlighted how paracrine signals were able to strongly influence heterogeneity, therefore indicating the importance of understanding secreted factors and their influence on cell phenotype and plasticity. I demonstrated a level of plasticity in some aspects of cell phenotype, including inflammatory gene expression and migration, in response to secreted factors. This provides a significantly reduced model of the complex make-up of the bone marrow microenvironment but highlights BMSC heterogeneity and plasticity and a potential for BMSCs to drive changes in other BMSCs phenotype through secreted factors, which may help to drive the exceptional diversity seen in single cell studies.

6.5 Secreted factors for selection of therapeutic populations

Periostin and aggrecan could be promising in the development of assays and strategies for identification of tripotent cell populations for regenerative therapies, and other more broad targets overlapping with Y101 population could be included if osteo-chondral differentiation is required. These targets have been determined following *in vitro* culture of immortalised clones and so confirmation of their specificity with primary cells will be important, although, immortalisation of BMSCs has been shown to maintain the phenotype of primary cells in terms of differentiation capacity, and the Y201 has previously been shown to preserve mechanoresponsiveness seen in primary cultures (Abdallah et al., 2005; Galarza Torre et al., 2018; Twine et al., 2018).

If secreted markers such as ECM products are identified as subtype/potency markers then this could result in new approaches to the selection of cell populations for therapeutic purposes (Figure 6.2). The use of ELISAs or antibody arrays may provide appropriate throughput/sensitivity, and there is even evidence for technologies capable of screening secreted factors at the single cell level (Hsu et al., 2018; Lu et al., 2013). The non-destructive nature of assaying secreted factors is also of benefit for clonal expansion and isolation of sufficient cell numbers for therapies. Furthermore this work reveals the secreted content of heterogeneous BMSCs, providing possible avenues for the development of conditioned media or secreted factor derived therapies through selection of

populations with more homogeneous and therapeutically viable assortment of proteins or EVs. Determination of how these heterogeneous secretomes may differ in various therapeutic settings may even provide a greater arsenal of therapeutics cell populations through understanding of the secreted factors of subtypes.

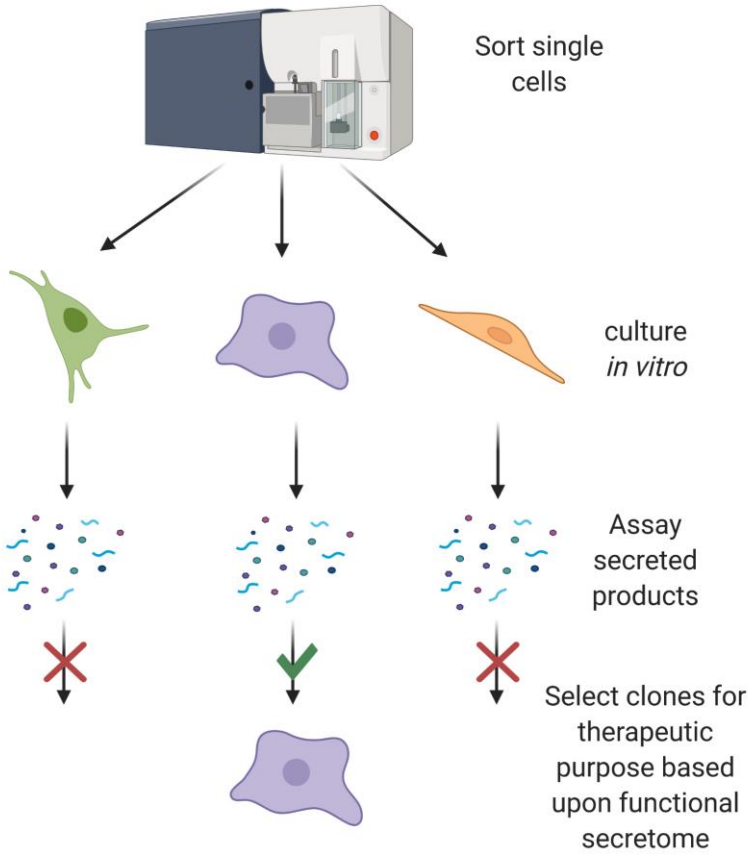

Figure 6.2 A strategy of using secreted products for the selection of cells for therapies
A potential pipeline for the isolation of therapeutically relevant BMSC populations from a heterogeneous mix. Sort individual cells (potentially in combination with cell surface markers) and expand cells *in vitro*. Use high sensitivity assays for detection of previously determined secreted markers of potency (such as ECM products) and select clones for applications based upon this approach.

6.6 Conclusions

The study of BMSC heterogeneity is important for fundamental understanding of the roles of specific subtypes in bone marrow during homeostasis and disease, as well as for selection of appropriate populations for therapeutics. The work presented in this thesis reinforces the necessity for improved scrutiny and characterisation of BMSC populations, particularly if they are to be developed for various therapeutic applications requiring selection of homogeneous, effective and reproducible populations (Wilson et al., 2019a). In

this thesis I aimed to demonstrate differences in BMSC subpopulation functions by a thorough characterisation of immortalised clonal lines. I provided clear evidence for differential protein secretion by heterogeneous BMSC clones and these secreted factors could prove predictive of BMSC phenotype, something that could be confirmed with follow-up studies. I specifically noted large differences in the expression of ECM proteins between clones, which proved effective as a novel strategy for the identification of subpopulations of BMSCs in vivo in combination with classical cell-surface markers. The ECM of specific BMSC subtypes may drive their phenotype or act as an indicator of distinct populations, a feature that could be confirmed with larger-scale assessments of primary BMSC cultures. I also observed plasticity in BMSC subtype morphological, migratory and inflammatory phenotypes that could be altered be secreted factors from other BMSCs which has consequences for the in vitro study of BMSCs and may need to be considered when drawing conclusions from mixed populations of cells from primary cultures.

The development of technologies to investigate heterogeneity at the single-cell level is likely to reveal increasingly heterogeneous populations of BMSCs. Investigation and compartmentalisation of populations by their transcriptomic profiles is informative, however, I propose that assessment of BMSC secretomes could prove useful as a non-destructive methods for characterisation and identification of functionally distinct cell subpopulations, as well as potentially improving selection of therapeutically effective populations.

7 Appendix

Supplementary Table 1 List of proteins and fold changes between 44 proteins significantly more abundant in Y201 vs Y202 total secretome

Protein	Log2 fold change Y201 vs Y202	Protein	Log2 fold change Y201 vs Y202	Protein	Log2 fold change Y201 vs Y202
ACAN	6.71	SULF1	3.44	LAMC1	1.93
POSTN	6.17	OLFML2B	3.39	THBS1	1.81
C2	6.06	THBS2	3.31	VCAN	1.81
CD248	4.93	THBS3	3.14	NOTCH3	1.77
CEMIP	4.92	CXCL12	2.99	LTBP1	1.70
COL5A3	4.56	ENPP2	2.93	ADIRF	1.68
HSPB6	4.56	SPOCK1	2.88	TNXB	1.60
SERPINB2	4.26	AKAP12	2.82	DCN	1.59
TNFRSF11B	4.16	S100A4	2.79	COL6A1	1.44
MASP1	4.13	MYLK	2.75	LTBP2	1.37
CRIP2	3.84	CYTL1	2.44	NOTCH2	1.32
LAMA2	3.80	JAG1	2.29	FN1	1.17
SCUBE3	3.68	MFAP2	2.22	FABP5	1.10
A2M	3.66	NOV	2.20	ADAMTS7	1.08
ADAMTS1	3.47	BGN	1.93		

Supplementary Table 2 List of proteins and fold changes between 129 proteins significantly more abundant in Y202 vs Y201 total secretome

Protein	Log2 Fold change Y202 vs Y201	Protein	Log2 Fold change Y202 vs Y201	Protein	Log2 Fold change Y202 vs Y201
DKK1	infinite	PSAT1	2.24	WARS	1.47
CES1	6.49	SRPX2	2.23	FLNB	1.46
IDS	5.23	AKR1B1	2.20	LTBP4	1.45
LCP1	4.78	HEXB	2.13	PLOD3	1.45
QPCT	4.59	MINPP1	2.09	PDXK	1.43
DSC3	4.39	FLRT2	2.08	GSS	1.43
COL4A5	4.38	HNRNPC	2.07	CLSTN1	1.42
IL18	4.20	HGS	2.06	RNASET2	1.42
PSG9	4.04	PSPH	2.01	FKBP4	1.40
IGFBP2	3.66	CAP2	1.99	WDR1	1.38
BCHE	3.61	PGM1	1.97	SEC31A	1.37
OLFML1	3.41	TARS	1.94	NPC2	1.35
EIF4A2	3.39	RCN1	1.92	ADAMTS5	1.33
PLOD2	3.36	ERP29	1.91	EZR	1.33
CPA4	3.36	PFKP	1.90	P3H1	1.30
MATN2	3.32	CFH	1.79	FHL2	1.29
LUM	3.28	PA2G4	1.79	CTSZ	1.28
AP2A1	3.23	CFB	1.77	KTN1	1.28
HSPA13	3.15	CDH8	1.75	PXDN	1.26
DKK3	3.08	HSPB1	1.72	GLRX3	1.23
MSLN	2.93	MAN2A1	1.71	CCT7	1.14
NPR3	2.92	HAGH	1.71	PSME2	1.14
PSMD1	2.89	AXL	1.69	CLTC	1.13
PRKACA	2.72	LRRFIP1	1.69	CNN2	1.10
SERPINB6	2.70	DAG1	1.69	FBN1	1.10
CRYAB	2.66	TALDO1	1.68	IQGAP1	1.10
ICAM1	2.64	RGMB	1.68	ANXA1	1.04
EMILIN2	2.55	BTD	1.67	UGGT1	1.01
NNMT	2.54	GBP1	1.67	CST3	0.99
LOXL3	2.52	FSTL1	1.65	CCT5	0.95
PGM3	2.51	GSTM3	1.65	FHL1	0.92
PDLIM1	2.49	COL5A2	1.64	PKM	0.90
PVR	2.40	CCT6A	1.63	KPNB1	0.87
TUBB2A	2.40	COL12A1	1.63	IDH1	0.87
ATP5B	2.38	SERBP1	1.61	RBMX	0.80
CLU	2.37	TWSG1	1.61	SCRN1	0.76
UCHL1	2.36	SERPINH1	1.57	OLFML3	0.73
P4HA1	2.36	HYOU1	1.56	XPNPEP1	0.73
NANS	2.35	CYR61	1.54	TAGLN2	0.72
ULBP2	2.31	UBA1	1.54	PABPC1	0.63
AKR1C3	2.31	SOD1	1.50	CSRP1	0.47
FAM3C	2.26	GGH	1.49	GSTO1	0.45
LGMN	2.25	CNDP2	1.48	PLOD1	0.45

Supplementary Table 3 List of proteins and fold changes between 162 proteins significantly more abundant in Y201 EVs vs Y202 EVs

Protein	Log2 Fold change Y201 vs Y202	Protein	Log2 Fold change Y201 vs Y202	Protein	Log2 Fold change Y201 vs Y202
AKAP12	9.17	MYO1D	2.40	DSTN	1.35
SLC26A1	8.56	PSAT1	2.32	LRRC17	1.35
SULF1	7.86	NRP1	2.31	AARS	1.34
HIST2H3A	6.52	IGSF8	2.29	ACTN1	1.34
BST1	4.81	MAPK1	2.28	CALM1	1.30
GJA1	4.75	PTP4A2	2.25	GLIPR2	1.29
CPNE2	4.41	PCOLCE	2.17	ITGA7	1.29
FLOT1	4.25	CDH11	2.14	SRC	1.29
HSPB6	4.13	ARPC1B	2.11	PGAM1	1.27
SLIT3	4.12	COL6A3	2.10	CPNE1	1.24
S100A4	4.11	WDR1	2.07	COL1A2	1.22
MAP1B	3.94	QSOX1	2.06	EHD2	1.22
SQSTM1	3.78	TGFBI	2.06	ERP29	1.21
ITGA11	3.70	COL6A2	1.96	VIM	1.20
40787	3.65	PDCD6IP	1.94	SARS	1.18
CPNE8	3.58	SCUBE3	1.92	ALPL	1.17
BGN	3.44	HTRA1	1.91	KPNB1	1.17
LRRC32	3.40	FN1	1.88	MYO1B	1.16
HEG1	3.33	RFTN1	1.88	CSRP1	1.12
PLAUR	3.31	CLIC4	1.86	RAB7A	1.10
CD63	3.30	EHD1	1.86	RAB32	1.10
CEMIP	3.25	PLXNB2	1.82	LDHB	1.09
FH	3.23	COL6A1	1.80	LMAN1	1.09
RHOC	3.19	SLC1A4	1.76	YWHAH	1.09
RECK	3.12	PAFAH1B1	1.76	ANXA2	1.08
ITGA4	3.06	COL1A1	1.74	ST13	1.08
FAP	3.03	WNT5B	1.74	RPL27	1.08
CAVIN1	2.99	ATP2B4	1.73	RAB6A	1.03
CALD1	2.83	LDHA	1.71	RPL10	1.01
PTTG1IP	2.80	RELN	1.70	STOM	1.00
SLC1A5	2.75	A2M	1.69	POSTN	0.98
PTGFRN	2.75	CHMP1A	1.69	RAB1B	0.97
LAMB2	2.75	CAPNS1	1.64	CD44	0.96
VTA1	2.74	ACTN4	1.59	PFN1	0.93
RNH1	2.73	TAOK3	1.59	HSPD1	0.92
KIDINS220	2.69	HNRNPM	1.59	GFPT1	0.91
MRGPRF	2.69	CD9	1.54	STAT1	0.89
COL4A2	2.67	CORO1C	1.53	RAC2	0.88
CD81	2.62	YWHAQ	1.50	YWHAG	0.86
CSPG4	2.62	UBB	1.49	HBA1	0.85
CHMP2A	2.61	NRAS	1.49	TFRC	0.84
RPL29	2.58	CPNE3	1.49	DPYS	0.81
SDCBP	2.57	CYFIP1	1.46	RPSA	0.80
TTYH3	2.57	RPL6	1.46	CLTC	0.78
ANPEP	2.54	COL4A1	1.45	HSPA8	0.76
ENAH	2.50	FSCN1	1.44	HSP90AA1	0.75
TGFB1	2.48	KCTD12	1.41	MAMDC2	0.70
DCN	2.48	CD59	1.41	EEF2	0.67
VDAC1	2.46	LAMP1	1.40	ACTB	0.66
GPC1	2.46	IQGAP1	1.39	TLN1	0.65
ADAM9	2.44	CAP1	1.38	FLNA	0.65
PDLIM5	2.42	STXBP2	1.37	GANAB	0.63
PODXL	2.41	RPL17	1.37	APOM	0.60
FARP1	2.40	PABPC1	1.35	TNXB	0.57

Supplementary Table 4 List of proteins and fold changes between 14 proteins significantly more abundant in Y202 EVs vs Y201 EVs

Protein	Log2 Fold change Y202 vs Y201
LTF	4.82
MATN2	4.08
RAB1A	2.71
NAV1	2.40
AFM	2.13
TSPAN14	2.05
UCHL1	1.97
TNC	1.92
FSTL1	1.66
LOXL3	1.62
PLOD2	1.34
PLSCR3	1.33
CTGF	1.11
JCHAIN	0.36

Supplementary Table 5 List of Matrisome annotated proteins that did not differ significantly in normalised abundance between Y201 and Y202 total secretome

Protein	Mean Normalized Abundance		Log2 FC	Protein	Mean Normalized Abundance		Log2 FC	Protein	Mean Normalized Abundance		Log2 FC
	Y201	Y202			Y201	Y202			Y201	Y202	
SPARC	1.24E+09	1.22E+09	0.02	SRGN	6.17E+06	7.44E+06	-0.27	SVEP1	5.10E+05	4.17E+05	0.29
COL1A2	8.68E+08	7.32E+08	0.25	TNC	5.72E+06	3.49E+06	0.71	PAMR1	5.01E+05	8.62E+05	-0.78
COL1A1	4.28E+08	4.47E+08	-0.06	SERPINE1	4.93E+06	1.52E+07	-1.62	SEMA5A	4.26E+05	2.33E+05	0.87
IGFBP7	3.98E+08	4.05E+08	-0.02	CRIM1	4.89E+06	6.80E+06	-0.47	PLAU	4.03E+05	1.20E+06	-1.57
TIMP1	1.86E+08	1.14E+08	0.71	CSPG4	3.93E+06	7.15E+06	-0.86	CSTB	3.70E+05	9.22E+05	-1.32
FBLN1	1.30E+08	5.57E+07	1.22	ADAM10	3.69E+06	3.16E+06	0.22	CCBE1	3.46E+05	1.12E+06	-1.70
ECM1	1.13E+08	7.05E+07	0.68	CD109	3.69E+06	2.60E+06	0.51	PAPPA	3.36E+05	5.81E+05	-0.79
COL6A2	1.08E+08	4.69E+07	1.21	LAMA4	3.69E+06	1.99E+06	0.89	SDC4	3.29E+05	1.94E+05	0.76
COL6A3	7.94E+07	2.73E+07	1.54	CTSL	3.67E+06	6.57E+06	-0.84	COL11A1	3.02E+05	1.92E+05	0.65
TGFBI	7.20E+07	1.37E+07	2.39	INHBA	3.43E+06	9.78E+05	1.81	ADAMTS2	2.88E+05	1.48E+05	0.96
COL4A2	7.19E+07	4.57E+07	0.65	SERPING1	3.35E+06	2.39E+06	0.49	SRPX	2.65E+05	6.49E+05	-1.30
LGALS1	6.41E+07	8.47E+07	-0.40	SEMA7A	3.30E+06	4.15E+06	-0.33	ADAM15	2.41E+05	1.51E+05	0.67
TIMP2	6.15E+07	5.80E+07	0.09	IGFBP1	3.23E+06	4.90E+06	-0.60	FST	2.40E+05	2.23E+05	0.11
PCOLCE	6.07E+07	3.63E+07	0.74	EFEMP2	3.06E+06	3.22E+06	-0.07	SERPINB1	2.11E+05	5.82E+05	-1.46
IGFBP6	6.02E+07	2.74E+07	1.14	AGRN	3.06E+06	1.39E+07	-2.18	LGALS3	2.01E+05	9.52E+04	1.08
COL3A1	5.63E+07	1.44E+08	-1.36	COL8A1	3.01E+06	2.51E+06	0.26	SMOC1	1.99E+05	2.21E+05	-0.15
IGFBP4	5.47E+07	3.82E+07	0.52	CTSD	2.50E+06	4.18E+06	-0.74	GAS6	1.92E+05	1.54E+05	0.32
HSPG2	5.21E+07	4.99E+07	0.06	EMILIN1	2.45E+06	3.08E+06	-0.33	PLAT	1.75E+05	2.13E+05	-0.28
COL4A1	5.08E+07	5.03E+07	0.01	NID2	2.19E+06	4.36E+06	-0.99	SBSPON	1.72E+05	2.67E+05	-0.64
CTSB	4.86E+07	2.62E+07	0.89	CSF1	2.15E+06	2.15E+06	0.00	WISP2	1.54E+05	8.07E+05	-2.39
EFEMP1	4.30E+07	8.44E+07	-0.97	GPC1	2.12E+06	2.33E+06	-0.14	ADAM12	1.18E+05	1.41E+05	-0.26
MMP2	3.81E+07	5.12E+07	-0.43	FBN2	1.98E+06	5.37E+06	-1.44	PRELP	1.01E+05	1.39E+05	-0.45
IGFBP3	2.23E+07	8.93E+06	1.32	CLEC11A	1.82E+06	3.08E+06	-0.76	NTN4	9.47E+04	4.40E+04	1.11
COL5A1	2.22E+07	2.83E+07	-0.35	FBLN5	1.57E+06	5.55E+05	1.51	SEMA3B	8.94E+04	2.95E+05	-1.72
MFAP5	2.14E+07	1.12E+07	0.93	FSTL3	1.56E+06	2.38E+06	-0.61	PCOLCE2	7.90E+04	3.53E+04	1.16
SERPINE2	1.96E+07	1.86E+07	0.07	LAMA1	1.49E+06	7.55E+05	0.98	LIF	7.85E+04	1.55E+05	-0.98
ITIH2	1.73E+07	8.98E+06	0.95	LOXL1	1.35E+06	3.03E+06	-1.17	MMP19	7.53E+04	1.33E+05	-0.82
MFGE8	1.61E+07	1.37E+07	0.23	MEGF6	1.31E+06	2.69E+06	-1.04	AGT	7.10E+04	8.95E+04	-0.33
HTRA1	1.35E+07	7.71E+06	0.81	LAMB2	1.28E+06	3.76E+05	1.77	ANXA6	6.81E+04	1.13E+05	-0.73
LAMB1	1.31E+07	8.20E+06	0.67	MMP1	1.25E+06	4.26E+06	-1.77	GDF15	4.60E+04	1.55E+05	-1.75
S100A11	1.27E+07	1.05E+07	0.28	HAPLN1	1.17E+06	3.90E+05	1.59	SERPINF1	4.16E+04	2.20E+03	4.24
LOX	1.11E+07	9.54E+06	0.22	FBLN7	1.09E+06	3.95E+05	1.46	ADAM17	3.74E+04	8.40E+04	-1.17
LOXL2	1.05E+07	9.83E+06	0.10	LAMA5	9.57E+05	2.99E+05	1.68	LTBP3	3.52E+04	1.13E+05	-1.68
NID1	9.96E+06	6.62E+06	0.59	S100A16	8.93E+05	6.61E+05	0.43	ANGPT1	3.30E+04	7.79E+04	-1.24
CLEC3B	9.53E+06	1.46E+07	-0.61	CTSA	8.15E+05	6.92E+05	0.24	SNED1	2.68E+04	8.93E+03	1.59
CTGF	7.95E+06	7.46E+06	0.09	ADAMTSL1	7.45E+05	1.63E+06	-1.13	VIT	2.35E+04	2.91E+04	-0.31
ABI3BP	7.95E+06	1.03E+07	-0.38	CTHRC1	7.41E+05	5.81E+04	3.67	SEMA3F	1.56E+04	5.67E+04	-1.86
RELN	7.83E+06	1.90E+06	2.04	VEGFC	6.51E+05	1.02E+06	-0.65	PAPPA2	8.62E+03	0.00E+00	infinity
BMP1	7.23E+06	7.78E+06	-0.11	EDIL3	6.42E+05	1.84E+06	-1.52	ESM1	4.68E+03	2.26E+04	-2.27
ANXA2	7.17E+06	5.57E+06	0.36	ANXA5	5.63E+05	5.00E+05	0.17	PDGFC	3.68E+03	3.87E+04	-3.39
ADAM9	7.14E+06	8.78E+06	-0.30	MMP14	5.13E+05	2.63E+05	0.97				

7.1 Code used for EV miRNA data processing

```
```{r setup, include=FALSE}
knitr::opts_chunk$set(echo = TRUE)
library(readxl)
library(tidyr)
library(data.table)
library(plyr)
library(dplyr)
library(ggplot2)
library(ggrepel)
library(pheatmap)
library(viridis)
source('mysummary.R')
```
#Read Data in
Read data in from Excel file

```{r Original import, include=FALSE}
miRNA <- read_excel("nanostring export table.xlsx")
```

```{r Tidying}
names(miRNA) <- c("miRNA",
"Accession",
"Class_Name",
"Analyte_Type",
"PC_Samples_above_Threshold",
"Y202_A",
"Y202_B",
"Y202_C",
"Y202_D",
"Y101_A",
"Y101_B",
"Y101_C",
"Y101_D",
"Y102_A",
"Y102_B",
"Y102_C",
"Y102_D",
"Y201_A",
"Y201_B",
"Y201_C",
"Y201_D",
"Y1015_A",
"Y1015_B",
"Y1015_C",
"Y1015_D",
"Y101_avg",
"Y102_avg",
"Y201_avg",
"Y202_avg",
"Y101.5_avg",
"Y202_st.dev",
"Y101_st.dev",
"Y102_st.dev",
"Y201_st.dev",
"Y101.5_st.dev")
miRNA <- miRNA[,1:25]

# column type indexes
Y202 <- which(colnames(miRNA) %like% "Y202_")
Y201 <- which(colnames(miRNA) %like% "Y201_")
Y101 <- which(colnames(miRNA) %like% "Y101_")
Y102 <- which(colnames(miRNA) %like% "Y102_")
Y101.5 <- which(colnames(miRNA) %like% "Y1015_")
```
```

```{r Stack gather data}
miRNA_stack <- miRNA %>%
  gather(key,value="count",
         -miRNA,
         -Accession,
         -Class_Name,
         -Analyte_Type,
         -PC_Samples_above_Threshold) %>%
  extract(key, c("celltype", "rep"),
          "(Y[0-9]{3,4})\\_(.)")

# Extract column name into two columns, celltype and replicate, Y[numbers]{3 or 4 numbers
in the sample name)}
# Gather data - value="count" renames value column to count
# %>% is called a pipe - instead of intermediate data frames pipe the output of one command
straight into the input of the next
```

```{r Calculate means}
miRNA_SUM <- mysummary(data=miRNA_stack, measurevar = "count", groupvars = c("celltype",
"miRNA"))
str(miRNA_SUM)
```
```{r}
############################################################
#
# identifying sig differences between all lines
#
############################################################

# factor levels
miRNA_List <- unique(miRNA_stack$miRNA)
# build lm of miRNA counts by cell type ~ lineage for each gene #unique makes list based
upon unique names (828 * 5*n4)
# miRNA_stack$miRNA is tidy: (Stacked data)
models <- sapply(miRNA_List, function(my) {
  lm(count ~ celltype, data = miRNA_stack, miRNA == my)
}, simplify = FALSE)

# apply ANOVA to lm for each gene
ANOVA.tables <- sapply(models, anova, simplify = FALSE)

ANOVA.tables[1]
# create table of miRNAs, p values and whether signifcant
# unpopulated table
miRNA_tests_all <- data.frame(miRNA = character(), F = numeric(), p = numeric(), sig =
logical())

#i is a convention used for index - when making a for loop it can be used to signify the
changing index
for(i in 1:length(ANOVA.tables)){
  F <- round(ANOVA.tables[[i]][["F value"]][1], 3)
  p <- round(ANOVA.tables[[i]][["Pr(>F)"]][1], 4)
  sig <- p <= 0.05
 miRNAnova <- names(ANOVA.tables[i])
  miRNA_tests_all <-  rbind(miRNA_tests_all, data.frame(miRNAnova, F, p, sig))
}

table(miRNA_tests_all$sig)

ggplot(data = miRNA_tests_all, aes(p)) +
  geom_histogram(bins = 20, fill = "white", color= "black")

```

#Make histogram of counts for all samples
```{r}
hist(miRNA_stack$count)
```
#Make a subset of 201s vs 202s
```{r}
miRNA_stack_201vs202 <- miRNA_stack[miRNA_stack$celltype %like% "Y20",]
```

```{r}
#add a tag to indicate whether a count is >20 and excludes loading controls and spike ins
as all true miRNA will have prefix "hsa-"
miRNA_stack_201vs202$filter <- miRNA_stack_201vs202$count >= 20 &
miRNA_stack_201vs202$miRNA %like% "hsa-"
#check how many individual samples have counts greater than 20
table(miRNA_stack_201vs202$filter)
#make list of unique miRNAs that have at least one sample with counts >=20
miRNA_over20 <- unique(miRNA_stack_201vs202$miRNA[miRNA_stack_201vs202$filter])
#select from miRNA stack where the miRNA is in the list
miRNA_filtered <- miRNA_stack_201vs202[miRNA_stack_201vs202$miRNA %in% miRNA_over20,]
```

```{r}
#############################################################
#
# identifying sig differences between all lines for Filtered set
#
#############################################################

# factor levels
miRNA_List <- unique(miRNA_filtered$miRNA)
# build lm of miRNA counts by cell type ~ lineage for each gene #unique makes list based
upon unique names (828 * 5*n4)
# miRNA_stack$miRNA is tidy: (Stacked data)
models <- sapply(miRNA_List, function(my) {
  lm(count ~ celltype, data = miRNA_filtered, miRNA == my)
}, simplify = FALSE)

# apply ANOVA to lm for each gene
ANOVA.tables <- sapply(models, anova, simplify = FALSE)

ANOVA.tables[1]
# create table of miRNAs, p values and whether signifcant
# unpopulated table
miRNA_tests_all <- data.frame(miRNA = character(), F = numeric(), p = numeric(), sig =
logical())

#i is a convention used for index - when making a for loop it can be used to signify the
changing index
for(i in 1:length(ANOVA.tables)){
  F <- round(ANOVA.tables[[i]][["F value"]][1], 3)
  p <- round(ANOVA.tables[[i]][["Pr(>F)"]][1], 4)
  sig <- p <= 0.05
 miRNAnova <- names(ANOVA.tables[i])
  miRNA_tests_all <-  rbind(miRNA_tests_all, data.frame(miRNAnova, F, p, sig))
}

table(miRNA_tests_all$sig)

ggplot(data = miRNA_tests_all, aes(p)) +
  geom_histogram(bins = 20, fill = "white", color= "black")

```

Make a subset of 201s vs 202s
```{r}
miRNA_stack_201vs202 <- miRNA_filtered[miRNA_filtered$celltype %like% "Y20",]
```
```{r}

#############################################################
#
# identifying sig differences between 201 and 202
#
#############################################################

# factor levels
miRNA_list_201vs202 <- unique(miRNA_stack_201vs202$miRNA)
# build lm of miRNA counts by cell type ~ lineage for each gene #unique makes list based
upon unique names (828 * 5*n4)
# miRNA_stack_201vs202$miRNA is tidy: (Stacked data)
models <- sapply(miRNA_list_201vs202, function(my) {
  lm(count ~ celltype, data = miRNA_stack_201vs202, miRNA == my)
}, simplify = FALSE)
```

```
# apply ANOVA to lm for each gene
ANOVA.tables <- sapply(models, anova, simplify = FALSE)

ANOVA.tables[1]
# create table of miRNAs, p values and whether signifcant
# unpopulated table
miRNA_tests_201vs202 <- data.frame(miRNA = character(), F = numeric(), numDf = numeric(),
denomDf = numeric(), p = numeric(), sig = logical())

#i is a convention used for index - when making a for loop it can be used to signify the
changing index
for(i in 1:length(ANOVA.tables)){
  F <- round(ANOVA.tables[[i]][["F value"]][1], 3)
  p <- round(ANOVA.tables[[i]][["Pr(>F)"]][1], 4)
  numDf <- ANOVA.tables[[i]][["Df"]][1]
  denomDf <- ANOVA.tables[[i]][["Df"]][2]
  sig <- p <= 0.05
  miRNAanova <- names(ANOVA.tables[i])
  miRNA_tests_201vs202 <-  rbind(miRNA_tests_201vs202, data.frame(miRNAanova, F, numDf,
denomDf, p, sig))
}

ANOVA.tables[[1]][["Df"]]

table(miRNA_tests_201vs202$sig)

write.table(miRNA_tests_201vs202, file="miRNA_tests_201vs202.csv", sep=",")

ggplot(data = miRNA_tests_201vs202, aes(p)) +
  geom_histogram(bins = 20, fill = "white", color= "black")
```
```{r}
#Multiple test correction - use package 'q-value'
#library(qvalue)
# miRNA_tests_201vs202$q <- qvalue(miRNA_tests_201vs202$p, fdr.level = 0.05, pi0 =
0.2125)$qvalues
#miRNA_tests_201vs202$q <- p.adjust(miRNA_tests_201vs202$p, method = "BH")
#miRNA_tests_201vs202$q_sig <- miRNA_tests_201vs202$q <= 0.05
```
```{r}
# making heatmap of p  miRNA differences 201 vs 202
Y201vsY202sig <- miRNA_tests_201vs202$miRNA[miRNA_tests_201vs202$sig]
Y201vsY202sig <- droplevels(Y201vsY202sig)
Y201vsY202sig <- as.character(Y201vsY202sig)
Heatmap201vs202 <- miRNA[miRNA$miRNA %in% Y201vsY202sig, ]
```

```{r}
Heatmap201vs202 <- as.data.frame(Heatmap201vs202)
row.names(Heatmap201vs202) <- Heatmap201vs202$miRNA
Heatmap <- Heatmap201vs202 %>% select(Y202_A, Y202_B, Y202_C, Y202_D, Y201_A, Y201_B,
Y201_C, Y201_D) %>% as.matrix()
cal_z_score <- function(x){
  (x-mean(x))/sd(x)
}
Heatmap_norm <- t(apply(Heatmap, 1, cal_z_score))
sample_col <- data.frame(lineage=rep(c("Y201", "Y202"),c(4,4)))
row.names(sample_col) <- colnames(Heatmap)
hclust201202 <- hclust(dist(Heatmap_norm), method="complete")
plot(hclust201202)
#miRNAclust <- cutree(tree=as.dendrogram(hclust201202), k=2)
pheatmap(Heatmap_norm, clustering_method="complete",
         annotation_col=sample_col,
         color = viridis(100),
         cutree_rows = 2,
         cutree_cols = 1)
```

Abbreviations

bFGF – basic fibroblast growth factor

BMSC – Bone marrow stromal cell

CAR cell – CXCL12 abundant reticular cell

CFU-F – Colony Forming Unit Fibroblast

CM – Conditioned media

CXCL12 – C-X-C motif chemokine 12/Stromal derived factor 1

DAPI - 4′,6-diamidino-2-phenylindole

DKK1 – Dickkopf related protein 1

DMEM – Dulbecco's Modified Eagle Medium

DMSO – Dimethyl sulfoxide

ECM – Extracellular Matrix

EDTA – Ethylenediaminetetraacetic acid

EV – Extracellular Vesicle

FA – Focal adhesion

FAK – Focal adhesion kinase

FAKi – Focal adhesion kinase inhibitor

FBS – Foetal Bovine Serum

FIBSEM – Focused ion beam scanning electron microscopy

GFP – Green fluorescent protein

GO – Gene ontology

HA – Hyaluronic acid

HSC – Haematopoietic Stem Cell

hTERT – Human telomerase reverse transcriptase

IFNγ – Interferon gamma

IFNγR1 – Interferon gamma receptor 1

IL10 – Interleukin-10

IL12 – Interleukin-12

IL18 – Interleukin-18

IL6 – Interleukin-6

IL8 – Interleukin-8

ISCT – International Society for Cell and Gene Therapy

ISEV – International Society for Extracellular Vesicles

LC-MS/MS – liquid chromatography tandem mass spectrometry

LPS – Lipopolysaccharide

LTBP(1,2,3 or 4) – Latent transforming growth factor beta binding protein (1, 2 ,3 & 4)

miRNA – Micro ribonucleic acid

mRNA – Messenger ribonucleic acid

MSC – Mesenchymal stem cell

NFκB – Nuclear factor kappa B

NK cell – Natural Killer cell

OSX – Osterix

PBMC – Peripheral blood mononuclear cell

PBS – Phosphate buffered saline

PDGFRα - Platelet derived growth factor receptor alpha

PDGFRβ - Platelet derived growth factor receptor beta

PFA – Paraformaldehyde

PRX1 – Peroxiredoxin 1

RNAseq – RNA sequencing

scRNAseq – single cell RNA sequencing

SE – Standard error

SEM – Scanning electron microscopy

TEM – Transmission electron microscopy

TGFβ – Transforming growth factor beta

TGFβR2 – Transforming growth factor beta receptor 2

TNFα – Tumour necrosis factor alpha

TSG-6 – TNFα stimulated gene 6

VEGF – Vascular endothelial growth factor

W/V – weight to volume

References

Abdallah, B.M., Haack-Sørensen, M., Burns, J.S., Elsnab, B., Jakob, F., Hokland, P., and Kassem, M. (2005). Maintenance of differentiation potential of human bone marrow mesenchymal stem cells immortalized by human telomerase reverse transcriptase gene despite of extensive proliferation. Biochemical and Biophysical Research Communications *326*, 527-538.

Aggarwal, S., and Pittenger, M.F. (2005). Human mesenchymal stem cells modulate allogeneic immune cell responses. Blood *105*, 1815-1822.

Al-Nbaheen, M., Vishnubalaji, R., Ali, D., Bouslimi, A., Al-Jassir, F., Megges, M., Prigione, A., Adjaye, J., Kassem, M., and Aldahmash, A. (2013). Human stromal (mesenchymal) stem cells from bone marrow, adipose tissue and skin exhibit differences in molecular phenotype and differentiation potential. Stem Cell Rev Rep *9*, 32-43.

Alexopoulos, L.G., Youn, I., Bonaldo, P., and Guilak, F. (2009). Developmental and osteoarthritic changes in Col6a1-knockout mice: biomechanics of type VI collagen in the cartilage pericellular matrix. Arthritis Rheum *60*, 771-779.

Anderson, J.D., Johansson, H.J., Graham, C.S., Vesterlund, M., Pham, M.T., Bramlett, C.S., Montgomery, E.N., Mellema, M.S., Bardini, R.L., Contreras, Z.*, et al.* (2016). Comprehensive Proteomic Analysis of Mesenchymal Stem Cell Exosomes Reveals Modulation of Angiogenesis via Nuclear Factor-KappaB Signaling. Stem cells (Dayton, Ohio) *34*, 601-613.

Andrzejewska, A., Catar, R., Schoon, J., Qazi, T.H., Sass, F.A., Jacobi, D., Blankenstein, A., Reinke, S., Krüger, D., Streitz, M.*, et al.* (2019). Multi-Parameter Analysis of Biobanked Human Bone Marrow Stromal Cells Shows Little Influence for Donor Age and Mild Comorbidities on Phenotypic and Functional Properties. Front Immunol *10*.

Annes, J.P., Chen, Y., Munger, J.S., and Rifkin, D.B. (2004). Integrin alphaVbeta6-mediated activation of latent TGF-beta requires the latent TGF-beta binding protein-1. J Cell Biol *165*, 723-734.

Arslan, F., Lai, R.C., Smeets, M.B., Akeroyd, L., Choo, A., Aguor, E.N., Timmers, L., van Rijen, H.V., Doevendans, P.A., Pasterkamp, G.*, et al.* (2013). Mesenchymal stem cell-derived exosomes increase ATP levels, decrease oxidative stress and activate PI3K/Akt pathway to enhance myocardial viability and prevent adverse remodeling after myocardial ischemia/reperfusion injury. Stem Cell Res *10*, 301-312.

Asano, Y., Ihn, H., Yamane, K., Jinnin, M., Mimura, Y., and Tamaki, K. (2005). Involvement of αvβ5 integrin–mediated activation of latent transforming growth factor β1 in autocrine transforming growth factor β signaling in systemic sclerosis fibroblasts. Arthritis & Rheumatism *52*, 2897-2905.

Augello, A., Tasso, R., Negrini, S.M., Cancedda, R., and Pennesi, G. (2007). Cell therapy using allogeneic bone marrow mesenchymal stem cells prevents tissue damage in collagen-induced arthritis. Arthritis & Rheumatism *56*, 1175-1186.

Baberg, F., Geyh, S., Waldera-Lupa, D., Stefanski, A., Zilkens, C., Haas, R., Schroeder, T., and Stühler, K. (2019). Secretome analysis of human bone marrow derived mesenchymal stromal cells. Biochimica et Biophysica Acta (BBA) - Proteins and Proteomics *1867*, 434-441.

Babicki, S., Arndt, D., Marcu, A., Liang, Y., Grant, J.R., Maciejewski, A., and Wishart, D.S. (2016). Heatmapper: web-enabled heat mapping for all. Nucleic acids research *44*, W147-153.

Baccin, C., Al-Sabah, J., Velten, L., Helbling, P.M., Grünschläger, F., Hernández-Malmierca, P., Nombela-Arrieta, C., Steinmetz, L.M., Trumpp, A., and Haas, S. (2020). Combined single-cell and spatial transcriptomics reveal the molecular, cellular and spatial bone marrow niche organization. Nature Cell Biology *22*, 38-48.

Bailey Dubose, K., Zayzafoon, M., and Murphy-Ullrich, J.E. (2012). Thrombospondin-1 inhibits osteogenic differentiation of human mesenchymal stem cells through latent TGF-β activation. Biochem Biophys Res Commun *422*, 488-493.

Bakondi, B., Shimada, I.S., Perry, A., Munoz, J.R., Ylostalo, J., Howard, A.B., Gregory, C.A., and Spees, J.L. (2009). CD133 Identifies a Human Bone Marrow Stem/Progenitor Cell Sub-population With a Repertoire of Secreted Factors That Protect Against Stroke. Molecular Therapy *17*, 1938-1947.

Balzano, M., De Grandis, M., Vu Manh, T.P., Chasson, L., Bardin, F., Farina, A., Sergé, A., Bidaut, G., Charbord, P., Hérault, L.*, et al.* (2019). Nidogen-1 Contributes to the Interaction Network Involved in Pro-B Cell Retention in the Peri-sinusoidal Hematopoietic Stem Cell Niche. Cell Rep *26*, 3257-3271.e3258.

Barreto, G., Senturk, B., Colombo, L., Brück, O., Neidenbach, P., Salzmann, G., Zenobi-Wong, M., and Rottmar, M. (2020). Lumican is upregulated in osteoarthritis and contributes to TLR4-induced pro-inflammatory activation of cartilage degradation and macrophage polarization. Osteoarthritis and Cartilage *28*, 92-101.

Bartholomew, A., Sturgeon, C., Siatskas, M., Ferrer, K., McIntosh, K., Patil, S., Hardy, W., Devine, S., Ucker, D., Deans, R.*, et al.* (2002). Mesenchymal stem cells suppress lymphocyte proliferation in vitro and prolong skin graft survival in vivo. Experimental hematology *30*, 42-48.

Baryawno, N., Przybylski, D., Kowalczyk, M.S., Kfoury, Y., Severe, N., Gustafsson, K., Kokkaliaris, K.D., Mercier, F., Tabaka, M., Hofree, M.*, et al.* (2019). A Cellular Taxonomy of the Bone Marrow Stroma in Homeostasis and Leukemia. Cell *177*, 1915-1932.e1916.

Baxter, M.A., Wynn, R.F., Jowitt, S.N., Wraith, J.E., Fairbairn, L.J., and Bellantuono, I. (2004). Study of telomere length reveals rapid aging of human marrow stromal cells following in vitro expansion. Stem cells (Dayton, Ohio) *22*, 675-682.

Bi, Y., Stuelten, C.H., Kilts, T., Wadhwa, S., Iozzo, R.V., Robey, P.G., Chen, X.-D., and Young, M.F. (2005). Extracellular Matrix Proteoglycans Control the Fate of Bone Marrow Stromal Cells*. Journal of Biological Chemistry *280*, 30481-30489.

Bindea, G., Mlecnik, B., Hackl, H., Charoentong, P., Tosolini, M., Kirilovsky, A., Fridman, W.-H., Pagès, F., Trajanoski, Z., and Galon, J. (2009). ClueGO: a Cytoscape plug-in to decipher functionally grouped gene ontology and pathway annotation networks. Bioinformatics (Oxford, England) *25*, 1091-1093.

Biswas, A., Roy, I.M., Babu, P.C., Manesia, J., Schouteden, S., Vijayakurup, V., Anto, R.J., Huelsken, J., Lacy-Hulbert, A., Verfaillie, C.M.*, et al.* (2020). The Periostin/Integrin-αv Axis Regulates the Size of Hematopoietic Stem Cell Pool in the Fetal Liver. Stem Cell Reports *15*, 340-357.

Bonaldo, P., Braghetta, P., Zanetti, M., Piccolo, S., Volpin, D., and Bressan, G.M. (1998). Collagen VI Deficiency Induces Early Onset Myopathy in the Mouse: An Animal Model for Bethlem Myopathy. Human Molecular Genetics *7*, 2135-2140.

Brittberg, M., Lindahl, A., Nilsson, A., Ohlsson, C., Isaksson, O., and Peterson, L. (1994). Treatment of Deep Cartilage Defects in the Knee with Autologous Chondrocyte Transplantation. New England Journal of Medicine *331*, 889-895.

Bruder, S.P., Kraus, K.H., Goldberg, V.M., and Kadiyala, S. (1998). The Effect of Implants Loaded with Autologous Mesenchymal Stem Cells on the Healing of Canine Segmental Bone Defects*. JBJS *80*.

Bühring, H.J., Battula, V.L., Treml, S., Schewe, B., Kanz, L., and Vogel, W. (2007). Novel markers for the prospective isolation of human MSC. Ann N Y Acad Sci *1106*, 262-271.

Buxboim, A., Ivanovska, I.L., and Discher, D.E. (2010). Matrix elasticity, cytoskeletal forces and physics of the nucleus: how deeply do cells 'feel' outside and in? Journal of Cell Science *123*, 297.

Calvi, L.M., Adams, G.B., Weibrecht, K.W., Weber, J.M., Olson, D.P., Knight, M.C., Martin, R.P., Schipani, E., Divieti, P., Bringhurst, F.R.*, et al.* (2003). Osteoblastic cells regulate the haematopoietic stem cell niche. Nature *425*, 841-846.

Caplan, A.I. (1991). Mesenchymal stem cells. Journal of orthopaedic research : official publication of the Orthopaedic Research Society *9*, 641-650.

Caplan, A.I., and Dennis, J.E. (2006). Mesenchymal stem cells as trophic mediators. Journal of cellular biochemistry *98*, 1076-1084.

Carlson, E.C., Lin, M., Liu, C.-Y., Kao, W.W.Y., Perez, V.L., and Pearlman, E. (2007). Keratocan and lumican regulate neutrophil infiltration and corneal clarity in lipopolysaccharide-induced keratitis by direct interaction with CXCL1. The Journal of biological chemistry *282*, 35502-35509.

Chaly, Y., Marinov, A.D., Oxburgh, L., Bushnell, D.S., and Hirsch, R. (2012). FSTL1 promotes arthritis in mice by enhancing inflammatory cytokine/chemokine expression. Arthritis Rheum *64*, 1082-1088.

Chan, C.K.F., Chen, C.-C., Luppen, C.A., Kim, J.-B., DeBoer, A.T., Wei, K., Helms, J.A., Kuo, C.J., Kraft, D.L., and Weissman, I.L. (2009). Endochondral ossification is required for haematopoietic stem-cell niche formation. Nature *457*, 490-494.

Chan, C.K.F., Gulati, G.S., Sinha, R., Tompkins, J.V., Lopez, M., Carter, A.C., Ransom, R.C., Reinisch, A., Wearda, T., Murphy, M.*, et al.* (2018). Identification of the Human Skeletal Stem Cell. Cell *175*, 43-56.e21.

Chan, Charles K.F., Seo, Eun Y., Chen, James Y., Lo, D., McArdle, A., Sinha, R., Tevlin, R., Seita, J., Vincent-Tompkins, J., Wearda, T.*, et al.* (2015). Identification and Specification of the Mouse Skeletal Stem Cell. Cell *160*, 285-298.

Chan, J.L., Tang, K.C., Patel, A.P., Bonilla, L.M., Pierobon, N., Ponzio, N.M., and Rameshwar, P. (2006). Antigen-presenting property of mesenchymal stem cells occurs during a narrow window at low levels of interferon-gamma. Blood *107*, 4817-4824.

Chaudhry, S.S., Cain, S.A., Morgan, A., Dallas, S.L., Shuttleworth, C.A., and Kielty, C.M. (2007). Fibrillin-1 regulates the bioavailability of TGFbeta1. J Cell Biol *176*, 355-367.

Chen, C.S., Mrksich, M., Huang, S., Whitesides, G.M., and Ingber, D.E. (1997). Geometric Control of Cell Life and Death. Science (New York, NY) *276*, 1425-1428.

Chen, L., Shi, K., Andersen, T.L., Qiu, W., and Kassem, M. (2019). KIAA1199 is a secreted molecule that enhances osteoblastic stem cell migration and recruitment. Cell Death & Disease *10*, 126.

Chen, X.-D., Dusevich, V., Feng, J.Q., Manolagas, S.C., and Jilka, R.L. (2007). Extracellular Matrix Made by Bone Marrow Cells Facilitates Expansion of Marrow-Derived Mesenchymal Progenitor Cells and Prevents Their Differentiation Into Osteoblasts. Journal of Bone and Mineral Research *22*, 1943-1956.

Chen, X., Hughes, R., Mullin, N., Hawkins, R.J., Holen, I., Brown, N.J., and Hobbs, J.K. (2020). Mechanical Heterogeneity in the Bone Microenvironment as Characterized by Atomic Force Microscopy. Biophysical Journal *119*, 502-513.

Chinnadurai, R., Rajan, D., Qayed, M., Arafat, D., Garcia, M., Liu, Y., Kugathasan, S., Anderson, L.J., Gibson, G., and Galipeau, J. (2018). Potency Analysis of Mesenchymal Stromal Cells Using a Combinatorial Assay Matrix Approach. Cell Reports *22*, 2504-2517.

Choi, H., Lee, R.H., Bazhanov, N., Oh, J.Y., and Prockop, D.J. (2011). Anti-inflammatory protein TSG-6 secreted by activated MSCs attenuates zymosan-induced mouse peritonitis by decreasing TLR2/NF-κB signaling in resident macrophages. Blood *118*, 330-338.

Choi, J.S., and Harley, B.A.C. (2017). Marrow-inspired matrix cues rapidly affect early fate decisions of hematopoietic stem and progenitor cells. Science advances *3*, e1600455-e1600455.

Christensen, S.E., Coles, J.M., Zelenski, N.A., Furman, B.D., Leddy, H.A., Zauscher, S., Bonaldo, P., and Guilak, F. (2012). Altered Trabecular Bone Structure and Delayed Cartilage Degeneration in the Knees of Collagen VI Null Mice. PLOS ONE *7*, e33397.

Coşkun, S., Chao, H., Vasavada, H., Heydari, K., Gonzales, N., Zhou, X., de Crombrugghe, B., and Hirschi, K.K. (2014). Development of the fetal bone marrow niche and regulation of HSC quiescence and homing ability by emerging osteolineage cells. Cell reports *9*, 581-590.

Coutu, D.L., Kokkaliaris, K.D., Kunz, L., and Schroeder, T. (2017). Three-dimensional map of nonhematopoietic bone and bone-marrow cells and molecules. Nature Biotechnology *35*, 1202-1210.

Coutu, D.L., Wu, J.H., Monette, A., Rivard, G.-É., Blostein, M.D., and Galipeau, J. (2008). Periostin, a Member of a Novel Family of Vitamin K-dependent Proteins, Is Expressed by Mesenchymal Stromal Cells. Journal of Biological Chemistry *283*, 17991-18001.

Crisan, M., Yap, S., Casteilla, L., Chen, C.-W., Corselli, M., Park, T.S., Andriolo, G., Sun, B., Zheng, B., Zhang, L.*, et al.* (2008). A Perivascular Origin for Mesenchymal Stem Cells in Multiple Human Organs. Cell stem cell *3*, 301-313.

Danielyan, L., Schwab, M., Siegel, G., Brawek, B., Garaschuk, O., Asavapanumas, N., Buadze, M., Lourhmati, A., Wendel, H.-P., Avci-Adali, M.*, et al.* (2020). Cell motility and migration as determinants of stem cell efficacy. EBioMedicine *60*.

Decker, M., Martinez-Morentin, L., Wang, G., Lee, Y., Liu, Q., Leslie, J., and Ding, L. (2017). Leptin-receptor-expressing bone marrow stromal cells are myofibroblasts in primary myelofibrosis. Nature Cell Biology *19*, 677-688.

Denker, A.E., Nicoll, S.B., and Tuan, R.S. (1995). Formation of cartilage-like spheroids by micromass cultures of murine C3H10T1/2 cells upon treatment with transforming growth factor-beta 1. Differentiation *59*, 25-34.

Dexter, T.M., Allen, T.D., and Lajtha, L.G. (1977). Conditions controlling the proliferation of haemopoietic stem cells in vitro. Journal of cellular physiology *91*, 335-344.

Di Nicola, M., Carlo-Stella, C., Magni, M., Milanesi, M., Longoni, P.D., Matteucci, P., Grisanti, S., and Gianni, A.M. (2002). Human bone marrow stromal cells suppress T-lymphocyte proliferation induced by cellular or nonspecific mitogenic stimuli. Blood *99*, 3838-3843.

Ding, L., and Morrison, S.J. (2013). Haematopoietic stem cells and early lymphoid progenitors occupy distinct bone marrow niches. Nature *495*, 231-235.

Ding, L., Saunders, T.L., Enikolopov, G., and Morrison, S.J. (2012). Endothelial and perivascular cells maintain haematopoietic stem cells. Nature *481*, 457-462.

Dominici, M., Le Blanc, K., Mueller, I., Slaper-Cortenbach, I., Marini, F., Krause, D., Deans, R., Keating, A., Prockop, D., and Horwitz, E. (2006). Minimal criteria for defining multipotent mesenchymal stromal cells. The International Society for Cellular Therapy position statement. Cytotherapy *8*, 315-317.

Donnelly, H., Salmeron-Sanchez, M., and Dalby, M.J. (2018). Designing stem cell niches for differentiation and self-renewal. Journal of The Royal Society Interface *15*, 20180388.

Duarte, D., Hawkins, E.D., Akinduro, O., Ang, H., De Filippo, K., Kong, I.Y., Haltalli, M., Ruivo, N., Straszkowski, L., Vervoort, S.J.*, et al.* (2018). Inhibition of Endosteal Vascular Niche Remodeling Rescues Hematopoietic Stem Cell Loss in AML. Cell stem cell *22*, 64-77.e66.

Duchamp de Lageneste, O., Julien, A., Abou-Khalil, R., Frangi, G., Carvalho, C., Cagnard, N., Cordier, C., Conway, S.J., and Colnot, C. (2018). Periosteum contains skeletal stem cells with high bone regenerative potential controlled by Periostin. Nature Communications *9*, 773.

Elman, J.S., Li, M., Wang, F., Gimble, J.M., and Parekkadan, B. (2014). A comparison of adipose and bone marrow-derived mesenchymal stromal cell secreted factors in the treatment of systemic inflammation. Journal of Inflammation *11*, 1.

Engler, A.J., Sen, S., Sweeney, H.L., and Discher, D.E. (2006). Matrix Elasticity Directs Stem Cell Lineage Specification. Cell *126*, 677-689.

Fierro, F.A., Kalomoiris, S., Sondergaard, C.S., and Nolta, J.A. (2011). Effects on proliferation and differentiation of multipotent bone marrow stromal cells engineered to express growth factors for combined cell and gene therapy. Stem cells (Dayton, Ohio) *29*, 1727-1737.

Frantz, C., Stewart, K.M., and Weaver, V.M. (2010). The extracellular matrix at a glance. Journal of Cell Science *123*, 4195.

Friedenstein, A.J., Chailakhjan, R.K., and Lalykina, K.S. (1970). The development of fibroblast colonies in monolayer cultures of guinea-pig bone marrow and spleen cells. Cell Tissue Kinet *3*, 393-403.

Friedenstein, A.J., Chailakhyan, R.K., Latsinik, N.V., Panasyuk, A.F., and Keiliss-Borok, I.V. (1974). Stromal cells responsible for transferring the microenvironment of the hemopoietic tissues. Cloning in vitro and retransplantation in vivo. Transplantation *17*, 331-340.

Friedenstein, A.J., Piatetzky-Shapiro, I.I., and Petrakova, K.V. (1966). Osteogenesis in transplants of bone marrow cells. Journal of Embryology and Experimental Morphology *16*, 381-390.

Galarza Torre, A., Shaw, J.E., Wood, A., Gilbert, H.T.J., Dobre, O., Genever, P., Brennan, K., Richardson, S.M., and Swift, J. (2018). An immortalised mesenchymal stem cell line maintains mechano-responsive behaviour and can be used as a reporter of substrate stiffness. Scientific reports *8*, 8981-8981.

Gattazzo, F., Urciuolo, A., and Bonaldo, P. (2014). Extracellular matrix: a dynamic microenvironment for stem cell niche. Biochim Biophys Acta *1840*, 2506-2519.

Geiss, G.K., Bumgarner, R.E., Birditt, B., Dahl, T., Dowidar, N., Dunaway, D.L., Fell, H.P., Ferree, S., George, R.D., Grogan, T.*, et al.* (2008). Direct multiplexed measurement of gene expression with color-coded probe pairs. Nat Biotechnol *26*, 317-325.

Gerecht, S., Burdick, J.A., Ferreira, L.S., Townsend, S.A., Langer, R., and Vunjak-Novakovic, G. (2007). Hyaluronic acid hydrogel for controlled self-renewal and differentiation of human embryonic stem cells. Proceedings of the National Academy of Sciences *104*, 11298-11303.

Gnecchi, M., He, H., Liang, O.D., Melo, L.G., Morello, F., Mu, H., Noiseux, N., Zhang, L., Pratt, R.E., Ingwall, J.S.*, et al.* (2005). Paracrine action accounts for marked protection of ischemic heart by Akt-modified mesenchymal stem cells. Nature medicine *11*, 367-368.

Gomariz, A., Helbling, P.M., Isringhausen, S., Suessbier, U., Becker, A., Boss, A., Nagasawa, T., Paul, G., Goksel, O., Székely, G.*, et al.* (2018). Quantitative spatial analysis of haematopoiesis-regulating stromal cells in the bone marrow microenvironment by 3D microscopy. Nature Communications *9*, 2532.

Goncharova, V., Serobyan, N., Iizuka, S., Schraufstatter, I., de Ridder, A., Povaliy, T., Wacker, V., Itano, N., Kimata, K., Orlovskaja, I.A.*, et al.* (2012). Hyaluronan expressed by the hematopoietic microenvironment is required for bone marrow hematopoiesis. The Journal of biological chemistry *287*, 25419-25433.

Greenbaum, A., Hsu, Y.-M.S., Day, R.B., Schuettpelz, L.G., Christopher, M.J., Borgerding, J.N., Nagasawa, T., and Link, D.C. (2013). CXCL12 in early mesenchymal progenitors is required for haematopoietic stem-cell maintenance. Nature *495*, 227-230.

Gronthos, S., Mankani, M., Brahim, J., Robey, P.G., and Shi, S. (2000). Postnatal human dental pulp stem cells (DPSCs) in vitro and in vivo. Proceedings of the National Academy of Sciences *97*, 13625-13630.

Guilak, F., Cohen, D.M., Estes, B.T., Gimble, J.M., Liedtke, W., and Chen, C.S. (2009). Control of stem cell fate by physical interactions with the extracellular matrix. Cell stem cell *5*, 17-26.

Hatzimichael, E., and Tuthill, M. (2010). Hematopoietic stem cell transplantation. Stem Cells Cloning *3*, 105-117.

Hernigou, P., Poignard, A., Beaujean, F., and Rouard, H. (2005). Percutaneous autologous bone-marrow grafting for nonunions. Influence of the number and concentration of progenitor cells. J Bone Joint Surg Am *87*, 1430-1437.

Herrmann, M., Hildebrand, M., Menzel, U., Fahy, N., Alini, M., Lang, S., Benneker, L., Verrier, S., Stoddart, M.J., and Bara, J.J. (2019). Phenotypic Characterization of Bone Marrow Mononuclear Cells and Derived Stromal Cell Populations from Human Iliac Crest, Vertebral Body and Femoral Head. International Journal of Molecular Sciences *20*, 3454.

Higgins, J.M., and Mahadevan, L. (2010). Physiological and pathological population dynamics of circulating human red blood cells. Proceedings of the National Academy of Sciences *107*, 20587-20592.

Hinz, B. (2015). The extracellular matrix and transforming growth factor-β1: Tale of a strained relationship. Matrix Biology *47*, 54-65.

Horiuchi, K., Amizuka, N., Takeshita, S., Takamatsu, H., Katsuura, M., Ozawa, H., Toyama, Y., Bonewald, L.F., and Kudo, A. (1999). Identification and Characterization of a Novel Protein, Periostin, with Restricted Expression to Periosteum and Periodontal Ligament and Increased Expression by Transforming Growth Factor β. Journal of Bone and Mineral Research *14*, 1239-1249.

Horwitz, E.M., Le Blanc, K., Dominici, M., Mueller, I., Slaper-Cortenbach, I., Marini, F.C., Deans, R.J., Krause, D.S., and Keating, A. (2005). Clarification of the nomenclature for MSC: The International Society for Cellular Therapy position statement. Cytotherapy *7*, 393-395.

Houlihan, D.D., Mabuchi, Y., Morikawa, S., Niibe, K., Araki, D., Suzuki, S., Okano, H., and Matsuzaki, Y. (2012). Isolation of mouse mesenchymal stem cells on the basis of expression of Sca-1 and PDGFR-α. Nature Protocols *7*, 2103-2111.

Hsu, M.N., Wei, S.-C., Guo, S., Phan, D.-T., Zhang, Y., and Chen, C.-H. (2018). Smart Hydrogel Microfluidics for Single-Cell Multiplexed Secretomic Analysis with High Sensitivity. Small *14*, 1802918.

Hynes, R.O., and Naba, A. (2012). Overview of the matrisome--an inventory of extracellular matrix constituents and functions. Cold Spring Harb Perspect Biol *4*, a004903-a004903.

Ilas, D.C., Baboolal, T.G., Churchman, S.M., Jones, W.G., Giannoudis, P.V., Bühring, H.-J., McGonagle, D., and Jones, E. (2020). The osteogenic commitment of CD271+CD56+ bone marrow stromal cells (BMSCs) in osteoarthritic femoral head bone. Scientific Reports *10*, 11145.

James, S., Fox, J., Afsari, F., Lee, J., Clough, S., Knight, C., Ashmore, J., Ashton, P., Preham, O., Hoogduijn, M.*, et al.* (2015). Multiparameter Analysis of Human Bone Marrow Stromal Cells Identifies Distinct Immunomodulatory and Differentiation-Competent Subtypes. Stem cell reports *4*, 1004-1015.

Jones, D.L., and Wagers, A.J. (2008). No place like home: anatomy and function of the stem cell niche. Nature Reviews Molecular Cell Biology *9*, 11-21.

Jones, E., English, A., Churchman, S.M., Kouroupis, D., Boxall, S.A., Kinsey, S., Giannoudis, P.G., Emery, P., and McGonagle, D. (2010). Large-scale extraction and characterization of CD271+ multipotential stromal cells from trabecular bone in health and osteoarthritis: Implications for bone regeneration strategies based on uncultured or minimally cultured multipotential stromal cells. Arthritis & Rheumatism *62*, 1944-1954.

Jones, E.A., Kinsey, S.E., English, A., Jones, R.A., Straszynski, L., Meredith, D.M., Markham, A.F., Jack, A., Emery, P., and McGonagle, D. (2002). Isolation and characterization of bone marrow multipotential mesenchymal progenitor cells. Arthritis & Rheumatism *46*, 3349-3360.

Kanehisa, M., and Goto, S. (2000). KEGG: Kyoto Encyclopedia of Genes and Genomes. Nucleic acids research *28*, 27-30.

Kawai, S., Azuma, Y., Fujii, E., Furugaki, K., Ozaki, S., Matsumoto, T., Kosaka, M., and Yamada-Okabe, H. (2008). Interferon-alpha enhances CD317 expression and the antitumor activity of anti-CD317 monoclonal antibody in renal cell carcinoma xenograft models. Cancer Sci *99*, 2461-2466.

Kay, A.G., Long, G., Tyler, G., Stefan, A., Broadfoot, S.J., Piccinini, A.M., Middleton, J., and Kehoe, O. (2017). Mesenchymal Stem Cell-Conditioned Medium Reduces Disease Severity and Immune Responses in Inflammatory Arthritis. Scientific Reports *7*, 18019.

Kern, S., Eichler, H., Stoeve, J., Klüter, H., and Bieback, K. (2006). Comparative Analysis of Mesenchymal Stem Cells from Bone Marrow, Umbilical Cord Blood, or Adipose Tissue. Stem cells (Dayton, Ohio) *24*, 1294-1301.

Khurana, S., Schouteden, S., Manesia, J.K., Santamaria-Martínez, A., Huelsken, J., Lacy-Hulbert, A., and Verfaillie, C.M. (2016). Outside-in integrin signalling regulates haematopoietic stem cell function via Periostin-Itgav axis. Nature Communications *7*, 13500.

Kiani, C., Chen, L., Wu, Y.J., Yee, A.J., and Yang, B.B. (2002). Structure and function of aggrecan. Cell Research *12*, 19-32.

Kiel, M.J., Yilmaz, Ö.H., Iwashita, T., Yilmaz, O.H., Terhorst, C., and Morrison, S.J. (2005). SLAM Family Receptors Distinguish Hematopoietic Stem and Progenitor Cells and Reveal Endothelial Niches for Stem Cells. Cell *121*, 1109-1121.

Kilian, K.A., Bugarija, B., Lahn, B.T., and Mrksich, M. (2010). Geometric cues for directing the differentiation of mesenchymal stem cells. Proc Natl Acad Sci U S A *107*, 4872-4877.

Kilpinen, L., Impola, U., Sankkila, L., Ritamo, I., Aatonen, M., Kilpinen, S., Tuimala, J., Valmu, L., Levijoki, J., Finckenberg, P.*, et al.* (2013). Extracellular membrane vesicles from umbilical cord blood-derived MSC protect against ischemic acute kidney injury, a feature that is lost after inflammatory conditioning. Journal of Extracellular Vesicles *2*, 10.3402/jev.v3402i3400.21927.

Kim, D.-H., and Wirtz, D. (2013). Focal adhesion size uniquely predicts cell migration. FASEB J *27*, 1351-1361.

Kim, H.-S., Choi, D.-Y., Yun, S.J., Choi, S.-M., Kang, J.W., Jung, J.W., Hwang, D., Kim, K.P., and Kim, D.-W. (2012). Proteomic Analysis of Microvesicles Derived from Human Mesenchymal Stem Cells. Journal of Proteome Research *11*, 839-849.

Kinnaird, T., Stabile, E., Burnett, M.S., Shou, M., Lee, C.W., Barr, S., Fuchs, S., and Epstein, S.E. (2004). Local Delivery of Marrow-Derived Stromal Cells Augments Collateral Perfusion Through Paracrine Mechanisms. Circulation *109*, 1543-1549.

Klein, E.A., Yin, L., Kothapalli, D., Castagnino, P., Byfield, F.J., Xu, T., Levental, I., Hawthorne, E., Janmey, P.A., and Assoian, R.K. (2009). Cell-Cycle Control by Physiological Matrix Elasticity and In Vivo Tissue Stiffening. Current Biology *19*, 1511-1518.

Klein, G., Müller, C.A., Tillet, E., Chu, M.L., and Timpl, R. (1995). Collagen type VI in the human bone marrow microenvironment: a strong cytoadhesive component. Blood *86*, 1740-1748.

Klinker, M.W., Marklein, R.A., Lo Surdo, J.L., Wei, C.-H., and Bauer, S.R. (2017). Morphological features of IFN-γ–stimulated mesenchymal stromal cells predict overall immunosuppressive capacity. Proceedings of the National Academy of Sciences *114*, E2598-E2607.

Kräter, M., Jacobi, A., Otto, O., Tietze, S., Müller, K., Poitz, D.M., Palm, S., Zinna, V.M., Biehain, U., Wobus, M.*, et al.* (2017). Bone marrow niche-mimetics modulate HSPC function via integrin signaling. Scientific Reports *7*, 2549.

Kshitiz, Ellison, D.D., Suhail, Y., Afzal, J., Woo, L., Kilic, O., Spees, J., and Levchenko, A. (2019). Dynamic secretome of bone marrow-derived stromal cells reveals a cardioprotective biochemical cocktail. Proceedings of the National Academy of Sciences *116*, 14374-14383.

Kucera, M., Isserlin, R., Arkhangorodsky, A., and Bader, G.D. (2016). AutoAnnotate: A Cytoscape app for summarizing networks with semantic annotations. F1000Res *5*, 1717-1717.

Kunisaki, Y., Bruns, I., Scheiermann, C., Ahmed, J., Pinho, S., Zhang, D., Mizoguchi, T., Wei, Q., Lucas, D., Ito, K.*, et al.* (2013). Arteriolar niches maintain haematopoietic stem cell quiescence. Nature *502*, 637-643.

Kurtzberg, J., Prockop, S., Teira, P., Bittencourt, H., Lewis, V., Chan, K.W., Horn, B., Yu, L., Talano, J.A., Nemecek, E.*, et al.* (2014). Allogeneic human mesenchymal stem

cell therapy (remestemcel-L, Prochymal) as a rescue agent for severe refractory acute graft-versus-host disease in pediatric patients. Biol Blood Marrow Transplant *20*, 229-235.

Kuznetsov, S.A., Krebsbach, P.H., Satomura, K., Kerr, J., Riminucci, M., Benayahu, D., and Robey, P.G. (1997). Single-colony derived strains of human marrow stromal fibroblasts form bone after transplantation in vivo. J Bone Miner Res *12*, 1335-1347.

Lacey, D.C., Simmons, P.J., Graves, S.E., and Hamilton, J.A. (2009). Proinflammatory cytokines inhibit osteogenic differentiation from stem cells: implications for bone repair during inflammation. Osteoarthritis and Cartilage *17*, 735-742.

Lai, R.C., Arslan, F., Lee, M.M., Sze, N.S., Choo, A., Chen, T.S., Salto-Tellez, M., Timmers, L., Lee, C.N., El Oakley, R.M*., et al.* (2010a). Exosome secreted by MSC reduces myocardial ischemia/reperfusion injury. Stem cell research *4*, 214-222.

Lai, R.C., Tan, S.S., Yeo, R.W.Y., Choo, A.B.H., Reiner, A.T., Su, Y., Shen, Y., Fu, Z., Alexander, L., Sze, S.K*., et al.* (2016). MSC secretes at least 3 EV types each with a unique permutation of membrane lipid, protein and RNA. Journal of Extracellular Vesicles *5*, 29828.

Lai, Y., Sun, Y., Skinner, C.M., Son, E.L., Lu, Z., Tuan, R.S., Jilka, R.L., Ling, J., and Chen, X.D. (2010b). Reconstitution of marrow-derived extracellular matrix ex vivo: a robust culture system for expanding large-scale highly functional human mesenchymal stem cells. Stem Cells Dev *19*, 1095-1107.

Lamprecht, M.R., Sabatini, D.M., and Carpenter, A.E. (2007). CellProfiler™: free, versatile software for automated biological image analysis. BioTechniques *42*, 71-75.

Le Blanc, K., Frassoni, F., Ball, L., Locatelli, F., Roelofs, H., Lewis, I., Lanino, E., Sundberg, B., Bernardo, M.E., Remberger, M*., et al.* (2008). Mesenchymal stem cells for treatment of steroid-resistant, severe, acute graft-versus-host disease: a phase II study. The Lancet *371*, 1579-1586.

Le Blanc, K., Rasmusson, I., Sundberg, B., Götherström, C., Hassan, M., Uzunel, M., and Ringdén, O. (2004). Treatment of severe acute graft-versus-host disease with third party haploidentical mesenchymal stem cells. Lancet *363*, 1439-1441.

Lee-Thedieck, C., Rauch, N., Fiammengo, R., Klein, G., and Spatz, J.P. (2012). Impact of substrate elasticity on human hematopoietic stem and progenitor cell adhesion and motility. Journal of Cell Science *125*, 3765-3775.

Lee, C., Mitsialis, S.A., Aslam, M., Vitali, S.H., Vergadi, E., Konstantinou, G., Sdrimas, K., Fernandez-Gonzalez, A., and Kourembanas, S. (2012). Exosomes mediate the cytoprotective action of mesenchymal stromal cells on hypoxia-induced pulmonary hypertension. Circulation *126*, 2601-2611.

Lee, J.H., Daugharthy, E.R., Scheiman, J., Kalhor, R., Yang, J.L., Ferrante, T.C., Terry, R., Jeanty, S.S.F., Li, C., Amamoto, R*., et al.* (2014a). Highly multiplexed subcellular RNA sequencing in situ. Science (New York, NY) *343*, 1360-1363.

Lee, R.H., Pulin, A.A., Seo, M.J., Kota, D.J., Ylostalo, J., Larson, B.L., Semprun-Prieto, L., Delafontaine, P., and Prockop, D.J. (2009). Intravenous hMSCs Improve Myocardial Infarction in Mice because Cells Embolized in Lung Are Activated to Secrete the Anti-inflammatory Protein TSG-6. Cell stem cell *5*, 54-63.

Lee, R.H., Yu, J.M., Foskett, A.M., Peltier, G., Reneau, J.C., Bazhanov, N., Oh, J.Y., and Prockop, D.J. (2014b). TSG-6 as a biomarker to predict efficacy of human mesenchymal stem/progenitor cells (hMSCs) in modulating sterile inflammation in vivo. Proceedings of the National Academy of Sciences *111*, 16766-16771.

Lee, W.C., Shi, H., Poon, Z., Nyan, L.M., Kaushik, T., Shivashankar, G.V., Chan, J.K.Y., Lim, C.T., Han, J., and Van Vliet, K.J. (2014c). Multivariate biophysical markers predictive of mesenchymal stromal cell multipotency. Proceedings of the National Academy of Sciences *111*, E4409-E4418.

Leimkühler, N.B., Gleitz, H.F.E., Ronghui, L., Snoeren, I.A.M., Fuchs, S.N.R., Nagai, J.S., Banjanin, B., Lam, K.H., Vogl, T., Kuppe, C.*, et al.* (2020). Heterogeneous bone-marrow stromal progenitors drive myelofibrosis via a druggable alarmin axis. Cell stem cell.

Li, G., Jin, R., Norris, R.A., Zhang, L., Yu, S., Wu, F., Markwald, R.R., Nanda, A., Conway, S.J., Smyth, S.S.*, et al.* (2010). Periostin mediates vascular smooth muscle cell migration through the integrins αvβ3 and αvβ5 and focal adhesion kinase (FAK) pathway. Atherosclerosis *208*, 358-365.

Liberzon, A., Subramanian, A., Pinchback, R., Thorvaldsdóttir, H., Tamayo, P., and Mesirov, J.P. (2011). Molecular signatures database (MSigDB) 3.0. Bioinformatics *27*, 1739-1740.

Liu, Y., Wang, L., Kikuiri, T., Akiyama, K., Chen, C., Xu, X., Yang, R., Chen, W., Wang, S., and Shi, S. (2011). Mesenchymal stem cell-based tissue regeneration is governed by recipient T lymphocytes via IFN-γ and TNF-α. Nature medicine *17*, 1594-1601.

Lu, G.-d., Cheng, P., Liu, T., and Wang, Z. (2020). BMSC-Derived Exosomal miR-29a Promotes Angiogenesis and Osteogenesis. Frontiers in Cell and Developmental Biology *8*.

Lu, Y., Chen, J.J., Mu, L., Xue, Q., Wu, Y., Wu, P.-H., Li, J., Vortmeyer, A.O., Miller-Jensen, K., Wirtz, D.*, et al.* (2013). High-Throughput Secretomic Analysis of Single Cells to Assess Functional Cellular Heterogeneity. Analytical Chemistry *85*, 2548-2556.

Ma, Z., Zhao, X., Deng, M., Huang, Z., Wang, J., Wu, Y., Cui, D., Liu, Y., Liu, R., and Ouyang, G. (2019). Bone Marrow Mesenchymal Stromal Cell-Derived Periostin Promotes B-ALL Progression by Modulating CCL2 in Leukemia Cells. Cell Reports *26*, 1533-1543.e1534.

Mackie, E.J., Ahmed, Y.A., Tatarczuch, L., Chen, K.S., and Mirams, M. (2008). Endochondral ossification: how cartilage is converted into bone in the developing skeleton. Int J Biochem Cell Biol *40*, 46-62.

Maeda, S., Hayashi, M., Komiya, S., Imamura, T., and Miyazono, K. (2004). Endogenous TGF-beta signaling suppresses maturation of osteoblastic mesenchymal cells. Embo j *23*, 552-563.

Maffioli, E., Nonnis, S., Angioni, R., Santagata, F., Calì, B., Zanotti, L., Negri, A., Viola, A., and Tedeschi, G. (2017). Proteomic analysis of the secretome of human bone marrow-derived mesenchymal stem cells primed by pro-inflammatory cytokines. Journal of Proteomics *166*, 115-126.

Malinowski, M., Pietraszek, K., Perreau, C., Boguslawski, M., Decot, V., Stoltz, J.-F., Vallar, L., Niewiarowska, J., Cierniewski, C., Maquart, F.-X*., et al.* (2012). Effect of Lumican on the Migration of Human Mesenchymal Stem Cells and Endothelial Progenitor Cells: Involvement of Matrix Metalloproteinase-14. PLOS ONE *7*, e50709.

Marrison, J., Räty, L., Marriott, P., and O'Toole, P. (2013). Ptychography – a label free, high-contrast imaging technique for live cells using quantitative phase information. Scientific Reports *3*, 2369.

Massagué, J. (2012). TGFβ signalling in context. Nature Reviews Molecular Cell Biology *13*, 616-630.

Matic, I., Matthews, B.G., Wang, X., Dyment, N.A., Worthley, D.L., Rowe, D.W., Grcevic, D., and Kalajzic, I. (2016). Quiescent Bone Lining Cells Are a Major Source of Osteoblasts During Adulthood. Stem cells (Dayton, Ohio) *34*, 2930-2942.

McBeath, R., Pirone, D.M., Nelson, C.M., Bhadriraju, K., and Chen, C.S. (2004). Cell Shape, Cytoskeletal Tension, and RhoA Regulate Stem Cell Lineage Commitment. Developmental Cell *6*, 483-495.

McMurray, R.J., Gadegaard, N., Tsimbouri, P.M., Burgess, K.V., McNamara, L.E., Tare, R., Murawski, K., Kingham, E., Oreffo, R.O.C., and Dalby, M.J. (2011). Nanoscale surfaces for the long-term maintenance of mesenchymal stem cell phenotype and multipotency. Nat Mater *10*, 637-644.

Medyouf, H., Mossner, M., Jann, J.-C., Nolte, F., Raffel, S., Herrmann, C., Lier, A., Eisen, C., Nowak, V., Zens, B*., et al.* (2014). Myelodysplastic Cells in Patients Reprogram Mesenchymal Stromal Cells to Establish a Transplantable Stem Cell Niche Disease Unit. Cell stem cell *14*, 824-837.

Meirelles, L.d.S., Chagastelles, P.C., and Nardi, N.B. (2006). Mesenchymal stem cells reside in virtually all post-natal organs and tissues. Journal of Cell Science *119*, 2204-2213.

Méndez-Ferrer, S., Michurina, T.V., Ferraro, F., Mazloom, A.R., Macarthur, B.D., Lira, S.A., Scadden, D.T., Ma'ayan, A., Enikolopov, G.N., and Frenette, P.S. (2010). Mesenchymal and haematopoietic stem cells form a unique bone marrow niche. Nature *466*, 829-834.

Mets, T., and Verdonk, G. (1981a). In vitro aging of human bone marrow derived stromal cells. Mech Ageing Dev *16*, 81-89.

Mets, T., and Verdonk, G. (1981b). Variations in the stromal cell population of human bone marrow during aging. Mech Ageing Dev *15*, 41-49.

Miyamae, T., Marinov, A.D., Sowders, D., Wilson, D.C., Devlin, J., Boudreau, R., Robbins, P., and Hirsch, R. (2006). Follistatin-Like Protein-1 Is a Novel Proinflammatory Molecule. The Journal of Immunology *177*, 4758-4762.

Mizukami, A., Thomé, C.H., Ferreira, G.A., Lanfredi, G.P., Covas, D.T., Pitteri, S.J., Swiech, K., and Faça, V.M. (2019). Proteomic Identification and Time-Course Monitoring of Secreted Proteins During Expansion of Human Mesenchymal Stem/Stromal in Stirred-Tank Bioreactor. Frontiers in Bioengineering and Biotechnology *7*.

Morikawa, S., Mabuchi, Y., Kubota, Y., Nagai, Y., Niibe, K., Hiratsu, E., Suzuki, S., Miyauchi-Hara, C., Nagoshi, N., Sunabori, T.*, et al.* (2009). Prospective identification, isolation, and systemic transplantation of multipotent mesenchymal stem cells in murine bone marrow. The Journal of experimental medicine *206*, 2483-2496.

Morrison, S.J., and Scadden, D.T. (2014). The bone marrow niche for haematopoietic stem cells. Nature *505*, 327-334.

Mu, D., Cambier, S., Fjellbirkeland, L., Baron, J.L., Munger, J.S., Kawakatsu, H., Sheppard, D., Broaddus, V.C., and Nishimura, S.L. (2002). The integrin alpha(v)beta8 mediates epithelial homeostasis through MT1-MMP-dependent activation of TGF-beta1. J Cell Biol *157*, 493-507.

Munger, J.S., Harpel, J.G., Giancotti, F.G., and Rifkin, D.B. (1998). Interactions between growth factors and integrins: latent forms of transforming growth factor-beta are ligands for the integrin alphavbeta1. Mol Biol Cell *9*, 2627-2638.

Muraglia, A., Cancedda, R., and Quarto, R. (2000). Clonal mesenchymal progenitors from human bone marrow differentiate in vitro according to a hierarchical model. Journal of Cell Science *113*, 1161-1166.

Murphy, J.M., Fink, D.J., Hunziker, E.B., and Barry, F.P. (2003). Stem cell therapy in a caprine model of osteoarthritis. Arthritis & Rheumatism *48*, 3464-3474.

Murphy, J.W., Cho, Y., Sachpatzidis, A., Fan, C., Hodsdon, M.E., and Lolis, E. (2007). Structural and Functional Basis of CXCL12 (Stromal Cell-derived Factor-1α) Binding to Heparin*. Journal of Biological Chemistry *282*, 10018-10027.

Mwale, F., Stachura, D., Roughley, P., and Antoniou, J. (2006). Limitations of using aggrecan and type X collagen as markers of chondrogenesis in mesenchymal stem cell differentiation. Journal of orthopaedic research : official publication of the Orthopaedic Research Society *24*, 1791-1798.

Naba, A., Clauser, K.R., Hoersch, S., Liu, H., Carr, S.A., and Hynes, R.O. (2012). The matrisome: in silico definition and in vivo characterization by proteomics of normal and tumor extracellular matrices. Mol Cell Proteomics *11*, M111.014647-M014111.014647.

Nakamura-Ishizu, A., Okuno, Y., Omatsu, Y., Okabe, K., Morimoto, J., Uede, T., Nagasawa, T., Suda, T., and Kubota, Y. (2012). Extracellular matrix protein tenascin-C is required in the bone marrow microenvironment primed for hematopoietic regeneration. Blood *119*, 5429-5437.

Neil, S.J.D., Zang, T., and Bieniasz, P.D. (2008). Tetherin inhibits retrovirus release and is antagonized by HIV-1 Vpu. Nature *451*, 425-430.

Nejadnik, H., Hui, J.H., Feng Choong, E.P., Tai, B.C., and Lee, E.H. (2010). Autologous bone marrow-derived mesenchymal stem cells versus autologous chondrocyte implantation: an observational cohort study. Am J Sports Med *38*, 1110-1116.

Ng, C.P., Mohamed Sharif, A.R., Heath, D.E., Chow, J.W., Zhang, C.B.Y., Chan-Park, M.B., Hammond, P.T., Chan, J.K.Y., and Griffith, L.G. (2014). Enhanced ex vivo expansion of adult mesenchymal stem cells by fetal mesenchymal stem cell ECM. Biomaterials *35*, 4046-4057.

Nilsson, S.K., Debatis, M.E., Dooner, M.S., Madri, J.A., Quesenberry, P.J., and Becker, P.S. (1998). Immunofluorescence Characterization of Key Extracellular Matrix Proteins in Murine Bone Marrow In Situ. Journal of Histochemistry & Cytochemistry *46*, 371-377.

Norris, R.A., Damon, B., Mironov, V., Kasyanov, V., Ramamurthi, A., Moreno-Rodriguez, R., Trusk, T., Potts, J.D., Goodwin, R.L., Davis, J.*, et al.* (2007). Periostin regulates collagen fibrillogenesis and the biomechanical properties of connective tissues. Journal of cellular biochemistry *101*, 695-711.

Novoseletskaya, E., Grigorieva, O., Nimiritsky, P., Basalova, N., Eremichev, R., Milovskaya, I., Kulebyakin, K., Kulebyakina, M., Rodionov, S., Omelyanenko, N.*, et al.* (2020). Mesenchymal Stromal Cell-Produced Components of Extracellular Matrix Potentiate Multipotent Stem Cell Response to Differentiation Stimuli. Frontiers in Cell and Developmental Biology *8*.

Nuttall, M.E., Patton, A.J., Olivera, D.L., Nadeau, D.P., and Gowen, M. (1998). Human Trabecular Bone Cells Are Able to Express Both Osteoblastic and Adipocytic Phenotype: Implications for Osteopenic Disorders. Journal of Bone and Mineral Research *13*, 371-382.

Oguro, H., Ding, L., and Morrison, S.J. (2013). SLAM family markers resolve functionally distinct subpopulations of hematopoietic stem cells and multipotent progenitors. Cell stem cell *13*, 102-116.

Okamoto, T., Aoyama, T., Nakayama, T., Nakamata, T., Hosaka, T., Nishijo, K., Nakamura, T., Kiyono, T., and Toguchida, J. (2002). Clonal heterogeneity in differentiation potential of immortalized human mesenchymal stem cells. Biochem Biophys Res Commun *295*, 354-361.

Omatsu, Y., Sugiyama, T., Kohara, H., Kondoh, G., Fujii, N., Kohno, K., and Nagasawa, T. (2010). The Essential Functions of Adipo-osteogenic Progenitors as the Hematopoietic Stem and Progenitor Cell Niche. Immunity *33*, 387-399.

Ono, N., Ono, W., Nagasawa, T., and Kronenberg, H.M. (2014). A subset of chondrogenic cells provides early mesenchymal progenitors in growing bones. Nature Cell Biology *16*, 1157-1167.

Pathan, M., Fonseka, P., Chitti, S.V., Kang, T., Sanwlani, R., Van Deun, J., Hendrix, A., and Mathivanan, S. (2018). Vesiclepedia 2019: a compendium of RNA, proteins, lipids and metabolites in extracellular vesicles. Nucleic acids research *47*, D516-D519.

Pathan, M., Keerthikumar, S., Ang, C.S., Gangoda, L., Quek, C.Y., Williamson, N.A., Mouradov, D., Sieber, O.M., Simpson, R.J., Salim, A.*, et al.* (2015). FunRich: An open access standalone functional enrichment and interaction network analysis tool. Proteomics *15*, 2597-2601.

Phinney, D.G., Kopen, G., Righter, W., Webster, S., Tremain, N., and Prockop, D.J. (1999). Donor variation in the growth properties and osteogenic potential of human marrow stromal cells. Journal of cellular biochemistry *75*, 424-436.

Pinho, S., Lacombe, J., Hanoun, M., Mizoguchi, T., Bruns, I., Kunisaki, Y., and Frenette, P.S. (2013). PDGFRα and CD51 mark human nestin+ sphere-forming

mesenchymal stem cells capable of hematopoietic progenitor cell expansion. The Journal of experimental medicine *210*, 1351-1367.

Pittenger, M.F., Mackay, A.M., Beck, S.C., Jaiswal, R.K., Douglas, R., Mosca, J.D., Moorman, M.A., Simonetti, D.W., Craig, S., and Marshak, D.R. (1999). Multilineage Potential of Adult Human Mesenchymal Stem Cells. Science (New York, NY) *284*, 143-147.

Poon, Z., Lee, W.C., Guan, G., Nyan, L.M., Lim, C.T., Han, J., and Van Vliet, K.J. (2015). Bone marrow regeneration promoted by biophysically sorted osteoprogenitors from mesenchymal stromal cells. Stem cells translational medicine *4*, 56-65.

Prasad, V.K., Lucas, K.G., Kleiner, G.I., Talano, J.A., Jacobsohn, D., Broadwater, G., Monroy, R., and Kurtzberg, J. (2011). Efficacy and safety of ex vivo cultured adult human mesenchymal stem cells (Prochymal™) in pediatric patients with severe refractory acute graft-versus-host disease in a compassionate use study. Biol Blood Marrow Transplant *17*, 534-541.

Preibisch, S., Saalfeld, S., and Tomancak, P. (2009). Globally optimal stitching of tiled 3D microscopic image acquisitions. Bioinformatics (Oxford, England) *25*, 1463-1465.

Qin, Y., Wang, L., Gao, Z., Chen, G., and Zhang, C. (2016). Bone marrow stromal/stem cell-derived extracellular vesicles regulate osteoblast activity and differentiation in vitro and promote bone regeneration in vivo. Scientific Reports *6*, 21961.

Quirici, N., Soligo, D., Bossolasco, P., Servida, F., Lumini, C., and Deliliers, G.L. (2002). Isolation of bone marrow mesenchymal stem cells by anti-nerve growth factor receptor antibodies. Experimental hematology *30*, 783-791.

Rackov, G., Garcia-Romero, N., Esteban-Rubio, S., Carrión-Navarro, J., Belda-Iniesta, C., and Ayuso-Sacido, A. (2018). Vesicle-Mediated Control of Cell Function: The Role of Extracellular Matrix and Microenvironment. Frontiers in Physiology *9*.

Rakian, R., Block, T.J., Johnson, S.M., Marinkovic, M., Wu, J., Dai, Q., Dean, D.D., and Chen, X.-D. (2015). Native extracellular matrix preserves mesenchymal stem cell “stemness” and differentiation potential under serum-free culture conditions. Stem Cell Research & Therapy *6*, 235.

Ranganath, S.H., Levy, O., Inamdar, M.S., and Karp, J.M. (2012). Harnessing the mesenchymal stem cell secretome for the treatment of cardiovascular disease. Cell stem cell *10*, 244-258.

Raposo, G., and Stoorvogel, W. (2013). Extracellular vesicles: Exosomes, microvesicles, and friends. Journal of Cell Biology *200*, 373-383.

Raterman, H.G., Vosslamber, S., de Ridder, S., Nurmohamed, M.T., Lems, W.F., Boers, M., van de Wiel, M., Dijkmans, B.A.C., Verweij, C.L., and Voskuyl, A.E. (2012). The interferon type I signature towards prediction of non-response to rituximab in rheumatoid arthritis patients. Arthritis Research & Therapy *14*, R95.

Reinisch, A., Etchart, N., Thomas, D., Hofmann, N.A., Fruehwirth, M., Sinha, S., Chan, C.K., Senarath-Yapa, K., Seo, E.-Y., Wearda, T.*, et al.* (2015). Epigenetic and in vivo comparison of diverse MSC sources reveals an endochondral signature for human hematopoietic niche formation. Blood *125*, 249-260.

Ren, G., Zhang, L., Zhao, X., Xu, G., Zhang, Y., Roberts, A.I., Zhao, R.C., and Shi, Y. (2008). Mesenchymal Stem Cell-Mediated Immunosuppression Occurs via Concerted Action of Chemokines and Nitric Oxide. Cell stem cell *2*, 141-150.

Rennerfeldt, D.A., Raminhos, J.S., Leff, S.M., Manning, P., and Van Vliet, K.J. (2019). Emergent heterogeneity in putative mesenchymal stem cell colonies: Single-cell time lapsed analysis. PLOS ONE *14*, e0213452.

Rilla, K., Mustonen, A.-M., Arasu, U.T., Härkönen, K., Matilainen, J., and Nieminen, P. (2019). Extracellular vesicles are integral and functional components of the extracellular matrix. Matrix Biology *75-76*, 201-219.

Ringdén, O., Uzunel, M., Rasmusson, I., Remberger, M., Sundberg, B., Lönnies, H., Marschall, H.-U., Dlugosz, A., Szakos, A., Hassan, Z.*, et al.* (2006). Mesenchymal Stem Cells for Treatment of Therapy-Resistant Graft-versus-Host Disease. Transplantation *81*.

Rios, H., Koushik, S.V., Wang, H., Wang, J., Zhou, H.-M., Lindsley, A., Rogers, R., Chen, Z., Maeda, M., Kruzynska-Frejtag, A.*, et al.* (2005). periostin null mice exhibit dwarfism, incisor enamel defects, and an early-onset periodontal disease-like phenotype. Mol Cell Biol *25*, 11131-11144.

Roddy, G.W., Oh, J.Y., Lee, R.H., Bartosh, T.J., Ylostalo, J., Coble, K., Rosa, R.H., Jr., and Prockop, D.J. (2011). Action at a distance: systemically administered adult stem/progenitor cells (MSCs) reduce inflammatory damage to the cornea without engraftment and primarily by secretion of TNF-α stimulated gene/protein 6. Stem cells (Dayton, Ohio) *29*, 1572-1579.

Roderburg, C., Urban, G.-W., Bettermann, K., Vucur, M., Zimmermann, H., Schmidt, S., Janssen, J., Koppe, C., Knolle, P., Castoldi, M.*, et al.* (2011). Micro-RNA profiling reveals a role for miR-29 in human and murine liver fibrosis. Hepatology *53*, 209-218.

Rohart, F., Mason, E.A., Matigian, N., Mosbergen, R., Korn, O., Chen, T., Butcher, S., Patel, J., Atkinson, K., Khosrotehrani, K.*, et al.* (2016). A molecular classification of human mesenchymal stromal cells. PeerJ *4*, e1845.

Romieu-Mourez, R., François, M., Boivin, M.-N., Bouchentouf, M., Spaner, D.E., and Galipeau, J. (2009). Cytokine Modulation of TLR Expression and Activation in Mesenchymal Stromal Cells Leads to a Proinflammatory Phenotype. The Journal of Immunology *182*, 7963-7973.

Russell, K.C., Phinney, D.G., Lacey, M.R., Barrilleaux, B.L., Meyertholen, K.E., and O'Connor, K.C. (2010). In vitro high-capacity assay to quantify the clonal heterogeneity in trilineage potential of mesenchymal stem cells reveals a complex hierarchy of lineage commitment. Stem cells (Dayton, Ohio) *28*, 788-798.

Sacchetti, B., Funari, A., Michienzi, S., Di Cesare, S., Piersanti, S., Saggio, I., Tagliafico, E., Ferrari, S., Robey, P.G., Riminucci, M.*, et al.* (2007). Self-Renewing Osteoprogenitors in Bone Marrow Sinusoids Can Organize a Hematopoietic Microenvironment. Cell *131*, 324-336.

Sacchetti, B., Funari, A., Remoli, C., Giannicola, G., Kogler, G., Liedtke, S., Cossu, G., Serafini, M., Sampaolesi, M., Tagliafico, E.*, et al.* (2016). No Identical “Mesenchymal Stem Cells” at Different Times and Sites: Human Committed Progenitors of Distinct Origin

and Differentiation Potential Are Incorporated as Adventitial Cells in Microvessels. Stem Cell Reports *6*, 897-913.

Saksela, O., Moscatelli, D., Sommer, A., and Rifkin, D.B. (1988). Endothelial cell-derived heparan sulfate binds basic fibroblast growth factor and protects it from proteolytic degradation. Journal of Cell Biology *107*, 743-751.

Samsonraj, R.M., Rai, B., Sathiyanathan, P., Puan, K.J., Rötzschke, O., Hui, J.H., Raghunath, M., Stanton, L.W., Nurcombe, V., and Cool, S.M. (2015). Establishing criteria for human mesenchymal stem cell potency. Stem cells (Dayton, Ohio) *33*, 1878-1891.

Sarugaser, R., Lickorish, D., Baksh, D., Hosseini, M.M., and Davies, J.E. (2005). Human umbilical cord perivascular (HUCPV) cells: a source of mesenchymal progenitors. Stem cells (Dayton, Ohio) *23*, 220-229.

Schofield, R. (1978). The relationship between the spleen colony-forming cell and the haemopoietic stem cell. Blood Cells *4*, 7-25.

Schultz-Cherry, S., Ribeiro, S., Gentry, L., and Murphy-Ullrich, J.E. (1994). Thrombospondin binds and activates the small and large forms of latent transforming growth factor-beta in a chemically defined system. J Biol Chem *269*, 26775-26782.

Scotti, C., Piccinini, E., Takizawa, H., Todorov, A., Bourgine, P., Papadimitropoulos, A., Barbero, A., Manz, M.G., and Martin, I. (2013). Engineering of a functional bone organ through endochondral ossification. Proceedings of the National Academy of Sciences *110*, 3997-4002.

Selich, A., Daudert, J., Hass, R., Philipp, F., von Kaisenberg, C., Paul, G., Cornils, K., Fehse, B., Rittinghausen, S., Schambach, A.*, et al.* (2016). Massive Clonal Selection and Transiently Contributing Clones During Expansion of Mesenchymal Stem Cell Cultures Revealed by Lentiviral RGB-Barcode Technology. Stem Cells Transl Med *5*, 591-601.

Shalek, A.K., Satija, R., Shuga, J., Trombetta, J.J., Gennert, D., Lu, D., Chen, P., Gertner, R.S., Gaublomme, J.T., Yosef, N.*, et al.* (2014). Single-cell RNA-seq reveals dynamic paracrine control of cellular variation. Nature *510*, 363-369.

Shannon, P., Markiel, A., Ozier, O., Baliga, N.S., Wang, J.T., Ramage, D., Amin, N., Schwikowski, B., and Ideker, T. (2003). Cytoscape: a software environment for integrated models of biomolecular interaction networks. Genome Res *13*, 2498-2504.

Shao, X., Taha, I.N., Clauser, K.R., Gao, Y., and Naba, A. (2019). MatrisomeDB: the ECM-protein knowledge database. Nucleic acids research *48*, D1136-D1144.

Shi, S., Gronthos, S., Chen, S., Reddi, A., Counter, C.M., Robey, P.G., and Wang, C.-Y. (2002). Bone formation by human postnatal bone marrow stromal stem cells is enhanced by telomerase expression. Nature Biotechnology *20*, 587-591.

Sidhom, K., Obi, P.O., and Saleem, A. (2020). A Review of Exosomal Isolation Methods: Is Size Exclusion Chromatography the Best Option? Int J Mol Sci *21*.

Sidhu, S.S., Yuan, S., Innes, A.L., Kerr, S., Woodruff, P.G., Hou, L., Muller, S.J., and Fahy, J.V. (2010). Roles of epithelial cell-derived periostin in TGF-β activation, collagen production, and collagen gel elasticity in asthma. Proceedings of the National Academy of Sciences *107*, 14170-14175.

Simonsen, J.L., Rosada, C., Serakinci, N., Justesen, J., Stenderup, K., Rattan, S.I.S., Jensen, T.G., and Kassem, M. (2002). Telomerase expression extends the proliferative life-span and maintains the osteogenic potential of human bone marrow stromal cells. Nature Biotechnology *20*, 592-596.

Sipp, D., Robey, P.G., and Turner, L. (2018). Clear up this stem-cell mess. Nature *561*, 455-457.

Sivasubramaniyan, K., Ilas, D.C., Harichandan, A., Bos, P.K., Santos, D.L., de Zwart, P., Koevoet, W.J.L.M., Owston, H., Bühring, H.-J., Jones, E.*, et al.* (2018). Bone Marrow-Harvesting Technique Influences Functional Heterogeneity of Mesenchymal Stem/Stromal Cells and Cartilage Regeneration. Am J Sports Med *46*, 3521-3531.

Spangrude, G.J., Heimfeld, S., and Weissman, I.L. (1988). Purification and characterization of mouse hematopoietic stem cells. Science (New York, NY) *241*, 58-62.

Stagg, J., Pommey, S., Eliopoulos, N., and Galipeau, J. (2006). Interferon-gamma-stimulated marrow stromal cells: a new type of nonhematopoietic antigen-presenting cell. Blood *107*, 2570-2577.

Stastna, M., and Van Eyk, J.E. (2012). Secreted proteins as a fundamental source for biomarker discovery. Proteomics *12*, 722-735.

Strauer, B.E., Brehm, M., Zeus, T., Köstering, M., Hernandez, A., Sorg, R.V., Kögler, G., and Wernet, P. (2002). Repair of Infarcted Myocardium by Autologous Intracoronary Mononuclear Bone Marrow Cell Transplantation in Humans. Circulation *106*, 1913-1918.

Subramanian, A., Tamayo, P., Mootha, V.K., Mukherjee, S., Ebert, B.L., Gillette, M.A., Paulovich, A., Pomeroy, S.L., Golub, T.R., Lander, E.S.*, et al.* (2005). Gene set enrichment analysis: A knowledge-based approach for interpreting genome-wide expression profiles. Proceedings of the National Academy of Sciences *102*, 15545-15550.

Sugiyama, T., Kohara, H., Noda, M., and Nagasawa, T. (2006). Maintenance of the Hematopoietic Stem Cell Pool by CXCL12-CXCR4 Chemokine Signaling in Bone Marrow Stromal Cell Niches. Immunity *25*, 977-988.

Sun, Y., Li, W., Lu, Z., Chen, R., Ling, J., Ran, Q., Jilka, R.L., and Chen, X.-D. (2011). Rescuing replication and osteogenesis of aged mesenchymal stem cells by exposure to a young extracellular matrix. The FASEB Journal *25*, 1474-1485.

Swain, S., Sarmanova, A., Mallen, C., Kuo, C.F., Coupland, C., Doherty, M., and Zhang, W. (2020). Trends in incidence and prevalence of osteoarthritis in the United Kingdom: findings from the Clinical Practice Research Datalink (CPRD). Osteoarthritis Cartilage *28*, 792-801.

Szabó, E., Fajka-Boja, R., Kriston-Pál, É., Hornung, Á., Makra, I., Kudlik, G., Uher, F., Katona, R.L., Monostori, É., and Czibula, Á. (2015). Licensing by Inflammatory Cytokines Abolishes Heterogeneity of Immunosuppressive Function of Mesenchymal Stem Cell Population. Stem Cells and Development *24*, 2171-2180.

Taipale, J., Miyazono, K., Heldin, C.H., and Keski-Oja, J. (1994). Latent transforming growth factor-beta 1 associates to fibroblast extracellular matrix via latent TGF-beta binding protein. Journal of Cell Biology *124*, 171-181.

Takahashi, K., Tanabe, K., Ohnuki, M., Narita, M., Ichisaka, T., Tomoda, K., and Yamanaka, S. (2007). Induction of pluripotent stem cells from adult human fibroblasts by defined factors. Cell *131*, 861-872.

Tang, F., Barbacioru, C., Wang, Y., Nordman, E., Lee, C., Xu, N., Wang, X., Bodeau, J., Tuch, B.B., Siddiqui, A.*, et al.* (2009a). mRNA-Seq whole-transcriptome analysis of a single cell. Nature Methods *6*, 377-382.

Tang, Y., Wu, X., Lei, W., Pang, L., Wan, C., Shi, Z., Zhao, L., Nagy, T.R., Peng, X., Hu, J.*, et al.* (2009b). TGF-beta1-induced migration of bone mesenchymal stem cells couples bone resorption with formation. Nature medicine *15*, 757-765.

Théry, C., Amigorena, S., Raposo, G., and Clayton, A. (2006). Isolation and Characterization of Exosomes from Cell Culture Supernatants and Biological Fluids. Current protocols in cell biology *30*, 3.22.21-23.22.29.

Théry, C., Witwer, K.W., Aikawa, E., Alcaraz, M.J., Anderson, J.D., Andriantsitohaina, R., Antoniou, A., Arab, T., Archer, F., Atkin-Smith, G.K.*, et al.* (2018). Minimal information for studies of extracellular vesicles 2018 (MISEV2018): a position statement of the International Society for Extracellular Vesicles and update of the MISEV2014 guidelines. Journal of Extracellular Vesicles *7*, 1535750.

Thomas, T., Gori, F., Khosla, S., Jensen, M.D., Burguera, B., and Riggs, B.L. (1999). Leptin Acts on Human Marrow Stromal Cells to Enhance Differentiation to Osteoblasts and to Inhibit Differentiation to Adipocytes*. Endocrinology *140*, 1630-1638.

Tikhonova, A.N., Dolgalev, I., Hu, H., Sivaraj, K.K., Hoxha, E., Cuesta-Domínguez, Á., Pinho, S., Akhmetzyanova, I., Gao, J., Witkowski, M.*, et al.* (2019). The bone marrow microenvironment at single-cell resolution. Nature *569*, 222-228.

Tillet, E., Gential, B., Garrone, R., and Stallcup, W.B. (2002). NG2 proteoglycan mediates beta1 integrin-independent cell adhesion and spreading on collagen VI. Journal of cellular biochemistry *86*, 726-736.

Timmers, L., Lim, S.K., Arslan, F., Armstrong, J.S., Hoefer, I.E., Doevendans, P.A., Piek, J.J., El Oakley, R.M., Choo, A., Lee, C.N.*, et al.* (2008). Reduction of myocardial infarct size by human mesenchymal stem cell conditioned medium. Stem Cell Research *1*, 129-137.

Todorovic, V., and Rifkin, D.B. (2012). LTBPs, more than just an escort service. Journal of cellular biochemistry *113*, 410-418.

Tormin, A., Li, O., Brune, J.C., Walsh, S., Schütz, B., Ehinger, M., Ditzel, N., Kassem, M., and Scheding, S. (2011). CD146 expression on primary nonhematopoietic bone marrow stem cells is correlated with in situ localization. Blood *117*, 5067-5077.

Twine, N.A., Harkness, L., Adjaye, J., Aldahmash, A., Wilkins, M.R., and Kassem, M. (2018). Molecular Phenotyping of Telomerized Human Bone Marrow Skeletal Stem Cells Reveals a Genetic Program of Enhanced Proliferation and Maintenance of Differentiation Responses. JBMR Plus *2*, 257-267.

Veevers-Lowe, J., Ball, S.G., Shuttleworth, A., and Kielty, C.M. (2011). Mesenchymal stem cell migration is regulated by fibronectin through α5β1-integrin-mediated activation of PDGFR-β and potentiation of growth factor signals. Journal of Cell Science *124*, 1288-1300.

Venkata Lokesh, B., Sabrina, T., Petra, M.B., Friederike, G., Helene, R., Peter de, Z., Ingo, M., Bernhard, S., Thomas, S., Willem, E.F.*, et al.* (2009). Isolation of functionally distinct mesenchymal stem cell subsets using antibodies against CD56, CD271, and mesenchymal stem cell antigen-1. Haematologica *94*, 173-184.

Vizoso, F.J., Eiro, N., Cid, S., Schneider, J., and Perez-Fernandez, R. (2017). Mesenchymal Stem Cell Secretome: Toward Cell-Free Therapeutic Strategies in Regenerative Medicine. International Journal of Molecular Sciences *18*.

Vlodavsky, I., Folkman, J., Sullivan, R., Fridman, R., Ishai-Michaeli, R., Sasse, J., and Klagsbrun, M. (1987). Endothelial cell-derived basic fibroblast growth factor: synthesis and deposition into subendothelial extracellular matrix. Proceedings of the National Academy of Sciences *84*, 2292-2296.

von Erlach, T.C., Bertazzo, S., Wozniak, M.A., Horejs, C.-M., Maynard, S.A., Attwood, S., Robinson, B.K., Autefage, H., Kallepitis, C., Del Río Hernández, A.*, et al.* (2018). Cell-geometry-dependent changes in plasma membrane order direct stem cell signalling and fate. Nat Mater *17*, 237-242.

Walsh, C.J., Goodman, D., Caplan, A.I., and Goldberg, V.M. (1999). Meniscus regeneration in a rabbit partial meniscectomy model. Tissue Eng *5*, 327-337.

Wang, H.-S., Hung, S.-C., Peng, S.-T., Huang, C.-C., Wei, H.-M., Guo, Y.-J., Fu, Y.-S., Lai, M.-C., and Chen, C.-C. (2004). Mesenchymal Stem Cells in the Wharton's Jelly of the Human Umbilical Cord. Stem cells (Dayton, Ohio) *22*, 1330-1337.

Watanabe, H., Cheung, S.C., Itano, N., Kimata, K., and Yamada, Y. (1997). Identification of Hyaluronan-binding Domains of Aggrecan. Journal of Biological Chemistry *272*, 28057-28065.

Waterman, R.S., Tomchuck, S.L., Henkle, S.L., and Betancourt, A.M. (2010). A New Mesenchymal Stem Cell (MSC) Paradigm: Polarization into a Pro-Inflammatory MSC1 or an Immunosuppressive MSC2 Phenotype. PLOS ONE *5*, e10088.

Watt, F.M., and Huck, W.T.S. (2013). Role of the extracellular matrix in regulating stem cell fate. Nature Reviews Molecular Cell Biology *14*, 467-473.

Whitfield, M.J., Lee, W.C.J., and Van Vliet, K.J. (2013). Onset of heterogeneity in culture-expanded bone marrow stromal cells. Stem Cell Research *11*, 1365-1377.

Wilson, A., Hodgson-Garms, M., Frith, J.E., and Genever, P. (2019a). Multiplicity of Mesenchymal Stromal Cells: Finding the Right Route to Therapy. Front Immunol *10*, 1112-1112.

Wilson, A., Webster, A., and Genever, P. (2019b). Nomenclature and heterogeneity: consequences for the use of mesenchymal stem cells in regenerative medicine. Regenerative medicine *14*, 595-611.

Wilson, J.G., Liu, K.D., Zhuo, H., Caballero, L., McMillan, M., Fang, X., Cosgrove, K., Vojnik, R., Calfee, C.S., Lee, J.-W.*, et al.* (2015a). Mesenchymal stem (stromal) cells for treatment of ARDS: a phase 1 clinical trial. Lancet Respir Med *3*, 24-32.

Wilson, N.K., Kent, D.G., Buettner, F., Shehata, M., Macaulay, I.C., Calero-Nieto, F.J., Sánchez Castillo, M., Oedekoven, C.A., Diamanti, E., Schulte, R.*, et al.* (2015b).

Combined Single-Cell Functional and Gene Expression Analysis Resolves Heterogeneity within Stem Cell Populations. Cell stem cell *16*, 712-724.

Winer, J.P., Janmey, P.A., McCormick, M.E., and Funaki, M. (2008). Bone Marrow-Derived Human Mesenchymal Stem Cells Become Quiescent on Soft Substrates but Remain Responsive to Chemical or Mechanical Stimuli. Tissue Engineering Part A *15*, 147-154.

Wolock, S.L., Krishnan, I., Tenen, D.E., Matkins, V., Camacho, V., Patel, S., Agarwal, P., Bhatia, R., Tenen, D.G., Klein, A.M.*, et al.* (2019). Mapping Distinct Bone Marrow Niche Populations and Their Differentiation Paths. Cell Reports *28*, 302-311.e305.

Wong, K.L., Lee, K.B.L., Tai, B.C., Law, P., Lee, E.H., and Hui, J.H.P. (2013). Injectable Cultured Bone Marrow–Derived Mesenchymal Stem Cells in Varus Knees With Cartilage Defects Undergoing High Tibial Osteotomy: A Prospective, Randomized Controlled Clinical Trial With 2 Years' Follow-up. Arthroscopy: The Journal of Arthroscopic & Related Surgery *29*, 2020-2028.

Wong, S.W., Lenzini, S., Cooper, M.H., Mooney, D.J., and Shin, J.-W. (2020). Soft extracellular matrix enhances inflammatory activation of mesenchymal stromal cells to induce monocyte production and trafficking. Science Advances *6*, eaaw0158.

Wong, T.Y., Chang, C.H., Yu, C.H., and Huang, L.L.H. (2017). Hyaluronan keeps mesenchymal stem cells quiescent and maintains the differentiation potential over time. Aging Cell *16*, 451-460.

Wu, F., Vij, N., Roberts, L., Lopez-Briones, S., Joyce, S., and Chakravarti, S. (2007). A novel role of the lumican core protein in bacterial lipopolysaccharide-induced innate immune response. J Biol Chem *282*, 26409-26417.

Wu, T., Liu, Y., Fan, Z., Xu, J., Jin, L., Gao, Z., Wu, Z., Hu, L., Wang, J., Zhang, C.*, et al.* (2015). miR-21 Modulates the Immunoregulatory Function of Bone Marrow Mesenchymal Stem Cells Through the PTEN/Akt/TGF-β1 Pathway. Stem cells (Dayton, Ohio) *33*, 3281-3290.

Xue, Q., Lu, Y., Eisele, M.R., Sulistijo, E.S., Khan, N., Fan, R., and Miller-Jensen, K. (2015). Analysis of single-cell cytokine secretion reveals a role for paracrine signaling in coordinating macrophage responses to TLR4 stimulation. Science Signaling *8*, ra59-ra59.

Yeo, G.C., and Weiss, A.S. (2019). Soluble matrix protein is a potent modulator of mesenchymal stem cell performance. Proceedings of the National Academy of Sciences *116*, 2042-2051.

Zhang, J., Niu, C., Ye, L., Huang, H., He, X., Tong, W.-G., Ross, J., Haug, J., Johnson, T., Feng, J.Q.*, et al.* (2003). Identification of the haematopoietic stem cell niche and control of the niche size. Nature *425*, 836-841.

Zhang, S., Ge, J., Sun, A., Xu, D., Qian, J., Lin, J., Zhao, Y., Hu, H., Li, Y., Wang, K.*, et al.* (2006). Comparison of various kinds of bone marrow stem cells for the repair of infarcted myocardium: Single clonally purified non-hematopoietic mesenchymal stem cells serve as a superior source. Journal of cellular biochemistry *99*, 1132-1147.

Zhang, S., Teo, K.Y.W., Chuah, S.J., Lai, R.C., Lim, S.K., and Toh, W.S. (2019). MSC exosomes alleviate temporomandibular joint osteoarthritis by attenuating inflammation and restoring matrix homeostasis. Biomaterials *200*, 35-47.

Zhao, M., Perry, J.M., Marshall, H., Venkatraman, A., Qian, P., He, X.C., Ahamed, J., and Li, L. (2014). Megakaryocytes maintain homeostatic quiescence and promote post-injury regeneration of hematopoietic stem cells. Nature Medicine *20*, 1321-1326.

Zheng, G., Huang, L., Tong, H., Shu, Q., Hu, Y., Ge, M., Deng, K., Zhang, L., Zou, B., Cheng, B.*, et al.* (2014). Treatment of acute respiratory distress syndrome with allogeneic adipose-derived mesenchymal stem cells: a randomized, placebo-controlled pilot study. Respir Res *15*, 39-39.

Zhou, Bo O., Yue, R., Murphy, Malea M., Peyer, J.G., and Morrison, Sean J. (2014). Leptin-Receptor-Expressing Mesenchymal Stromal Cells Represent the Main Source of Bone Formed by Adult Bone Marrow. Cell stem cell *15*, 154-168.

Zhou, T., Li, H.-Y., Liao, C., Lin, W., and Lin, S. (2020). Clinical Efficacy and Safety of Mesenchymal Stem Cells for Systemic Lupus Erythematosus. Stem Cells Int *2020*, 6518508-6518508.

Zhu, H., Mitsuhashi, N., Klein, A., Barsky, L.W., Weinberg, K., Barr, M.L., Demetriou, A., and Wu, G.D. (2006). The role of the hyaluronan receptor CD44 in mesenchymal stem cell migration in the extracellular matrix. Stem cells (Dayton, Ohio) *24*, 928-935.

Zyrafete, K., Julia, S., Hatixhe, L.-P., Sibylle, W., Stefan, S., Manuel, G., Halvard, B., Ulrike, K., Thomas, K., Peter, B.*, et al.* (2013). Clonal analysis of multipotent stromal cells derived from CD271+ bone marrow mononuclear cells: functional heterogeneity and different mechanisms of allosuppression. Haematologica *98*, 1609-1616.

Zysset, P.K., Edward Guo, X., Edward Hoffler, C., Moore, K.E., and Goldstein, S.A. (1999). Elastic modulus and hardness of cortical and trabecular bone lamellae measured by nanoindentation in the human femur. Journal of Biomechanics *32*, 1005-1012.